ASSESSING EFFICIENCIES IN VEGETABLE PRODUCTION: HYDROLOGIC MODELING OF SOIL-WATER DYNAMICS AND ESTIMATION OF GREENHOUSE GAS EMISSIONS

By

CURTIS DINNEEN JONES

A DISSERTATION PRESENTED TO THE GRADUATE SCHOOL
OF THE UNIVERSITY OF FLORIDA IN PARTIAL FULFILLMENT
OF THE REQUIREMENTS FOR THE DEGREE OF
DOCTOR OF PHILOSOPHY

UNIVERSITY OF FLORIDA

2013

To Callie, my family, my friends

ACKNOWLEDGMENTS

I would like to thank the members of my supervisory committee: Clyde Fraisse, Lincoln Zotarelli, John Schueller, Chris Martinez, and Kelly Morgan, for their advice and guidance. I would also like to thank Cheryl Porter and Jin Wu, for their collaboration and helpfulness with the DSSAT project. To Wayne Williams, my hole-digging partner, thanks for all the help setting up and maintaining equipment, and for the good talks. I would like to acknowledge Monica Ozores-Hampton for being an awesome collaborative partner. Thanks to Buck Nelson and the staff at the PSREU in Citra, for all their help setting up my field-experiment and keeping everything operational. Thanks to Robin Robbins and Irrigation Mart for their contribution of the drip tapes used in this study, which was a big help getting this study started. Thanks to my colleagues, especially Anna Linhoss, the late Arun Jain, Ahmed Al-Jumaili, Mackenzie Boyer, and Stacia Davis, for all the support and good company. Lastly, I want to thank all of my family and friends, for always being there.

TABLE OF CONTENTS

page

LIST OF TABLES

LIST OF FIGURES

LIST OF ABBREVIATIONS

ΔT	Time step
ΔX	Grid cell width
ΔZ	Grid cell height
C	Carbon
C_{EFF}	Nash-Sutcliffe coefficient of efficiency
CH_4	Methane
CO_2	Carbon dioxide
CO_2-EQ	Carbon dioxide equivalent
CSM	Cropping systems model
CVRMSE	Coefficient of variation of the root mean square error
CVRMSD	Coefficient of variation of the root mean square difference
D	Hydraulic diffusivity
DSSAT	Decision Support for Agrotechnology Transfer
DSSAT-2D	The modified two-dimensional DSSAT-CSM
ET	Evapotranspiration
GHG	Greenhouse gas
HDPE	High-density polyethylene
$H_{IN(I,J)}$	Horizontal in-flow to a grid cell in row i and cell j
$H_{OUT(I,J)}$	Horizontal out-flow from a grid cell in row i and cell j
K	Hydraulic conductivity
K_A	Bulk dielectric permittivity
K_S	Saturated hydraulic conductivity
LDPE	Low-density polyethylene
m	Van Genuchten fitting parameter

n	Van Genuchten fitting parameter
N	Nitrogen
N_2O	Nitrous oxide
NH_3	Ammonium
NO_3	Nitrate
P	Phosphorus
PA	Period average
Q_X	Horizontal water flux
Q_Z	Vertical water flux
R^2	Coefficient of determination
RMSD	Root mean squared difference
RMSE	Root mean squared error
SMRC	Soil moisture release curve
SSD	Sum of squares difference
$V_{OUT(I,J)}$	Vertical in-flow to a grid cell in row i and cell j
$V_{OUT(I,J)}$	Vertical out-flow from a grid cell in row i and cell j
VWC	Volumetric water content
α	Van Genuchten fitting parameter
Θ	Normalized water content
Θ	Soil water content
Θ_{1500}	Water content at 1500 kPa of tension
Θ_{33}	Water content at 33 kPa of tension
Θ_{DUL}	Drained upper limit water content
Θ_{LL}	Lower limit water content
Θ_R	Residual water content; also Van Genuchten fitting parameter

Θ_S	Saturation water content; also Van Genuchten fitting parameter
Ψ	Soil tension
Ψ_E	Air entry pressure

Abstract of Dissertation Presented to the Graduate School
of the University of Florida in Partial Fulfillment of the
Requirements for the Degree of Doctor of Philosophy

ASSESSING EFFICIENCIES IN VEGETABLE PRODUCTION: HYDROLOGIC MODELING OF SOIL-WATER DYNAMICS AND ESTIMATION OF GREENHOUSE GAS EMISSIONS

By

Curtis Dinneen Jones

May 2013

Chair: Clyde Fraisse
Major: Agricultural and Biological Engineering

The vegetable industry is economically important in Florida, with annual production valued at around 1.8 billion dollars spanning 300,000 acres. As such, these crops tend to be intensively managed to ensure optimal yields. However, in an atmosphere of increasing population and resource scarcity, both in Florida and globally, there is increasing pressure for agricultural commodities to be produced efficiently. To this end, cropping systems models (CSMs) are useful tools for identifying efficient production practices as they can be used to help understand complex relationships between management, system drivers, production, and environmental consequences. In this research the commonly used Decision Support System for Agrotechnology Transfer (DSSAT) CSM was amended to allow for water-limited simulation under cultural practices common for vegetable production, including drip irrigation. The modified model was evaluated to assess its utility in simulating soil-water dynamics, and simulation experiments were conducted to identify implications of management choices. Analyses demonstrated the relative importance of different drip irrigation management options as well as the importance of sensor placement for soil moisture sensor

controlled irrigation. As an added dimension, estimates of the greenhouse gas (GHG) emissions from typical tomato production systems were calculated. The estimates emphasize the importance of irrigation management, nutrient management, and productivity for minimizing these emissions.

CHAPTER 1
INTRODUCTION

Background

The vegetable industry is an economically important industry in Florida, with a value of 1.88 billion dollars in 2008 (Olson & Santos, 2011) spanning 300,000 acres (Cantliffe et al., 2009). The management practices of this large industry have many potential environment implications. Vegetables in Florida are typically produced on sandy soils with low water holding capacities (Dukes et al., 2006), commonly with plastic mulched raised beds and either drip or seepage irrigation. The potential to attain high water use efficiencies (Simonne et al., 2004) and fertilizer use efficiencies (Zotarelli, Dukes et al., 2009) has been demonstrated within these intensively managed systems given proper management. However, improper management can result in excessive water use and excessive nutrient loss, which are wasteful economically for the producer, damaging to the environment, and a drain on water resources.

Water shortages have become an increasing concern globally as naturally occurring rainfall shortages are intensified by population growth, land use change, and economic development (O'Connor et al., 2008). Vorosmarty et al. (2000) believe global water resources are already under significant stress based on the high ratio of water demand to sustainable water supply in many regions. Recent water shortages in the southeastern United States exemplify this global trend as regional droughts between 2005 and 2007 resulted in water shortages in this fast growing region, which is expected to have the largest net population growth between 2000 and 2030 of any region in the United States (Nagy et al., 2010). Water scarcity has long been an issue in the arid regions of the southwestern United States, but has become an increasingly

prevalent problem in the more humid southeastern United States, particularly in Florida (Asano et al., 2007) despite average annual rainfall of 114 to 152 cm (Smajstrla et al., 1999). Increased groundwater withdrawals in Florida have resulted in reduced river, lake, and aquifer levels throughout southwest Florida, saltwater intrusion into the Floridan aquifer in coastal Manatee, Sarasota, and Hillsborough counties, and caused the Southwest Florida Water Management District (SWFWMD) to create water use caution areas and tighten water permitting (Romero et al., 2008; SWFWMD, 2006). Lowered groundwater levels have also led to increased pumping costs, sinkhole formation and land subsidence (Molle & Berkoff, 2009), with pumping used for freeze protection of citrus and strawberries in Hillsborough County identified as causing many sinkholes in the area (Bengston, 1987).

Agriculture has a significant role in water resource issues. Agriculture is the largest user of water in the world, with Bruinsma (2003) estimating that 70% of global water use is for irrigation. Irrigation is the second largest user of water in the United States behind thermoelectric-power generation, accounting for 31% of all water withdrawals and 37% of freshwater withdrawals (Kenny et al., 2009). Irrigation also accounts for the largest withdrawal of groundwater in the United States at around 67% (Kenny et al., 2009). In Florida, irrigation is the largest user of freshwater, accounting for around 45% of all freshwater withdrawals, 62% of all fresh surface water withdrawals, and 35% of all groundwater withdrawals (Kenny et al., 2009). Rosenzweig et al. (2004) suggest that improvements in irrigation and crop technology will play an integral role in meeting the expected future increases in water demand.

Another issue important in agriculture that impacts production and the environment is nitrogen loading. Nutrient loss from agriculture has been shown to be significant. A United States Geological Survey (USGS) study (1998) conducted in Florida and Georgia demonstrated that 20% of water samples taken from surficial aquifers had nitrate-nitrogen concentrations in exceedance of the 10 mg/l United States Environmental Protection Agency (USEPA) drinking water standard, while 33% of samples collected from row-cropping areas exceeded this standard. Nitrates are a concern as elevated levels can have adverse health and ecological effects. Ecologically, a causal relationship has been shown between high nitrogen concentrations and plant and algal blooms in surface waters (Rosen, 2003) as well as fish poisoning (Di & Cameron, 2002). The problem is widespread, as agricultural nitrate losses have been identified as a source related to hypoxic zones in the Gulf of Mexico (Burkart & James, 1999) and elevated nitrate levels in the Baltic Sea (Tiemeyer et al., 2010). From a public health perspective, contaminated drinking water can also cause significant human health impacts, especially in infants, by inducing the potentially life threatening condition methemoglobinemia (Mueller & Helsel, 1996).

Drip irrigation is a technology which offers the ability to supply water to crops with increased efficiency, reducing water use as well as nutrient leaching compared to seepage irrigated systems (Dukes et al., 2010; Pitts et al., 1988; Sato et al., 2010). Micro-irrigation comprises 45% of the irrigated land in Florida, with most of this area comprised of microsprinklers used in citrus production, while seepage irrigation comprises 44% of irrigated lands (Dukes et al., 2010). However, due to the potential benefits of drip irrigation compared to seepage, there is increasing interest in

conversion of seepage-irrigated systems to drip irrigation (Dukes et al., 2010; Simonne, Hutchinson et al., 2010). This could result in an increased prevalence of drip irrigation for vegetable production in Florida, and increases the need to understand the system dynamics under drip irrigation to ensure the potential benefits of the technology are best realized.

In order to reduce nitrogen losses from agricultural production, management practices need to be developed to increase efficiency. Irrigation management is important for controlling these losses as irrigation practices have a strong impact on nitrate movement in soils, and thus nitrate loading. Due to the climate in the southeastern United States, most soil nitrogen is in the nitrate form because other forms are rapidly converted (Jansson & Persson, 1982). Nitrate moves rapidly with water, and under drip irrigation it has been shown that most of the nitrate collects near the fringe of the wetting front (Li et al., 2003). This behavior is even more significant on sandy soils as the low water holding capacities and high hydraulic conductivities encourage more vertical movement of the wetting front compared to heavier textured soils. Thus, the potential benefit from improved irrigation efficiency is two-fold as irrigation management has a large impact on both absolute water use and nutrient movement in soils.

The use of automated soil-moisture based irrigation has been shown to allow significant reduction in irrigation without reductions in yield (Smajstrla & Locascio, 1996; Dukes et al., 2003; Zotarelli et al., 2008; Zotarelli, Scholberg et al., 2009), with some estimates that irrigation can be cut in half compared to once or twice daily fixed-time irrigation approaches (Zotarelli, Dukes et al., 2009). However, the performance of these systems is dependent on decisions such as the sensor placement (Coelho & Or, 1996),

the soil moisture threshold value (Coelho & Or, 1996; Zotarelli et al., 2010), and the irrigation volume that is applied once the threshold moisture content has been reached (Zotarelli et al., 2010). Coelho and Or (1996) point out that while much work has been done to identify threshold soil moisture or matric values for optimal crop yields, most recommendations are general and empirical, ignoring site-specific soil water dynamics. Soil water models can be used to estimate the spatio-temporal dynamics of the system and thus make improved and more site-specific recommendations.

Another area for possible improvement in irrigation and fertilizer efficiency is the crop establishment phase of irrigation, during which irrigation is run for long durations after transplanting to encourage root development and prevent transplant shock (Simonne et al., 2004). The establishment of irrigation can account for a large portion of the seasonal nitrate leaching (Vazquez et al., 2005), especially when irrigation water is managed closely during the remainder of the season such that drainage is minimal (Zotarelli et al., 2007). This establishment phase has been identified as an area in which irrigation management efficiency can be improved (Schroder, 2006). Models can be used for estimating the irrigation durations necessary to maintain specific root-zone soil-moisture levels. This would allow water to be supplied in order to sustain young plants with poorly distributed and shallow roots while not supplying excess water beyond the shallow rooted depths. The frequency necessary to maintain high moisture levels in this region would also be important, and consideration of the site management capabilities would be necessary to determine if such irrigation frequencies would be feasible for real production applications.

Water use and nutrient losses need to be considered in the production of vegetables due to the effects they have on the environment and water resources locally and regionally. However, their impacts and the impacts of vegetable production as a whole also have global impacts through their influence on global GHG emissions. Atmospheric carbon dioxide levels are increasing, and the agricultural sector has been shown to account for 10-12% of anthropogenic GHG emissions (Smith et al., 2007). The Copenhagen Accord set a goal of keeping global temperature increases below 2 °C above preindustrial levels in order to avoid “dangerous anthropogenic interference with the climate system” (United Nations Framework Convention on Climate Change, 2009). However it appears that these increases are likely. For example, Rogelj et al. (2010), predict that based on current emissions pledges, there is a greater than 50% chance that an increase of more than 3 °C will in fact occur. A reasonable first step for reducing GHG emissions from the agricultural sector is to quantify emissions from specific sources within agricultural production and identify the most economically sensible actions for cutbacks. In similar production systems, irrigation and nitrogen fertilizer have been found to be among the largest sources of GHG emissions (Clyde Fraisse, personal communication, 2011). Thus, improvements in nitrogen and water use efficiencies could have major impacts on GHG emissions.

Objectives

It has been shown that the management of vegetable production has wide ranging impacts stemming from its impact on water demand, nutrient loss, and net GHG emissions. Irrigation practices have an influence on all of these areas. Frequent, low volume irrigation is considered the best method for providing sufficient water to the crop

while minimizing flow beyond the root zone (Locascio, 2005). However, while general recommendations are important, making site-specific recommendations that are more considerate of particular site, soil, crop, and management parameters can be beneficial. Investigations either need to be done site-specifically, which can be very costly, or models need to be created that are suitable for enhancing the details of such recommendations at lower cost. Therefore, the overall goal of this research was to create tools to help improve the efficiency of intensively managed vegetable production in order to reduce water use, nutrient leaching, and GHG emissions while maintaining competitive yields as well as to quantify the GHG emissions associated with typical tomato production practices. The specific objectives of this research were:

- To assist in the addition of a two-dimensional water balance model to the DSSAT-CSM which is capable of accounting for plastic mulch, raised beds, and drip irrigation
- To evaluate the performance of the amended DSSAT-CSM through a benchmark comparison with the HYDRUS-2D model
- To conduct field experiments to monitor the soil-water dynamics under different drip tape specifications and management scenarios
- To use the experimental data to evaluate the ability of the amended DSSAT-CSM to predict soil-water dynamics with different drip tapes and under different drip irrigation management scenarios
- To identify tangible management implications from simulation experiments using the amended DSSAT-CSM
- To estimate the GHG emissions associated with the production of open field-grown tomatoes under typical Florida production practices
- To identify the most promising areas of production for reducing GHG emissions from open-field Florida tomato production

CHAPTER 2
ADDITION OF A TWO-DIMENSIONAL WATER BALANCE MODEL TO THE DSSAT-CSM

Background

Agricultural production systems are complex, highly interactive systems. Crop models can be useful tools for understanding the relationships between crop, soil, climate, management actions, and the environment. An example of such a model is the DSSAT-CSM, a widely used modular software package that integrates of principles from experts in various fields to provide a unified model of cropping systems. DSSAT has been used in many regions and instances for addressing irrigation and fertilizer management strategies (Jones et al., 2003), making it a viable tool for improving the efficiencies in crop production.

However, while DSSAT has been widely applied to a range of cropping systems, it is in fact poorly suited for representing water or nutrient limited production under the production practices typical for vegetable production in Florida. The typical Florida vegetable production practices, which are not captured by DSSAT include the use of plastic mulch, raised beds, and drip irrigation. These production practices result in non-uniformities throughout the field that are not considered by the structure or water balance of DSSAT, and also include management options that are not available within DSSAT.

Conversely, HYDRUS-2D is a commonly used software package which can simulate soil-water dynamics under a wide range of boundary conditions. It has been shown to accurately predict soil-water flow under drip irrigation regimes (Provenzano, 2007; Roberts et al., 2009; Skaggs et al., 2004). However, unlike DSSAT, HYDRUS has a shortcoming in that it does not include a crop model, and thus cannot be used to

model interactions between management and crop growth and development. Additionally, HYDRUS is computationally intensive, requiring considerable time to complete simulations.

The soil water balance currently implemented in DSSAT (Ritchie, 1985; Ritchie, 1998) assumes one-dimensional, vertical flow. It operates on a daily time step, and considers water applied uniformly as either irrigation or rainfall. Runoff is calculated using the SCS curve number approach (United States Department of Agriculture, Soil Conservation Service, 1972) with modifications made by Williams et al. (1984) to account for layered soils and their moisture content, which was not considered in the original method. The soil is split into layers, with a maximum allowance of 20 layers, and each layer is characterized by its depth, saturation water content, drained upper limit water content, lower limit water content, and saturated hydraulic conductivity. Water which infiltrates the soil is added to the upper most layer, after which it is allowed to move using a “tipping bucket” approach modified with an empirical hydraulic conductivity by which water drains from upper layers if the water content exceeds the drained upper limit. The rate of this drainage is computed based on a general DSSAT drainage parameter which is a constant at all depths (Hoogenboom et al., 2003). This drainage rate is limited by the saturated hydraulic conductivity of that layer.

While one-dimensional modeling approaches have been shown to adequately represent water infiltration for rainfed, sprinkler, or flood irrigation systems (Brandt et al., 1971; Bresler et al., 1977), such an approach proves insufficient for drip irrigation systems. One reason for this is that under drip irrigation, the irrigation is applied non-uniformly. Since a one-dimensional reduction must assume uniform moisture

distribution across the field, it fails to correctly represent the system. Also, since the frequency of irrigation increases and the quantity of each irrigation decreases, the dynamics of the infiltration process become much more important. Thus the daily time-step becomes inadequately coarse in most instances.

These shortcomings of the one-dimensional approach arise because water movement under drip irrigation systems is truly a transient, three-dimensional process (Cote et al., 2003). However, because of difficulties for DSSAT developers to integrate a three-dimensional model (Gowdish & Muñoz-Carpena, 2009) within the DSSAT-CSM, a two-dimensional vertical plane flow approximation was made where uniformity was assumed in the direction of the crop row. Such an assumption is reasonable for drip-irrigated systems when emitters have a sufficiently small spacing (Bresler, 1977; Warrick, 1985), which has been reported to as being between 16 and 50 cm (Skaggs et al., 2004; Wang et al., 2000). This two-dimensional approximation has been made in many studies (Elmaloglou & Malamos, 2003; Rubin, 1968), and Schwartzman and Zur (1986) note that for row crops, emitters are typically spaced such that a fairly continuously wetted soil strip is created along the row, thus reasonably satisfying the assumption of uniformity in the row direction. The following will describe the theory behind and implementation of a two-dimensional water balance, which was developed by a group of DSSAT developers, within the DSSAT-CSM.

Model Description

Soil-Water Movement Calculations

The two-dimensional water flow theoretically can be computed using Richards equation, which is the most widely used model for soil water transport (Pachepsky et al., 2003). The equation originated when Richards (1931) demonstrated that Darcy's law,

which was derived from saturated flow experiments, could be applied to unsaturated flows if the saturated hydraulic conductivity parameter was replaced by the unsaturated hydraulic conductivity, which is a reduced value that is a function of the soil tension. Richards equation is derived by combining the continuity equation with Darcy's law. It is the equation which most accurately describes unsaturated water flow (Gowdish & Muñoz-Carpena, 2009). The original form of Richards equation is referred to as the potential-based form and is represented by equation (2-1), where θ is the soil water content (cm^3/cm^3), K is the hydraulic conductivity (cm/h), ψ is the soil suction head (cm), ∇ is a vector differential operator representing the gradient in space, t is the time (hr), and z is the vertical position (cm).

$$\frac{\partial \theta}{\partial t} = -\nabla\left[K(\psi)\nabla\psi\right] + \frac{\partial K}{\partial z} \tag{2-1}$$

The potential-based form is the most commonly used for numerical solutions, and it is applicable for variably-saturated and layered soils (Hillel, 1998). However, this form requires short time steps and small spatial intervals (Hillel, 1998). Implementations of this form are computationally intensive, require extensive soil property data, and generally involve fine spatial and temporal discretization. Additionally, Issues of convergence and instability are often found, sometimes impeding a solution to specific sets of initial and boundary conditions. Therefore mathematical manipulations were made to create an alternate water-content-based form which circumvents some of the issues encountered using the potential-based form. The form is represented by equations (2-2) and (2-3), where D is the hydraulic diffusivity (cm^2/hr).

$$\frac{\partial \theta}{\partial t} = -\nabla\left[D(\theta)\nabla\theta\right] + \frac{\partial K}{\partial z} \tag{2-2}$$

$$D(\theta) = K(\theta)\frac{d\psi}{d\theta} \quad (2\text{-}3)$$

The water-content-based form is less sensitive to the non-linear relationship of the soil hydraulic conductivity and pressure, and can tolerate much larger time and space intervals (Hillel, 1998). However, because it is a mathematical manipulation and not a physical representation of the system, it is not applicable for saturated flow, layered soils, or heterogeneous soils (Hillel, 1998). Taking this into consideration, it was decided that in order to create an approximate, practical model, which would have faster computational times, the water-content-based form would be implemented with some adjustments made to improve the performance under saturated and layered conditions.

The shortcoming of this form of Richards equation with saturated conditions is due to the hydraulic diffusivity, which approaches infinity as the water content approaches saturation. Therefore a hydraulic diffusivity limit of 417 cm^2/hr was imposed such that the value would not exceed the maximum value found in practice (Hillel, 1998). The shortcoming of this form in dealing with layered soils, as described by Talbot et al. (2004), has to do with discontinuities in the moisture content of different soil layers when in fact the matric potential varies continuously. This can result in erroneous flow predictions and potentially in predictions of flow in the opposite direction of the true flow, an illustration that water flow is dictated by the gradient of the total soil potential rather than by the difference in water contents. While this is a shortcoming of this form of the equation, in order to reduce the error, the normalized water content Θ was used in place of θ, as shown in equation (2-4), where θ_s is the saturated water content (cm^3/cm^3),θ_r is the residual water content (cm^3/cm^3), and θ is the actual water content (cm^3/cm^3). Thus by using Θ to drive soil-water flow, some of the error should be reduced when predicting

flow between differently textured soil layers. The horizontal and vertical flow can then be calculated as described in equations (2-5) and (2-6), where q_x is the horizontal flux (cm/hr) and q_z is the vertical flux (cm/hr). It should be noted that for homogenous soils, modeling soil-moisture flow using the normalized water-content is equivalent to using the actual water-content. As such, horizontal flows are unaffected by the adjustment since soil hydraulic properties are assumed uniform within each layer.

$$\Theta = \frac{\theta - \theta_r}{\theta_s - \theta_r} \tag{2-4}$$

$$q_x = -D(\theta)\frac{\partial \Theta}{\partial x} \tag{2-5}$$

$$q_z = -D(\theta)\frac{\partial \Theta}{\partial z} - K(\theta) \tag{2-6}$$

Parameterization Methodologies

In order to utilize Richards equation, it is necessary to provide the soil moisture release curve (SMRC) as well as the hydraulic conductivity and hydraulic diffusivity as functions of θ. There are many methodologies that can be used to relate $\theta(\psi)$, $K(\theta)$ and $D(\theta)$. Gardner and Mayhugh (1958) proposed an empirical equation to estimate the hydraulic diffusivity which is shown in equation (2-7), where a and b are fitting parameters. While this form does generally approximate $D(\theta)$, its unimodal shape poorly estimates $D(\theta)$ for low values of θ (Hillel, 1998) and the model parameters lack a physical basis.

$$D(\theta) = ae^{b\theta} \tag{2-7}$$

Gupta et al. (1974) estimated the hydraulic diffusivity as described in equation (2-8), where D_s is the soil diffusivity at saturation and α is a parameter with little sensitivity to the soil pore size distribution. This method was shown to perform well for a range of soil textures (Reichardt et al., 1972). However, the D_s and α parameters are unknown and must be determined experimentally, which makes it a poor approach for the DSSAT-2D model.

$$D(\theta) = D_s e^{\alpha(\theta-\theta_s)} \tag{2-8}$$

An additional method used the soil water retention curve predicted using the Saxton and Rawls (2006) methodology to estimate the hydraulic diffusivity, using the defining equation of hydraulic diffusivity previously described by equation (2-3). However, the soil water retention was calculated as a piecewise function, and its derivative resulted in a piecewise function which was discontinuous.

Ultimately the choice was made to use the Van Genuchten (1980) soil water retention curve model and the Mualem (1976) pore-size distribution model. These models were selected due to their wide use (Schaap & Leij, 2000; Tuller & Or, 2001; Kosugi et al., 2002; Ippisch et al., 2006). They have been found to be applicable to a wider variety of soils than other equations (Van Genuchten & Nielsen, 1985) and have been shown to predict soil water retention and unsaturated hydraulic conductivity better than other models on coarse sand and gravel (Mace et al., 1998). Certain models perform best for certain soil types and applications (Kosugi et al., 2002), but there is no model which performs best for all situations. However, the Van Genuchten and Mualem models were chosen due to their wide use and flexibility for characterizing many soil types and scenarios. The Van Genuchten parameters can be used to generate θ, K,

and D. The SMRC is described by equation (2-9), where θ_s, θ_r, α, m and n are the Van Genuchten fitting parameters. A common restriction of setting m = 1 - 1/n was made because it has been shown to perform better for most soils than any of the other common restrictions (Van Genucthen et al., 1991).The restriction was necessary because while the fitting is typically more accurate with no restrictions, it can suffer from poor convergence and correlated parameters with large uncertainty (Van Genucthen et al., 1991). With this restriction, K and D can be described by equations (2-10) and (2-11), where l is the pore-connectivity parameter.

$$\theta = \theta_r + \frac{\theta_s - \theta_r}{\left[1 + (\alpha h)^n\right]^m} \tag{2-9}$$

$$K(\Theta) = K_s \Theta^l \left[1 - (1 - \Theta^{\frac{1}{m}})^m\right]^2 \tag{2-10}$$

$$D(\Theta) = \frac{(1-m)K_s}{\alpha m(\theta_s - \theta_r)} \Theta^{(\frac{1}{2} - \frac{1}{m})} \left[(1 - \Theta^{\frac{1}{m}})^{-m} + (1 - \Theta^{\frac{1}{m}})^m - 2\right] \tag{2-11}$$

DSSAT allows a variety of soil properties to be input into the model. In order to operate the two-dimensional water balance, users are allowed the option of entering the Van Genuchten parameters directly for each soil layer. If the Van Genuchten parameters can be estimated from expert information or from fitting to SMRC data, this is preferred for improving the accuracy of simulations of the soil-water dynamics. However, in order to ensure that users with knowledge of only the standard soil properties for each soil layer can utilize the model, a methodology was developed to estimate the Van Genuchten parameters from the standard DSSAT soil property inputs.

Among the standard soil property inputs to DSSAT are the soil lower limit of plant extractable water (θ_{LL}), drained upper limit (θ_{DUL}), and saturation (θ_s) volumetric water

contents as well as the soil texture, and the sand, silt, clay, and organic matter soil fractions. The θ_{LL} is defined as the soil water content at which a crop can no longer extract water, while the θ_{DUL} is defined as the soil water content at which a previously saturated soil reaches once it has been allowed to drain until drainage ceases. Practically speaking, this is considered the point when the soil moisture content changes no more than 0.1% to 0.2% per day (Tsuji et al., 1994). The θ_{LL} is therefore analogous to the permanent wilting point while the θ_{DUL} is analogous to the field capacity. Thus, in order to estimate the necessary parameters for Richard's equation using the standard DSSAT model inputs, several steps were necessary, with each of these steps being performed for each soil layer.

First, the SMRC was derived using relationships reported by Saxton and Rawls (2006). Many equations have been proposed that relate soil water retention, soil texture, soil hydraulic properties, and other soil properties (Hillel, 1998; Rawls et al., 1992, Schaap & Leij, 2000). The Saxton and Rawls (2006) relationships were chosen due to their applicability to the DSSAT inputs, previous applications in agricultural hydrology (Caruso et al., 2013; Looper & Baxter, 2011; Shrestha et al., 2010), and reports of good performance compared to other methods (Gijsman et al., 2002), although the performance of various pedotransfer functions often varies strongly from site to site and thus performance conclusions are difficult outside of the locations at which they have been evaluated (Baroni et al., 2009). Following the Saxton and Rawls (2006) methodology, the tension at a particular moisture content $\psi(\theta)$ (cm water) was calculated as described by equation (2-12) for tensions between 1500 kPa and 33 kPa and equation (2-13) for tensions between 33 kPa and air entry pressure (ψ_e) (kPa),

where θ_{33} is the water content at a tension of 33 kPa (cm^3/cm^3), and θ_{1500} is the water content at a tension of 1500 kPa (cm^3/cm^3). The air entry pressure was calculated using relationships reported by Brooks and Corey (1966), and are described by equations (2-14) and (2-15), where λ is a fitting parameter, ψ_{DUL} is the tension at θ_{DUL}. ψ_{DUL} is assumed to be10 kPa for coarsely textured soils and 33 kPa for all other soils based on the recommendations of Cassel and Nielsen (1986). θ_r was estimated using the ratios of θ_r to θ_{LL} reported by Gowdish (2009) for 11 USDA textural classifications and the user inputted value of θ_{DUL}.

$$\psi(\theta) = 10.19716\left(e^{\ln(33)+\frac{\ln(1500)-\ln(33)}{\ln(\theta_{33})-\ln(\theta_{1500})}(\theta_{33})} \theta^{-\frac{\ln(1500)-\ln(33)}{\ln(\theta_{33})-\ln(\theta_{1500})}} \right) \tag{2-12}$$

$$\psi(\theta) = 10.19716\left(33 - \frac{(\theta-\theta_{33})(33-\psi_e)}{\theta_s-\theta_{33}} \right) \tag{2-13}$$

$$\psi_e = 1500\left(\frac{\theta_{LL}-\theta_r)}{\theta_s-\theta_r} \right)^{1/\lambda} \tag{2-14}$$

$$\lambda = \frac{\ln\left[(\theta-\theta_r)/(\theta_{LL}-\theta_r)\right]}{\ln(1500/\psi_{DUL})} \tag{2-15}$$

In order to extract the Van Genuchten parameters from the estimated SMRC, 38 points from the SMRC were computed and used as inputs for fitting the Van Genuchten parameters using the RETC code (Van Genuchten et al., 1991). The code uses Marquardt's maximum neighborhood method (Marquardt, 1963) to perform a non-linear least squares optimization to fit the retention data to the soil water function described by equation (2-9). Once the fitting process is completed for each soil layer, the estimation of the Van Genuchten parameters is complete.

Implementation within the DSSAT-CSM

To implement the soil-water movement calculations, the two-dimensional modeling space had to be discretized. It was decided that the modeling space would be split into a two-dimensional grid cell as depicted in Figure 2-1. The water balance assumes the water content to be uniform along the row length, and thus to only vary with distance perpendicular to the length of the row and depth. Additionally, due to symmetry only half of the bed is simulated because it is assumed that the other half will be a mirror. The model allows additional management capabilities, including the ability to input the depth and width of a raised bed, the option of applying plastic mulch to the bed, and the option of applying irrigation through drip tape with adjustable specifications. The model delineates the modeling space as either being within the raised bed, under the raised bed, within the furrow, or under the furrow. Cells are then created to fill the modeling space, with smaller cell sizes being used within the raised bed and at the soil surface. This method was implemented in order to ensure finer discretized cells were placed in locations where greater soil-water dynamics is expected, and coarser cells were placed in locations with less soil-water dynamics. The minimum cell size was 5 cm by 5 cm.

In order to operate the water balance, two-dimensional flux equations described by equations (2-5) and (2-6) had to be expressed in the context of the two-dimensional grid cell. Figure 2-2 depicts the cell layout, cell geometry, and flows necessary for updating the water balance to a new time step. Within this layout, the horizontal and vertical fluxes can be calculated as described by equations (2-16) and (2-17), where i is the cell row, j is the cell column, Δz is the cell height (cm), and Δx is the cell width (cm).

The horizontal ($H_{out(i,j)}$) and vertical ($V_{out(i,j)}$) flows can then be calculated as described by equations (2-18) and (2-19), where Δt is the time step (hours). The inflows are then related to the outflows as described by equations (2-20) and (2-21). No lateral flow is allowed across the center of the bed, the edge of the bed, or the edge of the furrow. Vertical flow is computed in the deepest soil layer by fixing $D(\theta)_{(i,j)}$ at zero, limiting deep percolation to gravitational flow at the limit of the soil extent. A special cell is the cell directly beneath the drip emitter. All drip irrigation water is input into this cell, which stores all applied irrigation until it flows out of the cell.

$$h_{out(i,j)} = \sqrt{D(\theta)_{(i,j)} D(\theta)_{(i,j+1)}} \frac{\theta_{(i,j)} - \theta_{(i,j+1)}}{\frac{\Delta x_{(i,j)} + \Delta x_{(i,j+1)}}{2}} \tag{2-16}$$

$$v_{out(i,j)} = \sqrt{D(\theta)_{(i,j)} D(\theta)_{(i+1,j)}} \frac{(\theta_{s(i,j)} - \theta_{r(i,j)}) + (\theta_{s(i+1,j)} - \theta_{r(i+1,j)})}{2} \frac{\Theta_{(i,j)} - \Theta_{(i+1,j)}}{\frac{\Delta z_{(i,j)} + \Delta z_{(i+1,j)}}{2}} +$$

$$\sqrt{K(\theta)_{(i,j)} K(\theta)_{(i+1,j)}} \tag{2-17}$$

$$H_{out(i,j)} = h_{out(i,j)} \Delta z_{(i,j)} \Delta t \tag{2-18}$$

$$V_{out(i,j)} = v_{out(i,j)} \Delta x_{(i,j)} \Delta t \tag{2-19}$$

$$H_{in(i,j+1)} = H_{out(i,j)} \tag{2-20}$$

$$V_{in(i+1,j)} = V_{out(i,j)} \tag{2-21}$$

The model operates on a variable time step, which is computed based on the dynamics within the system to assure stability and convergence. The minimum required time step is computed for each cell according to equation (2-22), and the overall minimum from all the cells is accepted as the required time step. Potential evaporation and transpiration demand are computed on a daily basis, using the original DSSAT

methodologies (Hoogenboom et al., 2009), with the daily demand being distributed across the day based on the distribution of solar radiation throughout a day. Actual evaporation depends on surface cover and water content. Actual root water uptake is limited by water content, root density, root distribution, and soil properties. Root growth is also computed on a daily basis according to standard DSSAT methodologies, with some adjustments to account for the added dimension. Root growth only occurs in the vertical direction in the first column. Once root growth in a row of the first column is fully penetrated with roots, horizontal growth begins to occur in that row. Root growth factors within the soil represent soil impacts on root growth, while horizontal and vertical root growth rates provided by the user adjust the crop's root development tendency. Daily rainfall infiltration is computed using the Soil Conservation Service runoff curve number method (United States Department of Agriculture, Soil Conservation Service, 1972). The daily infiltration is distributed across the day and evenly applied to non-mulched surface cells, with rainfall on mulched areas being routed to the furrowed area. At the end of each time step, the water content in each cell is updated, considering vertical and horizontal inflows and outflows, infiltration, and root water uptake.

$$\Delta t_{(i,j)} <= \frac{1}{\frac{2D(\theta)_{(i,j)}}{(\Delta z_{(i,j)})^2} + \frac{2D(\theta)_{(i,j)}}{(\Delta x_{(i,j)})^2} + \frac{10K(\theta)_{(i,j)}}{\Delta z_{(i,j)}}} \quad (2\text{-}22)$$

Summary

A two-dimensional water balance was added to the DSSAT-CSM by a group of DSSAT developers, using the Richards equation to drive soil-water flow and adapting the standard DSSAT methods for estimating evaporation, root water uptake, infiltration, and root growth within a two-dimensional framework. Additional management options

were added to DSSAT to allow the model to account for management practices common for vegetable production. An approximate form of the Richards equation was chosen in order to reduce the computational time required for model simulations. This increases the utility of the model for analyses which require large quantities of model runs, such as parameter estimation, uncertainty analysis, sensitivity analysis, large-scale GIS applications, and detailed simulation experiments. The model provides a detailed water balance model within the DSSAT modeling framework, allowing investigations of relationships between crop growth and development, soil-water dynamics, and management actions within these types of production systems.

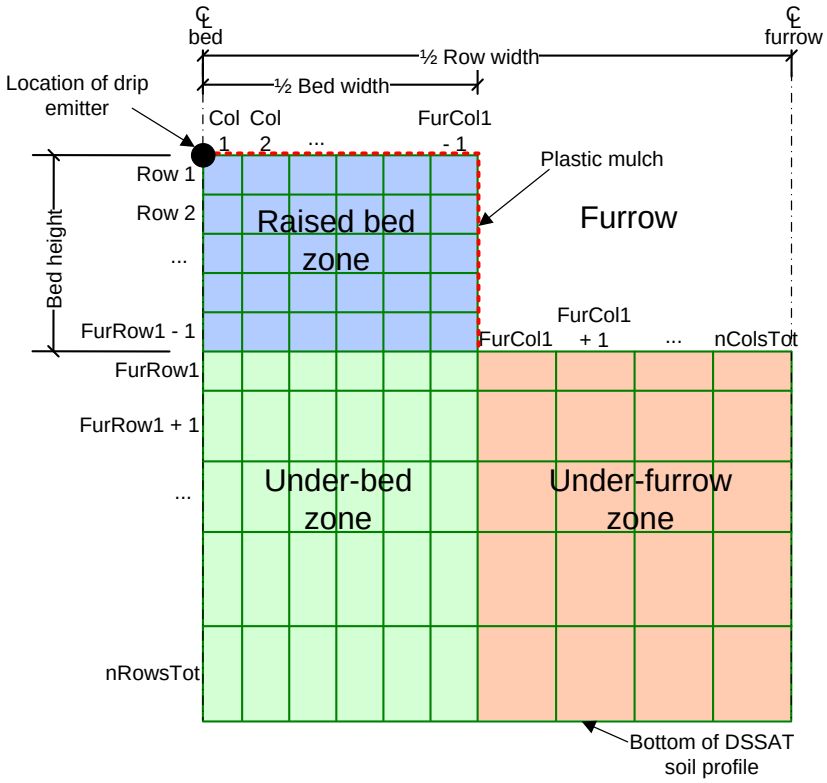

Figure 2-1. Cross section of half of a raised bed system as modeled by DSSAT-2D. Image created by and used with permission of Cheryl Porter.

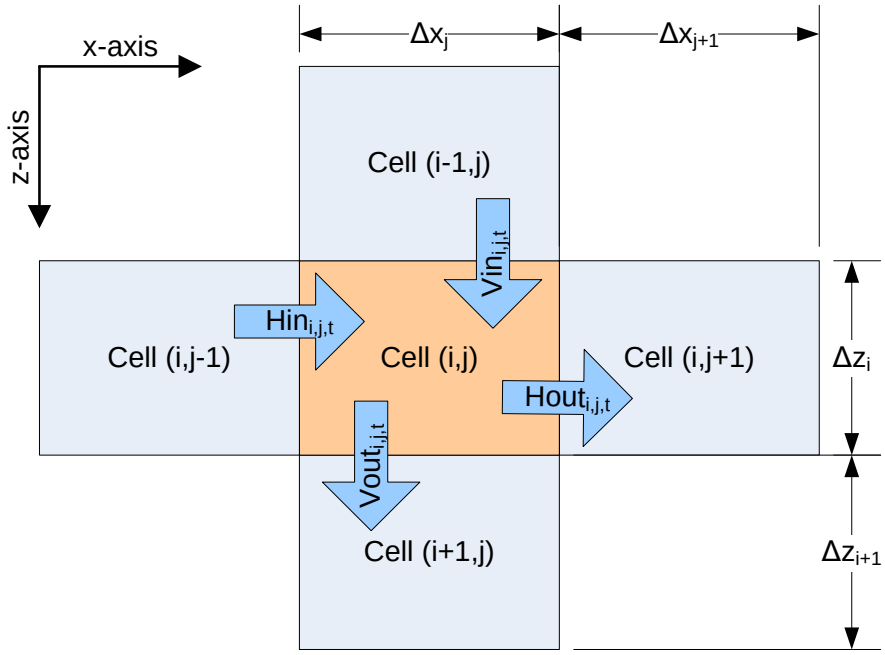

Figure 2-2. Definitions of the DSSAT-2D grid cell dimensions and layout. Image created by and used with permission of Cheryl Porter.

CHAPTER 3
EVALUATION OF A TWO-DIMENSIONAL WATER BALANCE WITHIN THE DSSAT-CSM

Background

As populations grow, water resources become increasingly limiting, and atmospheric GHG levels rise, there is increasing pressure for agriculture to produce food more efficiently and with less environmental effects. Thus it is important that tools and methods be developed that help the understanding of relationships between management actions, system drivers, production, and environmental loadings within these production systems. Crop models can be useful tools for understanding these relationships and interactions.

Vegetable production is an important industry in Florida, both economically and environmentally, in which a lot of efforts have been invested to improve production efficiency. However, there are currently no models available that can sufficiently simulate the soil-water dynamics and crop growth and development dynamics under the production practices typical of these production systems.

HYDRUS-2D is a commonly used software that can simulate soil-water dynamics under a wide range of boundary conditions, including those typical of Florida vegetable production systems. It has been shown to accurately predict soil-water flow under drip irrigation regimes (Provenzano, 2007; Roberts et al., 2009; Skaggs et al., 2004). However, HYDRUS-2D does not model crop growth or development. Thus HYDRUS-2D cannot be used to model interactions between management and crop growth and development. Additionally, HYDRUS-2D is computationally intensive, requiring considerable time to complete simulations, which limits its utility for analyses requiring large numbers of model runs.

The DSSAT-CSM (Hoogenboom et al., 2009) is a commonly used software that can simulate soil-plant-atmosphere interactions. Model runs are not computationally intensive, and it has been used in many regions and instances for addressing irrigation and fertilizer management strategies (Jones et al., 2003). However, it is limited in its ability to function under the management practices typical of these production systems.

Therefore the DSSAT-CSM was amended such that it could sufficiently characterize the soil-water dynamics occurring under management practices typical for Florida vegetable production. The modeling approach was more approximate compared to HYDRUS-2D in order to allow simple input requirements and shorter computational times. To this end, in comparison to HYDRUS-2D, the amended DSSAT-CSM operated with a coarser grid size, an approximate form of the Richards equation, and the option of calculating the necessary soil hydraulic parameters from only the standard DSSAT soil inputs.

However, this DSSAT-2D model requires evaluation to determine its ability to accurately characterize the soil-water dynamics of these systems. Thus, in order to evaluate the DSSAT-2D model, three approaches were used. First, the methodology for estimating the soil hydraulic parameters from the standard DSSAT inputs was evaluated. Second, the model was assessed through a benchmark comparison against HYDRUS-2D for different theoretical soil profiles. Finally, field experiments were conducted in order to evaluate the model's ability to predict the measured soil-water dynamics in a field setting.

Evaluation of the Parameterization Methodology

In order to evaluate the ability of the model to estimate the SMRC using only the standard DSSAT soil inputs, the three-point approximation methodology was evaluated against measured SMRC data from the Florida Soil Characterization Database (University of Florida Department of Soil and Water Science, 2012). Soil profiles were accepted from the database for the evaluation if they were a mineral soil, had SMRC measurements, had an average θ_{SAT} value greater than the average θ_{DUL} value, and had an average θ_{DUL} value greater than the average θ_{LL} value. The average measured θ_{SAT}, θ_{DUL}, and θ_{LL} values as well as the soil texture were used as inputs for the approximation procedure. θ_{DUL} was estimated by the volumetric water content (VWC) at a tension of 100 cm water for coarsely textured soils and the VWC at a tension of 345 cm water for all other soils. θ_{SAT} was estimated by the VWC at a tension of 3.5 cm water, and θ_{LL} was estimated by the VWC at a tension of 15295.7 cm water. The SMRCs in the database consisted of soil moisture measurements at tensions of 3.5, 20, 30, 45, 60, 80, 100, 150, 200, 345, and 15295.7 cm water. Thus, once the SMRC was estimated by the DSSAT approximation method for a soil sample, the predicted VWCs at the measured tensions were compared to the measured values to assess the prediction ability of the method. The calculated error metrics are listed in Table 3-1.

To further evaluate the DSSAT approximation methodology, a benchmark comparison was conducted, comparing the DSSAT approximation methodology to the commonly used hydraulic parameter estimation software RETC (Van Genuchten et al., 1991). The RETC software can fit a number of different parameter model types, but the Van Genuchten model was chosen with the common restriction of fixing m = 1 - 1/n because the parameter estimation process with this restriction has been shown to

perform better for most soils than with any of the other common restrictions (Van Genucthen et al., 1991). The RETC method uses Marquardt's maximum neighborhood method (Marquardt, 1963) to perform a non-linear least squares optimization to fit the retention data to the soil water retention function described by equation (2-9). Thus, the RETC method accepts all the SMRC data available, compared to the average values at the three soil tensions used by the DSSAT three-point approximation method. Once the model is fit, the predicted VWCs at the measured tensions from the database were compared to the measured values to assess the prediction ability of the method. The calculated error metrics are listed in Table 3-2.

Inspection of the error metrics in Tables 3-1 and 3-2 reveals a clear difference between the three-point DSSAT methodology and the RETC methodology, with the RETC methodology performing demonstrably better. This is to be expected, as the RETC approximation method has the advantage of utilizing a greater amount of input data for fitting the model to that data. Both methods have smaller prediction errors and better goodness-of-fit measures for the coarser soils, although the CVRMSE followed the inverse of this pattern, indicating some of this difference is due to the difference in magnitude of the VWC values among textures, which are higher in heavier textured soils and thus tend to increase error amounts. Figures 3-1 and 3-2 demonstrate that both methods are mostly unbiased, with the VWC prediction residuals approximately normally distributed with means very near zero. The figures also further confirm the shortcoming of the three-point DSSAT method, with the residuals having greater spread and thus greater magnitudes. Figures 3-3 and 3-4 show boxplots of the VWC prediction residuals at each soil tension for the two parameter estimation methods. These figures

explain the reason for the poorer prediction abilities of the three-point DSSAT method. While the RETC method demonstrated fairly consistent boxplots with medians near zero at all tensions, the DSSAT method demonstrates good predictions at tensions near the three input tensions of 0, 345, and 15295 cm water, but has VWC prediction residuals straying noticeably from zero at tensions distant from the inputted tensions. This confirms that the difference in model abilities stems from the inputs not being supplied over a sufficient range of tensions for the three-point DSSAT approximation method.

Benchmark Comparison of the Soil-Water Dynamics to HYDRUS-2D

In addition to the parameterization methodology evaluation, the two-dimensional DSSAT water balance model was further evaluated through a benchmark comparison with HYDRUS-2D (Simunek et al., 2006) soil-water dynamics simulations. HYDRUS-2D computes water flow using the Galerkin finite element method with linear basis functions to numerically solve the Richards equation for variably saturated flow. The modeling space is discretized into triangular and quadrilateral elements with nodes at each corner. Users can control the size of the elements, and are encouraged to use smaller elements in regions expected to have large hydraulic gradients. The element size is typically orders of magnitude smaller than the elements used in DSSAT-2D. HYDRUS-2D allows flexible boundary conditions and modeling space geometries, thus enabling it to be applied to typical vegetable production systems. For simulating half of a raised-bedded system, one notable difference between the HYDRUS-2D and DSSAT-2D approaches is that the shape of the surface drip flux boundary can be customized in HYDRUS-2D as a quarter circle of a specified radius, whereas DSSAT-2D applies water from the emitter to the element beneath the emitter, mixing the water uniformly to this element. Each time step evolves through an iterative process designed to keep the

absolute change in pressure head between iterations less than a small tolerance value. The length of each time step is bounded by minimum and maximum time limits and is a function of the number of iterations required to solve the previous time step.

Thus comparisons between DSSAT-2D and HYDRUS-2D can be used to understand the combined impacts of the Richards equation form, numerical solving technique, element size, element distribution, and drip-emitter boundary shape on soil-water dynamics. In order to compare the models, each model was run using different soil profiles to assess the relative model performance for differently textured uniform and layered soils. Analyses were conducted for four soil profiles consisting of two uniform soils and two layered soils. The uniform soils were a sand and a sandy clay textured soil chosen from the Florida Soil Characterization Database (University of Florida Department of Soil and Water Science, 2012) to represent a coarse and fine-textured soil. The two layered soils were combinations of the uniform soils, with one soil constituting the upper 20 cm and the other soil constituting the remainder of the soil profile. The hydraulic parameters characterizing these soil profiles are listed in Table 3-3. For uniform soils, the two forms of the Richards equation theoretically should essentially function equivalently for unsaturated flow, minimizing the importance of the equation form as a source of deviation between the models. The simulation space and boundary conditions were set up to be equivalent for the DSSAT-2D and HYDRUS-2D models, with the exception of the emitter boundary condition, with an 80 cm wide by 205 cm deep soil space. The 80 cm horizontal surface was set as a zero-flux boundary to represent a layer of impermeable plastic-mulch and to remove the effects of ET estimations from the model comparison. The 200 cm vertical edges were set as zero-

flux boundaries due to symmetry. The 80 cm horizontal bottom edge was set as free-drainage. For HYDRUS-2D, the drip-emitter flux boundary was represented by a quarter-circle with a 1 cm radius.

Since DSSAT-2D and HYDRUS-2D operate with different element sizes, shapes, and layouts, it is not possible to compare the model results directly. The grid layout for both models can be seen in Appendix A. Thus, for both models, the simulated VWC values from all the elements were interpolated onto a uniform grid via linear point kriging using Surfer (Golden Software Inc., 2011) software with a slope of one, anisotropy ratio of one, and anisotropy angle of zero. Contoured values were allowed to vary between 0.05 and 0.45 cm^3/cm^3 with an interval of 0.001 cm^3/cm^3. The grid was split such that there was a row and a column every two cm. Thus, the grid split the simulation space into 100 rows and 40 columns for the creation of a total of 4,000 points that were evenly spaced throughout the grid. In this manner, the points created from the DSSAT-2D and HYDRUS-2D simulations could be directly compared at each time step. However, since much of the soil will receive no changes in water content, the similarity between the models could be overestimated due to comparison of points in the simulation space that remain static during the entirety of the simulation period. To make a more informative comparison, the extent of the wetting front was calculated from each model. This was done by calculating the deepest grid node at each node distance from the row center that increased from its initial value by at least 0.001 cm^3/cm^3. The greatest depth at each distance calculated from the two models was used to determine the comparison points, such that if one model had a very different shape from the other model, the

union of the space of the two wetting fronts would be considered in the comparison calculations.

For each analysis, the soil was set to an initial soil tension of 336.5 cm water. Simulations were then conducted for a five-day period. Water was applied daily for four days, beginning at 1200 and being applied for 30 minutes at a rate of 1.617 $lh^{-1}m^{-1}$. For DSSAT-2D, this was expressed as a drip tape with an emitter spacing of 30.5 cm and an emitter rate of 0.1367 ml/s. For HYDRUS-2D, this was expressed as a line source represented by a quarter circle with a one cm radius and a flux rate of 123.34 cm/day. After the fourth irrigation event, the irrigation was cutoff for the remainder of the simulation period to allow soil-water redistribution.

To analyze the differences in soil-water dynamics between the two models, the simulated VWCs were compared at the nodes in the dynamic zone of the two models. The initial 12 hours were excluded from the comparison calculations because this was before the start of the first irrigation event and thus the soils were assumed to be at steady-state. Comparisons were made at a 15-minute temporal resolution from 0.5 days to 5 days. This temporal resolution and time period were chosen in order to capture the dynamics of the system, including the rapid changes near the drip tape during irrigation events and the slow changes over time during soil-water redistribution.

The overall results of the analyses for the four soils are listed in Table 3-4. For the Uniform 1 soil, the DSSAT-2D simulations were very similar to the HYDRUS-2D simulations. The RMSD between the two models was very small at 0.0010 cm^3/cm^3, and the correlation coefficient was very large at 0.985. The contour map in Figure 3-5 illustrates the two-dimensional model predictions at four different times, providing a

visual demonstration of the model similarity at each time. Analysis of the Uniform 2 soil, which is a heavier-textured soil, also indicates strong similarity between the two models with a very small RMSD of 0.0013 cm^3/cm^3, a very large correlation coefficient of 0.993, and visual similarity at four time steps as seen in Figure 3-6.

However, while the two models created very similar simulations for the uniform soils, a greater deviation was observed for the layered soils. For the Layered 1 soil with the DSSAT-2D model being driven by the normalized water-content, the RMSD was markedly higher at 0.0228 cm^3/cm^3 and the correlation coefficient was notably lower at 0.958. Visual observation of the two-dimensional VWC snapshots in Figure 3-7 revealed strong differences between the DSSAT-2D and HYDRUS-2D simulations. Primarily, the DSSAT-2D model failed to maintain the strong difference in VWC between the two layers that the HYDRUS-2D model predicted due to the sharp difference in soil properties. As such, the DSSAT-2D model predicted excessively high moisture in the sandy soil at the top of the profile and excessively low moisture in the clay soil in the remainder of the profile, especially near the interface of the two soils. This vertical movement of water was not associated with the drip irrigation events, but rather driven by the water content differential between the differently textured soils, which is why water movement was seen all the way out to 80 cm from the row center in the layered soils while neither of the uniform soils had movement beyond 59.5 cm from the row center.

For the Layered 1 soil with the DSSAT-2D model driven by the actual water-content, the deviations were greater than with the normalized water-content driven model. The RMSD rose to 0.0253 cm^3/cm^3, the correlation coefficient dropped to 0.947,

and the visual differences in Figure 3-7 were greater. Figure 3-7 again revealed a difficulty for the DSSAT-2D model to maintain the difference in VWC between the two layers, with an increased amount of vertical water flow that was not simulated by the HYDRUS-2D model. This behavior was even more pronounced for the actual water-content driven DSSAT-2D model than the normalized water-content driven DSSAT-2D model. The analysis of the Layered 2 soil was similar to the Layered 1 soil analysis, but with a greater agreeance with HYDRUS-2D. The normalized water-content driven DSSAT-2D model had a smaller RMSD of 0.0157 cm^3/cm^3, a greater coefficient of correlation of 0.975, and greater visual similarity in Figure 3-8. The actual water-content driven DSSAT-2D model had a greater RMSD of 0.0176 cm^3/cm^3, a smaller coefficient of correlation of 0.968, and less ability to maintain a VWC differential between the soil layers compared to the normalized water-content driven DSSAT-2D simulations in Figure 3-8.

In order to better understand the nature of the model differences, residuals were computed and plotted (Figure 3-9). The residual plots first demonstrate a clear deterioration in agreement between the HYDRUS-2D and DSSAT-2D VWC predictions for the layered soils. The prediction residuals are distributed much more closely to zero for the uniform soils than the layered soils. Further, this fit is much more consistent across VWC values. While the Uniform 1 soil does show some under-predictions at some of the higher VWC values, which is likely a function of the differences in grid sizes between the two models directly under the emitter during irrigation events, both uniform soils have similar distributions of residuals at all VWC values. Conversely, in all analyses the layered soils have much larger prediction differences, with consistent over-

predictions at lower water contents and consistent under-predictions at higher water contents. This trend is indicative of the DSSAT-2D model predicting flow of water from soil of high VWC to soil of low VWC at the interface of the differently textured soils, regardless of the orientation of the two layers, and is further indication of the inability of the water-content based form of the Richards equation to accurately predict soil-water dynamics for layered soils. The use of the normalized-water content as the system driver compared to the actual-water content resulted in some reduction in prediction residuals. However, the general pattern of erroneous flow predictions for sharply layered soils persisted despite this amendment.

Further, to analyze the differences between the models over time, the RMSD was calculated at each time step (Figure 3-10). It is first apparent that the RMSD values for the uniform soils are drastically smaller than for the layered soils. Further, for the uniform soils the model differences peak during irrigation application, likely due to the different emitter boundary conditions for the DSSAT-2D and the HYDRUS-2D models and the greater difference in grid size between the two models near the emitter. These differences then lessen during water redistribution as the soil-water distributions of the two models become increasingly similar. This indicates that the models are driving the soil-water dynamics to a similar steady-state if no further perturbations occur within the system. For the layered soils, however, the errors are the least at the beginning of the simulation, increasing during the simulation until the lack of dynamics in the system allows the error to remain at or near the maximum difference. For these layered soils, the system is largely insensitive to the irrigation events, as the error is being caused by the predicted water flow between the two layers. This is true for both the actual and

normalized water-content driven models, although the errors are greater for the actual water-content driven model. This is an indication that the DSSAT-2D model is consistently forcing the system to a different steady-state than the HYDRUS-2D model. It is also notable that while the DSSAT-2D model driven by the normalized-water content has less error compared to the actual-water content driven model, this difference is much more pronounced early in the simulation period. Later in the simulation period, the errors become increasingly similar. Thus, it appears that while driving the DSSAT-2D model with the normalized-water content is an improvement compared to using the actual-water content as the system driver, the improvement is the result of slowing the speed with which the erroneous water flow between the layers is predicted. Both methods, however, eventually result in a similar steady-state water distribution which fails to maintain the desired distinct difference in water content between layers. It is thus apparent that for sharply layered soils, the form of Richards equation used in the DSSAT-2D model forces considerably different soil-water flow predictions than the HYDRUS-2D model. While the use of the normalized water-content as the driver of flow in the DSSAT-2D model reduces these differences noticeably, the differences are still considerable.

Comparison of the Soil-Water Dynamics to Field Measurements

To further evaluate the model performance against field-measured data, a field experiment was conducted at the Plant Science Research and Education unit in Citra, FL. A plastic-mulched-raised bed was constructed with an 80 cm width and 20 cm height. Additional plastic was laid to extend 1.2 m from the edge of each side of the bed in order to reduce the impact of rainfall on the soil moisture pattern and thus better isolate the soil moisture dynamics to being controlled by the drip tape specifications and

irrigation management rather than ET and rainfall. The main drip tape specifications and irrigation management variables in the study were flow rate, emitter spacing, number of daily irrigation applications, and daily irrigation amount.

Different drip tapes were installed to obtain a variety of flow rates and emitter spacings, but within the restriction of drip tape availability. The six tapes selected for the experiment (Table 3-5) consist of three emitter spacings with two emitter rates at each spacing. There were two treatments for each drip tape, with one treatment applying the entire daily irrigation amount in one application starting at 1200, and the other applying the same daily irrigation amount in two split applications starting at 1000 and1400. Thus, the whole experiment consisted of 12 unique treatments. Following completion of the 12 treatments, half of the treatments were repeated.

Each of the first 12 treatments was conducted with four days of operation, followed by four days without irrigation. This was done to allow enough days of irrigation for the soil-moisture to adjust to a treatment, and enough non-irrigated days for the following treatment to begin at a similar soil-moisture state as the preceding treatment. Several of the repeated treatments were applied for additional days to allow for a longer model evaluation period.

Daily irrigation amounts were set at 5 mm, or 3.8 l/m per day. Thus, the duration of irrigation events were set such that each drip tape would apply this amount daily assuming application at the manufacturer specified flow rate. However, flow rates were measured in drip pans for each drip tape to more accurately estimate their flow rates under the experimental conditions. As such, the daily irrigation amounts varied between drip tapes. The experimental details for each treatment can be seen in Table 3-6. Water

use was measured using a DLJSJ50C water meter (Daniel L. Jerman Co., Hackensack, NJ) with a 1-gallon pulse output that was recorded using an H07-002-04 HOBO event logger (Onset Computer Corporation, Bourn, MA). Manual water meter readings were recorded with at least a weekly frequency, and manual readings were always taken at the start and end of a treatment.

Soil moisture was monitored by three sets of soil moisture probes installed at three distances along the row. The first set of probes were installed at the beginning of the experiment, with 12 CS616 (Campbell Scientific, Logan, UT) water content reflectometers installed at depths of 7.5, 22.5, 37.5, and 70 cm and at lateral distances from the row center of 0, 15, and 30 cm. The probe measurement rods were installed parallel to the row length, with an installed set of probes shown in Figure 3-11. The probe measurements were recorded every 15 minutes using a CR10X (Campbell Scientific, Logan, UT) datalogger, with the measured probe period average (PA; μs) converted to VWC by equation (3-1) (Campbell Scientific, 2011). This method is reported to provide accurate VWC conversions for mineral soils with bulk densities less than 1.55 g/cm^3, clay contents less than 30%, and bulk electrical conductivities less than 0.5 dS/m (Campbell Scientific, 2011). After each experimental treatment had been conducted once, two sets of 16 CS650 (Campbell Scientific, Logan, UT) water content reflectometer probes were installed, with each set being installed at different distances along the bed row. From each set of probes, 12 were installed at depths of 7.5, 22.5, 37.5, and 52.5 cm and lateral distances from the row center of 0, 15, and 30 cm. The remaining four probes from each set were installed at depths of 70 and 100 cm and at lateral distances from the row center of 0 and 15 cm. The probe measurements were

recorded every 15 minutes using a CR1000 (Campbell Scientific, Logan, UT) datalogger, with the measured bulk dielectric permittivity (K_a) converted to VWC via Topps equation (Topp, 1980), as shown in equation (3-2), which has been shown to work well in most mineral soils. Both the CS616 and CS650 probes have 30 cm measurement rods and a 7.5 cm sensing radius. A two-dimensional view of the 17 unique probe locations and approximate sensing volumes is shown in Figure 3-12.

$$VWC = -0.0663 - 0.0063(PA) + 0.0007(PA)^2 \quad (3\text{-}1)$$

$$VWC = -0.0663 - 0.0063(PA) + 0.0007(PA)^2 \quad (3\text{-}2)$$

In order to characterize the soil, several soil properties were measured. The soil was characterized as a Gainesville loamy sand (Soil Survey Staff, 2011). Bulk density measurements were taken at three different dates during the experiment at depths of 7.5, 22.5, 37.5, and 70 cm and lateral distances from the row center of 0, 15, and 30 cm. A total of 12 samples were collected for each unique sampling location with the exception of the 70 cm depth, for which only six samples were collected during the first sampling date since this depth was undisturbed by the bed formation process and thus not expected to change over time. Samples consisted of undisturbed soil cores of 5.4 cm diameter and 3 cm depth, with the bulk density determined according the field core method (Klute, 1986). The average bulk density from each measurement date and soil depth is shown in Figure 3-13. The average bulk density from all the measurements was 1.55 g/cm^3. Bulk density values remained fairly consistent over time, with an increase from the May 22 sampling at the 22.5 cm depth as the only marked temporal change. The 7.5 cm and 70 cm depth had nearly identical bulk densities that were

considerably less than the middle sampled depths. This is indicative of a plow pan layer somewhere above the 70 cm depth.

The particle density was determined by the Pycnometer method (Klute, 1986) using the May 22 samples, with four samples being used for each sampling depth. Results are shown in Table 3-7. The average particle density for all the samples was 2.63 g/cm^3. It was apparent that the particle density was very consistent at all the sampling depths.

The particle-size distribution was determined according to the USDA Soil Survey Lab Method (Soil Survey Staff, 2004) using four samples for each sampling depth from the May 22 sampling. Results are shown in Table 3-7. The overall average particle-size distribution consisted of 91.3 percent sand, 5.5 percent silt, and 3.2 percent clay. The particle-size distribution was also quite uniform with depth.

Finally, SMRCs and saturated hydraulic conductivities were determined using six samples from a 10 cm depth and five samples from a 45 cm depth taken on June 30. Soil samples were saturated with de-ionized water for 72 hours, then placed in Tempe cells (Soil Measurement Systems, Tucson, Arizona) that were connected to adjustable water columns for soil moisture determination at a range of pressures per Klute (1986). Moisture determinations were made at tensions of 10, 102, 183, 326, 571, 1019, 3220, 10190, and 15285 cm water. Samples were then re-saturated and the saturated hydraulic conductivities were determined according to Klute (1986). The geometric average of the saturated hydraulic conductivities was 25.4, 19.3, and 22.4 cm/hr for the 10 cm samples, 45 cm samples, and all samples, respectively, with average values of 26.1, 19.6, and 23.1 cm/hr. The results of the SMRC measurements are shown in

Figure 3-14. The average saturation water content, drained upper limit water content, and soil lower limit water content were 0.489, 0.172, and 0.058 cm^3/cm^3 for the 10 cm soil samples, 0.469, 0.170, and 0.060 cm^3/cm^3 for the 45 cm, and 0.480, 0.171, and 0.059 cm^3/cm^3 for all the samples.

Both the RETC and the three-point DSSAT parameter estimations methods were used to estimate the Van Genuchten parameters from the SMRCs. For the 10 cm samples, the RETC method estimated an α of 0.0274 cm^{-1}, an n of 2.17, and a θ_r of 0.062 cm^3/cm^3 while the three-point DSSAT method estimated an α of 0.0424 cm^{-1}, an n of 1.58, and a θ_r of 0.035 cm^3/cm^3. For the 45 cm samples, the RETC code estimated an α of 0.0235 cm^{-1}, an n of 2.38, and a θ_r of 0.061 cm^3/cm^3 while the three-point DSSAT method estimated an α of 0.0441 cm^{-1}, an n of 1.56, and a θ_r of 0.036 cm^3/cm^3. For all the samples, the RETC code estimated an α of 0.0258 cm^{-1}, an n of 2.25, and a θ_r of 0.062 cm^3/cm^3 while the three-point DSSAT method estimated an α of 0.0432 cm^{-1}, an n of 1.57, and a θ_r of 0.036 cm^3/cm^3. The DSSAT-2D model was run for each treatment using parameter estimates from each of the parameter estimation methodologies. The Van Genuchten parameters and the saturated hydraulic conductivity in the first 20 cm of the soil profile were set in the DSSAT soil file to be equal to the values estimated from the 10 cm samples. The parameters in the DSSAT soil profile from 20 to 35 cm depths were set based on the values estimated from all the samples, as this was in between the 10 and 45 cm sampling depths. Finally, the parameters in the DSSAT soil profile from 35 cm to the bottom of the profile were set based on the values estimated from the 45 cm samples.

To initialize the model for each treatment, the soil water content was initialized based on the measured probe values at the beginning of the day before the first irrigation event. This allowed the model to be given an accurate representation of the actual initial conditions in the soil as well as time for the model to settle before beginning model evaluation. Since the initial water content was set based on the probe measurements, it had to be set considering the 12 unique probe locations for the first 12 treatments and based on the 17 unique probe locations for the repeated treatments. In both cases, a grid within the soil with horizontal bounds that fall entirely within 7.5 cm horizontally from a probe column will have their initial VWC determined by a probe in that column only. Alternatively, if the horizontal bounds of a soil grid fall within 7.5 cm horizontally from two probe columns, its initial VWC will be determined by an average of probes from the two probe columns. Vertically, if a soil grid has its upper vertical extent above the line 7.5 cm vertically below a row of probes, it will have its initial VWC determined by the highest row of probes for which that is true. If, however, the highest vertical extent of a soil grid falls more than 7.5 cm below the deepest row of probes, the initial VWC will be determined by the deepest set of probes available.

Weather data was obtained from the Florida Automated Weather Network for the Citra location. The data was formatted and units were converted for use within the DSSAT-CSM. In order to account for the effect of the rain shelter, the recorded rainfall was changed to zero. The weather, however, was quite un-impactful on the probe measurements, as the plastic minimized the effects that rainfall or potential ET would have on the soil-moisture regime.

For each treatment, the model was evaluated against the 15-minute probe measurements from the beginning of the day of the first irrigation until the end of the day after the last irrigation. This was done in order to evaluate the model while the system was dynamic, including the days with irrigation as well as a day of soil-water redistribution with no irrigation events. During the experiment, there were several occasions where probe errors occurred or conditions existed which made the probe data erroneous. These issues were caused due to probe exposure, elevated salinity, and rainfall infiltration through the rain shelter. The probe exposure always occurred with the probe directly beneath the drip emitter, as the high flows and shallow probe placement resulted in inadequate soil coverage once enough soil was washed away. As soon as a probe was thought to be exposed, the plastic was removed to inspect, and additional soil was added and attempted to be packed to a representative density. Elevated salinity also only occurred in the probe directly beneath the emitter, because for some of the treatments solute was injected through the drip tape, and it had the highest concentration right after injection directly beneath the tape. At elevated electrical conductivity, the CS650 probes will not return VWC values. The CS616 probes, however, cannot measure the electrical conductivity and thus return erroneously elevated VWC values at high salinity levels. Measurements were no longer considered erroneous once irrigation commenced the following day, as the salinity was flushed from the system and readings returned to the expected levels. When rainfall infiltrated the rain shelter, the matrices that were affected were removed from the evaluation for the remainder of that treatment to allow time for the levels to return to normal. Probes which were not included in the evaluation for each treatment are shown in Table 3-6.

The evaluation was conducted by comparing the average probe measurements to the predicted probe measurements. However, since DSSAT-2D breaks the soil into rectangular grids of uniform VWC, the gridded DSSAT-2D VWC distribution had to be converted into a VWC value representative of the probe sensing area. Thus, a program was written to compute the percentage of the probe sensing area that intersected with each grid rectangle. This code can be seen in Appendix B. These percentages were then used to weigh the intersected grid VWCs in order to obtain an estimated probe VWC. These calculations were computed in R (R Development Core Team, 2011), using the gpclib package to compute the intersection areas, and were used as weights for estimating a probe VWC. These weights and grid cell locations were read into DSSAT-2D at the beginning of a simulation and used to calculate the probe VWC at each time step. This was conducted for each of the unique probe locations, which are shown in Figure 3-12.

The overall results of the model evaluation, using the average probe measurements at each probe location for comparison, are shown in Table 3-8. Error metrics are different for the first repetition of treatments compared to the additional repetitions in part due to the installation of additional probes and at additional measurement locations. Considering all the treatments, the model performs fairly well, with RMSE values of 0.0290 and 0.0248 cm^3/cm^3 and correlation coefficients of 0.590 and 0.567 for the simulations using the three-point DSSAT estimation method and the RETC estimation method, respectively. For both parameter estimation techniques, the model made more accurate simulations for the repeat treatments. Using the three-point DSSAT parameter estimation method, the model had RMSE values of 0.0305 and

0.0280 cm^3/cm^3 for the first repetition treatments and repeated treatments, respectively. Similarly, with the RETC estimated parameters, the model had RMSE values of 0.0267 and 0.0235 cm^3/cm^3 for the first repetition treatments and repeated treatments, respectively.

The repeated treatments may be more representative due to the increased number of measurement probes allowing the characteristic response to be better approximated. Further, the additional probes allowed for estimation of the uncertainty in the VWC measurements at each probe location. Using this information, it is possible to calculate uncertainty adjusted metrics. Thus, 95 percent confidence intervals were computed for the VWC at each time step and for each probe location. Then error was assumed to be zero if the predicted value fell within this uncertainty range, and as the difference from the nearest outer bound of the uncertainty range if the predicted value falls outside. The results of this analysis (Table 3-9) yielded reduced error evaluations. Using the three-point DSSAT parameter estimation method, the model predicted VWCs with an RMSE of 0.0212 cm^3/cm^3 and a correlation coefficient of 0.787. With the RETC estimated parameters, the model predicted VWCs with an RMSE of 0.0150 cm^3/cm^3 and a correlation coefficient of 0.775.

The evaluation metrics for individual treatments using the average probe measurements (Table 3-10) reveal the range of prediction error for the different treatments. For the three-point DSSAT estimated parameters, the RMSE ranged from 0.0220 to 0.0378 cm^3/cm^3, the correlation coefficient ranged from 0.286 to 0.661, and the Nash-Sutcliffe model efficiency coefficient ranged from -0.287 to 0.587. For the RETC estimated parameters, the RMSE ranged from 0.0209 to 0.0302 cm^3/cm^3, the

correlation coefficient ranged from 0.213 to 0.631, and the Nash-Sutcliffe model efficiency coefficient ranged from 0.371 to 0.623. While the model appeared to perform reasonably well and robustly across all the treatments, there was a noticeable range in model performance. Two of the treatments that were simulated using the three-point DSSAT parameter estimation method made predictions with a negative valued Nash-Sutcliffe coefficient, which indicates average predictions would have better predicted the soil-water dynamics than the model predictions. Uncertainty adjusted evaluation metrics were also computed for the individual treatments (Table 3-11). These are again based on the 95 percent confidence interval VWC at each time step for each probe location, and thus are only computed for the repeated treatments which had the additional probe installations. For the three-point DSSAT estimated parameters, the RMSE ranged from 0.0145 to 0.0271 cm^3/cm^3, the correlation coefficient ranged from 0.712 to 0.855, and the Nash-Sutcliffe model efficiency coefficient ranged from 0.504 to 0.748. For the RETC estimated parameters, the RMSE ranged from 0.0099 to 0.0142 cm^3/cm^3, the correlation coefficient ranged from 0.749 to 0.850, and the Nash-Sutcliffe model efficiency coefficient ranged from 0.683 to 0.829. The comparison of the model predictions to the probe measurements for each of the treatments can be visualized in Figure C-1 and Figure C-2 for the three-point DSSAT estimated parameters and the RETC estimated parameters, respectively. In general, the model predictions appear to respond similarly to the probe measurements, having the appropriate response to changes in flow rate, irrigation durations, and application splitting. It is notable, however, that the model does consistently over-predict the VWC values at the three measurement locations at the 7.5 cm depth. There were no noticeable patterns of

model prediction error relating to the emitter spacing, flow rate, application splitting, or daily irrigation amount, which varied between the treatments. Thus, field evaluations of the DSSAT-2D model indicate the model as robust in its ability to adequately simulate the soil-water dynamics under various drip irrigation regimes.

Summary

The amended DSSAT model was evaluated to provide some assessment of its ability to accurately characterize the soil-water dynamics of these systems. First, the methodology for estimating the soil hydraulic parameters from the standard DSSAT inputs was evaluated. The model was then evaluated against the HYDRUS-2D model for four hypothetical soil profiles. Finally, a field experiment was conducted in order to evaluate the model's prediction ability in a field setting.

The DSSAT three-point soil parameter estimation method was evaluated against 4447 SMRCs from soil profiles in a Florida soil database. Analyses revealed that the SMRCs were estimated fairly well by this method, although with notable error. Further, the method seemed to perform better for estimating coarser soils than for heavier textured soils. Overall, however, VWC prediction residuals were normally distributed with a mean near zero and the model bias was very near zero, indicating the methodology was functioning properly. The estimation methodology was further evaluated against the RETC estimation methodology, which is a commonly used method for estimating soil hydraulic parameters and can thus be used as a benchmark for model comparison. The RETC method showed a similar trend to the DSSAT approximation method in predicting the coarser soils more accurately than the more finely textured soils, indicating that some of this error is due to inherent sampling uncertainty. However, the RETC method predicted the SMRCs with notably improved

accuracy, which is to be expected since the methodology used all the available data rather than the limited data used for the approximate DSSAT method. It is thus concluded that the approximate DSSAT method is a functional solution for widening the model applicability for scenarios where the soil hydraulic parameters have not been well characterized. However, this comes at the cost of reduced model representation of the soil properties. Thus, it is recommended to use more detailed soil hydraulic measurements when possible.

Next, the DSSAT-2D soil-water flow calculations were evaluated against the HYDRUS-2D model to allow evaluation of the model performance under specific theoretical soil profiles. The two models produced very similar simulations for uniformly coarsely textured and uniformly finely textured soils under drip irrigation. This indicates that the grid-design and numerical solving technique used in DSSAT-2D perform comparably to those of HYDRUS-2D. However, the model simulations diverged notably for layered soils, with significantly higher error metrics and divergence between models that grew largely monotonically with simulation time. This indicates that the approximate form of the Richards equation used in the DSSAT-2D model results in questionable soil-flow predictions for sharply layered soils. The analysis also demonstrated that driving the DSSAT-2D model by the normalized water content rather than the actual water content reduced the deviations from the HYDRUS-2D model, although the deviations were still considerable. Further, the improvements appeared to be the result of the adjustment slowing the development of the deviations, not eliminating them.

The DSSAT-2D soil-water flow calculations were further evaluated through comparison with field-measured soil-moisture data. The soil was fairly uniform, with

largely uniform texture and some deviation with depth in hydraulic conductivity and soil-water retention likely due to structural compaction. The model demonstrated the ability to simulate the soil-water flow patterns fairly adeptly under different drip irrigation management regimes and drip tape specifications. Additionally, simulations using the three-point DSSAT soil hydraulic parameter estimation method were able to provide representative simulations, but with error notably greater than simulations with the soil hydraulic parameters estimated by the RETC method.

Table 3-1. Error metrics for predicting SMRCs using the three-point DSSAT methodology. SMRCs are from the Florida Soil Characterization Database.

Texture	Samples	RMSE (cm^3/cm^3)	CVRMSE (cm^3/cm^3)	Ceff	R^2	Bias (cm^3/cm^3)
Fine sand	2319	0.0393	0.1959	0.923	0.889	0.00355
Sand	1072	0.0528	0.3274	0.820	0.857	0.02218
Sandy loam	419	0.0576	0.2044	0.705	0.842	-0.03487
Sandy clay	532	0.0463	0.1375	0.673	0.731	0.00233
Clay	105	0.0619	0.1339	0.501	0.630	-0.00900
All	4447	0.0458	0.2090	0.899	0.900	0.00517

Table 3-2. Error metrics for predicting SMRCs using the RETC methodology. SMRCs are from the Florida Soil Characterization Database.

Texture	Samples	RMSE (cm^3/cm^3)	CVRMSE (cm^3/cm^3)	Ceff	R^2	Bias (cm^3/cm^3)
Fine sand	2319	0.0275	0.1369	0.962	0.967	-0.00952
Sand	1072	0.0244	0.1515	0.962	0.964	-0.00674
Sandy loam	419	0.0330	0.1171	0.903	0.904	-0.00109
Sandy clay	532	0.0298	0.0885	0.864	0.866	-0.00044
Clay	105	0.0354	0.0767	0.836	0.838	0.00232
All	4447	0.0277	0.1262	0.963	0.966	-0.00686

Table 3-3. Soil hydraulic parameters for the benchmark comparison of DSSAT-2D with HYDRUS-2D.

Analysis ID	Layer	Depth (cm)	Texture	K_s (cm/hr)	θ_r (cm^3/cm^3)	θ_s (cm^3/cm^3)	α (cm^{-1})	n
Uniform 1	1	0-200	Sand	7.7	0.050	0.360	0.024	2.123
Uniform 2	1	0-200	Sandy clay	1.7	0.163	0.426	0.052	1.270
Layered 1	1	0-20	Sand	7.7	0.050	0.360	0.024	2.123
Layered 1	2	20-200	Sandy clay	1.7	0.163	0.426	0.052	1.270
Layered 2	1	0-20	Sandy clay	1.7	0.163	0.426	0.052	1.270
Layered 2	2	20-200	Sand	7.7	0.050	0.360	0.024	2.123

Table 3-4. Difference metrics and closeness-of-fit measures between VWC predictions by DSSAT-2D and HYDRUS-2D.

Analysis ID	Water-Content Form	RMSE (cm^3/cm^3)	CVRMSE (cm^3/cm^3)	Ceff	R^2	Bias (cm^3/cm^3)	X_{max} (cm)	Z_{max} (cm)
Uniform 1	Normalized	0.0010	0.0124	0.982	0.985	0.00007	59.5	72.7
Uniform 2	Normalized	0.0013	0.0044	0.993	0.993	0.00012	43.1	48.5
Layered 1	Normalized	0.0228	0.1413	0.944	0.958	0.00150	80.0	46.5
Layered 1	Actual	0.0253	0.1507	0.932	0.947	0.00039	80.0	46.5
Layered 2	Normalized	0.0157	0.1123	0.972	0.975	-0.00059	80.0	78.8
Layered 2	Actual	0.0176	0.1262	0.965	0.968	-0.00058	80.0	78.8

Table 3-5. Drip tape manufacturer specifications.

Emitter Spacing (cm)	Flow Rate Level (High (H) or Low (L))	Emitter Rate (ml/s)
30.5	H	0.3155
30.5	L	0.1367
20.3	H	0.2804
20.3	L	0.1402
10.2	H	0.2804
10.2	L	0.1402

Table 3-6. Field experiment treatment details.

Treatment Spacing (cm) - Rate (H/L) - Splits	Emitter Spacing (cm)	Pan Measured Emitter Rate (ml/s)	Pan Measured Irrigation Amount (l/m/day)	Missing Matrix 1 Probes	Missing Matrix 2 Probes	Missing Matrix 3 Probes
30-H-1	30.5	0.3354	4.03	None	All	All
30-H-2	30.5	0.3354	4.09	None	All	All
30-L-1	30.5	0.1819	5.01	None	All	All
30-L-2	30.5	0.1819	5.01	None	All	All
20-H-1	20.3	0.3537	4.80	None	All	All
20-H-2	20.3	0.3537	4.80	None	All	All
10-H-2	10.2	0.3070	3.99	Probe 1* (all days)	All	All
10-H-1	10.2	0.3070	3.99	Probe 1* (all days)	All	All
20-L-1	20.3	0.1828	4.86	None	All	All
20-L-2	20.3	0.1828	4.86	None	All	All
10-L-2	10.2	0.1368	3.72	None	All	All
10-L-1	10.2	0.1368	3.72	None	All	All
10-H-1 Rep 2	10.2	0.2944	3.82	None	None	None
10-H-2 Rep 2	10.2	0.2944	3.82	None	None	None
10-H-2 Rep 3	10.2	0.2944	3.82	None	None	None
10-H-1 Rep 3	10.2	0.2944	3.82	Probe 1* (all days)	None	None
30-L-1 Rep 2	30.5	0.1917	5.28	Probe 1* (all days)	None	None
30-L-2 Rep 2	30.5	0.1917	5.28	Probe 1* (1 day)	All (2 days)	None
30-L-1 Rep 3	30.5	0.1917	5.28	Probe 1* (1 day)	All	None
30-L-2 Rep 3	30.5	0.1917	5.28	Probe 1* (1 day)	All	None
20-H-2 Rep 2	20.3	0.3278	4.45	Probe 1* (1 day)	None	None
20-H-1 Rep 2	20.3	0.3278	4.45	Probe 1* (1 day)	None	None

*Probe 1 is the probe inserted at a distance of 0 cm from the row center and a depth of 7.5 cm .

Table 3-7. Soil particle size, bulk density, and particle density averages by soil depth. Samples taken for the field experiment.

Depth (cm)	Sand (%)	Silt (%)	Clay (%)	Bulk density (g/cm^3)	Particle density (g/cm^3)
7.5	91.9	5.3	2.8	1.47	2.62
22.5	92.0	5.0	3.0	1.60	2.62
37.5	91.1	6.3	2.6	1.58	2.63
70.0	90.4	5.4	4.2	1.48	2.64

Table 3-8. Overall DSSAT-2D error metrics from the average probe measurements.

Treatments	Parameter Estimation Method	RMSE (cm^3/cm^3)	CVRMSE (cm^3/cm^3)	Ceff	R^2	Bias (cm^3/cm^3)
All	Three-point DSSAT	0.0290	0.2209	0.350	0.590	0.01240
Repetition 1	Three-point DSSAT	0.0305	0.2235	0.269	0.518	0.01314
Repeat	Three-point DSSAT	0.0280	0.2189	0.386	0.626	0.01193
All	RETC	0.0248	0.1888	0.525	0.567	0.00729
Repetition 1	RETC	0.0267	0.1954	0.442	0.504	0.00855
Repeat	RETC	0.0235	0.1838	0.567	0.600	0.00650

Table 3-9. Overall DSSAT-2D adjusted error metrics from the average probe measurements.

Treatments	Parameter Estimation Method	$RMSE_{adj}$ (cm^3/cm^3)	$CVRMSE_{adj}$ (cm^3/cm^3)	$Ceff_{adj}$	R^2_{adj}	$Bias_{adj}$ (cm^3/cm^3)
Repeat	Three-point DSSAT	0.0212	0.1622	0.627	0.787	0.00927
Repeat	RETC	0.0150	0.1162	0.730	0.775	0.00580

Table 3-10. DSSAT-2D error metrics from the average probe measurements for each treatment.

Treatment Spacing (cm) - Rate (H/L) - Splits	Parameter Estimation Method	RMSE (cm^3/cm^3)	CVRMSE (cm^3/cm^3)	R^2	Ceff	Bias (cm^3/cm^3)
30-H-1	Three-point DSSAT	0.0267	0.2018	0.435	0.331	0.01060
30-H-2	Three-point DSSAT	0.0262	0.1933	0.416	0.402	0.01180
30-L-1	Three-point DSSAT	0.0335	0.2490	0.404	-0.019	0.01880
30-L-2	Three-point DSSAT	0.0319	0.2430	0.445	0.012	0.01960
20-H-1	Three-point DSSAT	0.0324	0.2438	0.395	0.056	0.01780
20-H-2	Three-point DSSAT	0.0306	0.2266	0.418	0.221	0.01530
10-H-2	Three-point DSSAT	0.0254	0.1911	0.341	0.495	0.00820
10-H-1	Three-point DSSAT	0.0271	0.2045	0.326	0.436	0.01100
20-L-1	Three-point DSSAT	0.0337	0.2342	0.286	0.114	0.00790
20-L-2	Three-point DSSAT	0.0337	0.2312	0.310	0.236	0.01150
10-L-2	Three-point DSSAT	0.0309	0.2151	0.341	0.389	0.01020
10-L-1	Three-point DSSAT	0.0317	0.2308	0.346	0.307	0.01440
10-H-2 Rep 2	Three-point DSSAT	0.0232	0.1926	0.629	0.544	0.00590
10-H-2 Rep 3	Three-point DSSAT	0.0247	0.2028	0.596	0.459	0.00790
10-H-1 Rep 2	Three-point DSSAT	0.0220	0.1924	0.653	0.580	0.00510
10-H-1 Rep 3	Three-point DSSAT	0.0221	0.1790	0.652	0.587	0.00570
30-L-1 Rep 2	Three-point DSSAT	0.0260	0.2040	0.638	0.461	0.00890
30-L-1 Rep 3	Three-point DSSAT	0.0319	0.2459	0.614	0.025	0.01850
30-L-2 Rep 2	Three-point DSSAT	0.0265	0.2046	0.629	0.434	0.00990
30-L-2 Rep 3	Three-point DSSAT	0.0378	0.2786	0.585	-0.287	0.02380
20-H-1 Rep 2	Three-point DSSAT	0.0257	0.1966	0.661	0.545	0.01080
20-H-2 Rep 2	Three-point DSSAT	0.0263	0.1983	0.648	0.546	0.01050
30-H-1	RETC	0.0224	0.1696	0.330	0.527	0.00690
30-H-2	RETC	0.0243	0.1793	0.305	0.485	0.00770
30-L-1	RETC	0.0262	0.1947	0.306	0.377	0.01320
30-L-2	RETC	0.0250	0.1901	0.334	0.395	0.01400
20-H-1	RETC	0.0260	0.1961	0.299	0.389	0.01220
20-H-2	RETC	0.0250	0.1849	0.319	0.481	0.00980
10-H-2	RETC	0.0250	0.1884	0.249	0.509	0.00590
10-H-1	RETC	0.0270	0.2037	0.225	0.440	0.00850
20-L-1	RETC	0.0281	0.1956	0.213	0.382	0.00280
20-L-2	RETC	0.0294	0.2016	0.229	0.419	0.00550
10-L-2	RETC	0.0300	0.2091	0.228	0.422	0.00560
10-L-1	RETC	0.0302	0.2197	0.227	0.371	0.01010
10-H-2 Rep 2	RETC	0.0220	0.1825	0.600	0.591	0.00320
10-H-2 Rep 3	RETC	0.0226	0.1851	0.570	0.550	0.00490
10-H-1 Rep 2	RETC	0.0209	0.1822	0.631	0.623	0.00290
10-H-1 Rep 3	RETC	0.0216	0.1746	0.619	0.607	0.00260
30-L-1 Rep 2	RETC	0.0225	0.1765	0.615	0.596	0.00480

Table 3-10. Continued

Treatment Spacing (cm) -Rate (H/L) – Splits	Parameter Estimation Method	RMSE (cm3/cm3)	CVRMSE (cm3/cm3)	R2	Ceff	Bias (cm3/cm3)
30-L-1 Rep 3	RETC	0.0245	0.1886	0.570	0.427	0.01210
30-L-2 Rep 2	RETC	0.0224	0.1730	0.620	0.595	0.00550
30-L-2 Rep 3	RETC	0.0254	0.1869	0.562	0.421	0.01250
20-H-1 Rep 2	RETC	0.0245	0.1876	0.617	0.585	0.00580
20-H-2 Rep 2	RETC	0.0254	0.1915	0.612	0.577	0.00530

Table 3-11. DSSAT-2D adjusted error metrics from the average probe measurements for each treatment.

Treatment	Parameter Estimation Method	$RMSE_{adj}$ (cm^3/cm^3)	$CVRMSE_{adj}$ (cm^3/cm^3)	R^2_{adj}	$Ceff_{adj}$	$Bias_{adj}$ (cm^3/cm^3)
10-H-2 Rep 2	Three-point DSSAT	0.0162	0.1340	0.818	0.695	0.00550
10-H-2 Rep 3	Three-point DSSAT	0.0168	0.1354	0.816	0.674	0.00620
10-H-1 Rep 2	Three-point DSSAT	0.0157	0.1379	0.840	0.684	0.00560
10-H-1 Rep 3	Three-point DSSAT	0.0145	0.1172	0.855	0.748	0.00550
30-L-1 Rep 2	Three-point DSSAT	0.0190	0.1472	0.820	0.664	0.00740
30-L-1 Rep 3	Three-point DSSAT	0.0236	0.1700	0.733	0.531	0.00940
30-L-2 Rep 2	Three-point DSSAT	0.0190	0.1438	0.814	0.668	0.00740
30-L-2 Rep 3	Three-point DSSAT	0.0271	0.1839	0.712	0.504	0.01190
20-H-1 Rep 2	Three-point DSSAT	0.0176	0.1305	0.829	0.735	0.00680
20-H-2 Rep 2	Three-point DSSAT	0.0175	0.1280	0.827	0.739	0.00660
10-H-2 Rep 2	RETC	0.0114	0.0945	0.819	0.791	0.00260
10-H-2 Rep 3	RETC	0.0117	0.0940	0.805	0.774	0.00290
10-H-1 Rep 2	RETC	0.0107	0.0936	0.840	0.808	0.00250
10-H-1 Rep 3	RETC	0.0099	0.0798	0.850	0.829	0.00240
30-L-1 Rep 2	RETC	0.0118	0.0916	0.832	0.802	0.00300
30-L-1 Rep 3	RETC	0.0137	0.1001	0.759	0.683	0.00470
30-L-2 Rep 2	RETC	0.0118	0.0897	0.823	0.798	0.00290
30-L-2 Rep 3	RETC	0.0142	0.0989	0.749	0.688	0.00480
20-H-1 Rep 2	RETC	0.0124	0.0932	0.800	0.786	0.00280
20-H-2 Rep 2	RETC	0.0130	0.0960	0.785	0.777	0.00240

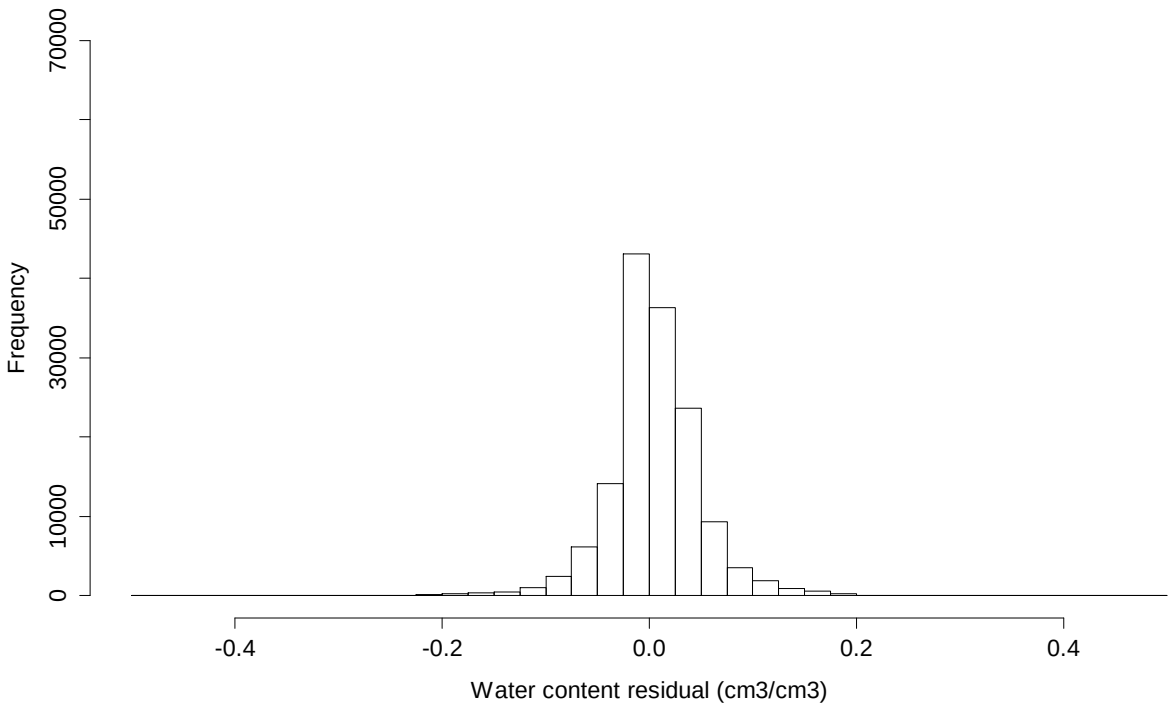

Figure 3-1. Distribution of VWC prediction residuals using the three-point DSSAT methodology. Residuals are derived from predictions of the SMRCs from the Florida Soil Characterization Database.

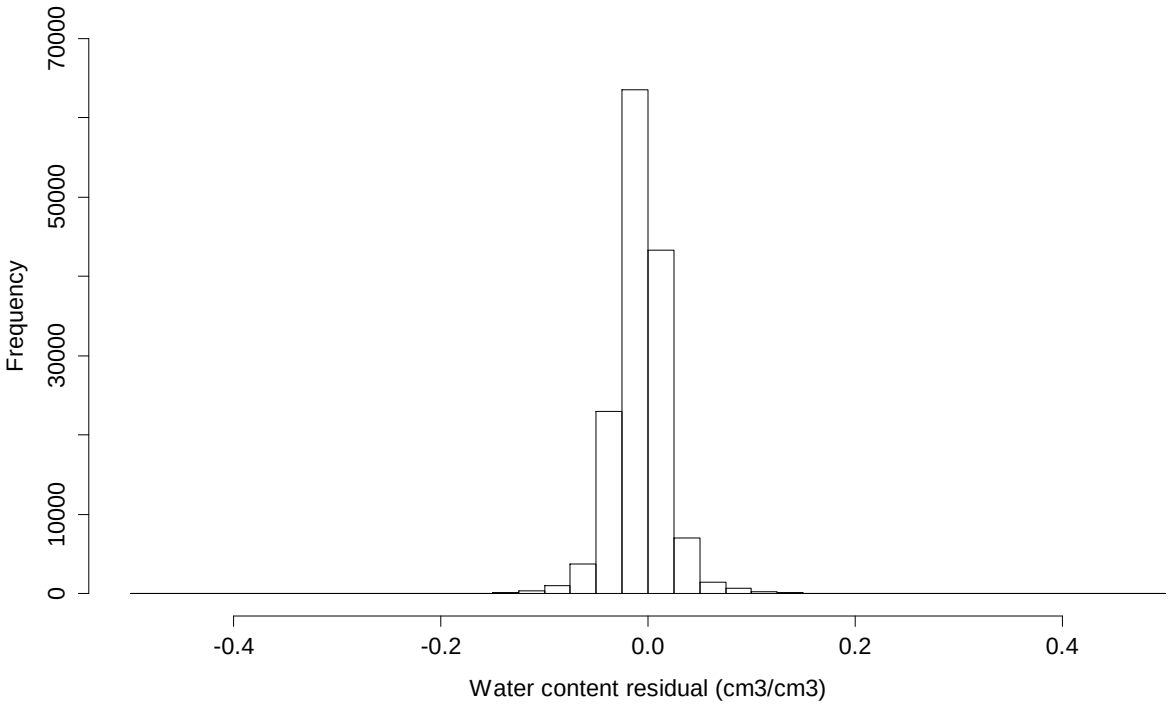

Figure 3-2. Distribution of VWC prediction residuals using the RETC methodology. Residuals are derived from predictions of the SMRCs from the Florida Soil Characterization Database.

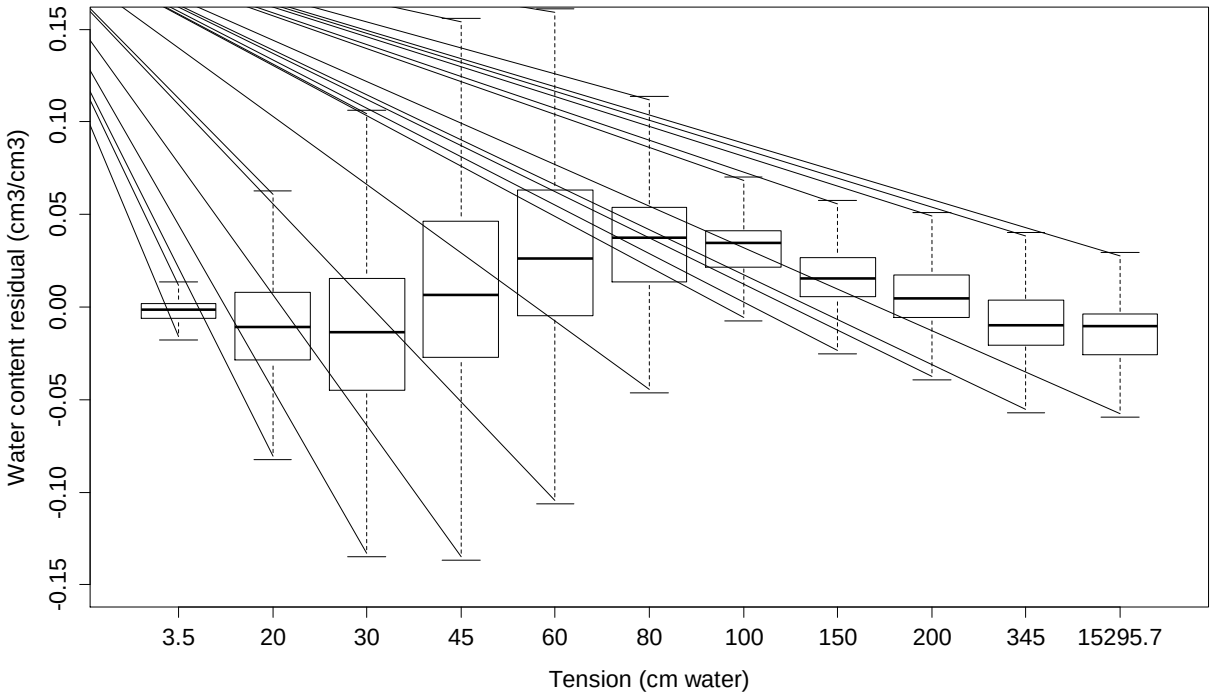

Figure 3-3. Boxplot of VWC prediction residuals vs. tension using the three-point DSSAT methodology. Residuals are derived from predicting SMRCs from the Florida Soil Characterization Database. The horizontal axis is not to scale.

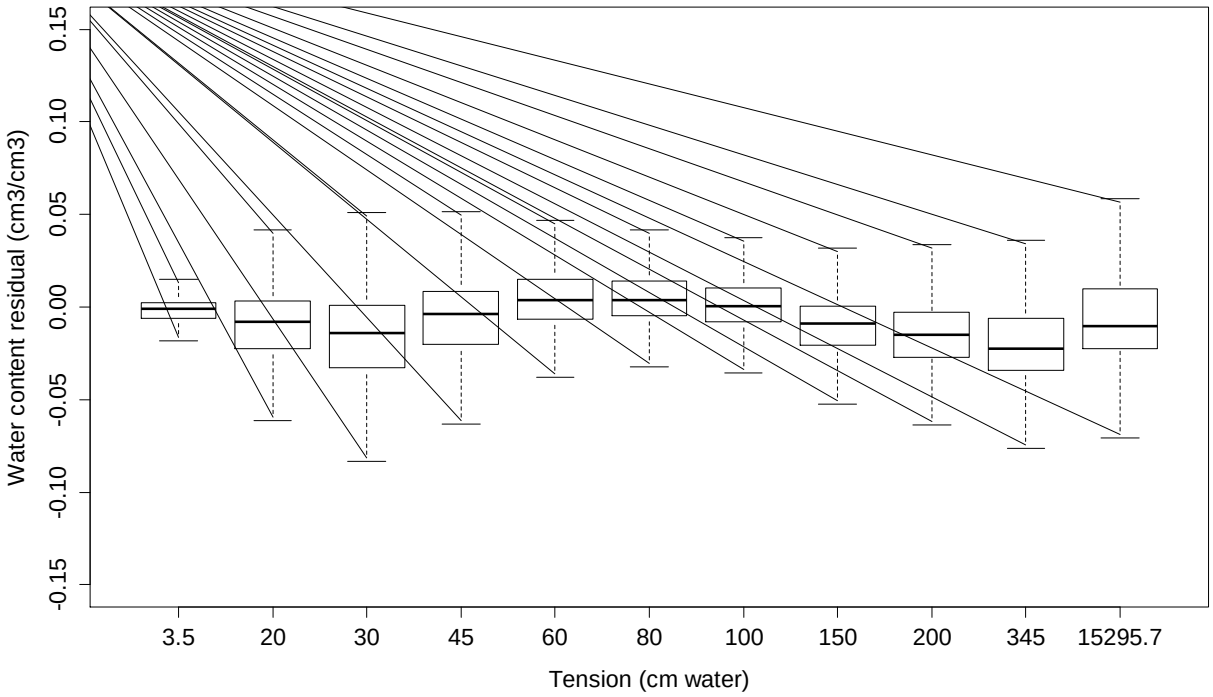

Figure 3-4. Boxplot of VWC prediction residuals vs. tension using the RETC methodology. Residuals are derived from predicting SMRCs from the Florida Soil Characterization Database. The horizontal axis is not to scale.

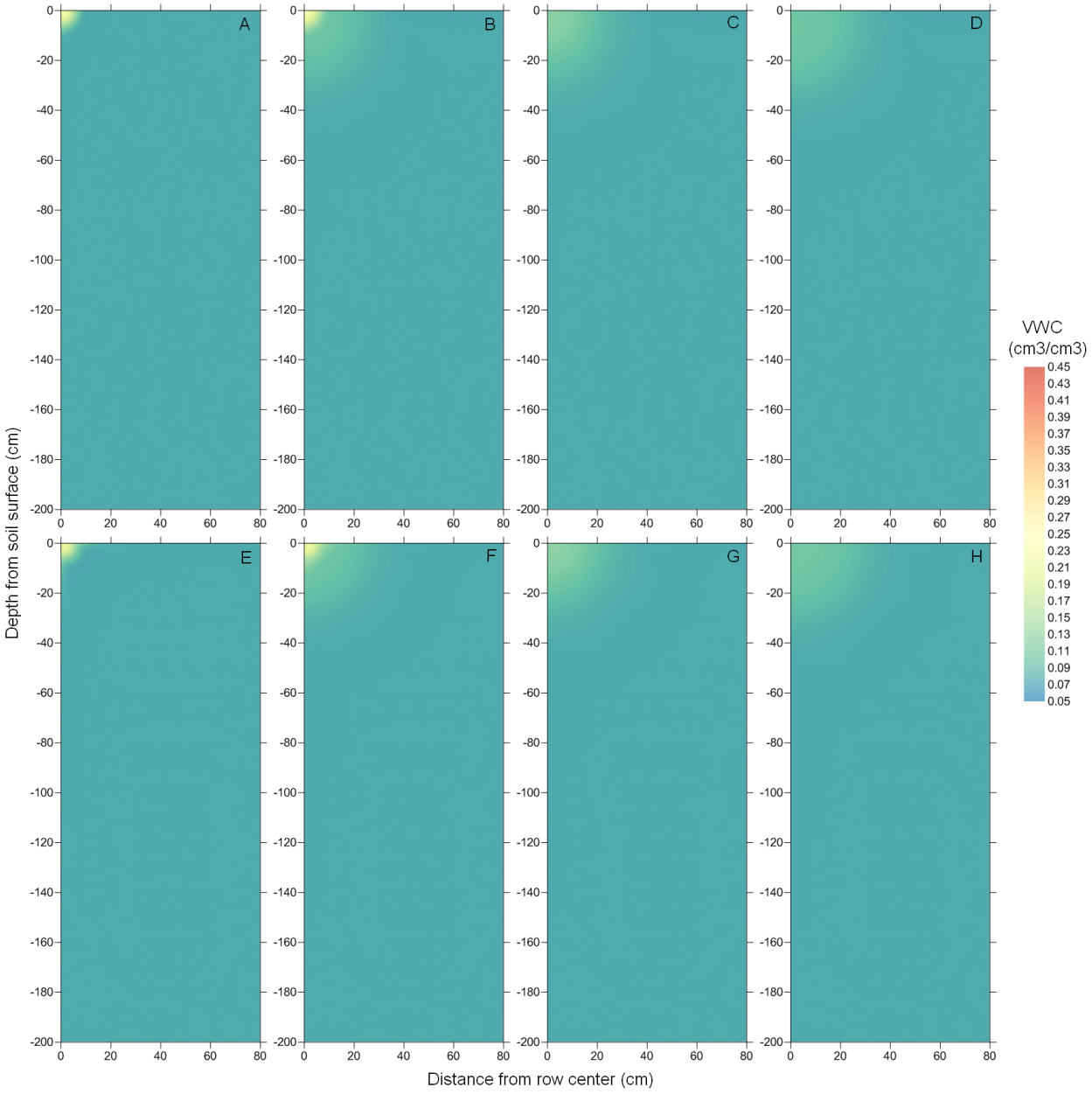

Figure 3-5. Simulated VWCs for the Uniform 1 soil. VWC values are plotted versus depth and distance for A) HYDRUS-2D at the end of the first irrigation event B) HYDRUS-2D at the end of the fourth irrigation event C) HYDRUS-2D four hours after the day four irrigation event D) HYDRUS-2D one day after the day four irrigation event E) DSSAT-2D with normalized-water content at the end of the first irrigation event F) DSSAT-2D with normalized-water content at the end of the fourth irrigation event G) DSSAT-2D with normalized-water content four hours after the fourth irrigation event H) DSSAT-2D with normalized-water content one day after the fourth irrigation event.

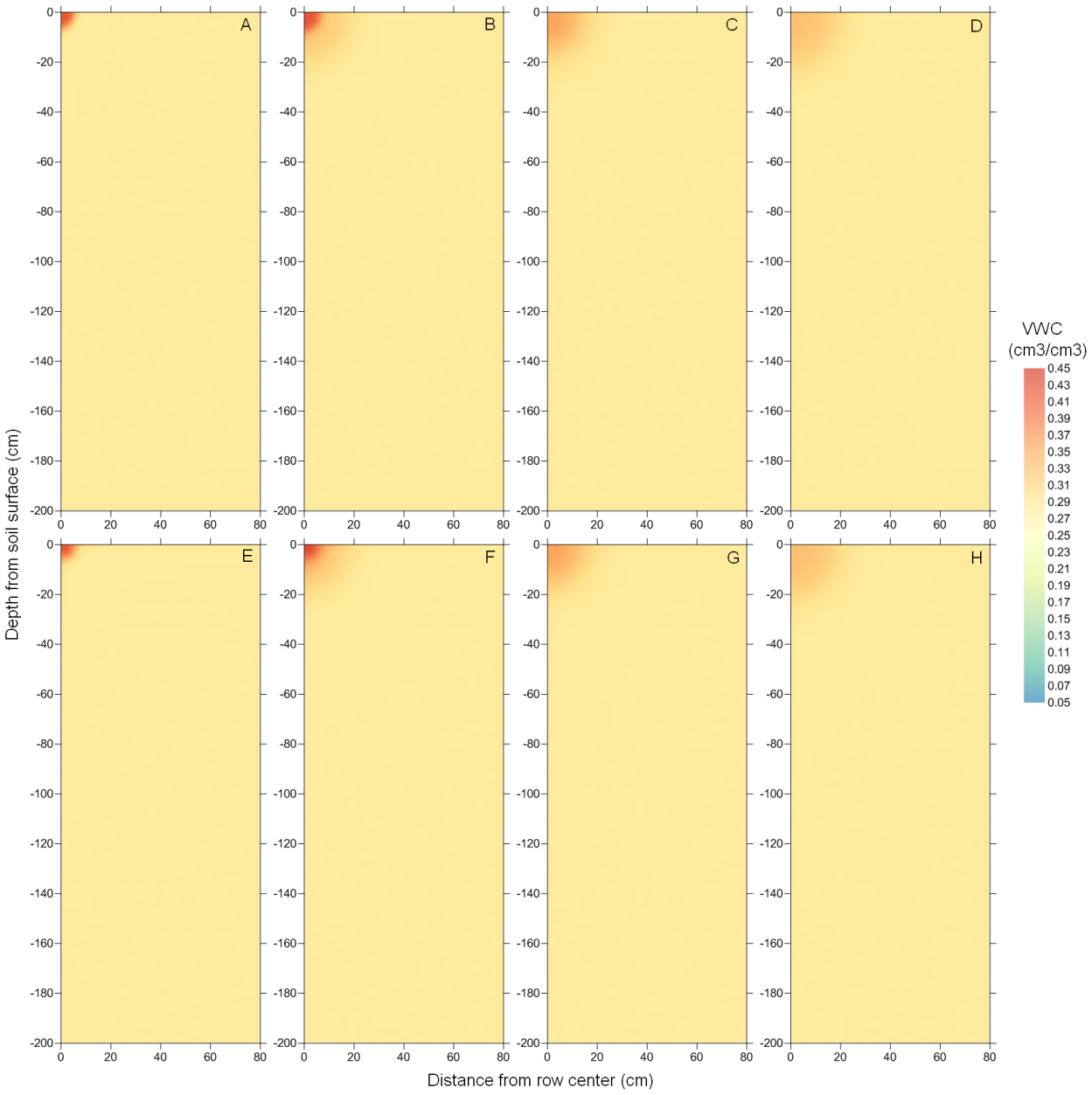

Figure 3-6. Simulated VWCs for the Uniform 2 soil. VWC values are plotted versus depth and distance for A) HYDRUS-2D at the end of the first irrigation event B) HYDRUS-2D at the end of the fourth irrigation event C) HYDRUS-2D four hours after the day four irrigation event D) HYDRUS-2D one day after the day four irrigation event E) DSSAT-2D with normalized-water content at the end of the first irrigation event F) DSSAT-2D with normalized-water content at the end of the fourth irrigation event G) DSSAT-2D with normalized-water content four hours after the fourth irrigation event H) DSSAT-2D with normalized-water content one day after the fourth irrigation event.

Figure 3-7. Simulated VWCs for the Layered 1 soil. VWC values are plotted versus depth and distance for A) HYDRUS-2D at the end of the first irrigation event B) HYDRUS-2D at the end of the fourth irrigation event C) HYDRUS-2D four hours after the day four irrigation event D) HYDRUS-2D one day after the day four irrigation event E) DSSAT-2D with normalized-water content at the end of the first irrigation event F) DSSAT-2D with normalized-water content at the end of the fourth irrigation event G) DSSAT-2D with normalized-water content four hours after the fourth irrigation event H) DSSAT-2D with normalized-water content one day after the fourth irrigation event I) DSSAT-2D with actual-water content at the end of the first irrigation event J) DSSAT-2D with actual-water content at the end of the fourth irrigation event K) DSSAT-2D with actual-water content four hours after the fourth irrigation event L) DSSAT-2D with actual-water content one day after the fourth irrigation event.

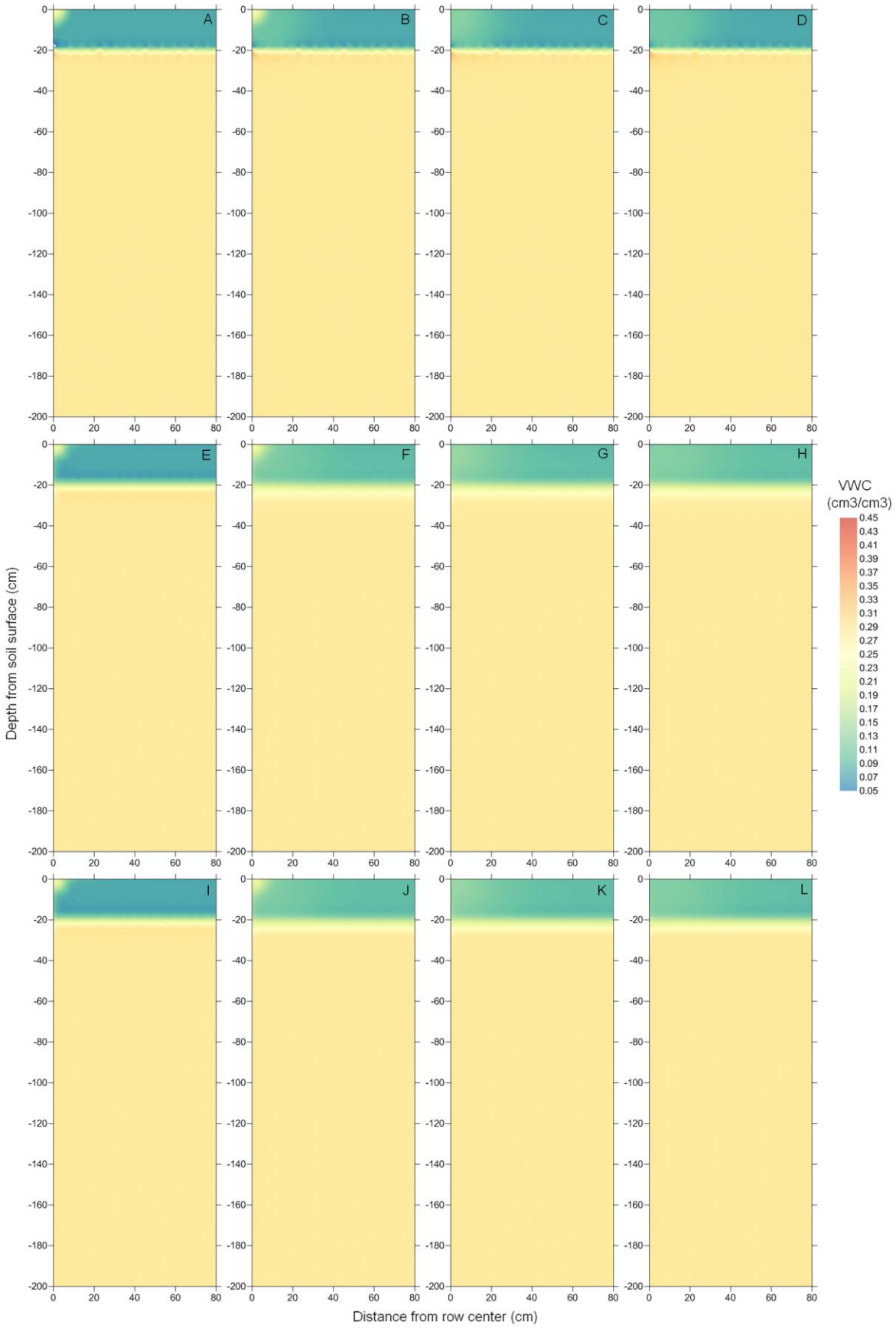
A
B
C
D
E
F
G
H
I
J
K
L
Depth from soil surface (cm)
Distance from row center (cm)
VWC
(cm3/cm3)
0.45
0.43
0.41
0.39
0.37
0.35
0.33
0.31
0.29
0.27
0.25
0.23
0.21
0.19
0.17
0.15
0.13
0.11
0.09
0.07
0.05

Figure 3-8. Simulated VWCs for the Layered 2 soil. VWC values are plotted versus depth and distance for A) HYDRUS-2D at the end of the first irrigation event B) HYDRUS-2D at the end of the fourth irrigation event C) HYDRUS-2D four hours after the day four irrigation event D) HYDRUS-2D one day after the day four irrigation event E) DSSAT-2D with normalized-water content at the end of the first irrigation event F) DSSAT-2D with normalized-water content at the end of the fourth irrigation event G) DSSAT-2D with normalized-water content four hours after the fourth irrigation event H) DSSAT-2D with normalized-water content one day after the fourth irrigation event I) DSSAT-2D with actual-water content at the end of the first irrigation event J) DSSAT-2D with actual-water content at the end of the fourth irrigation event K) DSSAT-2D with actual-water content four hours after the fourth irrigation event L) DSSAT-2D with actual-water content one day after the fourth irrigation event.

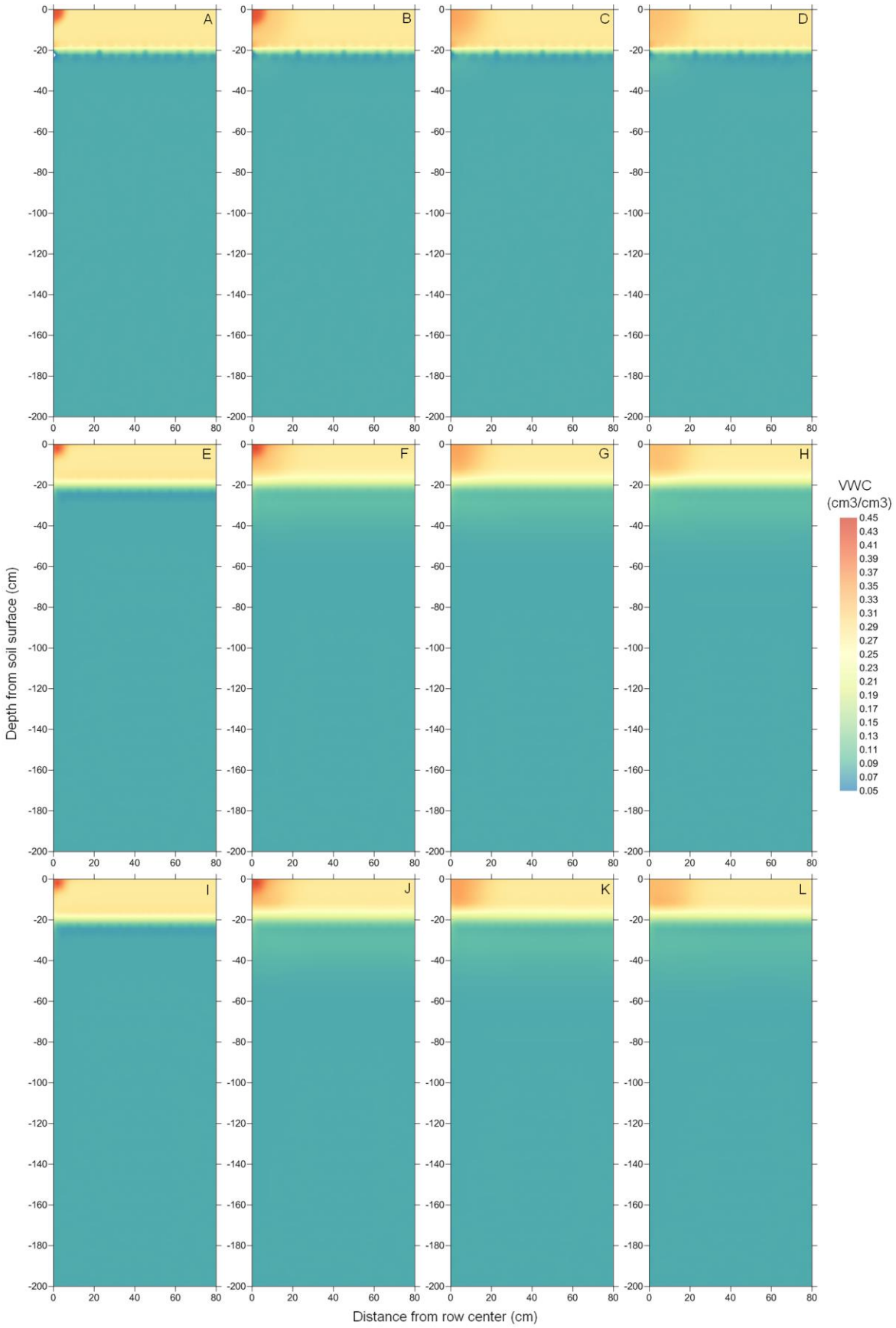
A
B
C
D
E
F
G
H
I
J
K
L
Depth from soil surface (cm)
Distance from row center (cm)
VWC
(cm3/cm3)
0.45
0.43
0.41
0.39
0.37
0.35
0.33
0.31
0.29
0.27
0.25
0.23
0.21
0.19
0.17
0.15
0.13
0.11
0.09
0.07
0.05

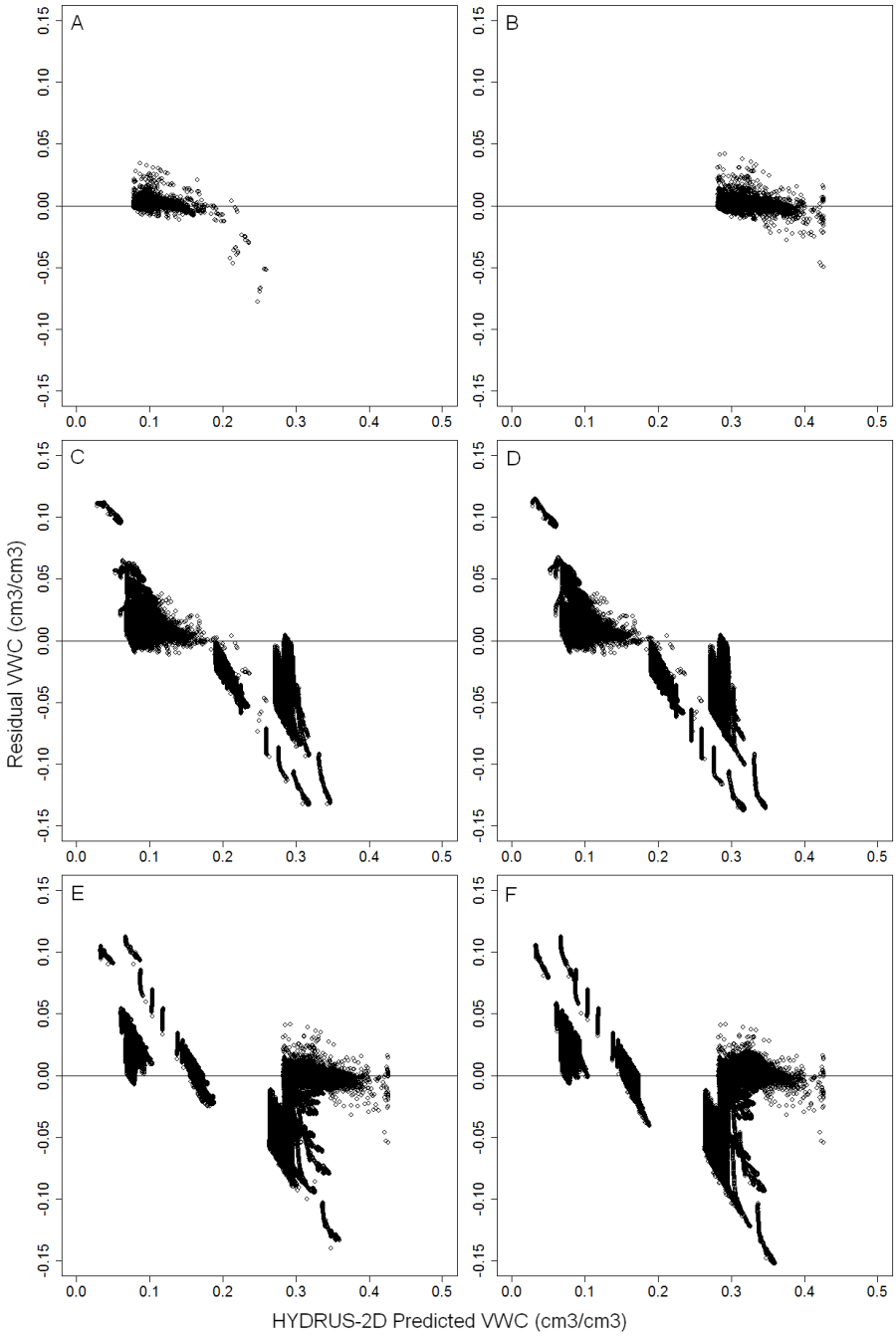

Figure 3-9. Plot of residuals between DSSAT-2D and HYDRUS-2D VWC predictions. Plots are for A) Uniform 1 soil, B) Uniform 2 soil, C) Layered 1 soil with DSSAT-2D driven by normalized-water content, D) Layered 1 soil with DSSAT-2D driven by actual-water content, E) Layered 2 soil with DSSAT-2D driven by normalized-water content, F) Layered 2 soil with DSSAT-2D driven by actual-water content.

Figure 3-10. The RMSD value over time between DSSAT-2D and HYDRUS-2D VWC predictions. This includes the RMSD value at each simulation time step between the VWC predictions of HYRDUS-2D and A) DSSAT-2D with normalized-water content for the Uniform 1 soil, B) DSSAT-2D with normalized-water content for the Uniform 2 soil, C) DSSAT-2D with normalized-water content for the Layered 1 soil , D) DSSAT-2D with actual-water content for the Layered 1 soil, E) DSSAT-2D with normalized-water content for the Layered 2 soil, F) DSSAT-2D with actual-water content for the Layered 2 soil.

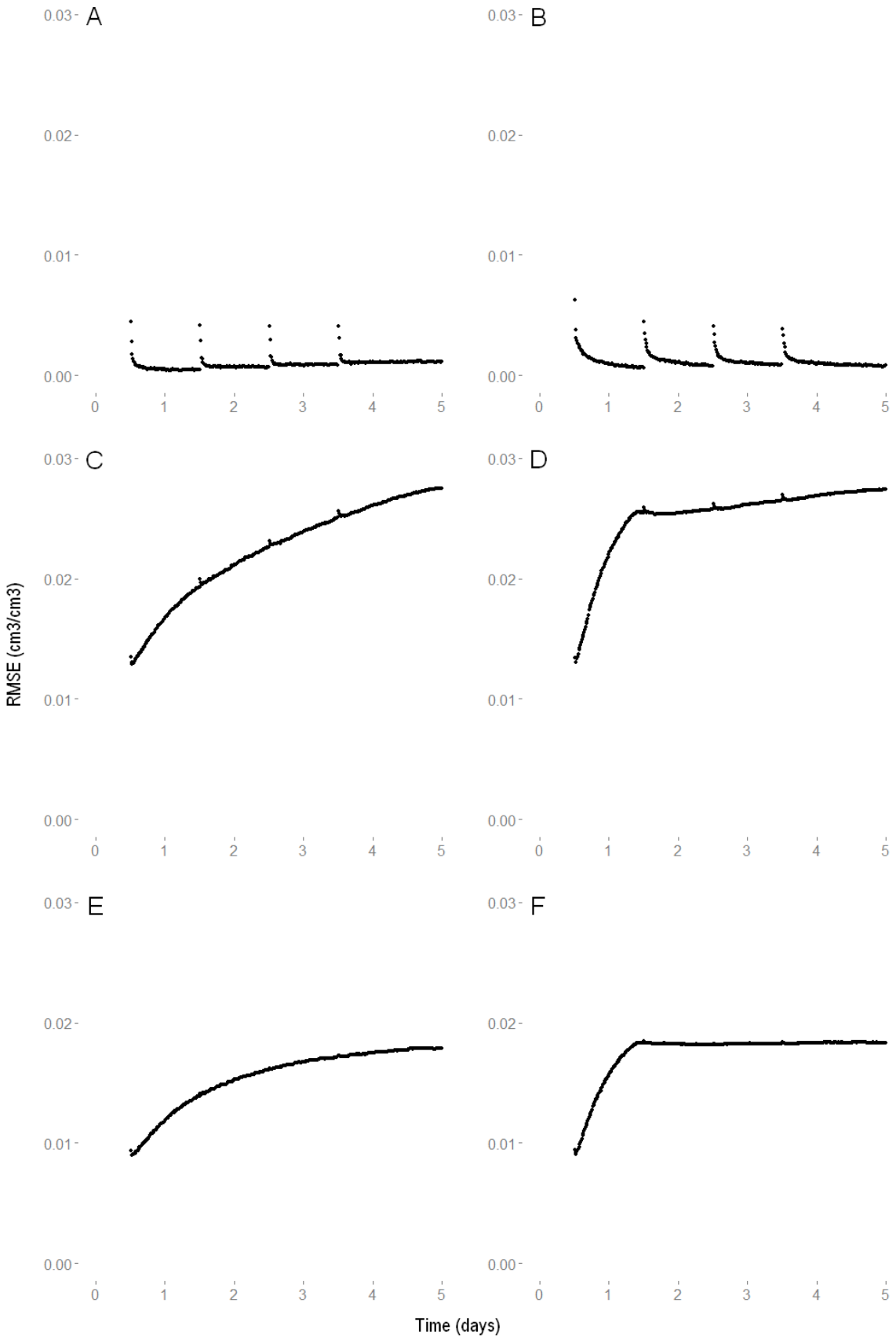
A
B
C
D
E
F
0.03
0.02
0.01
0.00
0
1
2
3
4
5
RMSE (cm3/cm3)
Time (days)

Figure 3-11. A set of water content reflectometer probes installed with measurement rods inserted parallel to the length of the bed row.

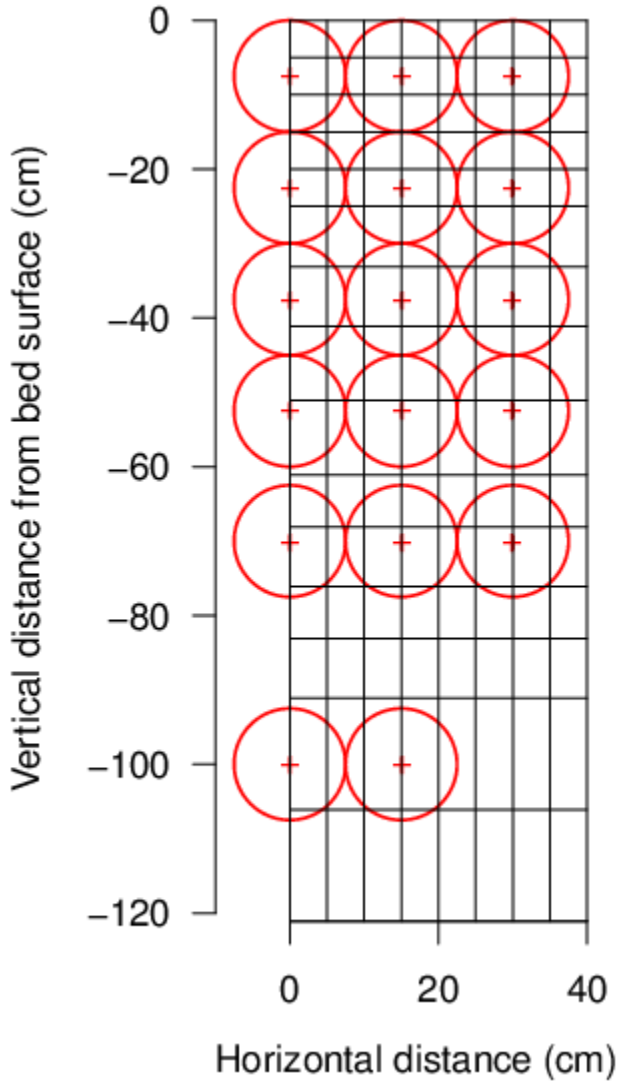

Figure 3-12. Two-dimensional representation of the 17 unique probe locations and sensing areas. The + at the center of a circle represents the probe installation location, and the 7.5 cm radius circle represents its approximate sensing area.

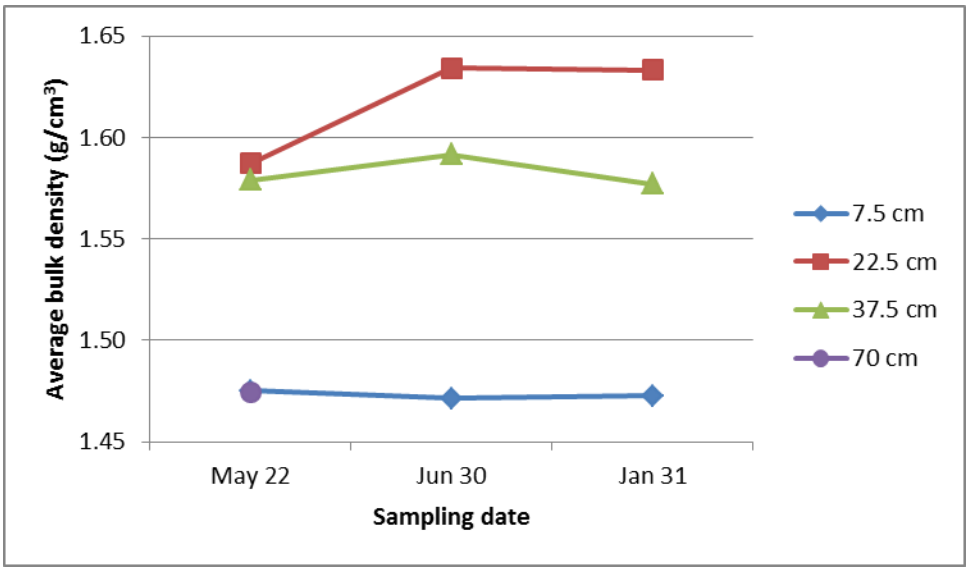

Figure 3-13. Average bulk density measurements vs. sampling date for each soil depth. Samples taken for the field experiment.

Figure 3-14. Boxplots of the field measured SMRCs. This includes boxplots for A) the samples at a 10 cm depth B) the samples at a 45 cm depth, C) all the samples. Note that the horizontal axis is not to scale.

A

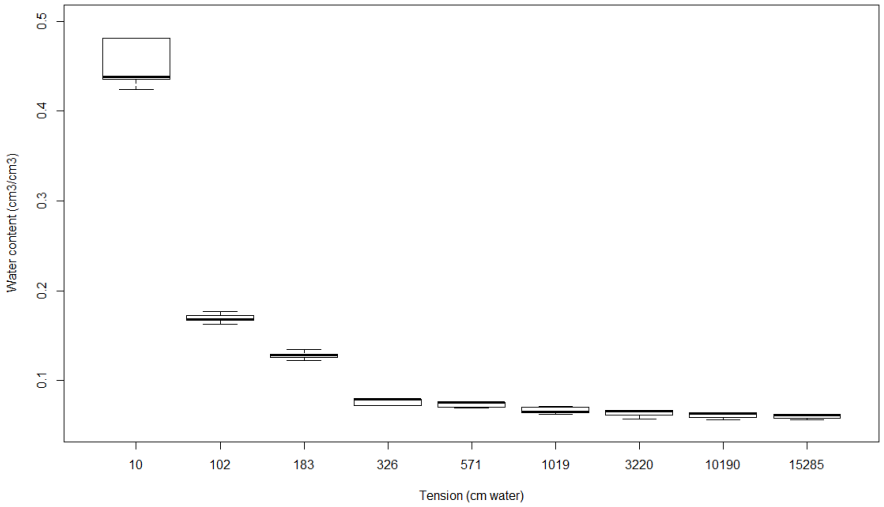
Water content (cm3/cm3)
0.1
0.2
0.3
0.4
0.5
10
102
183
326
571
1019
3220
10190
15285
Tension (cm water)

B

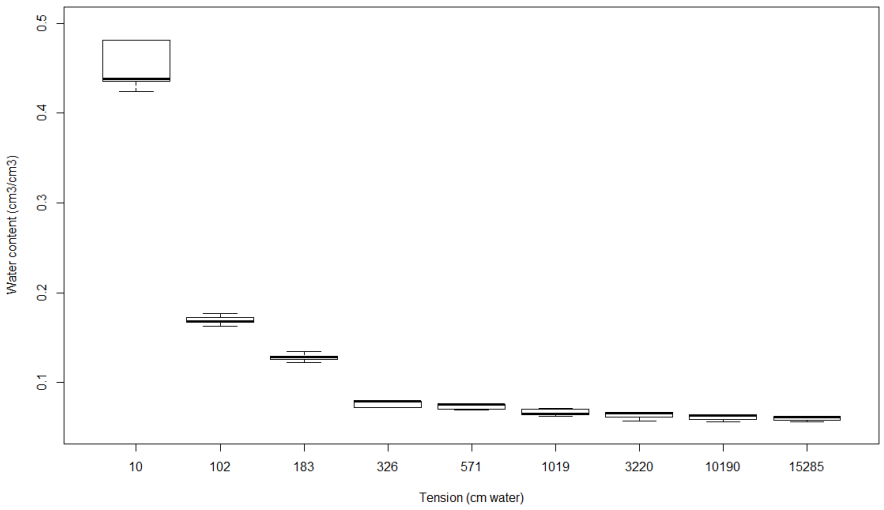
Water content (cm3/cm3)
0.1
0.2
0.3
0.4
0.5
10
102
183
326
571
1019
3220
10190
15285
Tension (cm water)

C

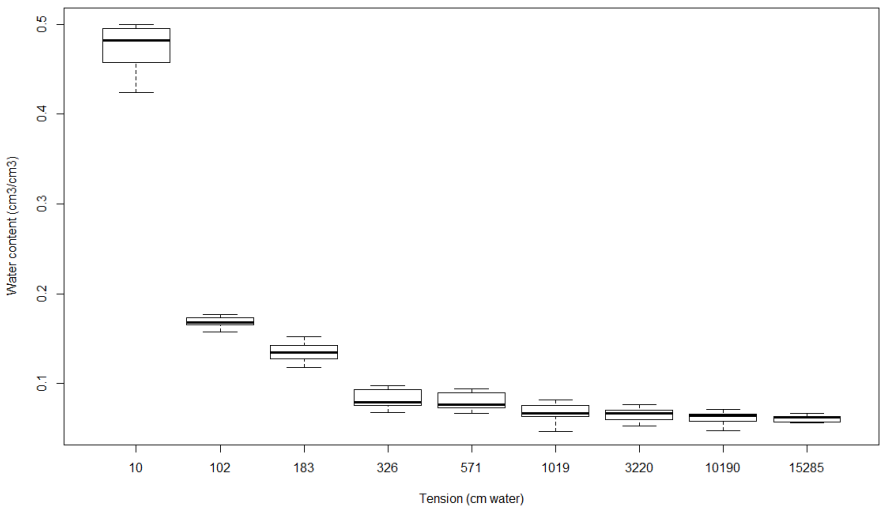
Water content (cm3/cm3)
0.1
0.2
0.3
0.4
0.5
10
102
183
326
571
1019
3220
10190
15285
Tension (cm water)

CHAPTER 4
DRIP IRRIGATION MANGEMENT IMPLICATIONS

Background

Vegetable production in Florida is typically done on sandy soils with low water holding capacities (Dukes et al., 2006). Production on these soils necessitates close management to maintain soil-moisture and nutrient levels conducive for optimal crop production. The combination of coarse soils requiring intensive irrigation and nutrient applications presents the potential for high water-use and nutrient leaching, for which there is increasing pressure to minimize. It thus becomes increasingly complicated to manage these production systems to meet both economic and environmental goals.

Vegetable production systems are typically irrigated using either seepage or drip irrigation. Drip irrigation has been shown to have the potential to increase water and nutrient use efficiencies and reduce nutrient leaching compared to seepage irrigation (Dukes et al., 2010; Pitts et al., 1988; Sato et al., 2010). Around 44 percent of irrigated lands in Florida are irrigated via seepage (Dukes et al., 2010). Thus, conversion of irrigation systems from seepage to drip has been suggested as a possible measure for reducing water use and nutrient leaching (Dukes et al., 2010; Sato et al., 2010).

However, while drip systems offer the potential for improved production efficiencies, system management is the key for realizing these potential reductions. Surveys have shown that it is common industry practice to apply fertilizer at rates in excess of the recommended amounts (Cantliffe et al., 2009). One facet of drip irrigation’s potential for improved nutrient use efficiency is the ability to split fertilizer applications throughout the growing season through fertigation. Thus, fertilizer can be applied more synchronously with the crop demand, resulting in less nutrients in the soil

at any one time and a system that is less susceptible to leaching during heavy rainfall events. Ironically, however, improper management can result in excessive nutrients to be applied as fertigation. This has been observed in surveys that have shown instances of producers using drip-systems using more fertilizer than those using seepage-systems (Jones et al., 2012). With the potentially increasing prevalence of drip-systems in the future, it is essential that these systems be managed properly.

Research has shown that, given proper management, high water use efficiencies (Simonne et al., 2004) and fertilizer use efficiencies (Zotarelli, Dukes et al., 2009) can be attained within these intensively managed systems. Nutrient and irrigation management are intrinsically linked, as nutrient movement is driven by soil-water dynamics. Nitrates especially move with soil-water flow, tending to collect near the fringe of wetting fronts under drip irrigation regimes (Li et al., 2003). Simonne and Ozores-Hampton (2006) argue that nutrient management should be approached by first attempting to improve the irrigation management, since nutrient requirements cannot be properly established until proper irrigation management is in place.

It is apparent that there is a need for proper irrigation management of drip-irrigated systems. Models can be useful tools for identifying the impacts of management decisions. Models can relate the complex system interactions between management, soil, climate, crop, and environment. DSSAT-2D is a modified version of the DSSAT-CSM that was designed and evaluated for simulating the soil-water dynamics under management practices and conditions typical of vegetable production systems. It was therefore the goal of this research to apply the DSSAT-2D model to analyze the impact

of different drip tape designs and irrigation management options on the soil-water regime and the implications on root-zone moisture and water loss from the root-zone.

Irrigation Management Impacts

Assessing the impacts of different irrigation management options requires the establishment of quantitative indicators of effectiveness. With a reliable crop model, the natural indicators would be simulated crop water stress, crop yield, and water use. In the absence of a validated crop component, however, it is necessary to consider the soil-moisture conditions that are conducive to crop growth. This scenario is analogous to irrigation during crop establishment, when root water uptake is essentially zero. The indicators selected were the average root-zone moisture content and the water flowing out of the root-zone, with higher root-zone moisture content considered better for crop growth and less water flow out of the root-zone considered better for minimizing water use and nutrient loss.

Analyses were conducted for a specific field layout. A plastic mulched raised bedded system of 20 cm height and 80 cm width with a row spacing of 180 cm was simulated. The soil was uniform, with a lower limit water content of 0.047 cm^3/cm^3, drained upper limit water content of 0.170 cm^3/cm^3, saturation water content of 0.480 cm^3/cm^3, saturated hydraulic conductivity of 23.1 cm/hr, 3.2 percent clay, and 5.2 percent silt. The Van Genuchten parameters were uniformly set with an α of 0.043 cm^{-1}, an n of 1.57, and a θ_r of 0.036 cm^3/cm^3. The initial soil water-content was set at 0.10 cm^3/cm^3. Model implications from these analyses can be generalized, but site-specific applicability is a strength of physically-based models.

The main drip irrigation management options are flow rate, daily irrigation amount, and method of splitting irrigation applications. Application splitting is the

practice of applying a desired irrigation amount in multiple applications instead of in a single application. On coarse soils with low water holding capacities and at periods of high demand, this is considered a good practice for keeping irrigation water in the root-zone. This is because at times of high ET demand, daily irrigation requirements can exceed the water holding capacity of the root-zone. Thus, the necessary irrigation amount must be applied in two or more split applications, with each application targeted to not exceed the root-zone water holding capacity. The daily irrigation amount was varied between 9 and 189 cm^2 in increments of 9 cm^2. The irrigation rate was varied between 0.1 and 0.8 lpm/m in increments of 0.1 lpm/m. Applications were split as either one application at 1200, two applications at 1000 and 1400, or four applications at 0800, 1000, 1200, and 1400. Results are shown in Figure 4-1, with only the extreme application splitting and irrigation rates being shown for simplicity of visual interpretation. It is apparent that the irrigation amount is the dominant management factor for influencing the soil-water regime, with increased irrigation amounts resulting in greater water loss from the root-zone and water storage in the root-zone. The response of water leaching to irrigation amount is such that with 47 cm^2 of daily irrigation or less, nearly no water leaches from the root-zone. Beyond this amount, however, leaching responds more rapidly to increases in irrigation amount until the response becomes approximately linear. Increases in irrigation amount result in increases in root-zone storage as well. However, the response is much more rapid at lower application amounts, with increased irrigation amounts resulting in only slight root-zone storage increases in regions of high irrigation amounts. At equivalent irrigation amounts the system showed increased root-zone storage and reduced leaching for irrigation applied

at lower rates and increased application splitting. These effects were minor, however, relative to the impacts of the irrigation amount.

To assess the response of the system to application rate and application splitting in greater detail, the model was run for a range of irrigation rates and application splitting methods while maintaining fixed daily irrigation amounts. Simulations were run with daily irrigation amounts of 20 cm^2. Flow rates were set to 0.100, 0.150, 0.200, 0.250, 0.300, and 0.375 cm^2/min. Application splitting methods consisted of, as before, one application at 1200 or two applications at 1000 and 1400. However, in addition to the number of splits, the distribution of the splits throughout the day is another factor that determines the effectiveness of splitting applications. Thus, applications were also split into three applications at 1000, 1200, and 1400, which has the same first and last irrigation start times as the two-split application, as well as a more spread out splitting of applications into three applications at 0900, 1300, and 1700. The three-split applications are thus referred to as the 3 narrow and 3 wide split applications. In order to assess any interactive response with application amount, the same analysis was also conducted with daily irrigation amounts of 40 and 60 cm^2.

The results of this analysis, which are shown in Figure 4-2, demonstrate consistent reduction of water leaching from the root-zone for lower application rates. A general pattern of reduced water leaching was also observed for greater split applications. However, while the 3 wide split applications was the best application splitting method in almost all the considered instances, the 3 narrow split method in fact consistently resulted in greater water leaching from the root-zone than the two-split method. It should be noted that while the 3 narrow split method utilizes an additional

application event, if one considers the total daily irrigation application time as the difference between the start of the first irrigation event and the end of the last irrigation event, the two-split method actually applies the irrigation water over a larger application time compared to the 3 narrow split method. This is because the first and last daily irrigation events start at the same time for the two splitting methods, but each event is longer for the two-split method. This trend of irrigation time truly influencing soil-water flow rather than phenomena associated with irrigation rates or application splitting is similar to observations by Skaggs et al. (2010). By this way of thinking, the root-zone leaching reductions associated with lower application rates are in fact due to the longer application times required to apply the fixed amounts at slower rates. This concept is further supported by the variable effect that changing application rates had under different split methods. The application rate had notably greater impact on the root-zone leaching for the splitting methods that resulted in shorter irrigation durations. Conversely, changes in application rate had the least impact on root-zone leaching for the 3 wide splitting method. This supports the application time concept because for single daily applications, the application rate has a large influence over the total irrigation time, thus making changes in application rate very influential. However, if the splitting method is already serving to separate the first and last irrigation events by a large amount of time, changes in application rate will have a relatively small influence over the application time.

It should also be noted that the application rate and the application splitting method had different influences at the different daily application amounts. At low daily application amounts, there are clear distinctions in root-zone leaching between the

application splitting methods, and smaller differences between the application rates. At higher daily application amounts, however, the daily application rates become much more impactful. This in turn results in variable effectiveness of different splitting methods depending on application rate, as a splitting method may outperform another at a certain application rate, but perform worse at a different application rate. The increased impact of application rates and reduced impact of application splitting method on root-zone leaching at higher daily application amounts is to be expected. With greater daily flow, irrigation durations must increase to reach the flow target. As such, changes in flow rate result in increasing changes in application time. The reduced impact of the splitting method also stands to reason because as irrigation times increase, the periods of rest between irrigations imposed by the splitting method become increasingly small. For example, if the splitting method dictates a two-hour difference between the start of two irrigation events, if the irrigation amount dictates that water be applied for two hours in each split, the split method becomes rendered meaningless as the two-applications have merged into a single continuous application. However, the logical extension would indicate that by a certain irrigation amount and at a fixed application rate, all the split methods would observe equivalent root-zone water leaching. However, it is observed that in several instances, and at equivalent application rates, the single daily application method observed reduced leaching compared to other split methods.

An additional analysis was conducted in which, in addition to varying the application rate and application splitting method, different combinations of daily ET rate and daily irrigation amount were imposed. Daily ET rates were set by simulating tomato

crop growth and varying daily solar radiation until the 10 day average of solar radiation between 45 and 55 days after transplanting reached the desired ET rate. It should be noted that the DSSAT-2D model has not been properly calibrated or evaluated for simulating crop growth and development. As such, this analysis should be considered as a proof-of-concept analysis. Results of the analysis, which can be seen in Figure 4-3, indicate that the ET rate has a similar impact on root-zone water leaching as the irrigation amount. The relative insignificance of the application rate and application splitting method are also very noticeable. The analysis most notably underlines the importance of matching irrigation amount with ET demand in order to meet the crop water requirements while minimizing root-zone water leaching.

Soil Moisture Sensor Controlled Irrigation

Soil-moisture sensor based irrigation has been shown as a technology capable of allowing significant reduction in irrigation without reductions in yield compared to traditional irrigation management practices (Smajstrla & Locascio, 1996; Dukes et al., 2003; Zotarelli et al., 2008; Zotarelli et al., 2009b). However, the performance of these systems depends on decisions such as the sensor placement (Coelho & Or, 1996) and soil moisture threshold value for triggering irrigation (Coelho & Or, 1996; Zotarelli et al., 2010). Coelho and Or (1996) point out that while much work has been done to identify threshold soil moisture or matric values for optimal crop yields, most recommendations are general and empirical, ignoring site-specific soil water dynamics. Thus, it is attempted to use the DSSAT-2D model to evaluate the impact of sensor location and threshold value on the soil-water dynamics. The analysis is conducted for the same field layout described previously, but can be applied to any field setup to provide site-specific recommendations.

To evaluate the impact of different soil-moisture sensor locations and threshold values, the DSSAT-2D code first had to be modified to simulate soil moisture sensor-based irrigation. This was done by allowing the depth and distance of the probe to be inputted into the model as well as the threshold VWC and the probe-sensing radius. Different soil-moisture probes have varying soil-moisture sensing radiuses, but for this study the radius was set to 7.5 cm, as this is a common probe specification. Since DSSAT-2D breaks the soil into rectangular grids of uniform VWC, this grid information had to be translated into a representative probe VWC. Thus, a program was written to compute the percentage of the probe sensing area that intersected with each grid area. This code can be seen in Appendix B. These percentages were then used as weights for the intersected grid VWCs to obtain an estimated probe VWC. These calculations were computed in R, using the gpclib package to compute the intersection areas. These weights and grid cell locations were read into DSSAT-2D at the beginning of a simulation and used to calculate the probe VWC at each time step. Irrigation events were thus triggered to occur at any time the probe VWC dropped below the threshold value.

Additionally, in order to conduct this analysis, measurements had to be established on which to evaluate the probe performance. The main goals of an irrigation system are to maintain a certain level of root-zone soil-moisture with a minimum amount of water-use. Thus, the closeness-of-fit of the root-zone soil-moisture to a desired moisture level was considered to evaluate the adequacy of an irrigation setup for meeting the crop-water requirement. As such, the desired root-zone soil-moisture was set as 0.15 cm^3/cm^3, and the closeness-of-fit was measured as the SSD between the

simulated root-zone soil-moisture and 0.15. The root-zone was considered the soil within 30 cm from the row center and at a depth of no more than 45 cm. The irrigation amount for a particular irrigation setup was then considered for assessing the water-use with that setup.

To conduct the analysis, probe locations were considered within the entire space of the root-zone. A grid of locations was created to cover this space, starting at 7.5 cm depth because of the sensing radius and going down to 45 cm deep, and ranging from 0 cm from the row center to 30 cm from the row center. In each direction, the probe location was moved in increments of 2.5 cm for a total of 208 probe locations. The soil-moisture thresholds were varied from 0.10 to 0.18 cm^3/cm^3. Thus, in order to evaluate all combinations of location and threshold, 1,664 unique irrigation management scenarios were created.

For all analyses, irrigation events were fixed to apply 7.5 cm^2 of water, which represents a small application amount such that irrigation can be more finely controlled by the sensors. Additionally, irrigation was applied with a 30 cm emitter spacing and at an emitter rate of 0.2 ml/s. Irrigation was started on day 100 and terminated on day 220 to represent a standard planting date and growing season for tomatoes grown in North Central Florida. Weather data was used from the Florida Automated Weather Network database for the Citra weather station.

The first analysis was conducted with no crop and with rainfall set to zero. This isolated the effect of probe location from rainfall and ET effects, resulting in a highly controlled system with minimal noise and strong repeatability throughout the season. Preliminary analysis demonstrated precise system repeatability between years. Since

this system was so unaffected by weather, simulations were only run for a single year of weather, for a total of 1,664 simulations. The second analysis also had no crop, but considered the impact of rainfall on the system. Thus, simulations were run for 12 years of weather data, from 2001 to 2012. This necessitated 19,968 simulations. For each of the 1,664 unique automated irrigation setups, total SSD and irrigation water use were computed from the 12 years of simulations to evaluate the cumulative performance of each system setup. The final analysis considered rainfall as well as a planted tomato crop, which was transplanted on day 100 with a density of 1.20 plants/m^2, initial planting depth of 1 cm, transplant dry weight of 3 kg/ha, transplant age of 28 days, and transplant greenhouse temperature of 25 °C. This analysis also considered simulations from years 2001 to 2012. It should again be noted that since the DSSAT-2D model has not been properly calibrated or evaluated for simulating crop growth and development, this particular analysis should be considered as a proof-of-concept analysis.

In order to visualize the implications of probe locations on the ability to meet the target root-zone soil-moisture, at each probe location the simulation with the VWC threshold value that resulted in the best SSD was accepted as the best possible SSD for a system with a probe at that location. These SSD values were then interpolated onto a uniform grid via linear point kriging using Surfer (Golden Software Inc., 2011) software with a slope of 1, an anisotropy ratio of 1, and an anisotropy angle of 0. Contour graphs from these analyses (Figure 4-4) reveal different implications of probe location choices, and how these impacts depend on the production system conditions. With no crop and no rain, the system can be quite precisely controlled, with RMSD values ranging between 0.0031 and 0.0173 cm^3/cm^3. The optimal probe placement area

is also fairly well defined, with an arced shape reminiscent of the characteristic flow pattern of the wetting front of drip regimes ranging from around 17 to 26 cm depths directly below the emitter to between 16 and 26 cm from the row center at 7.5 cm below the surface. There is a clear pattern that locations very close to the emitter are sub-optimal, and locations beyond the optimal range increasingly deteriorate in quality as well.

With the addition of rainfall to the un-cropped system, the ability of the system to control the root-zone moisture regime is hampered considerably, with RMSD values ranging between 0.0293 and 0.0335 cm^3/cm^3. This jump in deviation from the desired moisture levels is due to large rainfall events, which increase the moisture in the root-zone far beyond the desired levels. This effect is exacerbated by the plastic mulch and lack of crop, which essentially eliminate ET within the root-zone and result in the system remaining at these elevated moisture levels for long periods of time. With the spring planting, these rainfall events are much more prevalent during the later months. The optimal probe location area is more poorly defined, but remains in a similar location as the non-rainfall scenario, though favoring locations slightly more distant from the emitter. Locations very close to the emitter and very distant from the emitter again perform the worst. However, with the addition of rainfall to the un-cropped system, the difference between probe locations becomes less impactful.

When considering a cropped system, however, the system regains some ability to control the root-zone moisture near the desired level, with RMSD values ranging between 0.0128 and 0.031 cm^3/cm^3. This improved ability is due to the effect of root water uptake, which allows the moisture levels in the root-zone to drop to threshold

values more quickly following large rainfall events. This increased dependence on the irrigation regime allows the system to exact more control over the soil-moisture levels. This results in a more clearly defined optimal probe location area, which extends a bit further from the emitter, ranging from beneath the emitter at depths of around 22 to 30 cm and 18 to 26 cm from the row center at 7.5 cm below the soil surface. The cropped system results in the strongest negative effect of probe locations that are very close to the emitter. This is illustrated in Figure 4-5, which compares the root-zone VWC over time with a probe placed in a well-suited location and a probe placed directly below the emitter. The well-placed probe controls the irrigation fairly similarly throughout the season, consistently remaining near the 0.15 cm^3/cm^3 target with the exception of during a few large rainfall events where the root-zone VWC peaks. Conversely, control with the probe under the emitter results in over-irrigation in the beginning of the season, when root water uptake is concentrated near the emitter and the probe VWC is not representative of the root-zone VWC. Later in the season, the system is strongly under-irrigated, as the roots extract water from a greater portion of the root-zone and the area near the emitter now under-estimates the needs for moisture in the root-zone.

In order to evaluate the impact of the probe location on the proper probe threshold value, the optimal threshold value at each probe location was also interpolated via kriging. These graphs, which can be seen in Figure 4-6, demonstrate the general need to set thresholds to higher values nearer the emitter. This higher threshold is necessitated due to the quicker feedback with probes near the emitter. Irrigation events reach the probes near the emitter more quickly, resulting in frequent, short irrigations. Thus to supply water to an adequate level in the root-zone, higher

thresholds are necessitated. It should also be noted that the system with rainfall and no crop required much lower thresholds than the system with no rainfall and no crop, as the rainfall events supplied moisture to the system and reduced thresholds allowed the system to accept more rainfall with smaller increases beyond the desired levels. Similarly, adding the crop to the system required increased threshold levels to meet the increased demand for water. Importantly, however, the greatest changes in threshold values between these scenarios occurred at locations near the emitter, while locations in the optimal range showed the least changes in threshold values between scenarios. This further supports these locations as optimal, as their functionality is not dependent on altering the threshold value to fit varying system demand scenarios, but instead are more flexibly applicable.

Summary

The DSSAT-2D model was applied to evaluate the impacts of different drip-irrigation management options on irrigation efficiency. Model experiments implied that irrigation amount, especially as it relates to ET rates, is very impactful on root-zone storage and water leaching from the root-zone. Increasing application amounts increased root-zone storage and root-zone leaching. However, root-zone storage and root-zone leaching responded inversely to increases in daily application amounts, with root-zone storage responding with diminishing increases to increases at high daily application amounts, while root-zone leaching responded strongly at high daily application amounts. Root-zone leaching and storage are inherently linked, as minimizing leaching will maximize storage increases. However, at lower daily application amounts, increases in application amount are able to result in increased

root-zone storage with minimal increases in root-zone leaching. This is an optimal region to be in for efficient irrigation.

Although considerably less impactful, lower application rates and increased spreading of applications through application splitting were shown to result in increased root-zone storage and reduced root-zone leaching. Model responses generally coincided with the belief that the effect of application splitting and application rate was not due to flow phenomena associated with these management practices, but instead due to the impact each practice has on spreading the total irrigation application duration.

Model experiments were also conducted with DSSAT-2D to consider the impact of different management options for soil moisture sensor automated irrigation systems. A methodology was demonstrated for a site-specific evaluation that can be applied for other specific production sites and setups using automated drip systems. A clear area of optimal probe locations was identified for the site-specific analysis. This area was additionally shown to have the most consistent optimal soil-moisture threshold values under differing system scenarios, similar to its ability to represent the whole of the root-zone during both early season low-ET periods and late season high-ET periods. Conversely, probe locations near the emitter resulted in early-season over-irrigation and late-season under irrigation. Probe locations far from the emitter were insensitive to the root-zone ET, resulting in few and large irrigation events. While rainfall events introduce some randomness to the system and thus reduce the ability of the irrigation system to control the moisture levels precisely, crop growth restored some control to the system as root-water extraction allowed the root-zone to more rapidly fall to desirable moisture

levels following these events. This is additionally beneficial for spring plantings, as the Florida climate is conducive to a greater prevalence of large summer rainfall events, which coincides with late season high ET demand.

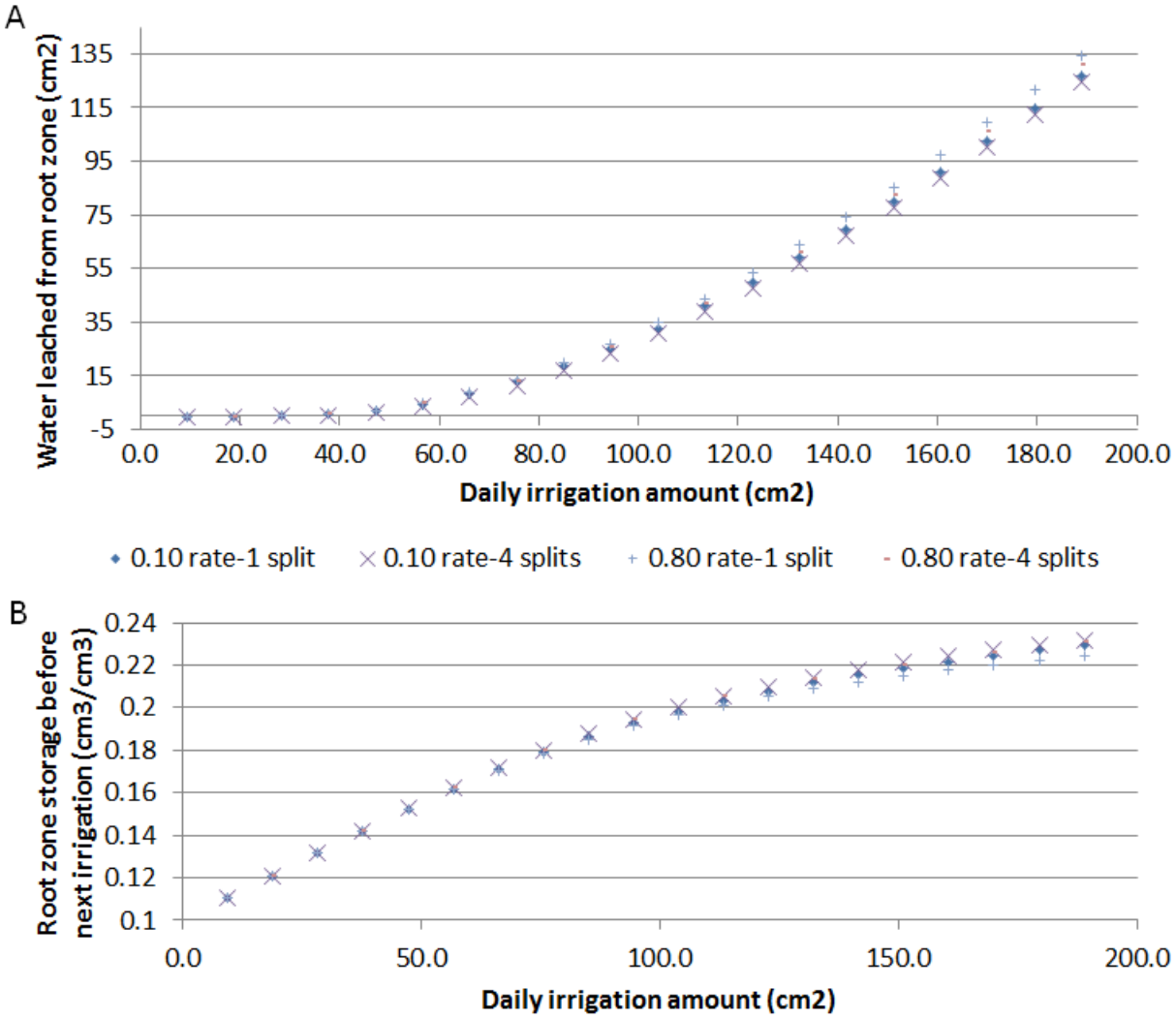

Figure 4-1. System response to changes in irrigation amount, rate, and application splitting. This includes A) DSSAT-2D predicted leaching from root-zone for various irrigation amounts, rates, and application splitting, B) DSSAT-2D root-zone storage for various irrigation amounts, rates, and application splitting.

Figure 4-2. DSSAT-2D predicted water leaching from the root-zone at different applications rates and application splitting methods. Analyses are shown with daily irrigation amounts fixed at A) 20 cm^2, B) 40 cm^2, C) 60 cm^2.

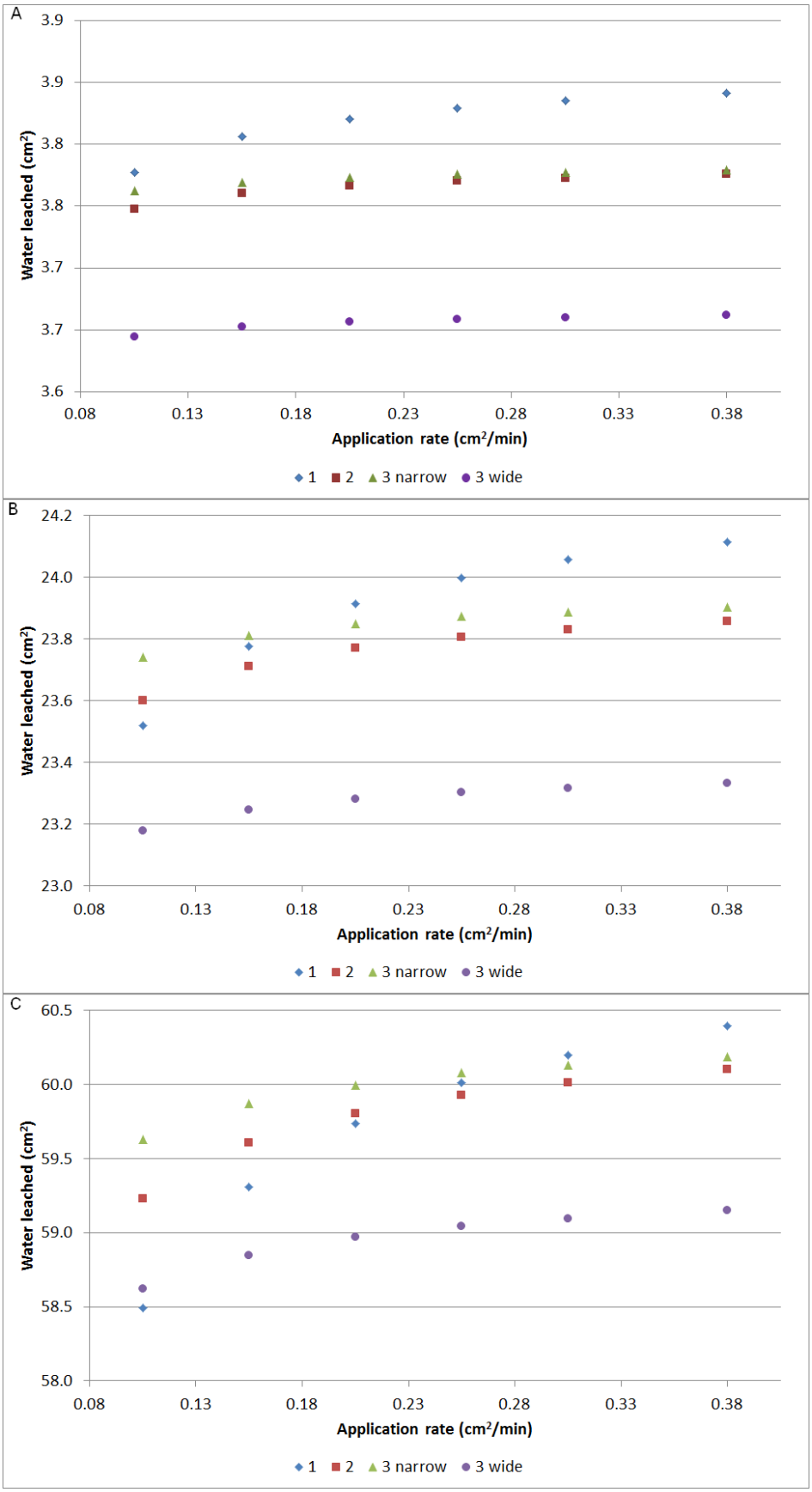
A
3.9
3.9
3.8
3.8
3.7
3.7
3.6
Water leached (cm²)
0.08
0.13
0.18
0.23
0.28
0.33
0.38
Application rate (cm²/min)
1
2
3 narrow
3 wide
B
24.2
24.0
23.8
23.6
23.4
23.2
23.0
Water leached (cm²)
0.08
0.13
0.18
0.23
0.28
0.33
0.38
Application rate (cm²/min)
1
2
3 narrow
3 wide
C
60.5
60.0
59.5
59.0
58.5
58.0
Water leached (cm²)
0.08
0.13
0.18
0.23
0.28
0.33
0.38
Application rate (cm²/min)
1
2
3 narrow
3 wide

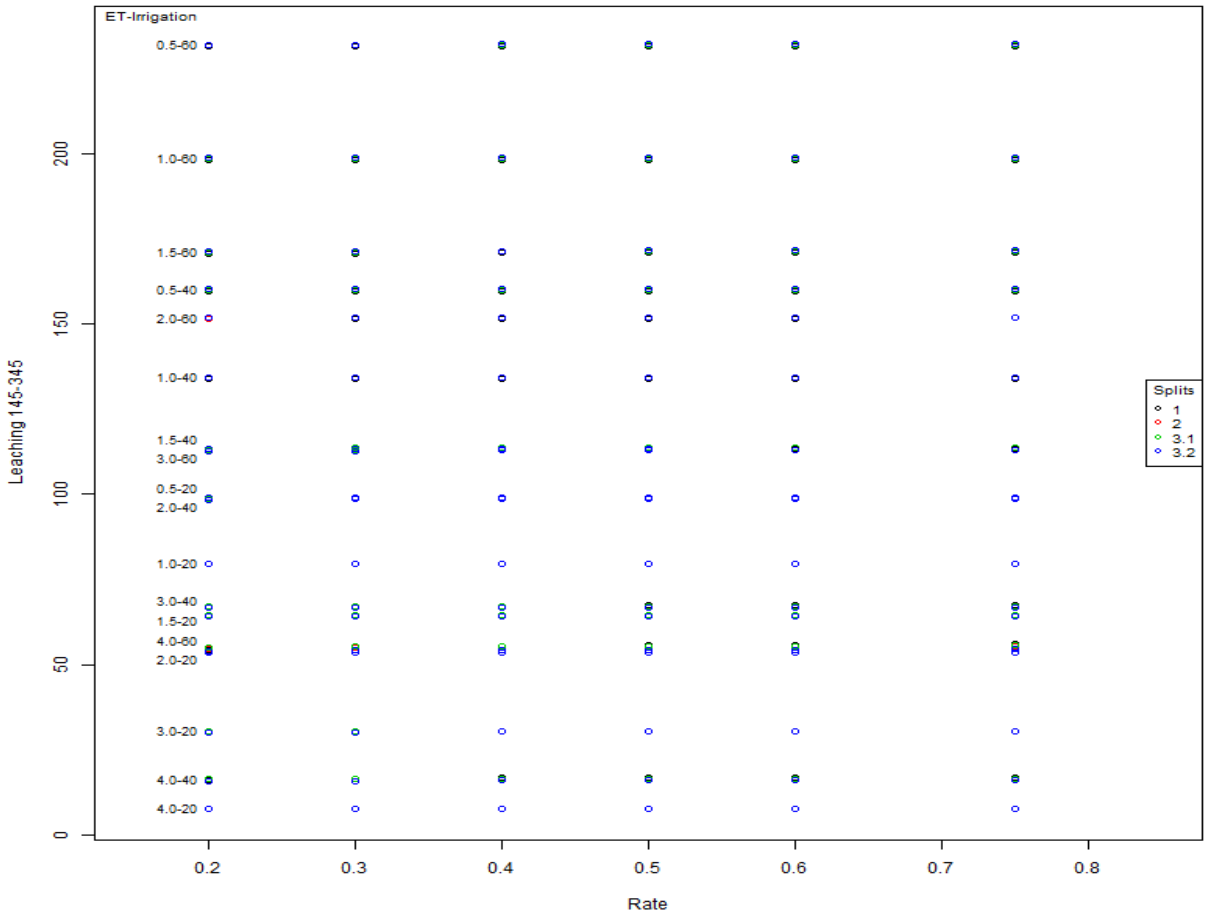

Figure 4-3. DSSAT-2D predicted water leaching from the root-zone under different scenarios. Scenarios include various application rates, split methods, and combinations of daily ET rate and irrigation amount.

Figure 4-4. Impact of probe location on the efficacy of soil moisture sensor controlled irrigation systems. Efficacy here is considered the ability to control the root-zone soil moisture content with A) no rain and no crop, B) rain and no crop, C) rain and crop.

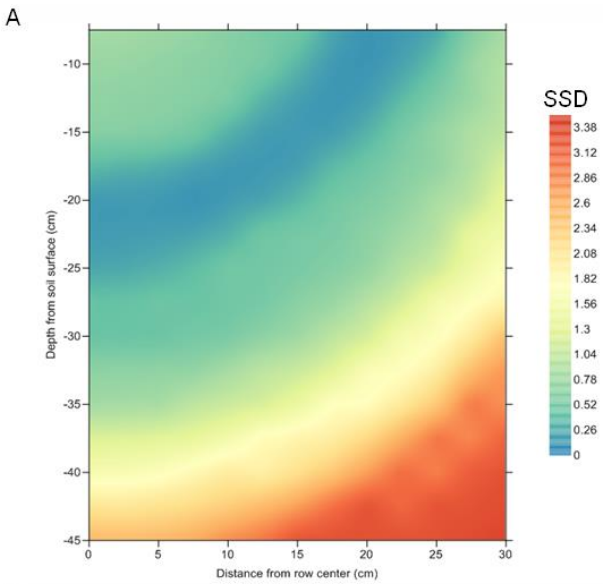
A
SSD
3.38
3.12
2.86
2.6
2.34
2.08
1.82
1.56
1.3
1.04
0.78
0.52
0.26
0
Depth from soil surface (cm)
-10
-15
-20
-25
-30
-35
-40
-45
0
5
10
15
20
25
30
Distance from row center (cm)

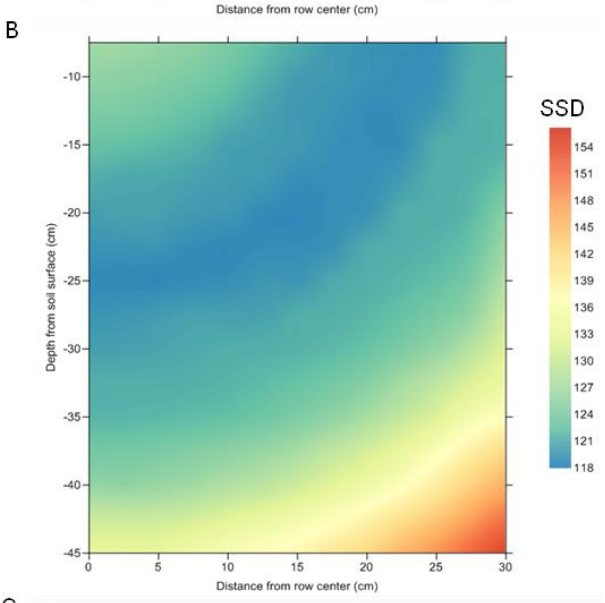
B
SSD
154
151
148
145
142
139
136
133
130
127
124
121
118
Depth from soil surface (cm)
-10
-15
-20
-25
-30
-35
-40
-45
0
5
10
15
20
25
30
Distance from row center (cm)

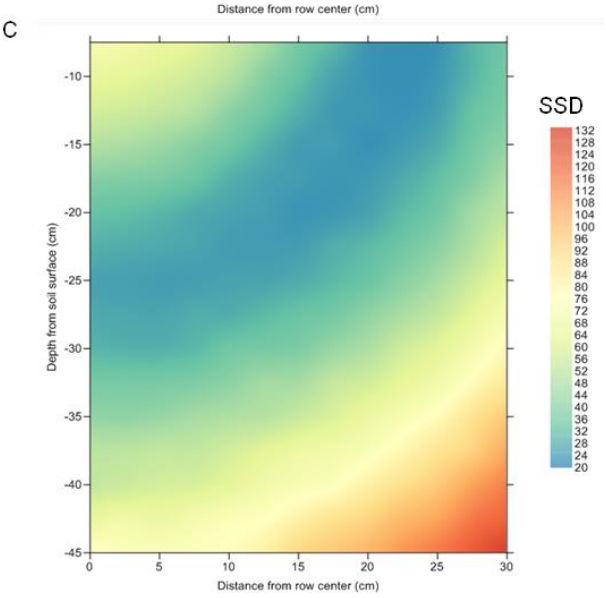
C
SSD
132
128
124
120
116
112
108
104
100
96
92
88
84
80
76
72
68
64
60
56
52
48
44
40
36
32
28
24
20
Depth from soil surface (cm)
-10
-15
-20
-25
-30
-35
-40
-45
0
5
10
15
20
25
30
Distance from row center (cm)

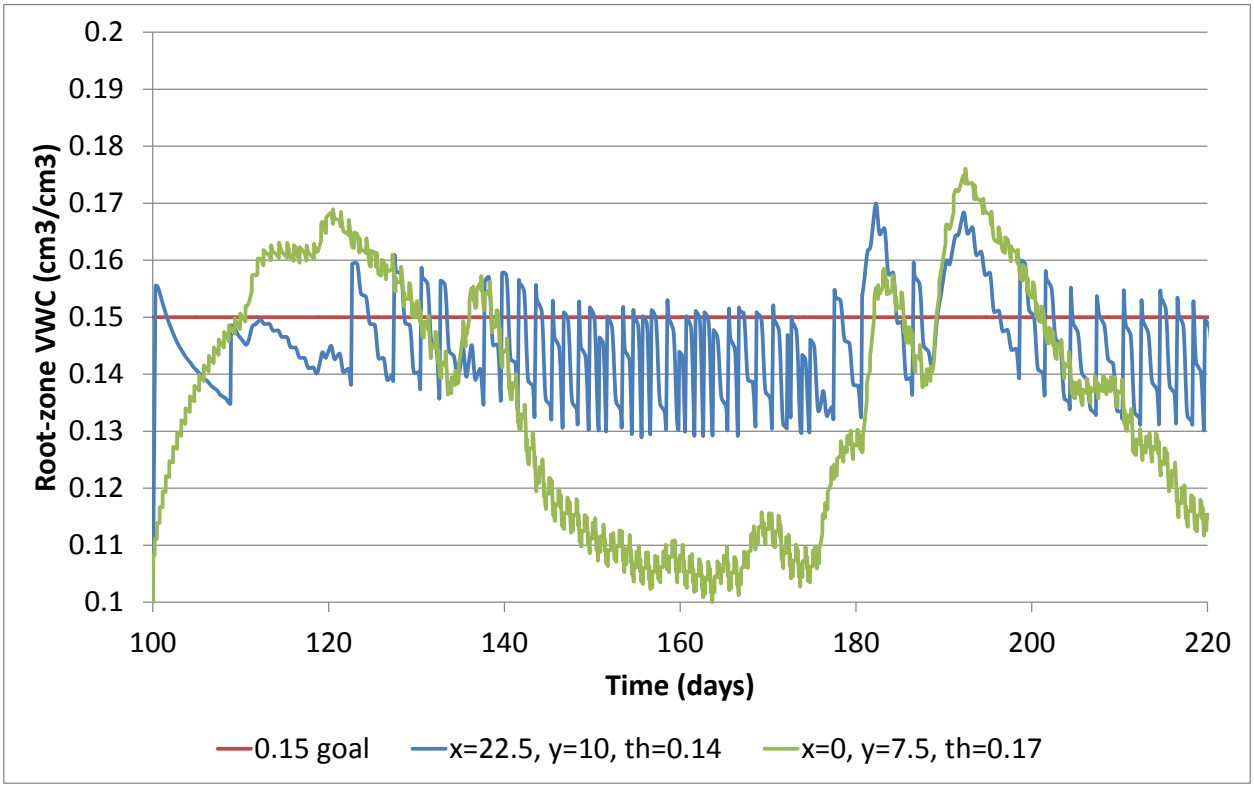

Figure 4-5. Root-zone VWC over time with different probe locations and thresholds for automated irrigation control.

Figure 4-6. Impact of probe location on the best threshold value for sensor controlled irrigation systems. Threshold values are assessed based on the system ability to control the root-zone soil moisture content with A) no rain and no crop, B) rain and no crop, C) rain and crop.

A

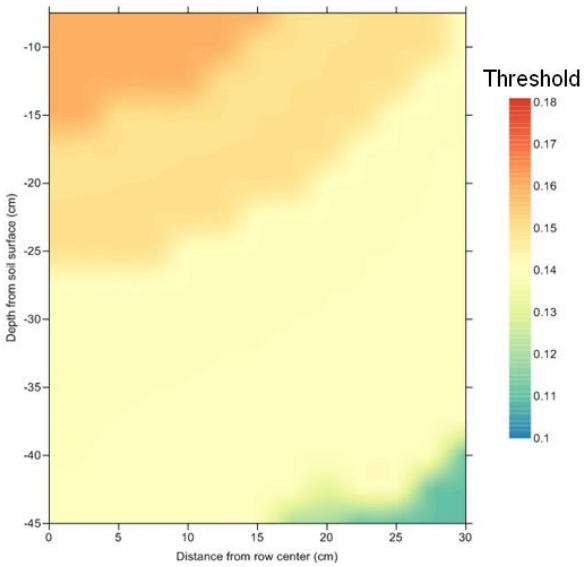
Threshold
0.18
0.17
0.16
0.15
0.14
0.13
0.12
0.11
0.1
Depth from soil surface (cm)
-10
-15
-20
-25
-30
-35
-40
-45
0
5
10
15
20
25
30
Distance from row center (cm)

B

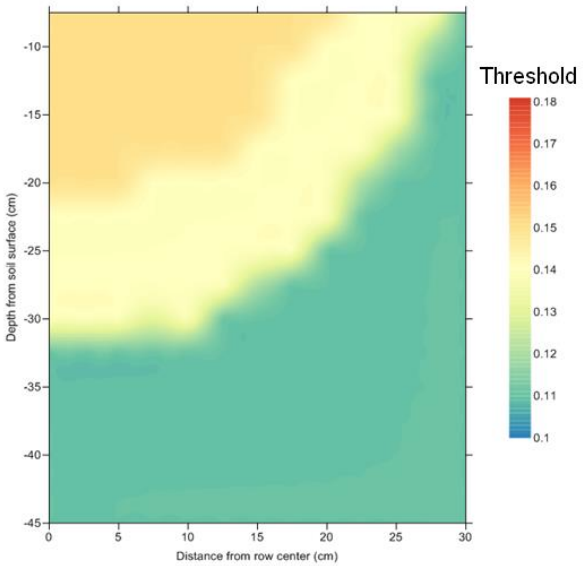
Threshold
0.18
0.17
0.16
0.15
0.14
0.13
0.12
0.11
0.1
Depth from soil surface (cm)
-10
-15
-20
-25
-30
-35
-40
-45
0
5
10
15
20
25
30
Distance from row center (cm)

C

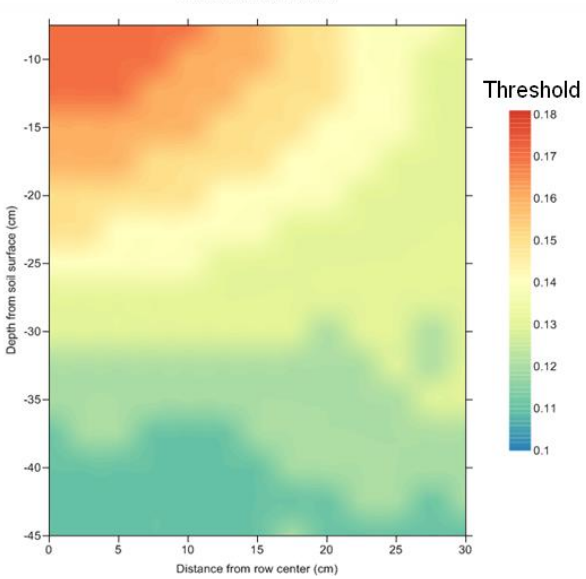
Threshold
0.18
0.17
0.16
0.15
0.14
0.13
0.12
0.11
0.1
Depth from soil surface (cm)
-10
-15
-20
-25
-30
-35
-40
-45
0
5
10
15
20
25
30
Distance from row center (cm)

CHAPTER 5
QUANTIFICATION OF GREENHOUSE GAS EMISSIONS FROM OPEN FIELD-GROWN FLORIDA TOMATO PRODUCTION

Background

Atmospheric carbon dioxide (CO_2) concentrations have been rising over the past several centuries from pre-industrial levels (World Meteorological Organization, 2006). The atmospheric concentration of CO_2 had risen to 380 ppmv in 2006 compared to 280 ppmv in the 1700s (World Meteorological Organization, 2006). Existing projections consistently estimate 2030 levels 25-90% higher than in the year 2000 (Rogner et al., 2007). This projected increase has the potential to affect the world's climate. Mid to late 21st century projections by Bernstein et al. (2007) show a likelihood for increased frequency of drought, heavy rainfall events, heat waves, and cyclones due to elevated atmospheric levels of GHGs. Hansen et al. (2006) considered a 1 °C temperature increase above 2000 levels to be dangerous based on predictions that this would cause sea level rise that could damage human populations and cause species extinction. The Copenhagen Accord set a goal of keeping global temperature increases within 2 °C of preindustrial levels in order to avoid "dangerous anthropogenic interference with the climate system" (Copenhagen Accord, 2009). Rogelj et al. (2010), however, argue that based on current emissions pledges, there is a greater than 50% probability that an increase of greater than 3 °C will occur. While the details of predictions are a subject for debate, due to uncertainty of and differences among climate projections, most in the scientific community agree that temperature increases of this magnitude would result in significant negative impacts and stresses on human developments and ecosystems (Fischlin et al., 2007; Meehl et al., 2007). Nevertheless, it is believed that these occurrences can be avoided with significant reductions in GHG emissions

(Meinshausen et al., 2009). It is therefore important to understand emissions from various actions and resources and to identify potential areas for emissions reductions.

The primary source of GHG emissions is fossil fuel used for transportation, construction, and energy (Del Grosso et al., 2008). Fossil fuel burning accounts for more than 75% of global CO_2 emissions (Snyder et al., 2009). However, the agricultural sector is considered a significant contributor (Smith et al., 2007). In 2005, agriculture was estimated to produce 10-12% of the global anthropogenic GHG emissions (Smith et al., 2007). However, a relatively low proportion of agricultural emissions (13%) are as CO_2 (Del Grosso et al., 2008). Instead, agriculture contributed to approximately 60% of global anthropogenic nitrous oxide (N_2O) emissions and 50% of global anthropogenic methane (CH_4) emissions (Smith et al., 2007). While other sectors contribute substantially greater total GHG emissions, mitigation in agriculture offers more cost-effective options (Smith et al., 2007). Therefore, a reasonable first step in GHG reductions in agriculture is to quantify emissions from specific sources in production and identify the most economically sensible options for reduction.

Studies have been conducted on the GHG emissions from many different agricultural products including wheat (*Triticum aestivum* L.; Brentrup et al., 2004), sugar cane (*Saccharum officinarum* L.; Barretto de Figueiredo et al., 2010), cotton (*Gossypium hirsutum* L.; Weinheimer et al., 2010), milk (Casey and Holden, 2003), beef (Beauchemin et al., 2010), and corn (*Zea mays* L.; Kendall and Change, 2009). Most of these studies involved agronomic crops or livestock, while a limited number of them have focused on high-value specialty vegetable crops, especially in the US.

Fresh field grown tomato (*Solanum lycopersicum*) production has historically been an important commodity in Florida, representing the state's second most valuable crop, accounting for 40% of total US fresh market production and 7.8% of Florida's total agricultural receipts value (Florida Department of Agriculture and Consumer Services, 2010). Florida ranks second nationally in fresh market vegetable production with 92,000 ha planted, depending on the season, with a farm value of US $1.9 billion in 2008-2009 (Florida Department of Agriculture and Consumer Services, 2010). Reports of GHG emissions from tomato production typically describe indoor greenhouse production (Muñoz et al., 2004; Antón et al., 2005), emissions from processing tomatoes (Andersson et al., 1998), or European production systems. Greenhouse tomato production is drastically different from field-grown tomato production. Processing tomato production differs from fresh market production by its use of a single mechanized harvesting event, lack of plastic-mulched-beds, and absence of plant staking or tying. However, reports of emissions for US field-grown tomato production are currently unavailable in the literature. Greenhouse gas emissions have also been shown to vary largely depending on location and implementation of varying management practices. Thus, the objective of this study was to quantify the GHG emissions of field-grown Florida tomatoes for the fresh market under typical production practices. Additionally, potential areas for emissions reductions were identified.

Estimation of Greenhouse Gas Emissions

Description of Typical Tomato Production System in Florida

Florida is an important production area for winter fresh-market tomatoes in the US with more than 13,000 ha planted annually (Florida Department of Agriculture and Consumer Services, 2010). Depending on market conditions, statewide production

value ranges from US $400 to $600 million annually. The tomato production system in Florida, which generally includes raised beds, polyethylene mulch, and seepage or drip irrigation, has been very effective in producing high tomato yields with production costs of US $37,000 per hectare (Olson et al., 2010). In seepage production, fertilizer is applied pre-plant during bed formation, while with drip it is applied both pre-plant and during the season through the drip tubing as 'fertigation'. Additional fertilizer can be added to seepage irrigated production systems but can be labor intensive and costly. The crop is planted from transplants produced within the State near tomato producing areas. Transplants are four to five weeks old depending on rate of development. Tomato beds are typically formed with 1.8 m spacing, with a plant spacing ranging from 46 to 66 cm and bed widths of 61 to 91 cm. Florida's warm and humid subtropical climate results in high insect, weed, and disease pressure that necessitate significant pesticide applications for protection of the high-value crop. Transplants are in the ground for 16-19 weeks, although extended seasons occur under certain circumstances. Fresh tomato harvesting is done manually, with workers filling buckets and carrying them to harvest trucks. At the end of the season the polyethylene mulch is removed, herbicide is applied to the crop, and the desiccated crop is disked into the soil to ensure decomposition.

System Boundaries

In order to quantify the GHG emissions from a season of typical Florida tomato production, the system boundaries needed to be determined. The emissions considered included those associated with the use of material inputs and farm operations, and include both direct emissions, which are emissions occurring on the farm due to production activities, and indirect emissions, which are released off-site but occur due to

the crop production. Farm operations account for both mobile and stationary tasks, while material emissions account for the GHGs released during the manufacturing, storage, packaging, and transportation of the material inputs. Thus, this analysis included primary and secondary emissions. For practicality purposes, tertiary emissions, which would include emissions involved in the manufacturing of equipment and structures, were not considered. This was for several reasons. For one, it could be difficult to characterize the typical amounts of machinery, building area, and irrigation infrastructure typically used. Second, appropriate emission factors that are accurate and updated are difficult to find in the literature (Roos et al., 2010). Lastly, many studies do not consider these tertiary emissions (Hillier et al., 2009; Kim et al., 2009; Robertson et al., 2000; Spreen et al., 2010), and in many cases, the tertiary emissions do not contribute significantly to overall emissions. Graboski (2002) estimated that less than 1% of the energy used in the production of corn ethanol is from the manufacturing of equipment and structures, such as irrigation systems and tractors. Ceschia et al. (2010) conducted a study of 11 crops in nine European countries and estimated the primary and tertiary emissions of various field operations. The tertiary emissions accounted for 3.3% of the total emissions from the field operations, which accounts for an even smaller percentage of the total emissions. Considering the input intensiveness of Florida tomato production, it is expected that the tertiary emissions in these systems would be minor relative to the other emissions and high crop yields. The analysis took into account the delivery of transplants to the farm, the manufacturing, transportation, and storage of material inputs, farm operations including field preparation, planting, spraying, irrigation, harvesting, terminating the crop, and transportation of seedlings to

the farm and of fruit to the packing-house. The analysis did not consider the production of the transplants, the packaging of fruits, or the delivery of fruits to market.

Input Data

A survey of the Florida tomato industry was conducted from January to July of 2011 in order to characterize the typical production practices in the region and the fuel usage associated with these practices. The producers surveyed constituted 65% of the average planted area for tomato production in Florida, with 65% of the area under seepage irrigation and 35% of the area under drip irrigation. The survey was conducted through personal interviews, phone interviews, and mailed questionnaires. Grower information was grouped by irrigation method, with seepage and drip systems being the predominant methods, since the irrigation method has an impact on management factors and pumping characteristics. Pumping fuel requirements were also affected by the water source, as surface water required less energy compared to ground water per volume of water pumped. The information collected consisted of the diesel fuel used in mobile management activities involving farm machinery, fuel usage for the transportation of tomato seedlings and fruit, irrigation pumping fuel requirements, fertilizer and lime application rates, standard cultural practices, and crop yields. This information is listed in Tables 5-1, 5-2, 5-3, 5-4, and 5-5. Fuel used for transportation was based on vehicle fuel efficiency, transport distance, carrying capacity of the vehicle, and amount of material to be transported. The length of polyethylene mulch and drip tubing used was computed based on a 1.8 m bed spacing, which equates to 5,468 meters of linear bed (lbm) per ha. The typical polyethylene mulch width used is 51 to 61 cm greater than the bed width to ensure adequate covering of the side of the beds and sufficient material for anchoring the mulch (Olson, 2011). The estimates used in these

calculations assumed the use of polyethylene mulch with a width of 147 cm, 1 mm thickness, and weight of 0.023 kg/m^2. The drip tape was assumed to weigh 0.010 kg/m. The surveyed fresh market yields were in the range of attainable yields reported in the literature (Scholberg, 1996). Average amounts of insecticide, herbicide, fungicide, and fumigant were estimated based on interviews conducted prior to this study by Glades Crop Care, Inc. (1999) with growers in tomato producing areas of Florida. Bacteriophage was not included in these calculations, as it is a biological control not a manufactured chemical, which would require specialized calculation of GHG emissions associated with its production.

Calculations

Due to the complexity and heterogeneity of vegetable production systems, detailed modeling requires detailed site-specific information. The goal of this study was to provide a useful approximation of GHG emissions for a typical field tomato production operation in Florida while requiring only commonly available inputs. Since tomato production in Florida occurs with a range of growing conditions and production practices, general methods were used to quantify GHG emissions from the various sources.

Emissions were expressed as CO_2 equivalents (CO_2-eq), which considers the global warming potential of various emission forms using a common unit. Conversion between emission gases was made according to the standard suggested by the Intergovernmental Panel on Climate Change (IPCC; Eggleston et al., 2006). One unit of CO_2 emission was defined as one unit of CO_2-eq, while one unit of CH_4 emitted was equivalent to 25 units of CO_2-eq, and one unit of N_2O was equivalent to 298 units of CO_2-eq. Absolute emissions represent the emissions associated with one tomato

growing season. Relative emissions were expressed as a season's emissions per unit fruit yield. All resulting emissions estimates are calculated using average input, operation, and emission factor values. Total emissions, however, were computed for low, average, and high values, thus giving a range of estimated emissions.

The emissions from crop agrochemical inputs were estimated using documented emissions values and input quantities. The agrochemicals, operations, and materials considered in the calculations are included in Tables 5-1, 5-2, 5-3, 5-4, and 5-5. The emissions occurring due to the manufacturing, storage, and transportation of these materials were estimated using emission factors presented by Lal (2004) and can be seen in Table 5-6. Uncertainties in these values are represented with the provision of low, average, and high values.

Diesel fuel usage for farm management and transportation was converted into carbon (C) content and then CO_2-eq using conversion factors defined by the United States Environmental Protection Agency (USEPA; 2005). Therefore, 1 L of diesel was assumed to have 0.73 kg of C, and one unit of C was assumed to have 3.67 units of CO_2.

Carbon dioxide emissions from the burning of polyethylene mulch and drip tape, which is a common practice in the industry, were calculated using the USEPA (2010) methodology for estimating CO_2 emissions from plastic combustion. By this method, high-density polyethylene (HDPE) or low-density polyethylene (LDPE) were both assumed to be constituted of 86% C and to have an oxidation fraction of 98%. The CO_2 emitted was then calculated as the product of the amount of plastic, the C content, the fraction oxidized, and a C to CO_2 conversion factor. Additionally the manufacturing of

plastic contributes GHG emissions in the forms of CO_2 and CH_4. Emissions were computed according to IPCC guidelines (Eggleston et al., 2006), with emissions factors of 3 kg CO_2/kg plastic and 1 kg CH_4/kg plastic.

In addition to the GHG emissions associated with the manufacturing and acquirement of N fertilizer, the application of N to the soil also results in the emission of GHG in the form of N_2O. These emissions occur both directly (on site) through nitrification and denitrification, and indirectly (off site) following leaching, runoff, and ammonia (NH_3) volatilization. While the emission of N_2O due to applied N has been shown to vary site-specifically (Snyder et al., 2009) as well as non-linearly with application rate (McSwiney and Robertson, 2005), a linear response of emissions to N application was assumed following the tier 1 IPCC guidelines (Eggleston et al., 2006). The emission factors used by these guidelines are shown in Table 5-7. Direct emissions were computed as the product of the direct N_2O emissions factor and the amount of N applied. Indirect N_2O emissions were broken down into those due to volatilization and those due to leaching or runoff. Each indirect emission path was calculated as the product of the amount of N applied, the fraction of N lost through that emission path, and the emission factor for that path. The only applied N considered was as applied fertilizer. While N in irrigation water can be a significant N source, its contribution is considered minor when irrigation water has a nitrate (NO_3) concentration of less than 45 ppm (Tak et al., 2012). A study of shallow groundwater samples, which generally have significantly higher NO_3 concentrations than surface water samples (Mueller and Helsel, 1996), from agricultural lands in Florida and Georgia found NO_3 concentrations generally well below 45 ppm, with a median concentration of 4.2 ppm (Berndt et al.,

1998). Thus, irrigation water was ignored as a source of N in the GHG emissions calculations.

Due to typically intense tillage practices and low initial soil organic matter that is typical of tomato production in this area, it was assumed that the soil neither sequestered nor released C. Thus, all tomato stem and root biomass was not considered as a C sink. It was assumed that tomato fruit would be respired following consumption. Therefore, C captured as fruit was also not considered a C sink in the calculations.

Emissions Estimates

The total average estimated GHG emissions due to the manufacture, storage, and transport of agrochemicals for seepage and drip irrigation systems were 9,728 kg CO_2-eq ha^{-1} and 9,889 kg CO_2-eq ha^{-1}, respectively, as shown in Figure 5-1. The largest contributors were N fertilizer, fungicide, and soil fumigant, accounting for 16.7%, 16.9%, and 33.8% of the average agrochemical emissions in drip systems, and 15.4%, 17.2%, and 34.4% of average emissions in seepage systems. Phosphorus (P) and potassium fertilizer resulted in low GHG emissions, accounting for 0.7% and 3.1% of the average agrochemical related emissions in drip systems, and 0.8% and 3.2% in seepage systems. All of the agrochemical GHG emissions were relatively equivalent between the two irrigation systems except the N fertilizer, which was 1,656 kg CO_2-eq ha^{-1} in the drip system compared to 1,496 kg CO_2-eq ha-1 in the seepage system. This is due to the typically higher application rates of N observed in drip compared to seepage systems, despite the potential for greater N use efficiency in drip systems compared to seepage systems.

The total GHG emissions from the operation of farm machinery was 1,276 kg CO_2-eq ha^{-1} for seepage irrigation systems and 1,180 kg CO_2-eq ha^{-1} for drip systems, as can be seen in Figure 5-2. The difference in emissions between the two irrigation systems is due to ditch maintenance being required in seepage systems while it is unnecessary in drip systems, which do not use ditches for supplying irrigation water. The field leveling, fungicide and insecticide spraying, and bed lying are the largest GHG emission categories, accounting for 19.7%, 16.8%, and 11.8% of the total machine operation emissions in seepage systems, and 21.3%, 18.1%, and 12.8% of the emissions in drip systems.

Additional GHGs were emitted because of chemical conversions in the field. The total GHGs released as field emissions were 3,089 kg CO_2-eq ha^{-1} for drip systems and 2,865 kg CO_2-eq ha^{-1} for seepage systems. The distribution of these emissions through different pathways is shown in Figure 5-3. The largest amount of GHGs was emitted through nitrification and denitrification, which accounted for 51.3% of all field emissions in average seepage systems and 52.7% in drip systems. Emissions that resulted from the field were considered direct emissions, while losses of substances from the field that are assumed to result in emissions away from the field are considered indirect emissions. Since lime dissolution results in the emission of CO_2 from the field, GHGs emitted through this pathway were considered direct emissions. Nitrification and denitrification occur within the soil and result in losses of N_2O directly from the field; therefore, they were also considered a direct emission. Volatilization results in the loss of NH_3 from the field. Ammonia is not a GHG, but some of this N in the atmosphere can return to the soil through atmospheric deposition, of which a certain amount will be

nitrified, denitrified, or lost as N_2O. Since this release is occurring off the farm, this is considered an indirect emission. Similarly, N lost through leaching, erosion, or runoff is not directly lost from the field as GHGs. However, some of this N will eventually be returned to a field, where some of it will be nitrified or denitrified, resulting in the release of N_2O. Thus, this pathway also results in indirect emissions. Indirect emissions accounted for 21.8% of the field emissions in seepage systems and 22.4% of these emissions in drip systems. The main source of field emissions was N fertilizer, as 73.1% and 75.1% of the field emissions were due to N fertilizer in the seepage and drip irrigation systems, respectively. The difference in emissions between the two irrigation systems was due to the typically higher use of N fertilizer in drip irrigation systems, as mentioned previously.

The use of pumps for supplying irrigation water resulted in GHG emissions dependent on both the irrigation type and water source used. The overall average emissions results are shown in Figure 5-4. Systems with drip irrigation and surface water had emissions of 996 kg CO_2-eq ha^{-1}. Systems with drip irrigation and well water had emissions of 5,976 kg CO_2-eq ha^{-1}. Systems with seepage irrigation and surface water had emissions of 449 kg CO_2-eq ha^{-1}, while systems with seepage irrigation and well water had emissions of 2,696 kg CO_2-eq ha^{-1}.

The use of plastic also results in the emission of GHGs. These emissions are due to both the manufacturing of the plastic and the disposal of the plastic (i.e., burning). This resulted in the emission of 735 kg CO_2-eq ha^{-1} in the manufacture of plastic for drip irrigation systems compared to 571 kg CO_2-eq ha^{-1} for seepage irrigation systems as well as the emission of 751 kg CO_2-eq ha^{-1} from burning of the plastic for

drip irrigation systems compared to 583 kg CO_2-eq ha^{-1} in seepage irrigation systems. Overall, plastic manufacturing and burning results in the emission of 1,486 kg CO_2-eq ha^{-1} in drip irrigation systems compared to 1,154 kg CO_2-eq ha^{-1} in seepage irrigation systems. The difference in emissions between the two systems is due to the absence of drip tape in seepage systems, which results in less plastic manufacturing and burning, while both systems utilize polyethylene mulch.

The transport of transplants from the nursery to the field accounted for a negligible amount (2 kg CO_2-eq ha^{-1}) of GHG emissions due to the large number of seedlings that could be carried on each truck as well as the proximity of transplant houses to tomato production areas. The transport of the fruit from the field to the packinghouse, however, resulted in the emission of 708 kg CO_2-eq ha^{-1}.

Overall, the least GHGs were emitted from the seepage irrigation system with a surface water supply, which resulted in an average estimated emission of 16,183 kg CO_2-eq ha^{-1} or 0.19 kg CO_2-eq kg $fruit^{-1}$. Seepage irrigation systems with well water supplies resulted in greater emissions of 18,429 kg CO_2-eq ha^{-1} or 0.22 kg CO_2-eq kg fruit-1. Drip irrigation systems with surface water supplies resulted in comparable emissions of 17,446 kg CO_2-eq ha^{-1} or 0.21 kg CO_2-eq kg $fruit^{-1}$, while drip irrigation systems with well water supplies resulted in the largest emissions of 22,426 kg CO_2-eq ha-1 or 0.27 kg CO_2-eq kg $fruit^{-1}$. Thus the average total GHG emissions from the different irrigation type-water source combinations ranged from 16,183 kg CO_2-eq ha^{-1} (0.19 kg CO_2-eq kg $fruit^{-1}$) to 22,426 kg CO_2-eq ha^{-1} (0.27 kg CO_2-eq kg $fruit^{-1}$). Considering the uncertainty range of the emission factors, the total GHG emissions ranged from 8,267 kg CO_2-eq ha^{-1} (0.10 kg CO_2-eq kg $fruit^{-1}$) to 40,307 kg CO_2-eq ha-1

(0.48 kg CO_2-eq kg $fruit^{-1}$). Finally, when accounting for the uncertainty range of the emission factors and of the production practices, the total GHG emissions ranged from 6,318 kg CO_2-eq ha^{-1} (0.06 kg CO_2-eq kg $fruit^{-1}$) to 52,813 kg CO_2-eq ha-1 (0.75 kg CO_2-eq kg $fruit^{-1}$).

Implications

The GHG emissions estimated from this study for fresh field grown Florida tomato production are consistent with emissions from production of other fruit and vegetable crops. The emissions estimates of this study are similar to estimates of 0.24-0.48 kg CO_2-eq kg $pineapple^{-1}$ for pineapple (*Ananas comosus*) produced in Costa Rica (Ingwersen, 2012), 0.27-1.36 kg CO_2-eq kg $strawberry^{-1}$ for strawberries (*Fragaria ananassa*) produced in Spain and the United Kingdom (Mordini et al., 2009), and 0.08-0.33 kg CO_2-eq kg $orange^{-1}$ for oranges (*Citrus sinensi*) produced in Spain, Italy, and Brazil (Mordini et al., 2009). This study's estimates were generally higher than estimates of 0.10-0.16 kg CO_2-eq kg $potato^{-1}$ for potato (*Solanum tuberosum*) produced in Sweden (Roos et al., 2010) and 0.10-0.14 kg CO_2-eq kg $carrot^{-1}$ for carrot (*Daucus carota*) produced in Denmark, the Netherlands, Germany, Great Britain, Italy, and Sweden (Carlsson, 1997). This study's estimates were generally lower than those of grain and oilseed crops, with estimates of 0.45-0.52 kg CO_2-eq kg $seed^{-1}$ for oilseeds (*Brassica napus*, *Brassica rapa*, *Brassica juncea*, *Brassica juncea*, *Sinapis alba*) grown in Canada (Gan et al., 2012), 0.80 kg CO_2-eq kg $wheat^{-1}$ for wheat produced in the United Kingdom (Williams et al., 2006), 1.7 kg CO_2-eq kg $seed^{-1}$ for rape seed (*Brassica napus*) produced in the United Kingdom (Williams et al., 2006), and 0.25-0.82 kg CO_2-eq kg $corn^{-1}$ for corn produced in the United States (Kim et al., 2009). Studies of tomatoes grown in many European countries reported emissions of 0.43-9.4 kg CO_2-eq

kg tomato^{-1} (Carlsson, 1997; Williams et al., 2006). The upper end of this emissions range were much higher than this study's emissions estimates due to the production having occurred in greenhouses in cold climates where the dominant emissions source was heating. The lower end of this emissions range was estimated from tomato production in Spain, where open-field production is used. These estimates were similar to this study's estimates, although on the high end of the estimated emissions range.

Results indicated that irrigation and agrochemicals were the leading categories for GHG emissions, with irrigation accounting for 2.8% to 26.6% of average emissions estimates and agrochemicals accounting for 44.1% to 60.1%, depending on irrigation method and water source. For systems with lower pumping demand, agrochemicals become an increasingly dominant factor for GHG emissions. For systems with high pumping demand, irrigation becomes a greater emissions source. Field GHG emissions were the third largest emissions category, ranging from 13.8% to 17.7% of the average estimated total GHG emissions depending on irrigation method and water source. Considering that 73.1% to 75.1% of these GHG emissions were due to N fertilizer, and that 15.4% to 16.7% of the average agrochemical related emissions are due to N fertilizer, it should be noted that the impact of N fertilizer could be significant. This underlines the importance of efficient N and irrigation management.

Recent surveys show that common industry practice is to apply N at significantly higher rates than recommended, especially in southern areas of Florida, on seepage irrigated fields, and during the fall season, which is characterized by high temperatures and rainfall (Cantliffe et al., 2009). The current N rate recommendation by the University of Florida/Institute of Food and Agricultural Sciences (UF/IFAS) is 224 kg N/ha plus a

13.7 kg N/ha supplemental N application for tomato grown at any location, using any irrigation method and any planting season (Olson et al., 2010). N application rates observed in this study exceeded this recommendation. Considering that between 17.7% and 22.8% of the average total GHG emissions in this study were due to N fertilizer, it is evident that major emission reductions could be obtained by more efficient N fertilizer management. The potential for savings can be significant as the recommended rates are intended to reflect the crop nutrient requirement. This means that any residual plant available N in the soil or supplied from irrigation water or other non-fertilizer sources will contribute an amount that does not need to be supplied as fertilizer and thus can be subtracted from the recommended N rate application. Thus, the excess fertilizer applied is likely underestimated by the simple difference between the actual application rate and the maximum recommended rate. Additionally, there is evidence that N_2O emissions increase rapidly when fertilizer is applied beyond yield response (McSwiney and Robertson, 2005), thus the potential for savings may be underestimated by this study.

Realistically, the N application rates cannot be expected to match the recommended rates as it is uncertain whether recommendations accurately reflect the dynamics occurring under particular growing conditions. Numerous studies have reported that temporary water table rises during heavy rainfall periods and/or for frost protection events, different lengths of growing season, the use of vigorous hybrid cultivars, and/or denitrification justify the use of fertilizer beyond the recommended rates (Simonne and Ozores-Hampton, 2006; Fraisse et al., 2010). Additionally, extra fertilizer offers an inexpensive insurance at a cost that is offset by very small yield increases (Cantliffe et al., 2009). It has been suggested that the situation can be improved,

gradually and iteratively, through the creation of flexible recommendations reflective of farm operational realities and continual communication with producers (Simonne and Ozores-Hampton, 2006). Therefore, improved management could result not only in the typically motivating reductions in N runoff and leaching, but also in reduced GHG emissions to mitigate the severity of adverse impacts of global climate change.

While N management is impactful on GHG emissions from tomato production, irrigation management is even more so, as its influence is two-fold. First, irrigation accounted for significant GHG emissions, ranging from 2.8% to 26.6% of average estimated total emissions. Second, irrigation has a fundamental effect on nutrient management, as an ample amount of nutrients will be rendered insufficient if the water is improperly managed. Simonne and Ozores-Hampton (2006) suggest that pollution reductions should be approached with the goal of improving water management rather than reducing N fertilizer application. Nitrate moves rapidly with water, and under drip irrigation it has been shown that most of the nitrate collects near the fringe of the wetting front (Li et al., 2003). In Florida, where sandy soils are common, the low water holding capacities and high hydraulic conductivities encourage more vertical movement of the wetting front. Therefore, drip systems must be managed to supply adequate amounts of water while containing NO_3 within the root-zone and minimizing leaching. Under seepage systems, the water table should be maintained at appropriate depths throughout the season based on the crop development stage. Shukla and Jaber (2005) demonstrated that under seepage irrigation, the water table in soils typical to South Florida raised an average of 16 times the rainfall amount. Pollutant outflows from such production systems have become an increasing public concern as such production

areas have been considered a major contributor to surface water quality degradation (Breve et al., 1997). Appropriate irrigation management can help reduce some of these undesirable contributions, as well as reducing GHG emissions from pumping and N fertilizer application.

In such a highly interactive system, it is interesting to examine the consequences of particular management decisions. The use of polyethylene mulch, for example, accounts for between 5.1% and 7.1% of the average estimated total GHG emissions. However, in many other ways, polyethylene mulch applications help reduce GHG emissions. Polyethylene mulched beds have been shown to reduce N leaching due to heavy rain events by promoting water flow around, rather than through, the fertilized bed (Hochmuth et al., 2008). This can reduce the fertilizer rate needed and reduce the indirect GHG emissions from leached N. Polyethylene mulch has also been shown to reduce evapotranspiration (ET) 10% to 30% (Simonne, Dukes et al., 2010), which allows for reduced irrigation requirements and thus reduced GHG emissions due to pumping. Additionally, polyethylene mulch reduces weed growth and increases crop yields, allows for reduced herbicide application and greater yield per unit of emission. Thus, overall, the use of polyethylene mulch represents a net GHG emission savings despite the emissions associated with its manufacturing and disposal. Nevertheless, approximately half of the GHG emissions associated with polyethylene mulch were released from the burning of the polyethylene mulch for disposal. Alternative methods of disposal, especially ones that could recycle or re-purpose it, could further reduce production related GHG emissions.

Intensive agricultural production results in large emissions per unit area of production. However, when intensive production results in elevated yields, it can result in more efficient crop production from an emissions standpoint. The impact of high yields is two-fold, as higher yields also led to a reduction of the emissions per unit weight of fruit produced. It has been shown that intensive high-yielding production systems result in reductions in net reduction in GHG emission per unit of production compared to less intensive production (Burney et al., 2010). Maintaining highly productive land or increasing the productivity of land can also reduce the need to develop new lands. This can prevent significant amounts of GHG emissions, as typically between 30 and 50% of the carbon present in native ecosystems is lost when converted to agriculture (Guo and Gifford, 2002). Thus, management that maintains optimal yields should be essential, from both an economic and a GHG emission perspective.

These calculations were intended to provide a simplified, practicable estimate of the GHG emissions from these production systems. Yet, there is certainly a great degree of uncertainty in many of the estimates. For example, the GHG emissions estimates for the manufacturing, transportation, and storage of N used estimates from Lal (2004), which were based on a range of values reported in the literature. However, these estimates may not accurately reflect other systems due to the particular N fertilizer type, the factory efficiency, and locations of the factory, distributor, and farming operation specific to each system. For particular systems, these details could be determined more accurately, and could be entered into the framework of this methodology on a site-specific basis.

However, the GHG emissions due to the application of N were calculated based on a simplified representation of the system dynamics, and a more complex methodology would be needed to capture the dynamics that vary site-specifically. Denitrification typically converts NO_3- to N_2, but an amount of N is released as N_2O gas at a rate depending on dynamics involving NO_3- concentration, water content, temperature, C , and other factors (Bedard-Haughn, 2006). Nitrification typically converts NH_4+ into NO_3-, but when nitrifying bacteria is oxygen limited, nitrite is used as a terminal electron acceptor instead, resulting in the release of nitrous oxide and nitric oxide as well (International Fertilizer Industry Association and the Food and Agriculture Organization of the United Nations, 2001). Further, indirect GHG emissions can be created from N volatilization that will eventually be returned to soils through deposition and a portion eventually emitted as N_2O, and through NO_3- runoff and leaching, which will result in N_2O emissions offsite through denitrification (Del Grosso et al., 2006). The overall rate of N_2O production can vary largely and depends on site-specific conditions including climate, N fertilizer management, soil drainage, soil texture, soil pH, soil organic matter, crop type, tillage, and irrigation (International Fertilizer Industry Association and the Food and Agriculture Organization of the United Nations, 2001). As such, site-specific estimates would need to consider more detailed information than was intended for the purpose of this study. Thus a simplified approach was adopted, as has been done in similar studies (e.g., Hillier et al., 2011), in order to provide a reasonable yet feasible estimate. However, it could be argued that higher GHG emission factors should be chosen due to the warm, humid climate, intensive fertilizer rates, elevated water tables, and sandy soils prevalent in typical Florida growing conditions. It could

also be argued that denitrification rates should be higher under seepage systems compared to drip irrigation due to the greater volume of soil being held at high water contents. Nevertheless, detailed measurements would be necessary to dictate such adjustments.

Summary

The average estimated total GHG emissions associated with typical production of fresh open field-grown Florida tomatoes was estimated to range from 16,183 kg CO_2-eq ha^{-1} (0.19 kg CO_2-eq kg $fruit^{-1}$) to 22,426 kg CO_2-eq ha^{-1} (0.27 kg CO_2-eq kg $fruit^{-1}$), depending on irrigation type and water source. Considering uncertainties in the emission factors, the average estimated emissions ranged from 8,267 kg CO_2-eq ha^{-1} (0.10 kg CO_2-eq kg $fruit^{-1}$) to 40,307 kg CO_2-eq ha^{-1} (0.48 kg CO_2-eq kg $fruit^{-1}$). While these represent typical GHG emissions, site-specific information could be used within this methodology to estimate more accurately the GHG emissions of a particular tomato producer. Emissions estimates considering the range of production practices and the emission factor uncertainty ranged from 6,318 kg CO_2-eq ha^{-1} (0.06 kg CO_2-eq kg $fruit^{-1)}$ to 52,813 kg CO_2-eq ha^{-1} (0.75 kg CO_2-eq kg $fruit^{-1}$). Similar methodologies could also be applied to other crops and production areas. Improvements in irrigation management, N management, and polyethylene mulch disposal were identified as areas with the greatest and most feasible potential for GHG emissions reductions.

Table 5-1. Diesel fuel use by machine operation for typical Florida tomato production practices. Data determined from Florida tomato grower survey.

Machine Operations	Diesel (l/ha)		
	Low	Average	High
Disking	18.7	35.5	35.5
False bedding	18.7	37.4	37.4
Bottom fertilizer mix application	16.8	22.4	22.4
Making beds	35.5	56.1	56.1
Plastic application	9.4	18.7	18.7
Cutting ditches	9.4	11.2	11.2
Punching holes	7.0	9.4	9.4
Planting	7.0	9.4	9.4
Driving stakes	15.0	15.0	28.1
Ditch Maintenance	14.0	35.5	35.5
Fungicide & insecticide	53.0	79.5	79.5
Herbicide	9.2	13.1	13.1
Drip - Surface Water	251.7	370.1	575.8
Drip - Well Water	1,510.1	2,220.7	3,455.1
Seepage - Surface Water	133.6	167.0	225.9
Seepage - Well Water	801.4	1,001.8	1,355.4
Leveling	74.8	93.5	93.5
Mowing	7.0	9.4	9.4
Lifting plastic	25.7	28.1	28.1

Table 5-2. Agrochemical use for typical Florida tomato production practices. Data determined from Florida tomato grower survey.

Agrochemical	Amount Applied (kg/ha)		
	Low	Average	High
Nitrogen (Drip)	291	347	404
Nitrogen (Seepage)	269	314	359
Phosphorus	67	101	135
Potassium	448	560	673
Fungicide	45[a]	117 [a]	204 [a]
Insecticide	41 [a]	47 [a]	55 [a]
Herbicide	39 [a]	42 [a]	45 [a]
Fumigant	117 [a]	234 [a]	336 [a]
Lime	1121	1681	2242

[a]Denotes active ingredient

Table 5-3. Plastic use for typical Florida tomato production practices. Data determined from Florida tomato grower survey.

Plastic material	Amount
Meters of linear bed per hectare	5,468
Polyethylene mulch width (cm)	147
Polyethylene mulch weight (kg/m^2)	0.023
Drip tube weight (kg/m)	0.010
Plastic disposal method	Burning

Table 5-4. Transportation practices for typical Florida tomato production practices. Data determined from Florida tomato grower survey.

Transportation detail	Amount
Number of seedlings per truck	169,400
Distance from nursery to field (km)	64
Truck fuel efficiency (km/l)	5.1
Bins of fruit shipped per truck (1 bin = 227 kg)	48
Distance from field to packing house (km)	72
Truck fuel efficiency (km/l)	2.1
Pallets Shipped per truck	24
Boxes of fruit per pallet (1 box = 11.3 kg)	70
Truck fuel efficiency (km/l)	2.1

Table 5-5. Crop production details for typical Florida tomato production. Data determined from Florida tomato grower survey.

Production	Low	Average	High
Plant density (plants/ha)	8,270	9,630	11,860
Crop yield (kg/ha)	70,000	84,000	98,000
Growing period (weeks)	16	17	20

Table 5-6. Carbon emissions for the manufacturing, transporation, and storage of input materials or agrochemicals. Includes low, average, and high value estimates according to Lal (2004).

Material	Carbon emission (kg C/kg substance)		
	Low	Average	High
Nitrogen fertilizer	0.90	1.30	1.80
Phosphorus fertilizer	0.10	0.20	0.30
Potassium fertilizer	0.10	0.15	0.20
Lime	0.03	0.16	0.23
Herbicide	1.70	6.30	12.6
Insecticide	1.20	5.10	8.10
Fungicide/fumigant	1.20	3.90	8.00

Table 5-7. Emission factors used for estimating N_2O emissions from N fertilizer and lime. Includes low, average, and high estimates derived from the IPCC (Eggleston et al., 2006) guidelines.

Emission Factor	Low	Average	High
Emission factor for direct N_2O emissions	0.0030	0.0100	0.0300
Fraction of N fertilizer that volatilizes	0.0500	0.2000	0.5000
Emission factor for volatilized N	0.0020	0.0100	0.0500
Fraction of N fertilizer that leaches	0.1000	0.3000	0.8000
Emission factor for leached N	0.0005	0.0075	0.0250
Emission factor for applied lime	0.1200	0.1250	0.1300

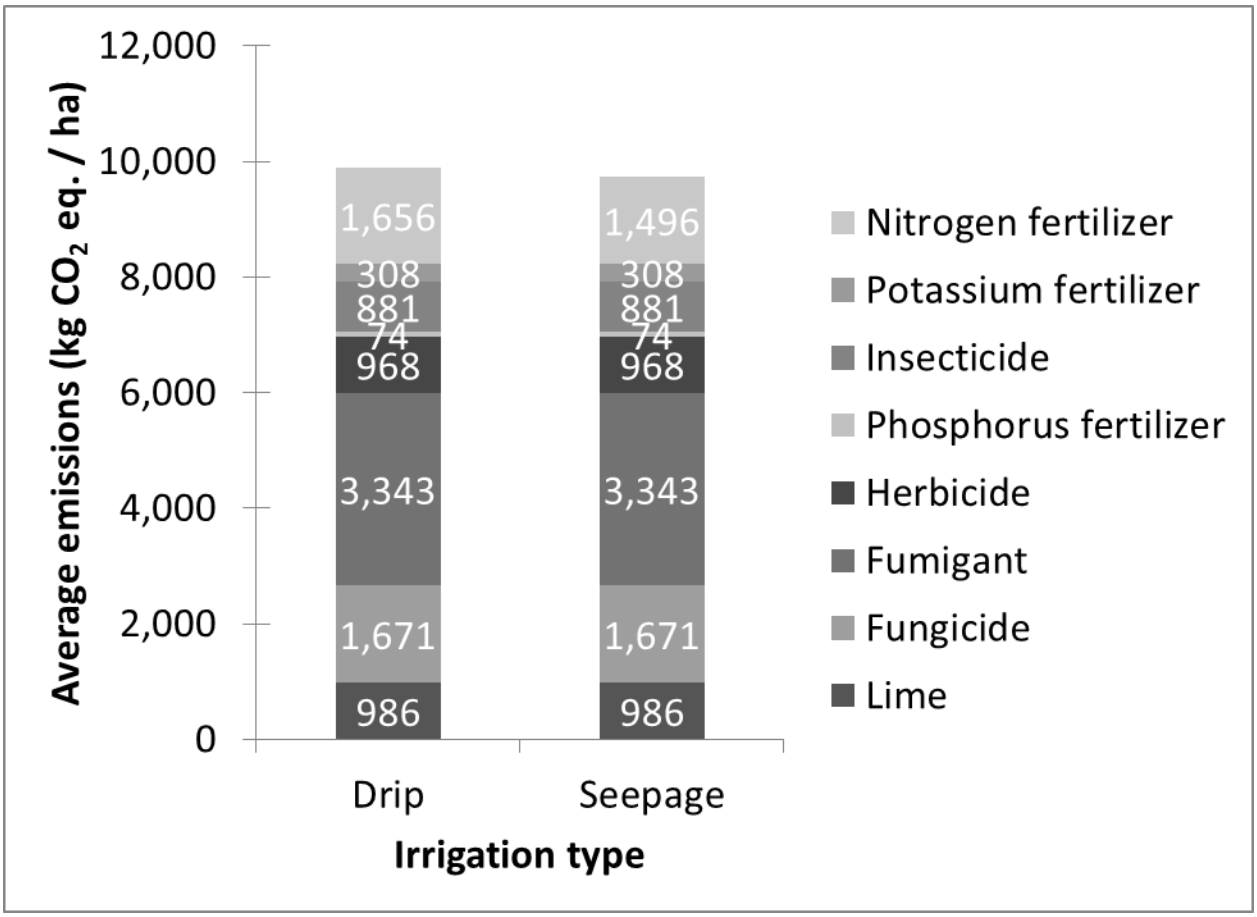

Figure 5-1. Greenhouse gas emissions due to production, transportation, and storage of agrochemicals. Emissions are estimated for typical drip and seepage irrigated tomato production systems in South Florida.

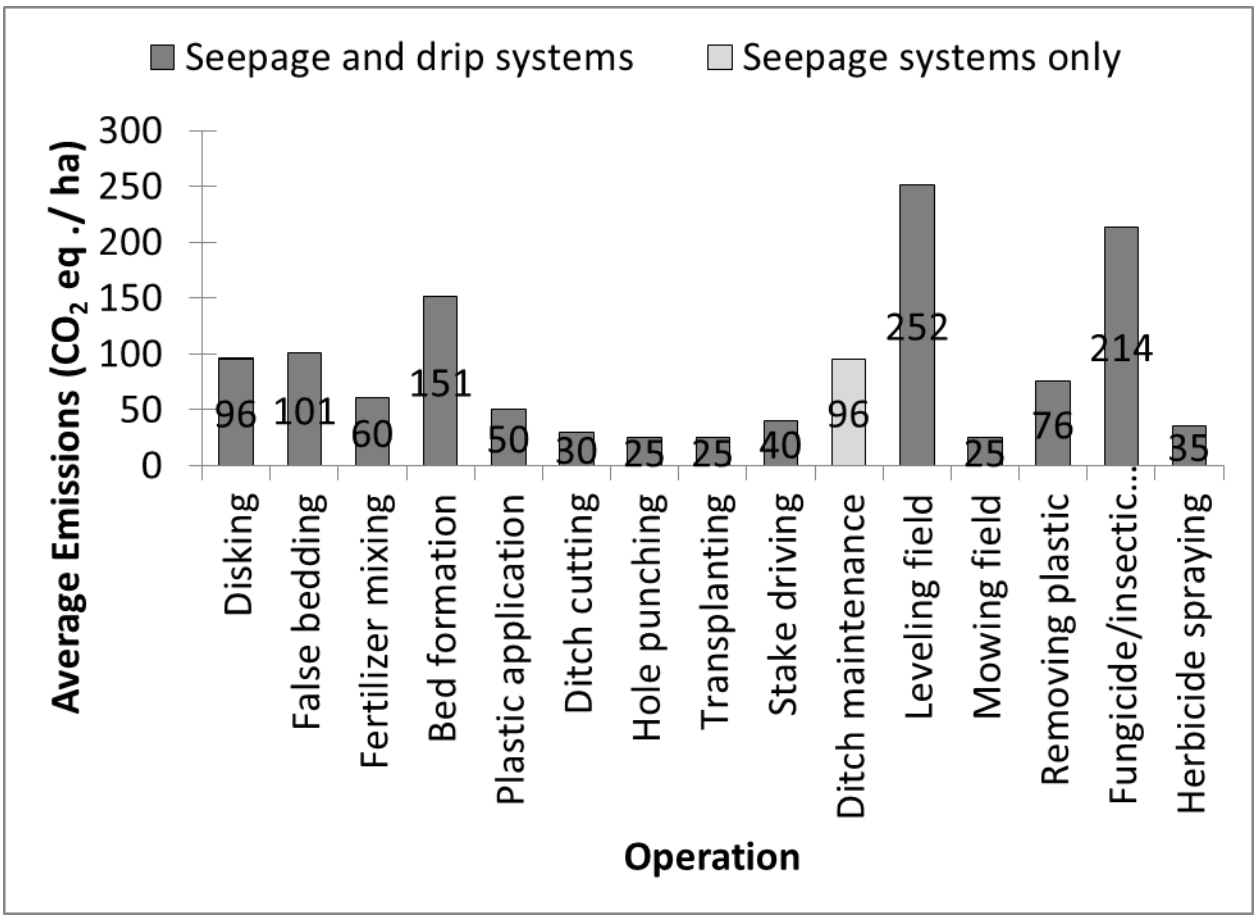

Figure 5-2. Greenhouse gas emissions due to farm machinery operations. Emissions are estimated for typical tomato production systems in South Florida.

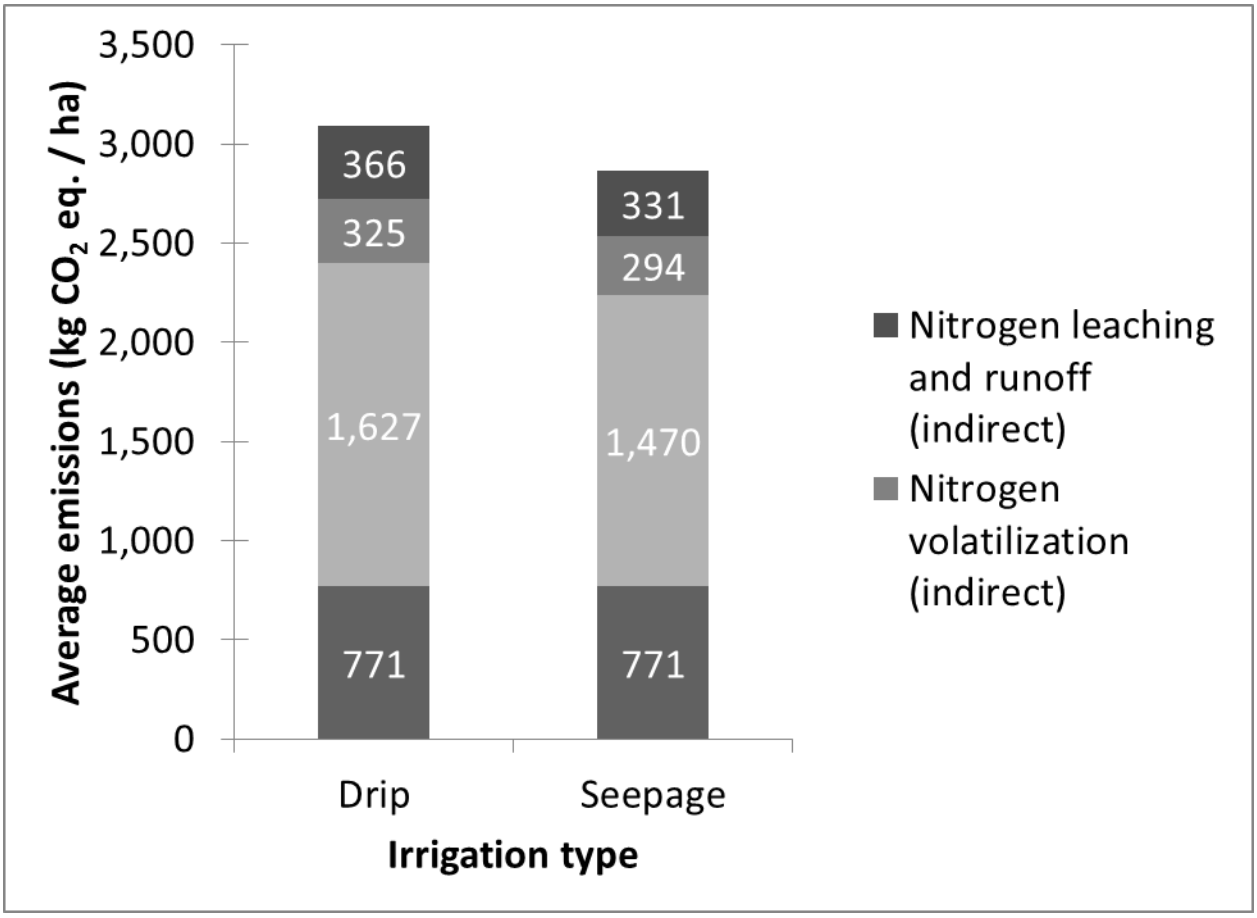

Figure 5-3. Greenhouse gas emissions from field losses. Emissions are for typical drip and seepage irrigated tomato production systems in South Florida.

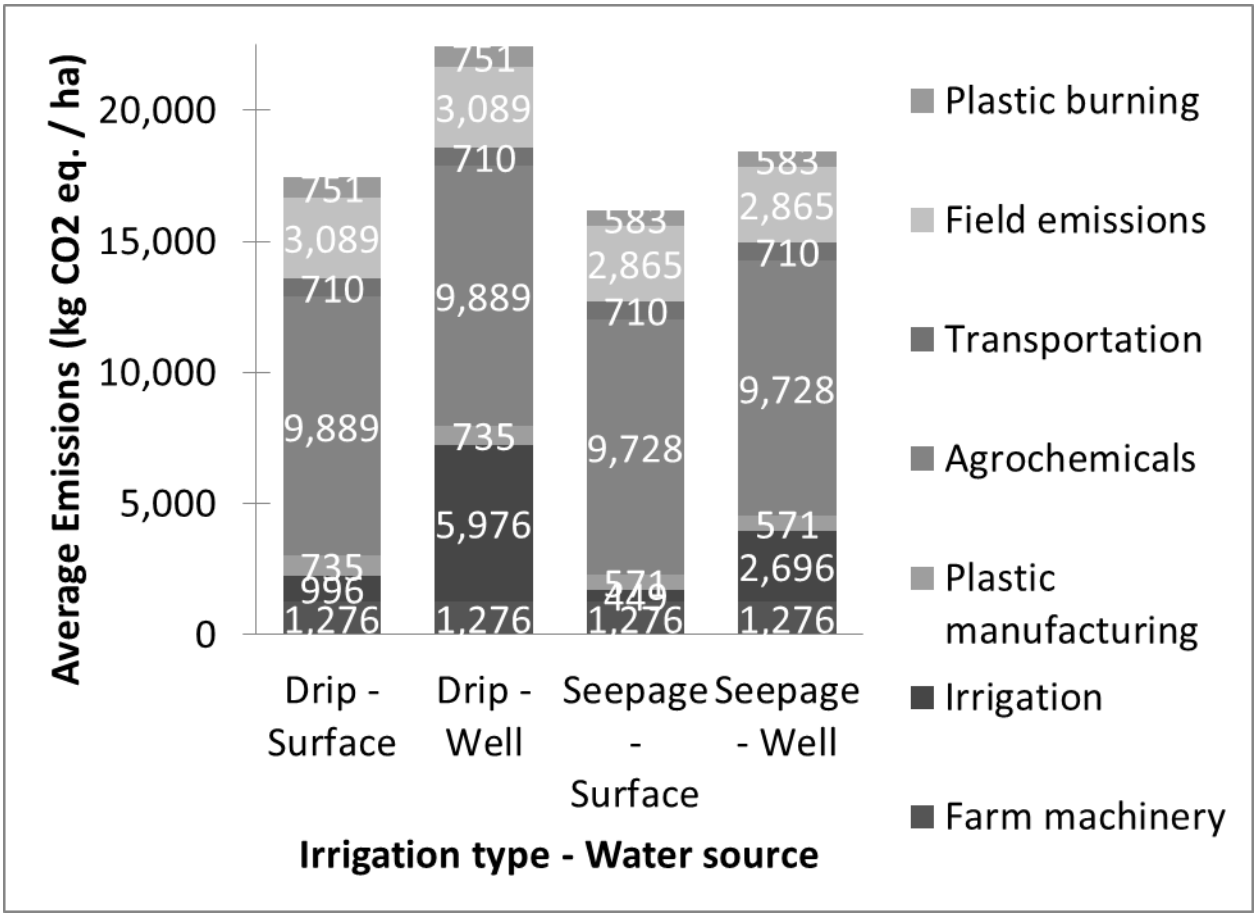

Figure 5-4. Total greenhouse gas emissions estimates. Emissions are reported for drip and seepage irrigated tomato productions systems with surface and well water sources.

CHAPTER 6
CONCLUSIONS

This research consisted of the development and utilization of methods for quantitatively estimating the impacts of agricultural production and management on production efficiency and environmental impacts. An emphasis was placed on drip irrigation management, which is an already common technology in Florida vegetable production that is likely to become more widespread as pressure grows to improve production efficiency. While much of this research focused on irrigation management, emphasis was also placed on the complex interactions within these systems, including the intrinsic link between soil-water dynamics and soil-nitrogen dynamics, both of which have major impacts on the GHG emissions associated with production.

Specifically, a two-dimensional water balance model was implemented within the DSSAT-CSM by a group of DSSAT developers in order to allow this widely used software to simulate water-limited production under drip irrigation and production practices typical for vegetable production in Florida. The water balance was designed to provide a practical, simple, and computationally efficient solution. As such, flexibility was allowed for the input requirements to operate the model, with an approximate parameterization method being created to allow the model to be run using only the standard DSSAT soil hydraulic property inputs.

The DSSAT-2D model was evaluated against lab measurements, benchmark models, and field-measured data to assess its ability to simulate soil-water dynamics under drip irrigation regimes. The evaluation of the three-point DSSAT parameter estimation methodology indicated that overall the methodology provided unbiased characterization of SMRCs. However, the limited range of measurements utilized for

these estimates reduced the predictive ability. As such, predictions were shown to perform more accurately at tensions near the three measurements points and to perform much less accurately at tensions distant from these measurement points. Characterization of SMRCs was improved when estimated using the RETC software, which utilized all available SMRC measurements. Thus, detailed measurements of soil hydraulic properties would be expected to improve the accuracy of the model parameter estimations and, consequentially, soil-moisture simulations.

Benchmark comparison of DSSAT-2D against HYDRUS-2D revealed great similarity between the two models for uniformly textured soils. These similarities indicated that the different numerical solving techniques, boundary conditions for representing drip tape, and discretization of the soil-simulation space of the two models resulted in comparable predicted outcomes. However, the large and persistent divergence between the model simulations for layered soils indicated that for sharply layered soils, DSSAT-2D simulations should be considered with caution. Steps were taken to improve simulation performance for layered soils. However, while these modifications were shown to improve the model performance, the adjusted model still produced simulations that were consistently divergent from the expected system behavior in layered soils.

Field trials were conducted in order to evaluate the combined parameterization and soil-water flow calculation methodologies of DSSAT-2D in an applied setting. The evaluation indicated that, overall, the model sufficiently simulates the soil-water dynamics of an unplanted, drip-irrigated, and fairly uniform soil. Model runs using the parameters estimated from more detailed soil hydraulic property measurements were

shown to improve the accuracy of the soil-moisture simulations compared to simulations using the parameters estimated using the three-point DSSAT methodology. However, simulations using both parameter sets were representative of the measured soil-water dynamics. When the uncertainty in the soil-water measurements is considered, the model simulations appear increasingly apt.

Model simulation experiments yielded many implications for drip irrigation management. Model simulations indicated that the soil-moisture dynamics of a particular soil are dominated by the irrigation amount and ET demand. Thus, managers will increase their water use efficiency the greatest if they can apply irrigation in amounts synchronous with crop demand and in consideration of the soil conditions and hydraulic properties. Simulation experiments did indicate that, while of much less importance, water application splitting and irrigation application rate do have an effect on soil-moisture dynamics. Leaching of water from the root-zone was consistently reduced at lower emitter rates. Splitting applications generally reduced water loss from the root-zone, but the effect depended on the manner in which the splitting method distributed the irrigation events rather than the actual number of irrigation events over which the method split the total irrigation.

Simulation experiments were also conducted to consider the impact of different implementations of automated soil moisture sensor based drip irrigation systems. A methodology was demonstrated for the site-specific identification of optimal probe locations and soil-moisture threshold values. This methodology can be applied for other specific production sites and setups using automated drip systems. The analysis also identified the impacts that rainfall, ET rate, and distribution of root water uptake have on

the ability of automated irrigation to control the soil moisture within desirable ranges. The impact of the implementation of automated soil moisture sensors on water use and ability to maintain desirable root-water content is further indication that these systems must be managed properly in order to maximize the potential benefits.

While the focus of this research was on irrigation efficiency, agricultural production systems are very interactive. Soil-water flow is known to have a strong effect on soil-nutrient movement. This is especially true for nitrate-N, which moves rapidly with water and has been shown to tend to collect around the extent of the wetting front (Li et al., 2003). Irrigation has a strong impact on soil-water dynamics. This is especially true under plastic-mulched raised beds, which reduce the influence of rainfall on the soil-water regime. Thus, irrigation management practices which more efficiently provide the necessary root-available water for optimal crop growth while reducing the flow of water beyond the root-zone will meet producer needs while reducing N leaching. This will result in reduced water use and reduced N loss, which in turn will allow crop nutrient requirements to be met with lower nutrient application rates.

While soil-nutrient movement is strongly related to soil-water movement, GHG emissions from agricultural production are a function of all aspects of production. Methodologies were aggregated for estimating GHG emissions from typical open-field tomato production. This provided a framework for estimating the emissions impact of different production management options. Based on the typical Florida producer, irrigation and nitrogen fertilization were identified as the most impactful management areas that could be improved in order to reduce emissions while maintaining optimal yields. Reductions in water application will result in direct emissions reductions due to

reduced pumping requirements. Similarly, reductions in nitrogen fertilizer application will result in reduced emissions due to the production, transport, and storage of the fertilizer. However, improved irrigation management can additionally result in reduced N leaching. These reduced N losses allow N applications to be reduced while maintaining similar soil-N levels, which reduces the direct emissions from the production, transport, and storage of the fertilizer. Additionally, reduced N losses will result in reduced indirect GHG emissions associated with the eventual conversion of some of the leached N to N_2O. This underscores the importance of efficient irrigation for improving agricultural efficiency by many measures.

Overall, the DSSAT-2D CSM provides a tool that can be used to improve irrigation management as well as address various production issues that require a more detailed water balance model for adequate system characterization. It is hoped that the model can aid in the process of improving the efficiency of vegetable production. Applications of the model in this research focused mainly on investigating the impact of irrigation management practices on soil-water dynamics, identifying practices which are believed to allow water to be applied in a manner that more efficiently maintain desirable root-zone soil-moisture levels with minimal flow of water beyond the root-zone. Further, improvements in irrigation efficiency that could be realized based on these identified practices should result in benefits beyond reduced water use. Improvements in irrigation efficiency should also result in reduced nutrient losses, reduced nitrogen application rates, and reduced GHG emissions. Future development of the DSSAT-2D model should include refinement of the crop growth and development routines within the 2D model as well as developing and evaluating a model for soil-

nitrogen dynamics. This would allow the model to be applied for further investigation of irrigation and fertilizer management as they relate to crop production and environmental impact.

APPENDIX A
DSSAT-2D AND HYDRUS-2D GRID LAYOUTS

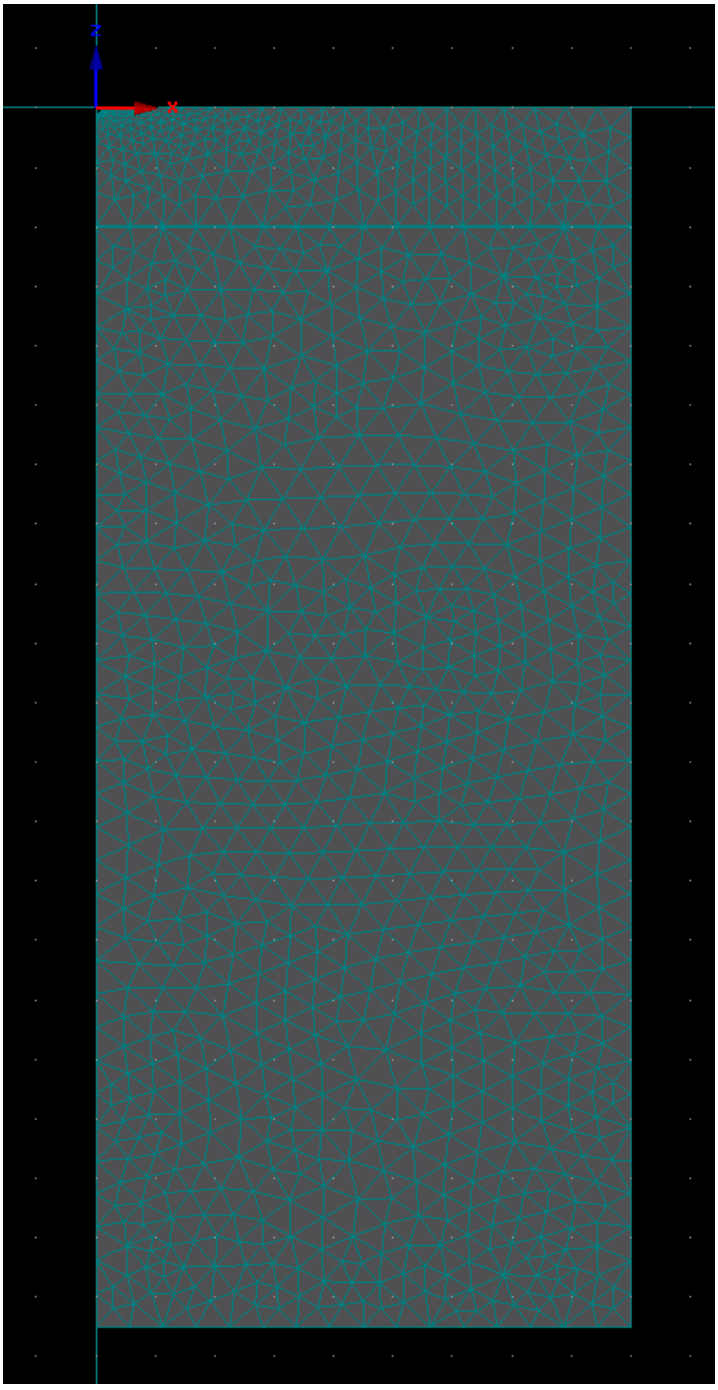

Figure A-1. Grid layout for the HYDRUS-2D simulations that were used for comparison with the DSSAT-2D simulations. Note the grid goes from 0 to 80 cm horizontally and from 0 to -205 cm vertically.

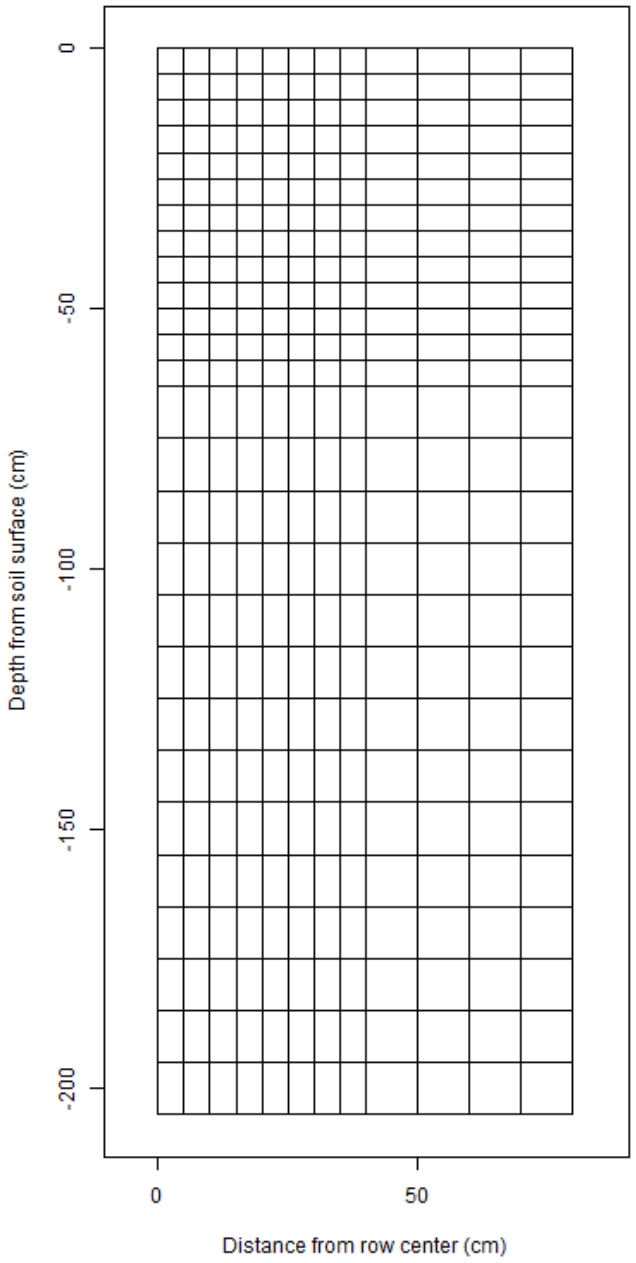

Figure A-2. Grid layout for the DSSAT-2D simulations that were used for comparison with the HYDRUS-2D simulations. Note the grid goes from 0 to 80 cm horizontally and from 0 to -205 cm vertically.

APPENDIX B
CODE FOR EXTRACTING PROBE VWC FROM GRIDDED DSSAT-2D VWC VALUES

The following is the R code used for computing the intersection weights between the sensing area of a probe and the grids in the DSSAT-2D grid space. This example is for a probe placed 0 cm from the row center and 7.5 cm from the soil surface with a sensing volume of 7.5 cm.

```
library(gpclib)
xGrids <- c( 0, 5, 10, 15, 20, 25, 30, 35, 40 )
yGrids <- c( 0, -5, -10, -15, -20, -25, -30, -35, -40, -45, -50, -55, -60, -65, -75, -85, -95, -
105, -115, -125, -135, -145, -155, -165, -175, -185, -195,-205 )
probeX <- 0.0
probeY <- -7.5
radius = 7.5
getCircle <- function(myX, myY, myR)
{
x <- array(0,360)
y <- array(0,360)
for(i in 0:360)
{
th=i*2*pi/360
x[i] <- myX + myR*cos(th)
y[i] <- myY + myR*sin(th)
}
return(cbind(x,y))
}
fillPercentage <- array( 0, c( length(yGrids)-1, length(xGrids)-1 ) )
intersectedArea <- array( 0, c( length(yGrids)-1, length(xGrids)-1 ) )
probeAreaPercentage <- array( 0, c( length(yGrids)-1, length(xGrids)-1 ) )
myCircle <- getCircle(probeX, probeY, radius)
myCircle <- as(myCircle, "gpc.poly")
myPlot <- myCircle
for(j in 1:(length(yGrids)-1))
{
for(k in 1:(length(xGrids)-1))
{
myRectangle <- cbind( c(xGrids[k],xGrids[k],xGrids[k+1],xGrids[k+1]) ,
c(yGrids[j],yGrids[j+1],yGrids[j+1],yGrids[j]) )
myRectangle <- as(myRectangle, "gpc.poly")
intersectionArea <- area.poly(intersect(myCircle,myRectangle))
intersectedArea[j,k] <- intersectionArea
rectangleArea <- area.poly(myRectangle)
fillPercentage[j,k] <- intersectionArea/rectangleArea
```

```
myPlot <- append.poly(myPlot,myRectangle)
}
}
for(j in 1:(length(yGrids)-1))
{
for(k in 1:(length(xGrids)-1))
{
probeAreaPercentage[j,k] <- ( intersectedArea[j,k] / sum(intersectedArea[,]) )
}
}
sink("AutoProbeWeights.txt", append=FALSE, split=FALSE)
cat("Row,Column,Weight")
for(j in 1:(length(yGrids)-1))
{
for(k in 1:(length(xGrids)-1))
{
if(probeAreaPercentage[j,k]>0){
cat("\n")
cat(j,k,probeAreaPercentage[j,k],sep=",")
}
}
}
sink()
```

APPENDIX C
TIME EVOLUTION GRAPHS OF THE MEASURED AND SIMULATED VWC VALUES AT EACH PROBE MEASUREMENT LOCATION

Figure C-1. Time evolution at each probe location of the measured and simulated VWCs using DSSAT-2D with the three-point DSSAT estimated soil parameters. Plots for each probe location include the predicted VWCs, average probe measured VWCs, and 95% probe measured VWC confidence intervals vs. time for treatments A) 30-H-1 rep 1, B) 30-H-2 rep 1, C) 30-L-1 rep 1, D) 30-L-2 rep 1, E) 20-H-1 rep 1, F) 20-H-2 rep 1, G) 10-H-2 rep 1, H)10-H-1 rep 1, I) 20-L-1 rep 1, J) 20-L-2 rep 1, K) 10-L-2 rep 1, L) 10-L-1 rep 1, M) 10-H-2 rep 2, N) 10-H-2 rep 3, O) 10-H-1 rep 2, P) 10-H-2 rep 3, Q) 30-L-1 rep 2, R) 30-L-1 rep 3, S) 30-L-2 rep 2, T) 30-L-2 rep 3, U) 20-H-1 rep 2, V) 20-H-2 rep 2.

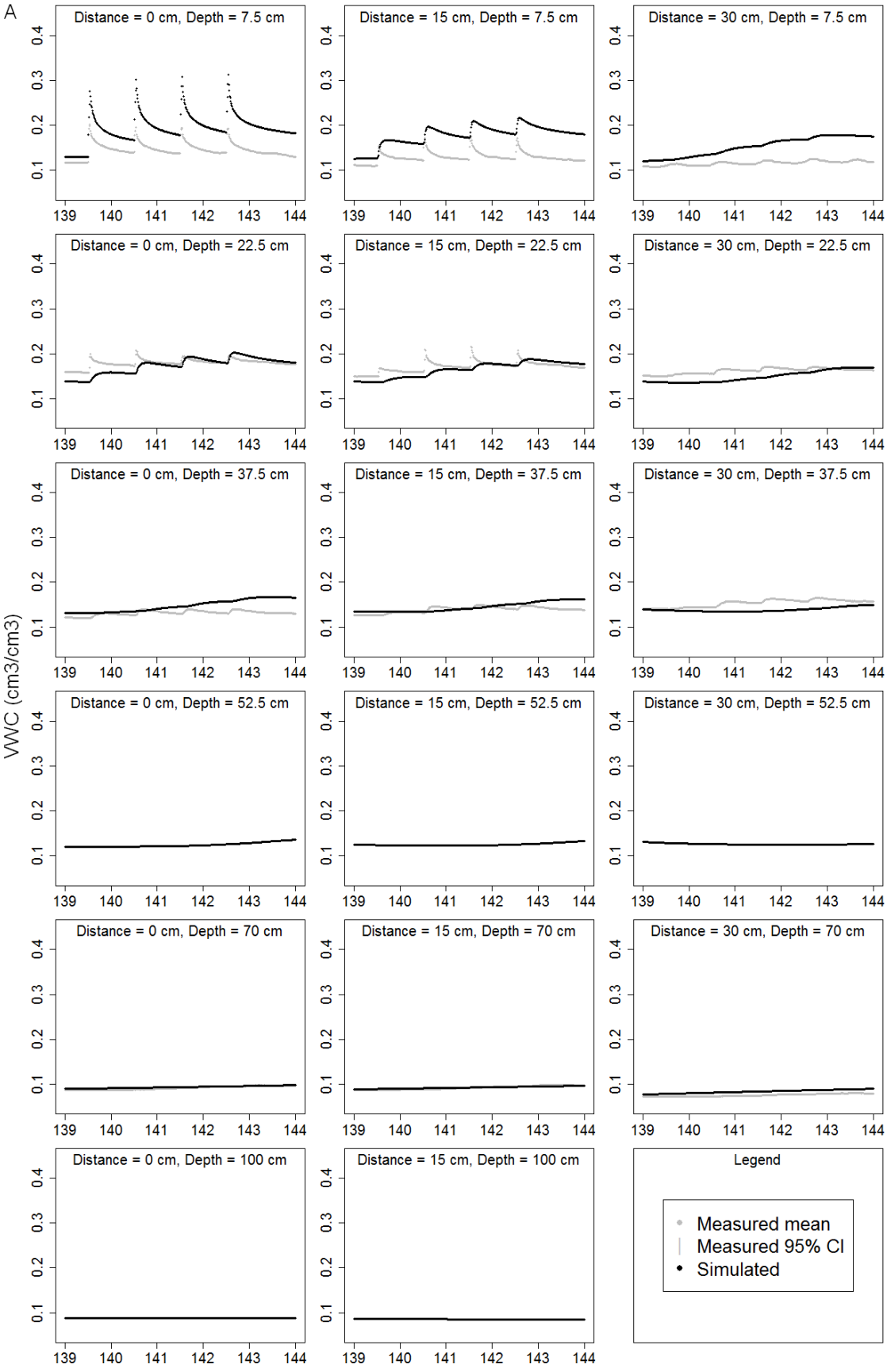
A
Distance = 0 cm, Depth = 7.5 cm
Distance = 15 cm, Depth = 7.5 cm
Distance = 30 cm, Depth = 7.5 cm
Distance = 0 cm, Depth = 22.5 cm
Distance = 15 cm, Depth = 22.5 cm
Distance = 30 cm, Depth = 22.5 cm
Distance = 0 cm, Depth = 37.5 cm
Distance = 15 cm, Depth = 37.5 cm
Distance = 30 cm, Depth = 37.5 cm
Distance = 0 cm, Depth = 52.5 cm
Distance = 15 cm, Depth = 52.5 cm
Distance = 30 cm, Depth = 52.5 cm
Distance = 0 cm, Depth = 70 cm
Distance = 15 cm, Depth = 70 cm
Distance = 30 cm, Depth = 70 cm
Distance = 0 cm, Depth = 100 cm
Distance = 15 cm, Depth = 100 cm
Legend
Measured mean
Measured 95% CI
Simulated
VWC (cm3/cm3)
0.1
0.2
0.3
0.4
139
140
141
142
143
144

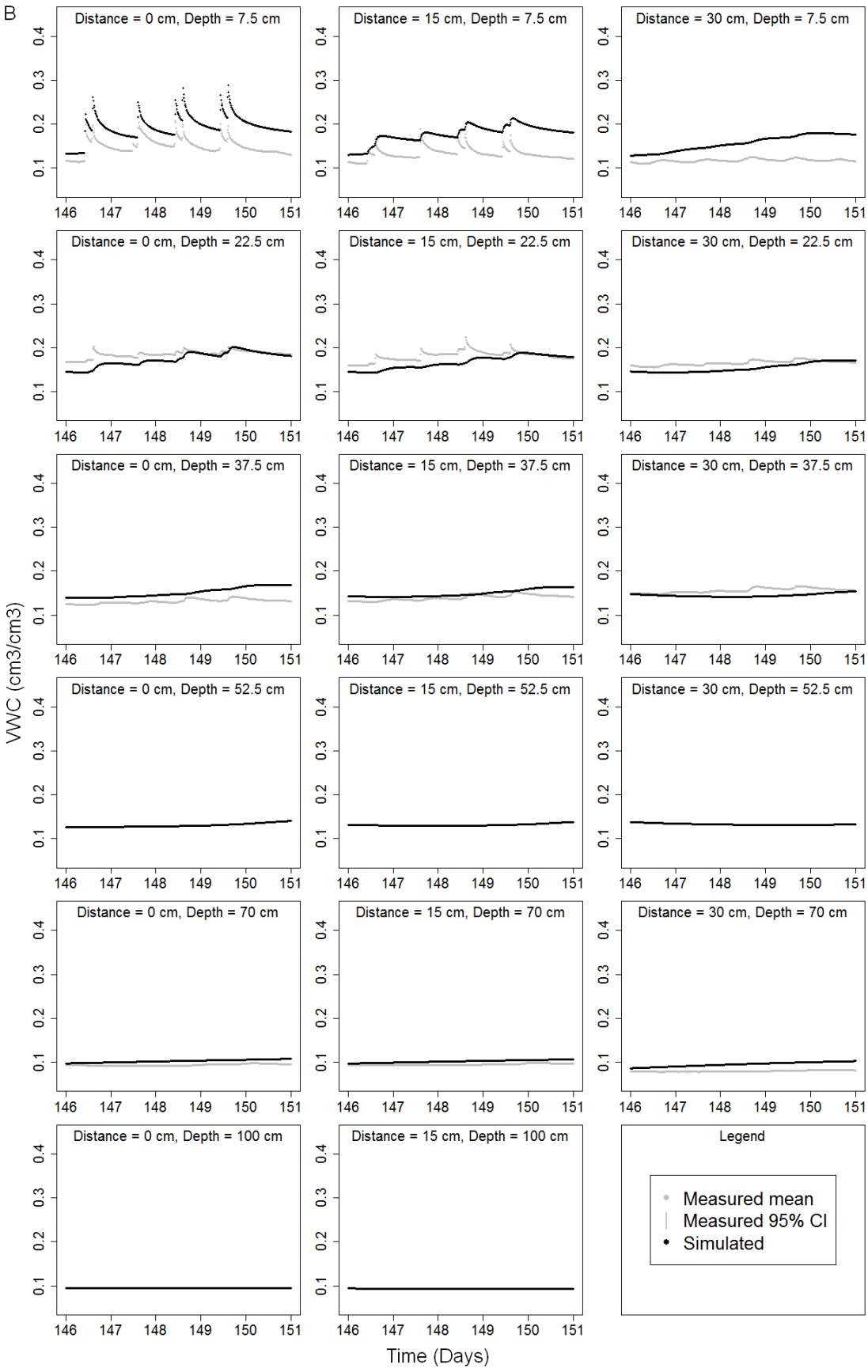
B
Distance = 0 cm, Depth = 7.5 cm
Distance = 15 cm, Depth = 7.5 cm
Distance = 30 cm, Depth = 7.5 cm
Distance = 0 cm, Depth = 22.5 cm
Distance = 15 cm, Depth = 22.5 cm
Distance = 30 cm, Depth = 22.5 cm
Distance = 0 cm, Depth = 37.5 cm
Distance = 15 cm, Depth = 37.5 cm
Distance = 30 cm, Depth = 37.5 cm
Distance = 0 cm, Depth = 52.5 cm
Distance = 15 cm, Depth = 52.5 cm
Distance = 30 cm, Depth = 52.5 cm
Distance = 0 cm, Depth = 70 cm
Distance = 15 cm, Depth = 70 cm
Distance = 30 cm, Depth = 70 cm
Distance = 0 cm, Depth = 100 cm
Distance = 15 cm, Depth = 100 cm
Legend
Measured mean
Measured 95% CI
Simulated
VWC (cm3/cm3)
Time (Days)
0.1
0.2
0.3
0.4
146
147
148
149
150
151

C

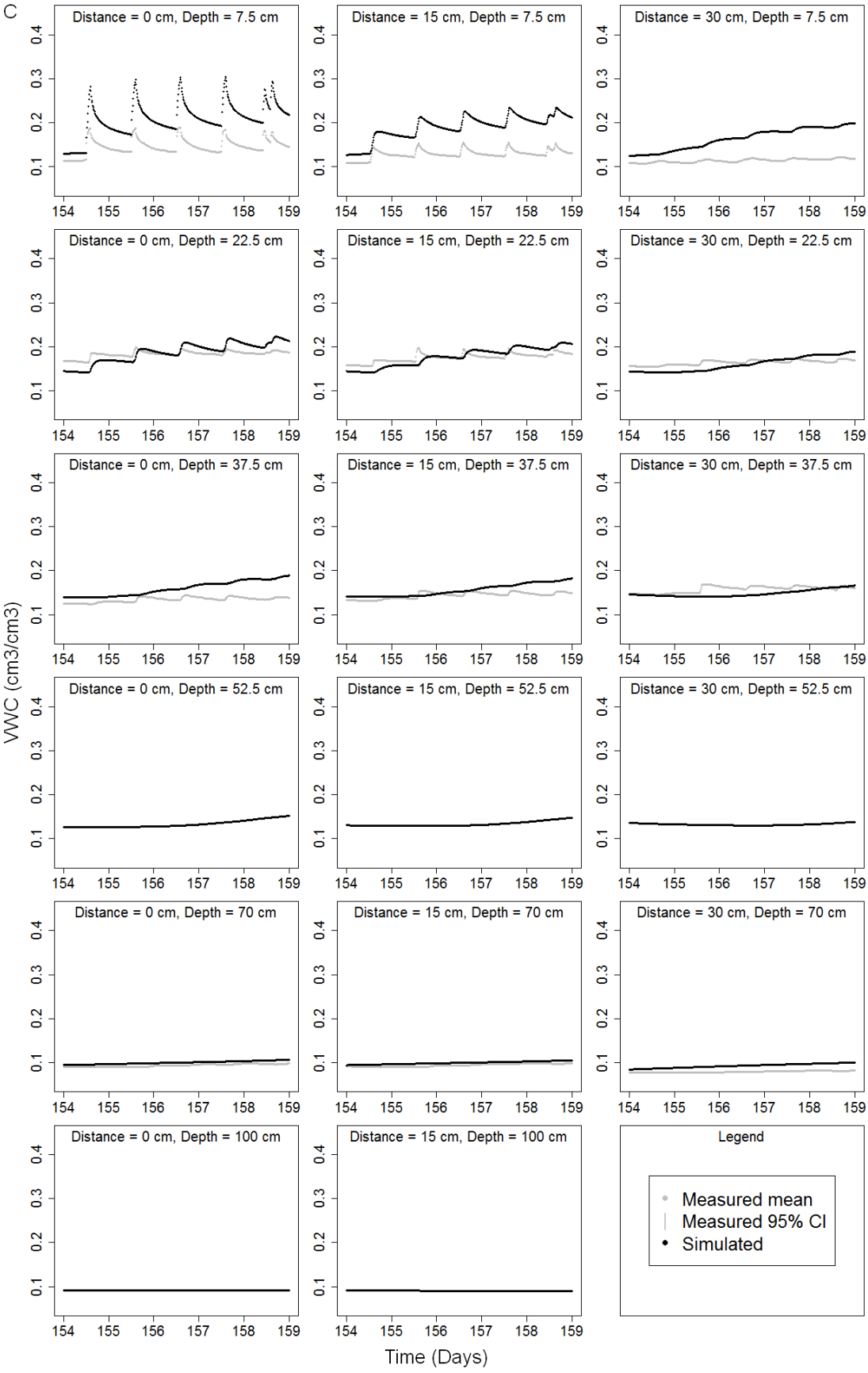
Distance = 0 cm, Depth = 7.5 cm
Distance = 15 cm, Depth = 7.5 cm
Distance = 30 cm, Depth = 7.5 cm
Distance = 0 cm, Depth = 22.5 cm
Distance = 15 cm, Depth = 22.5 cm
Distance = 30 cm, Depth = 22.5 cm
Distance = 0 cm, Depth = 37.5 cm
Distance = 15 cm, Depth = 37.5 cm
Distance = 30 cm, Depth = 37.5 cm
Distance = 0 cm, Depth = 52.5 cm
Distance = 15 cm, Depth = 52.5 cm
Distance = 30 cm, Depth = 52.5 cm
Distance = 0 cm, Depth = 70 cm
Distance = 15 cm, Depth = 70 cm
Distance = 30 cm, Depth = 70 cm
Distance = 0 cm, Depth = 100 cm
Distance = 15 cm, Depth = 100 cm
Legend
Measured mean
Measured 95% CI
Simulated
VWC (cm3/cm3)
Time (Days)

D

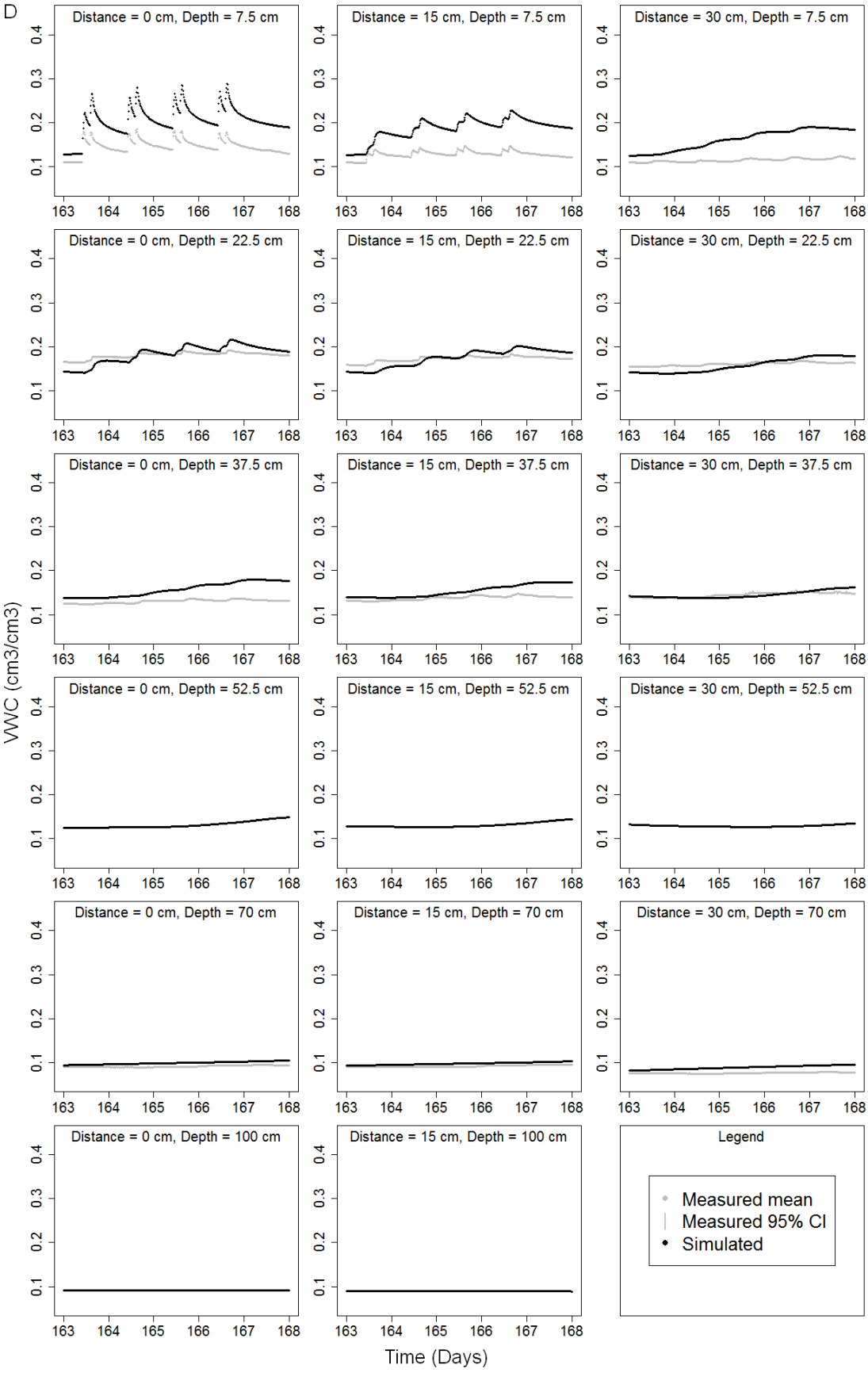
Distance = 0 cm, Depth = 7.5 cm
Distance = 15 cm, Depth = 7.5 cm
Distance = 30 cm, Depth = 7.5 cm
Distance = 0 cm, Depth = 22.5 cm
Distance = 15 cm, Depth = 22.5 cm
Distance = 30 cm, Depth = 22.5 cm
Distance = 0 cm, Depth = 37.5 cm
Distance = 15 cm, Depth = 37.5 cm
Distance = 30 cm, Depth = 37.5 cm
Distance = 0 cm, Depth = 52.5 cm
Distance = 15 cm, Depth = 52.5 cm
Distance = 30 cm, Depth = 52.5 cm
Distance = 0 cm, Depth = 70 cm
Distance = 15 cm, Depth = 70 cm
Distance = 30 cm, Depth = 70 cm
Distance = 0 cm, Depth = 100 cm
Distance = 15 cm, Depth = 100 cm
Legend
Measured mean
Measured 95% CI
Simulated
VWC (cm3/cm3)
Time (Days)

E

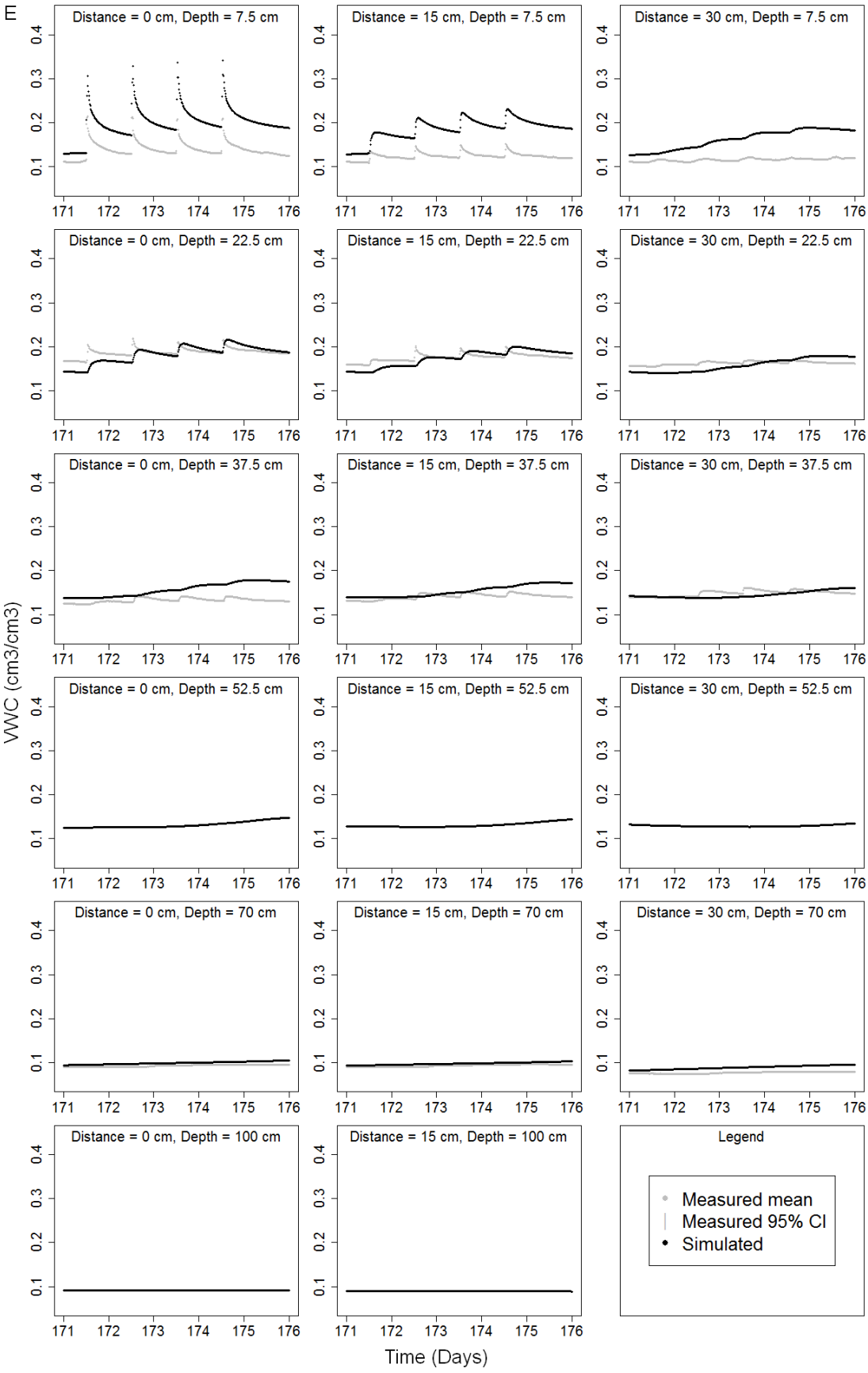
Distance = 0 cm, Depth = 7.5 cm
Distance = 15 cm, Depth = 7.5 cm
Distance = 30 cm, Depth = 7.5 cm
Distance = 0 cm, Depth = 22.5 cm
Distance = 15 cm, Depth = 22.5 cm
Distance = 30 cm, Depth = 22.5 cm
Distance = 0 cm, Depth = 37.5 cm
Distance = 15 cm, Depth = 37.5 cm
Distance = 30 cm, Depth = 37.5 cm
Distance = 0 cm, Depth = 52.5 cm
Distance = 15 cm, Depth = 52.5 cm
Distance = 30 cm, Depth = 52.5 cm
Distance = 0 cm, Depth = 70 cm
Distance = 15 cm, Depth = 70 cm
Distance = 30 cm, Depth = 70 cm
Distance = 0 cm, Depth = 100 cm
Distance = 15 cm, Depth = 100 cm
Legend
Measured mean
Measured 95% CI
Simulated
VWC (cm3/cm3)
Time (Days)

F

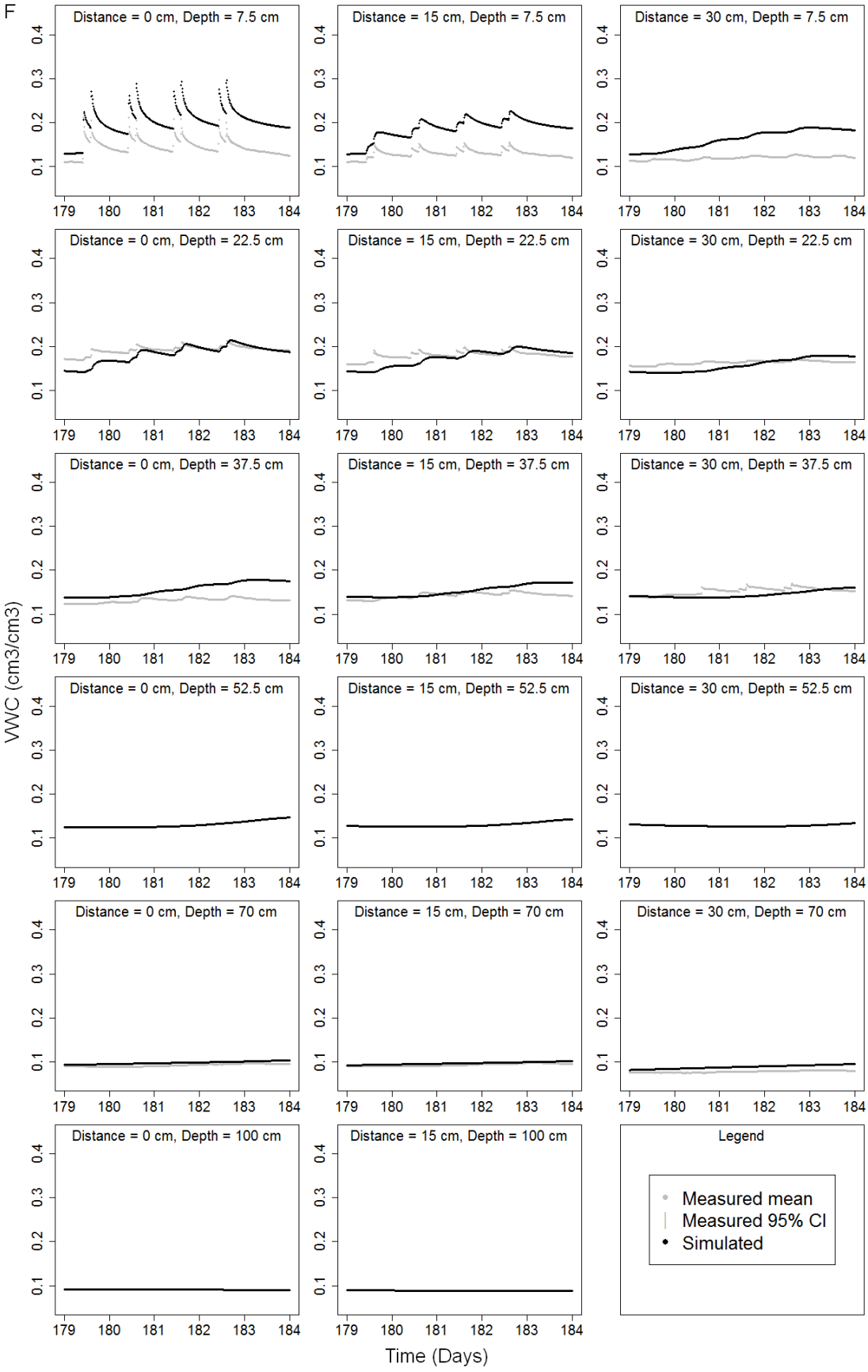
Distance = 0 cm, Depth = 7.5 cm
Distance = 15 cm, Depth = 7.5 cm
Distance = 30 cm, Depth = 7.5 cm
Distance = 0 cm, Depth = 22.5 cm
Distance = 15 cm, Depth = 22.5 cm
Distance = 30 cm, Depth = 22.5 cm
Distance = 0 cm, Depth = 37.5 cm
Distance = 15 cm, Depth = 37.5 cm
Distance = 30 cm, Depth = 37.5 cm
Distance = 0 cm, Depth = 52.5 cm
Distance = 15 cm, Depth = 52.5 cm
Distance = 30 cm, Depth = 52.5 cm
Distance = 0 cm, Depth = 70 cm
Distance = 15 cm, Depth = 70 cm
Distance = 30 cm, Depth = 70 cm
Distance = 0 cm, Depth = 100 cm
Distance = 15 cm, Depth = 100 cm
Legend
Measured mean
Measured 95% CI
Simulated
VWC (cm3/cm3)
Time (Days)
0.1
0.2
0.3
0.4
179
180
181
182
183
184

G

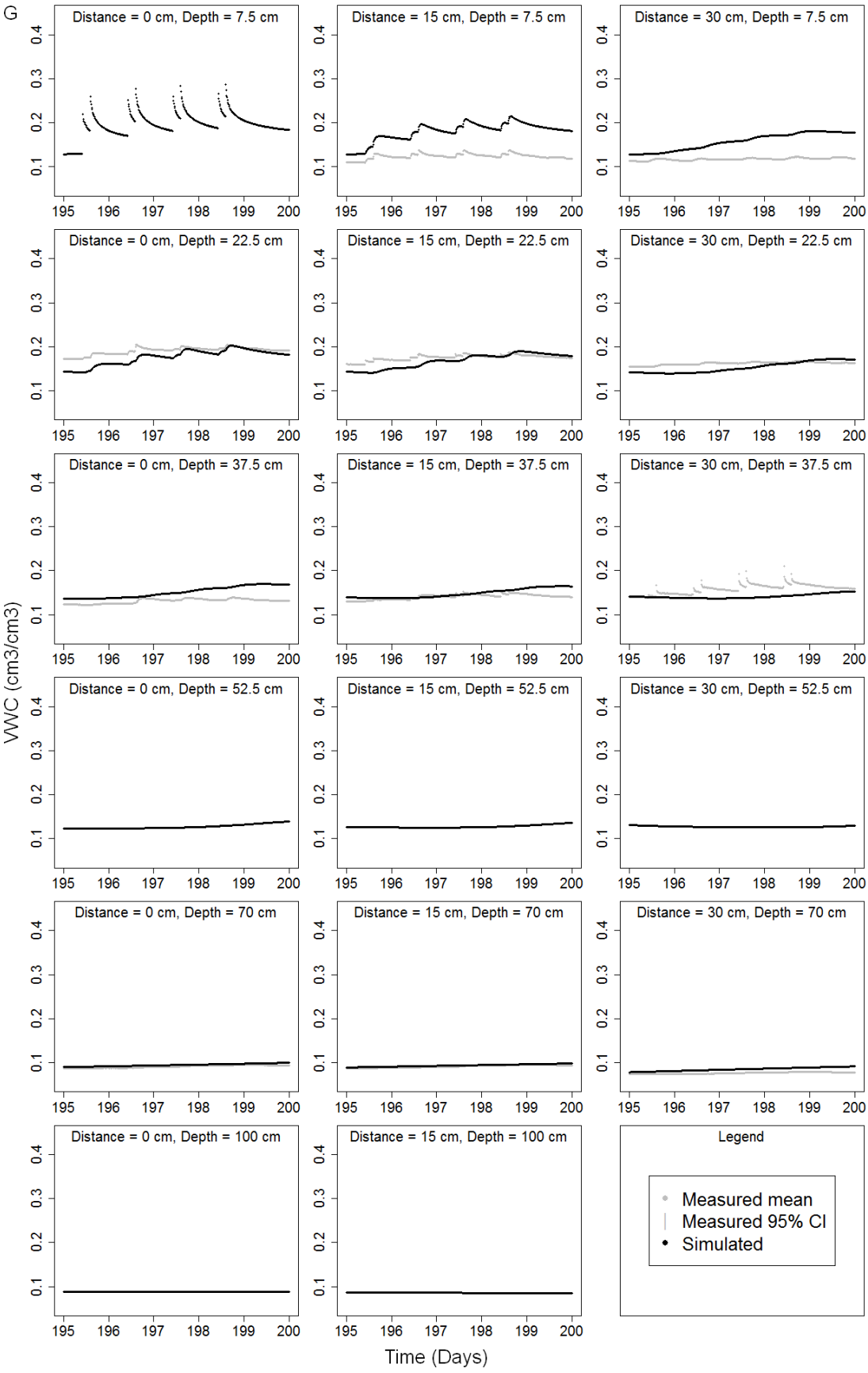
Distance = 0 cm, Depth = 7.5 cm
Distance = 15 cm, Depth = 7.5 cm
Distance = 30 cm, Depth = 7.5 cm
Distance = 0 cm, Depth = 22.5 cm
Distance = 15 cm, Depth = 22.5 cm
Distance = 30 cm, Depth = 22.5 cm
Distance = 0 cm, Depth = 37.5 cm
Distance = 15 cm, Depth = 37.5 cm
Distance = 30 cm, Depth = 37.5 cm
Distance = 0 cm, Depth = 52.5 cm
Distance = 15 cm, Depth = 52.5 cm
Distance = 30 cm, Depth = 52.5 cm
Distance = 0 cm, Depth = 70 cm
Distance = 15 cm, Depth = 70 cm
Distance = 30 cm, Depth = 70 cm
Distance = 0 cm, Depth = 100 cm
Distance = 15 cm, Depth = 100 cm
Legend
Measured mean
Measured 95% CI
Simulated
VWC (cm3/cm3)
Time (Days)
0.1
0.2
0.3
0.4
195
196
197
198
199
200

H

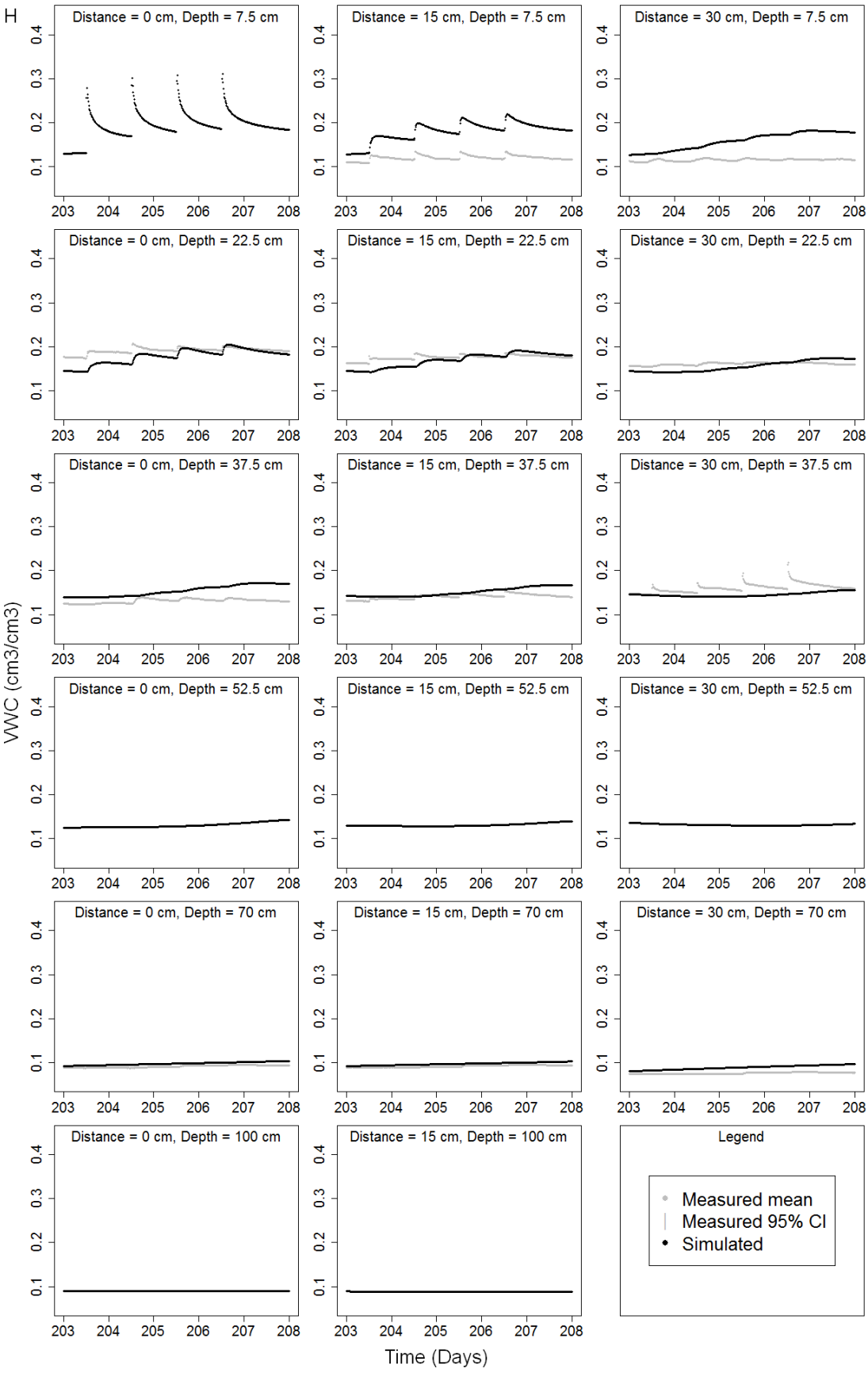
Distance = 0 cm, Depth = 7.5 cm
Distance = 15 cm, Depth = 7.5 cm
Distance = 30 cm, Depth = 7.5 cm
Distance = 0 cm, Depth = 22.5 cm
Distance = 15 cm, Depth = 22.5 cm
Distance = 30 cm, Depth = 22.5 cm
Distance = 0 cm, Depth = 37.5 cm
Distance = 15 cm, Depth = 37.5 cm
Distance = 30 cm, Depth = 37.5 cm
Distance = 0 cm, Depth = 52.5 cm
Distance = 15 cm, Depth = 52.5 cm
Distance = 30 cm, Depth = 52.5 cm
Distance = 0 cm, Depth = 70 cm
Distance = 15 cm, Depth = 70 cm
Distance = 30 cm, Depth = 70 cm
Distance = 0 cm, Depth = 100 cm
Distance = 15 cm, Depth = 100 cm
Legend
Measured mean
Measured 95% CI
Simulated
VWC (cm3/cm3)
Time (Days)

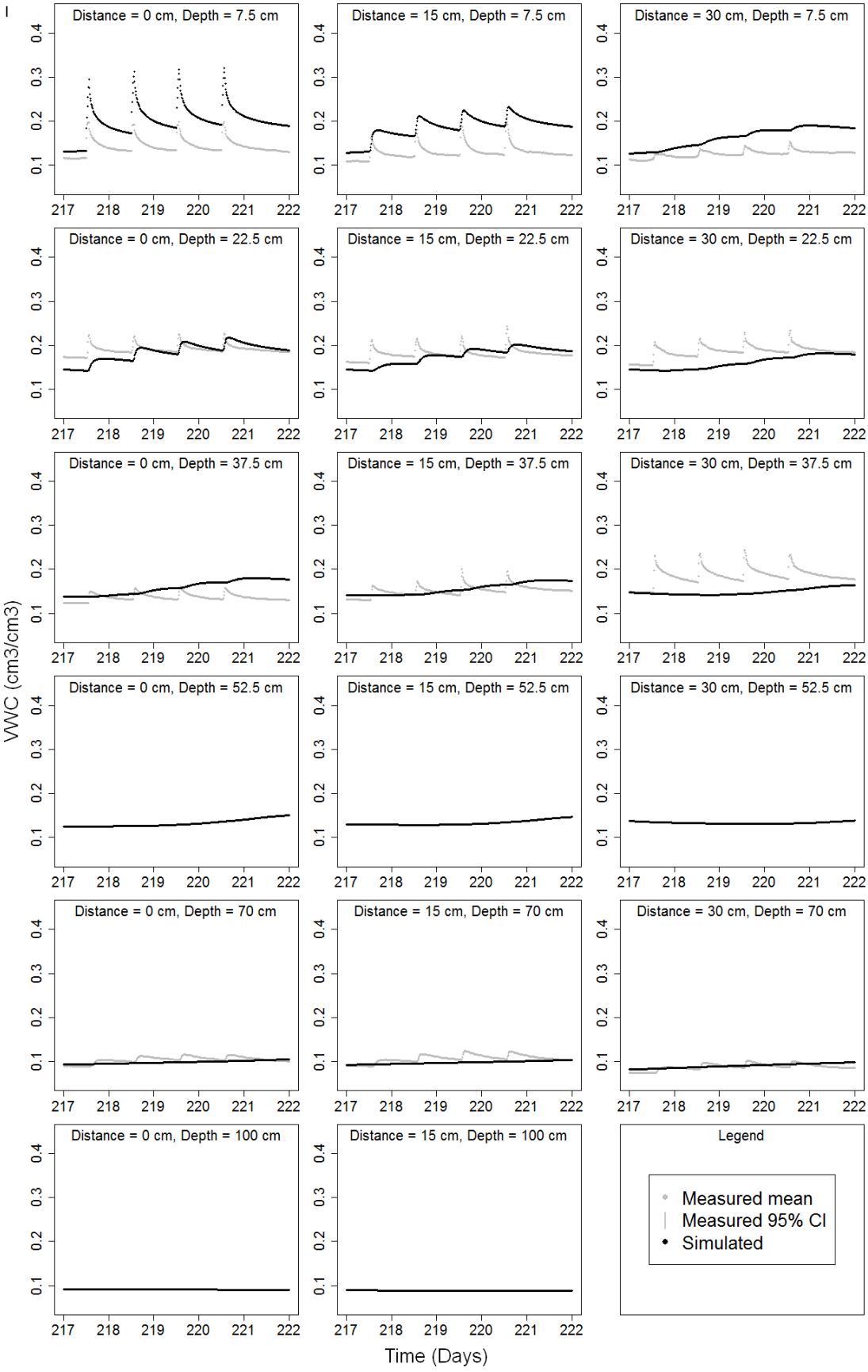
Distance = 0 cm, Depth = 7.5 cm
Distance = 15 cm, Depth = 7.5 cm
Distance = 30 cm, Depth = 7.5 cm
Distance = 0 cm, Depth = 22.5 cm
Distance = 15 cm, Depth = 22.5 cm
Distance = 30 cm, Depth = 22.5 cm
Distance = 0 cm, Depth = 37.5 cm
Distance = 15 cm, Depth = 37.5 cm
Distance = 30 cm, Depth = 37.5 cm
Distance = 0 cm, Depth = 52.5 cm
Distance = 15 cm, Depth = 52.5 cm
Distance = 30 cm, Depth = 52.5 cm
Distance = 0 cm, Depth = 70 cm
Distance = 15 cm, Depth = 70 cm
Distance = 30 cm, Depth = 70 cm
Distance = 0 cm, Depth = 100 cm
Distance = 15 cm, Depth = 100 cm
Legend
Measured mean
Measured 95% CI
Simulated
VWC (cm3/cm3)
Time (Days)
0.1
0.2
0.3
0.4
217
218
219
220
221
222

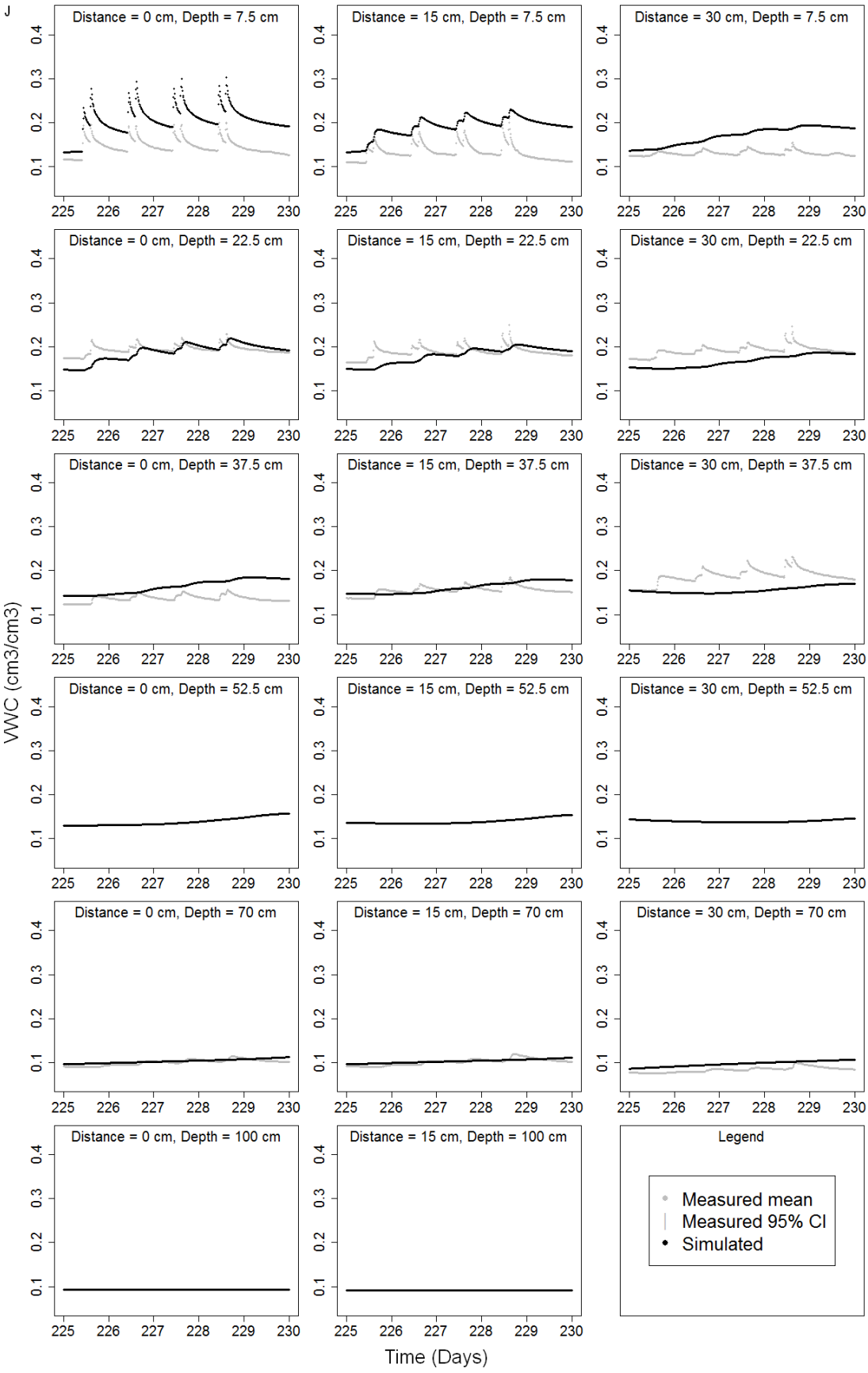
J
Distance = 0 cm, Depth = 7.5 cm
Distance = 15 cm, Depth = 7.5 cm
Distance = 30 cm, Depth = 7.5 cm
Distance = 0 cm, Depth = 22.5 cm
Distance = 15 cm, Depth = 22.5 cm
Distance = 30 cm, Depth = 22.5 cm
Distance = 0 cm, Depth = 37.5 cm
Distance = 15 cm, Depth = 37.5 cm
Distance = 30 cm, Depth = 37.5 cm
Distance = 0 cm, Depth = 52.5 cm
Distance = 15 cm, Depth = 52.5 cm
Distance = 30 cm, Depth = 52.5 cm
Distance = 0 cm, Depth = 70 cm
Distance = 15 cm, Depth = 70 cm
Distance = 30 cm, Depth = 70 cm
Distance = 0 cm, Depth = 100 cm
Distance = 15 cm, Depth = 100 cm
Legend
Measured mean
Measured 95% CI
Simulated
VWC (cm3/cm3)
Time (Days)
0.1
0.2
0.3
0.4
225
226
227
228
229
230

K

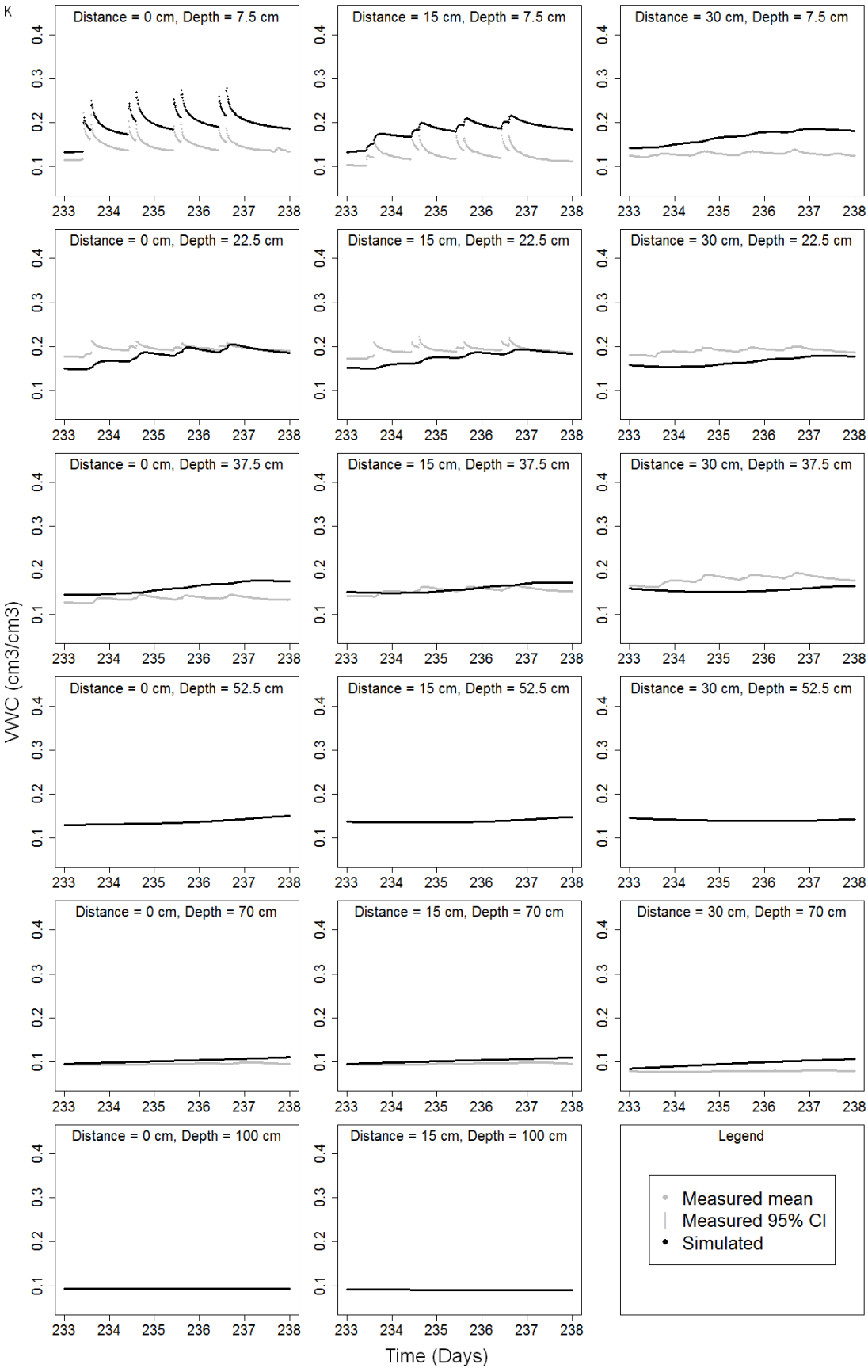
Distance = 0 cm, Depth = 7.5 cm
Distance = 15 cm, Depth = 7.5 cm
Distance = 30 cm, Depth = 7.5 cm
Distance = 0 cm, Depth = 22.5 cm
Distance = 15 cm, Depth = 22.5 cm
Distance = 30 cm, Depth = 22.5 cm
Distance = 0 cm, Depth = 37.5 cm
Distance = 15 cm, Depth = 37.5 cm
Distance = 30 cm, Depth = 37.5 cm
Distance = 0 cm, Depth = 52.5 cm
Distance = 15 cm, Depth = 52.5 cm
Distance = 30 cm, Depth = 52.5 cm
Distance = 0 cm, Depth = 70 cm
Distance = 15 cm, Depth = 70 cm
Distance = 30 cm, Depth = 70 cm
Distance = 0 cm, Depth = 100 cm
Distance = 15 cm, Depth = 100 cm
Legend
Measured mean
Measured 95% CI
Simulated
VWC (cm3/cm3)
Time (Days)
0.1
0.2
0.3
0.4
233
234
235
236
237
238

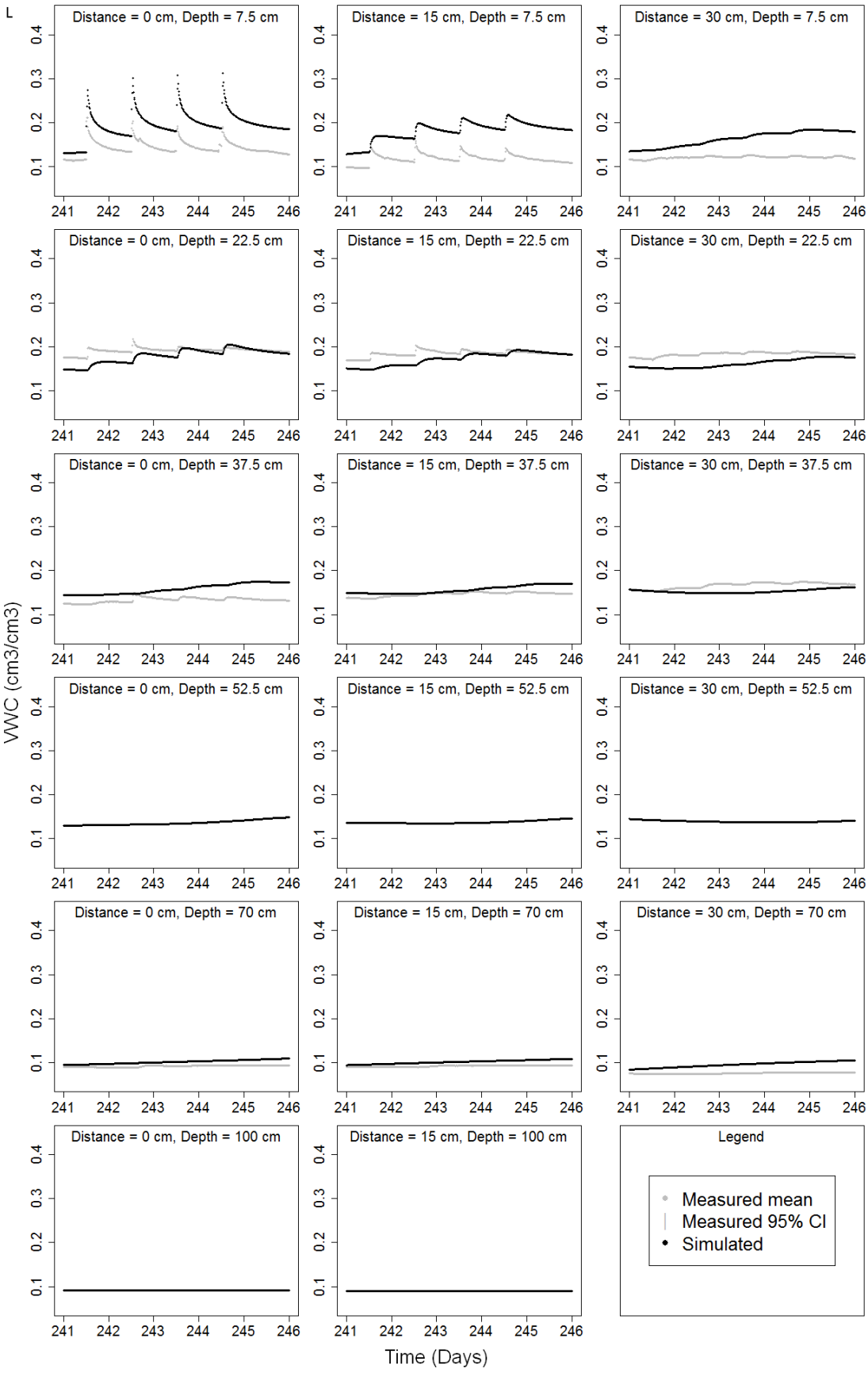
L
Distance = 0 cm, Depth = 7.5 cm
Distance = 15 cm, Depth = 7.5 cm
Distance = 30 cm, Depth = 7.5 cm
Distance = 0 cm, Depth = 22.5 cm
Distance = 15 cm, Depth = 22.5 cm
Distance = 30 cm, Depth = 22.5 cm
Distance = 0 cm, Depth = 37.5 cm
Distance = 15 cm, Depth = 37.5 cm
Distance = 30 cm, Depth = 37.5 cm
Distance = 0 cm, Depth = 52.5 cm
Distance = 15 cm, Depth = 52.5 cm
Distance = 30 cm, Depth = 52.5 cm
Distance = 0 cm, Depth = 70 cm
Distance = 15 cm, Depth = 70 cm
Distance = 30 cm, Depth = 70 cm
Distance = 0 cm, Depth = 100 cm
Distance = 15 cm, Depth = 100 cm
Legend
Measured mean
Measured 95% CI
Simulated
VWC (cm3/cm3)
Time (Days)
0.1
0.2
0.3
0.4
241
242
243
244
245
246

M

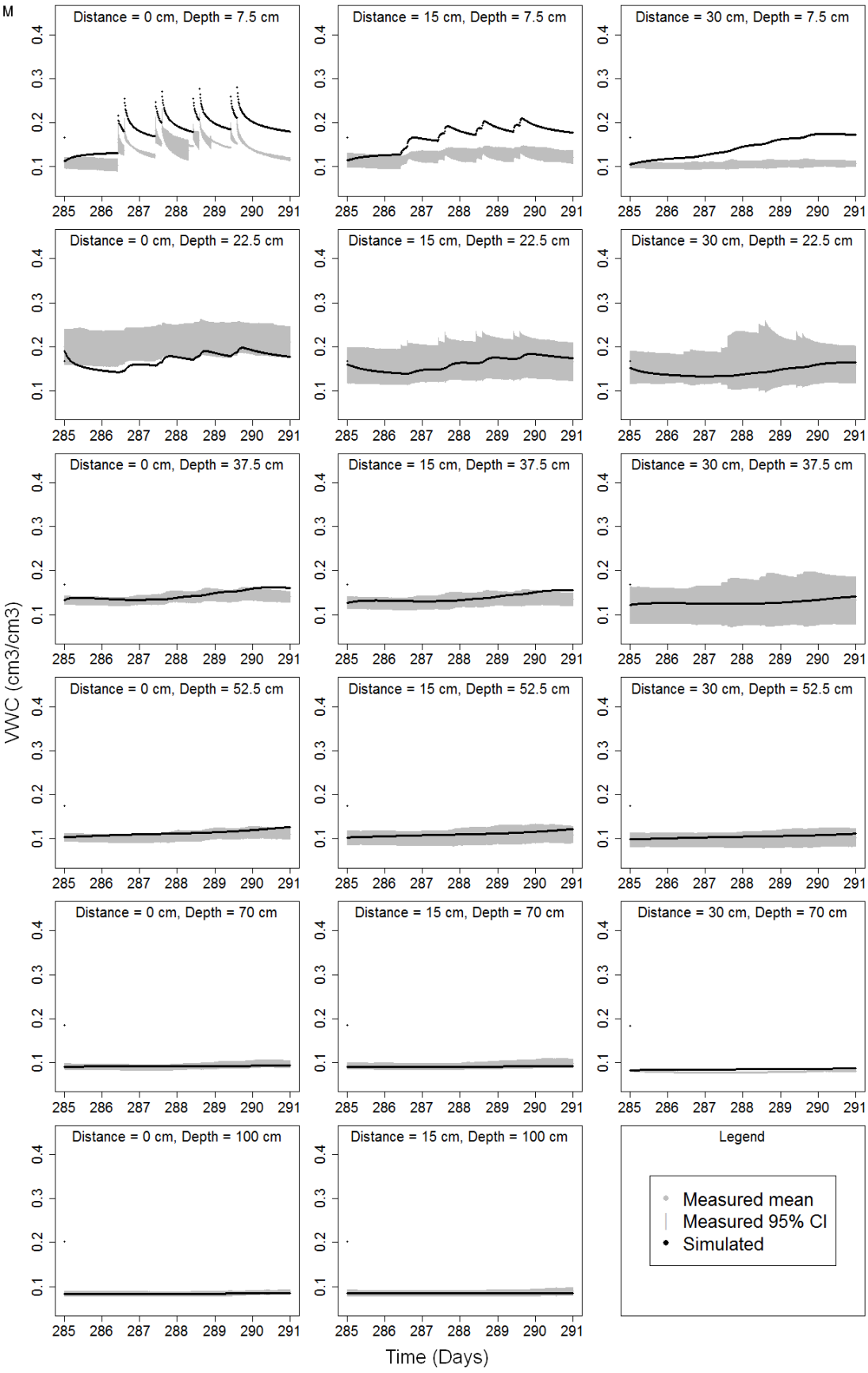
Distance = 0 cm, Depth = 7.5 cm
Distance = 15 cm, Depth = 7.5 cm
Distance = 30 cm, Depth = 7.5 cm
Distance = 0 cm, Depth = 22.5 cm
Distance = 15 cm, Depth = 22.5 cm
Distance = 30 cm, Depth = 22.5 cm
Distance = 0 cm, Depth = 37.5 cm
Distance = 15 cm, Depth = 37.5 cm
Distance = 30 cm, Depth = 37.5 cm
Distance = 0 cm, Depth = 52.5 cm
Distance = 15 cm, Depth = 52.5 cm
Distance = 30 cm, Depth = 52.5 cm
Distance = 0 cm, Depth = 70 cm
Distance = 15 cm, Depth = 70 cm
Distance = 30 cm, Depth = 70 cm
Distance = 0 cm, Depth = 100 cm
Distance = 15 cm, Depth = 100 cm
Legend
Measured mean
Measured 95% CI
Simulated
VWC (cm3/cm3)
Time (Days)

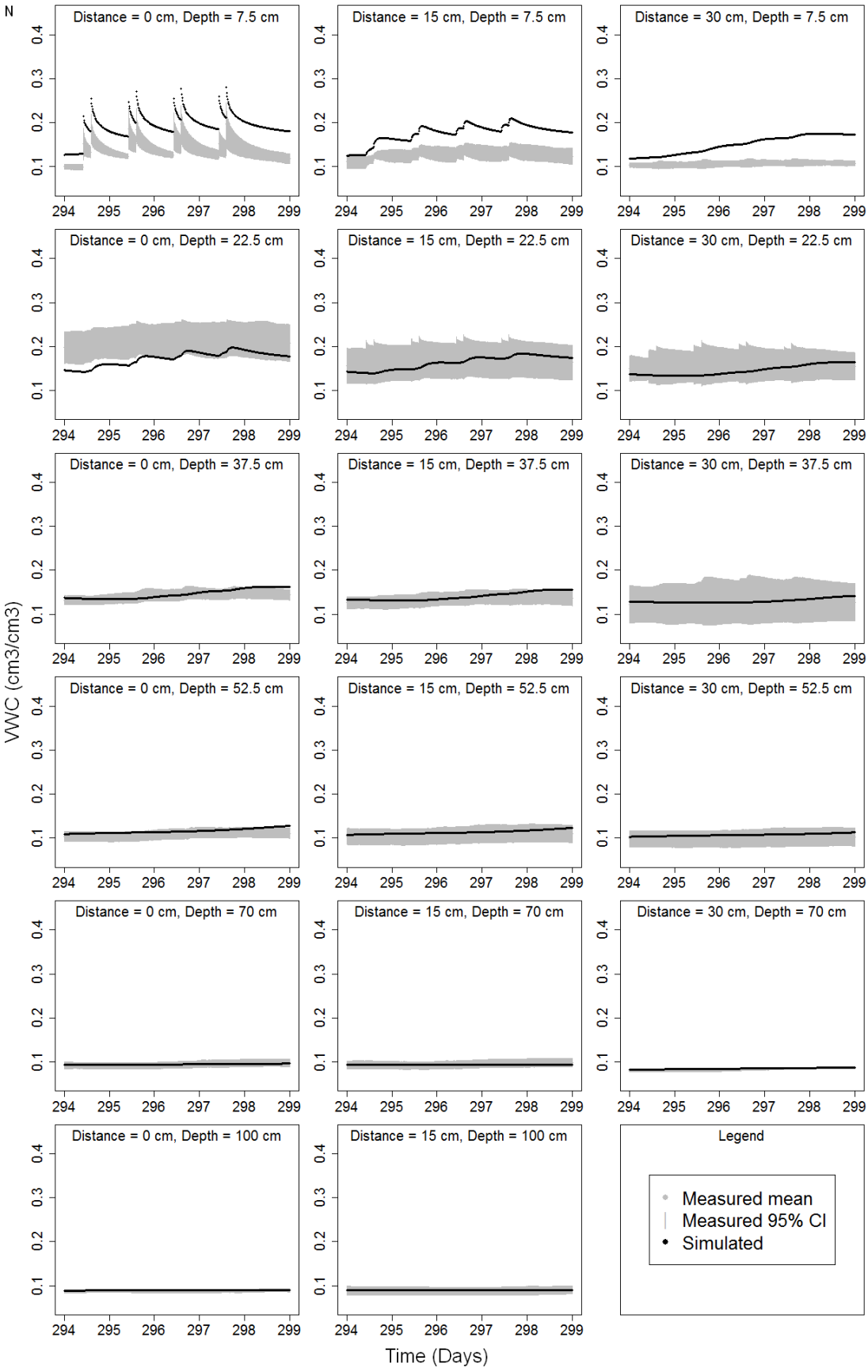
Distance = 0 cm, Depth = 7.5 cm
Distance = 15 cm, Depth = 7.5 cm
Distance = 30 cm, Depth = 7.5 cm
Distance = 0 cm, Depth = 22.5 cm
Distance = 15 cm, Depth = 22.5 cm
Distance = 30 cm, Depth = 22.5 cm
Distance = 0 cm, Depth = 37.5 cm
Distance = 15 cm, Depth = 37.5 cm
Distance = 30 cm, Depth = 37.5 cm
Distance = 0 cm, Depth = 52.5 cm
Distance = 15 cm, Depth = 52.5 cm
Distance = 30 cm, Depth = 52.5 cm
Distance = 0 cm, Depth = 70 cm
Distance = 15 cm, Depth = 70 cm
Distance = 30 cm, Depth = 70 cm
Distance = 0 cm, Depth = 100 cm
Distance = 15 cm, Depth = 100 cm
Legend
Measured mean
Measured 95% CI
Simulated
VWC (cm3/cm3)
Time (Days)
0.1
0.2
0.3
0.4
294
295
296
297
298
299

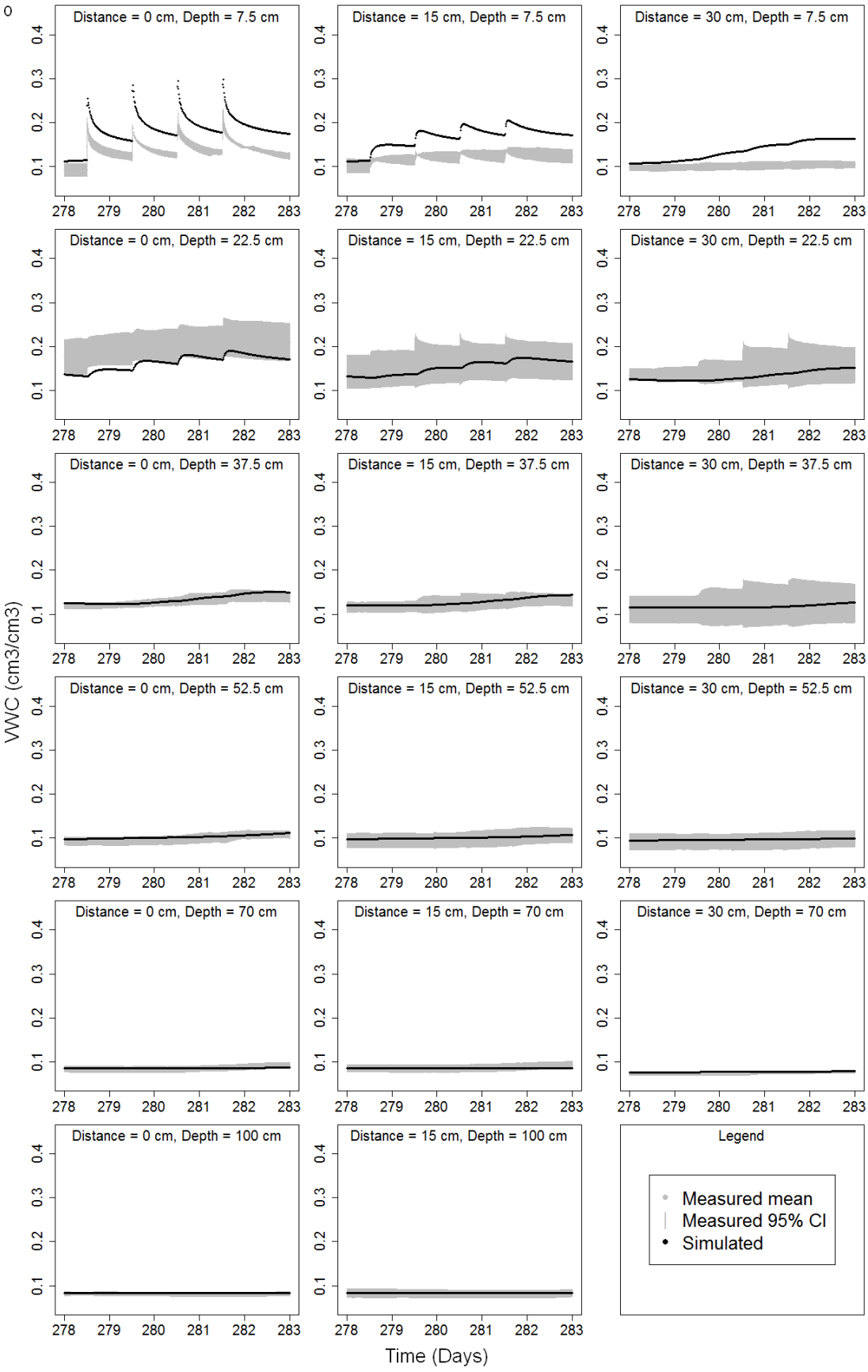
Distance = 0 cm, Depth = 7.5 cm
Distance = 15 cm, Depth = 7.5 cm
Distance = 30 cm, Depth = 7.5 cm
Distance = 0 cm, Depth = 22.5 cm
Distance = 15 cm, Depth = 22.5 cm
Distance = 30 cm, Depth = 22.5 cm
Distance = 0 cm, Depth = 37.5 cm
Distance = 15 cm, Depth = 37.5 cm
Distance = 30 cm, Depth = 37.5 cm
Distance = 0 cm, Depth = 52.5 cm
Distance = 15 cm, Depth = 52.5 cm
Distance = 30 cm, Depth = 52.5 cm
Distance = 0 cm, Depth = 70 cm
Distance = 15 cm, Depth = 70 cm
Distance = 30 cm, Depth = 70 cm
Distance = 0 cm, Depth = 100 cm
Distance = 15 cm, Depth = 100 cm
Legend
Measured mean
Measured 95% CI
Simulated
VWC (cm3/cm3)
Time (Days)
0.1
0.2
0.3
0.4
278
279
280
281
282
283

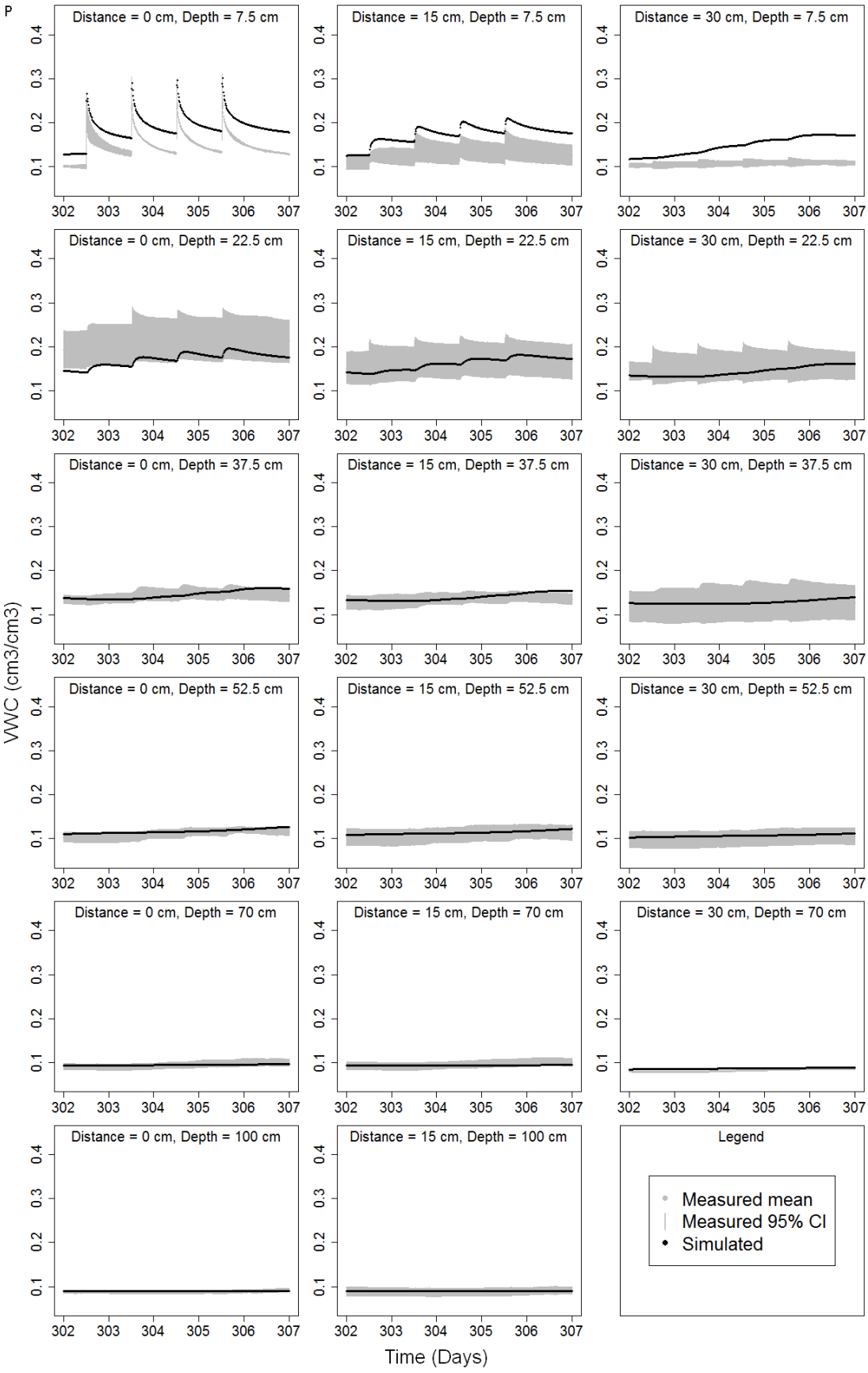
P
Distance = 0 cm, Depth = 7.5 cm
Distance = 15 cm, Depth = 7.5 cm
Distance = 30 cm, Depth = 7.5 cm
Distance = 0 cm, Depth = 22.5 cm
Distance = 15 cm, Depth = 22.5 cm
Distance = 30 cm, Depth = 22.5 cm
Distance = 0 cm, Depth = 37.5 cm
Distance = 15 cm, Depth = 37.5 cm
Distance = 30 cm, Depth = 37.5 cm
Distance = 0 cm, Depth = 52.5 cm
Distance = 15 cm, Depth = 52.5 cm
Distance = 30 cm, Depth = 52.5 cm
Distance = 0 cm, Depth = 70 cm
Distance = 15 cm, Depth = 70 cm
Distance = 30 cm, Depth = 70 cm
Distance = 0 cm, Depth = 100 cm
Distance = 15 cm, Depth = 100 cm
Legend
Measured mean
Measured 95% CI
Simulated
VWC (cm3/cm3)
Time (Days)
0.1
0.2
0.3
0.4
302
303
304
305
306
307

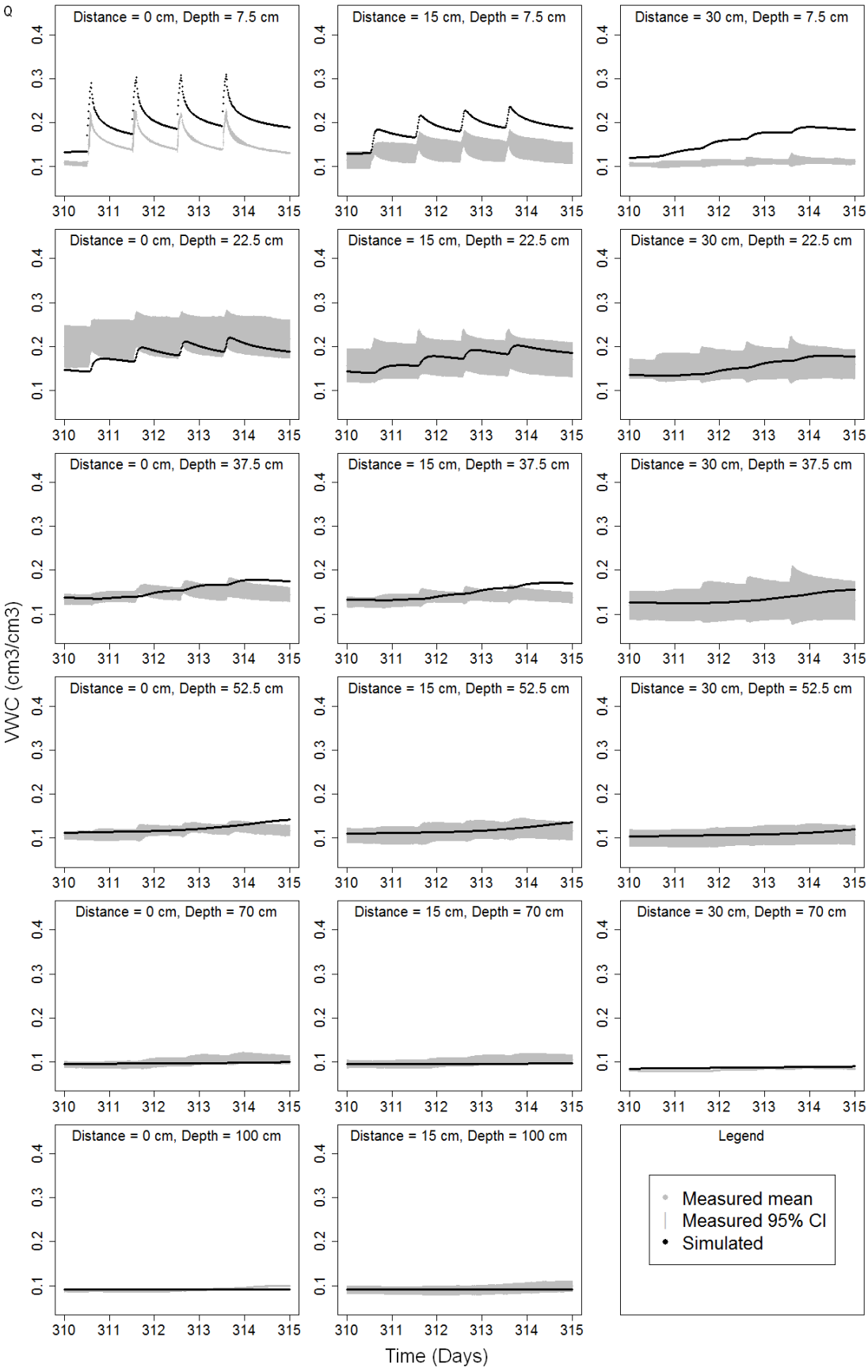
Q
Distance = 0 cm, Depth = 7.5 cm
Distance = 15 cm, Depth = 7.5 cm
Distance = 30 cm, Depth = 7.5 cm
Distance = 0 cm, Depth = 22.5 cm
Distance = 15 cm, Depth = 22.5 cm
Distance = 30 cm, Depth = 22.5 cm
Distance = 0 cm, Depth = 37.5 cm
Distance = 15 cm, Depth = 37.5 cm
Distance = 30 cm, Depth = 37.5 cm
Distance = 0 cm, Depth = 52.5 cm
Distance = 15 cm, Depth = 52.5 cm
Distance = 30 cm, Depth = 52.5 cm
Distance = 0 cm, Depth = 70 cm
Distance = 15 cm, Depth = 70 cm
Distance = 30 cm, Depth = 70 cm
Distance = 0 cm, Depth = 100 cm
Distance = 15 cm, Depth = 100 cm
Legend
Measured mean
Measured 95% CI
Simulated
VWC (cm3/cm3)
Time (Days)
0.1
0.2
0.3
0.4
310
311
312
313
314
315

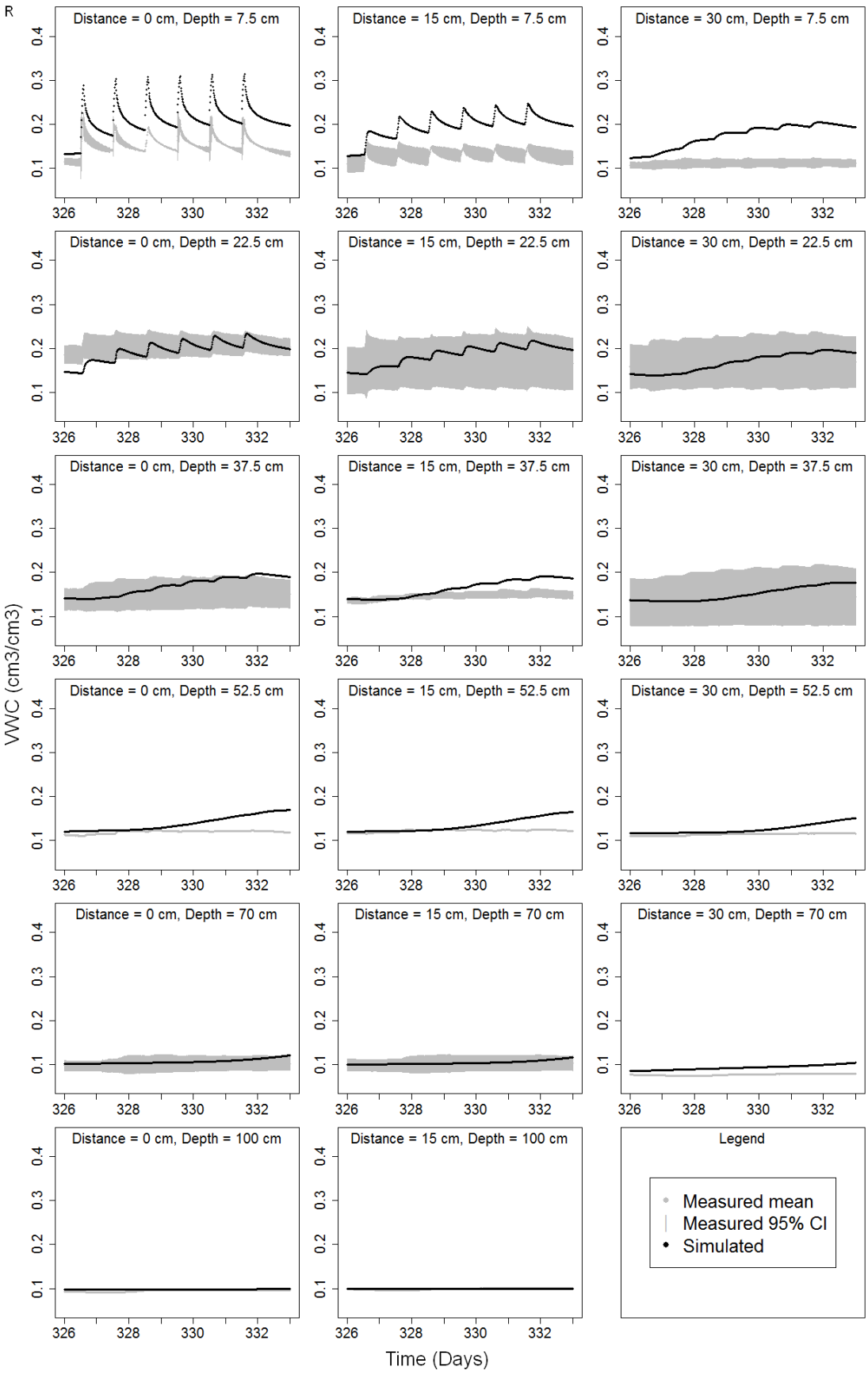
R
Distance = 0 cm, Depth = 7.5 cm
Distance = 15 cm, Depth = 7.5 cm
Distance = 30 cm, Depth = 7.5 cm
Distance = 0 cm, Depth = 22.5 cm
Distance = 15 cm, Depth = 22.5 cm
Distance = 30 cm, Depth = 22.5 cm
Distance = 0 cm, Depth = 37.5 cm
Distance = 15 cm, Depth = 37.5 cm
Distance = 30 cm, Depth = 37.5 cm
Distance = 0 cm, Depth = 52.5 cm
Distance = 15 cm, Depth = 52.5 cm
Distance = 30 cm, Depth = 52.5 cm
Distance = 0 cm, Depth = 70 cm
Distance = 15 cm, Depth = 70 cm
Distance = 30 cm, Depth = 70 cm
Distance = 0 cm, Depth = 100 cm
Distance = 15 cm, Depth = 100 cm
Legend
Measured mean
Measured 95% CI
Simulated
VWC (cm3/cm3)
Time (Days)
0.1
0.2
0.3
0.4
326
328
330
332

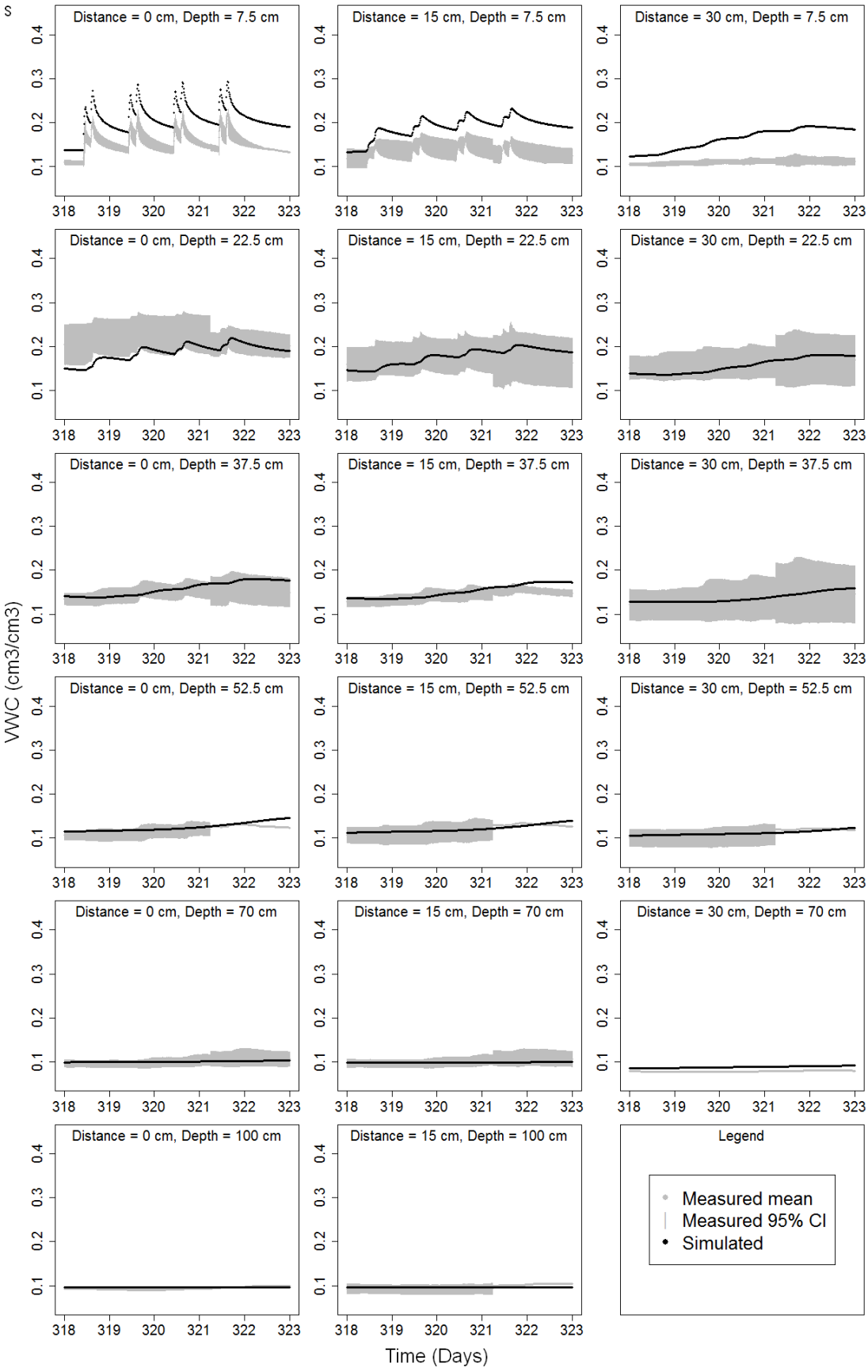
S
Distance = 0 cm, Depth = 7.5 cm
Distance = 15 cm, Depth = 7.5 cm
Distance = 30 cm, Depth = 7.5 cm
Distance = 0 cm, Depth = 22.5 cm
Distance = 15 cm, Depth = 22.5 cm
Distance = 30 cm, Depth = 22.5 cm
Distance = 0 cm, Depth = 37.5 cm
Distance = 15 cm, Depth = 37.5 cm
Distance = 30 cm, Depth = 37.5 cm
Distance = 0 cm, Depth = 52.5 cm
Distance = 15 cm, Depth = 52.5 cm
Distance = 30 cm, Depth = 52.5 cm
Distance = 0 cm, Depth = 70 cm
Distance = 15 cm, Depth = 70 cm
Distance = 30 cm, Depth = 70 cm
Distance = 0 cm, Depth = 100 cm
Distance = 15 cm, Depth = 100 cm
Legend
Measured mean
Measured 95% CI
Simulated
VWC (cm3/cm3)
Time (Days)
0.1
0.2
0.3
0.4
318
319
320
321
322
323

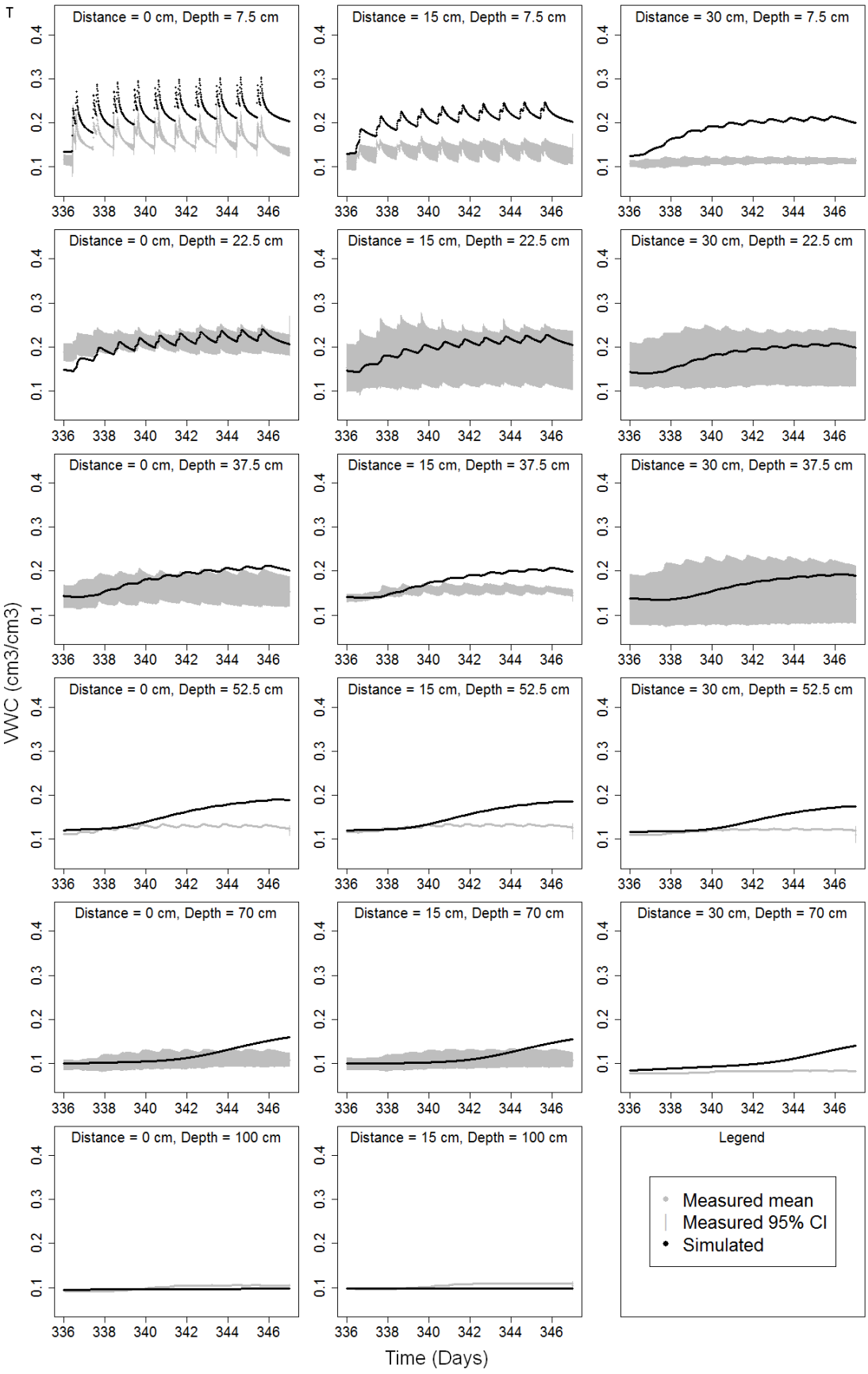
T
Distance = 0 cm, Depth = 7.5 cm
Distance = 15 cm, Depth = 7.5 cm
Distance = 30 cm, Depth = 7.5 cm
Distance = 0 cm, Depth = 22.5 cm
Distance = 15 cm, Depth = 22.5 cm
Distance = 30 cm, Depth = 22.5 cm
Distance = 0 cm, Depth = 37.5 cm
Distance = 15 cm, Depth = 37.5 cm
Distance = 30 cm, Depth = 37.5 cm
Distance = 0 cm, Depth = 52.5 cm
Distance = 15 cm, Depth = 52.5 cm
Distance = 30 cm, Depth = 52.5 cm
Distance = 0 cm, Depth = 70 cm
Distance = 15 cm, Depth = 70 cm
Distance = 30 cm, Depth = 70 cm
Distance = 0 cm, Depth = 100 cm
Distance = 15 cm, Depth = 100 cm
Legend
Measured mean
Measured 95% CI
Simulated
VWC (cm3/cm3)
Time (Days)
0.1
0.2
0.3
0.4
336
338
340
342
344
346

U

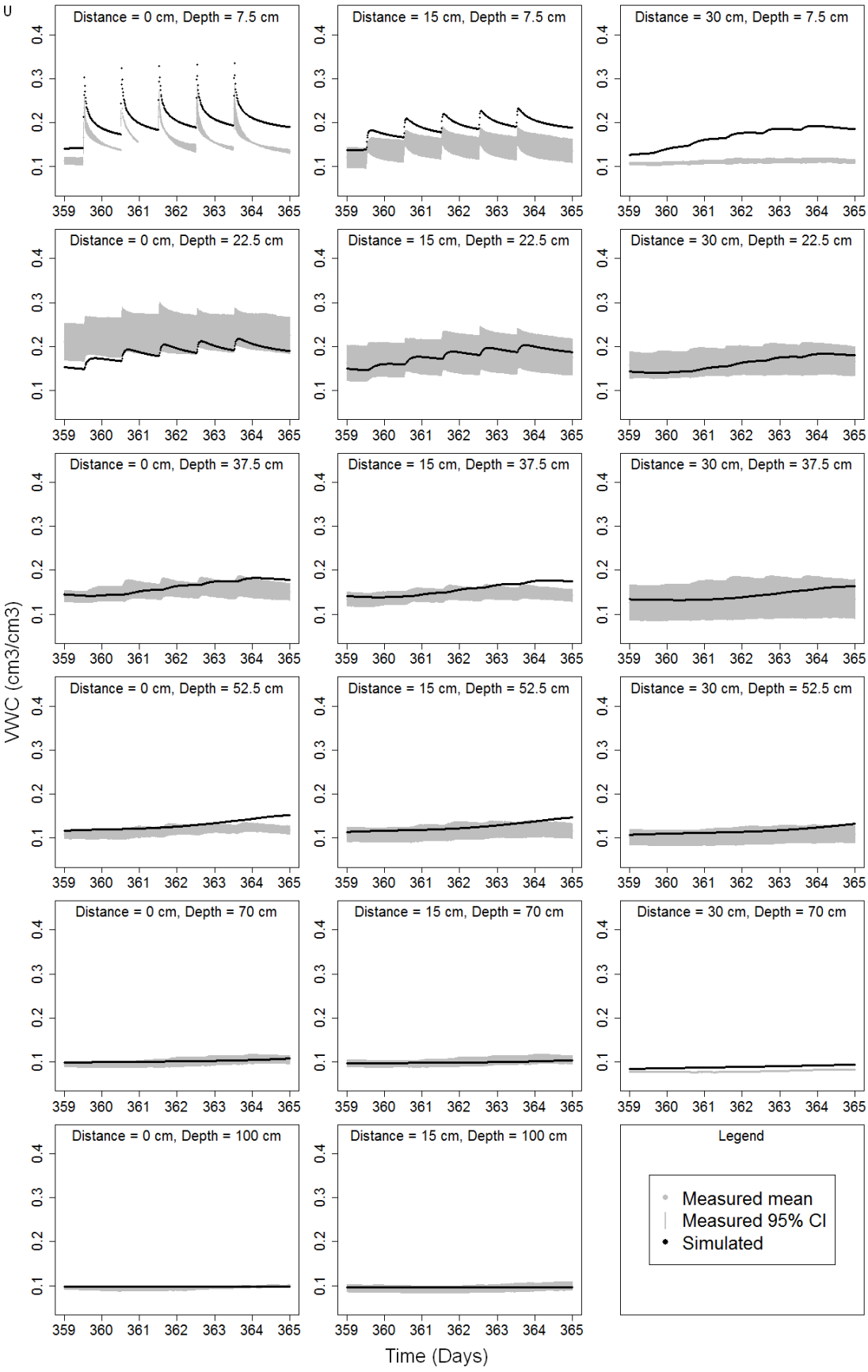
Distance = 0 cm, Depth = 7.5 cm
Distance = 15 cm, Depth = 7.5 cm
Distance = 30 cm, Depth = 7.5 cm
Distance = 0 cm, Depth = 22.5 cm
Distance = 15 cm, Depth = 22.5 cm
Distance = 30 cm, Depth = 22.5 cm
Distance = 0 cm, Depth = 37.5 cm
Distance = 15 cm, Depth = 37.5 cm
Distance = 30 cm, Depth = 37.5 cm
Distance = 0 cm, Depth = 52.5 cm
Distance = 15 cm, Depth = 52.5 cm
Distance = 30 cm, Depth = 52.5 cm
Distance = 0 cm, Depth = 70 cm
Distance = 15 cm, Depth = 70 cm
Distance = 30 cm, Depth = 70 cm
Distance = 0 cm, Depth = 100 cm
Distance = 15 cm, Depth = 100 cm
Legend
Measured mean
Measured 95% CI
Simulated
VWC (cm3/cm3)
Time (Days)
0.1
0.2
0.3
0.4
359
360
361
362
363
364
365

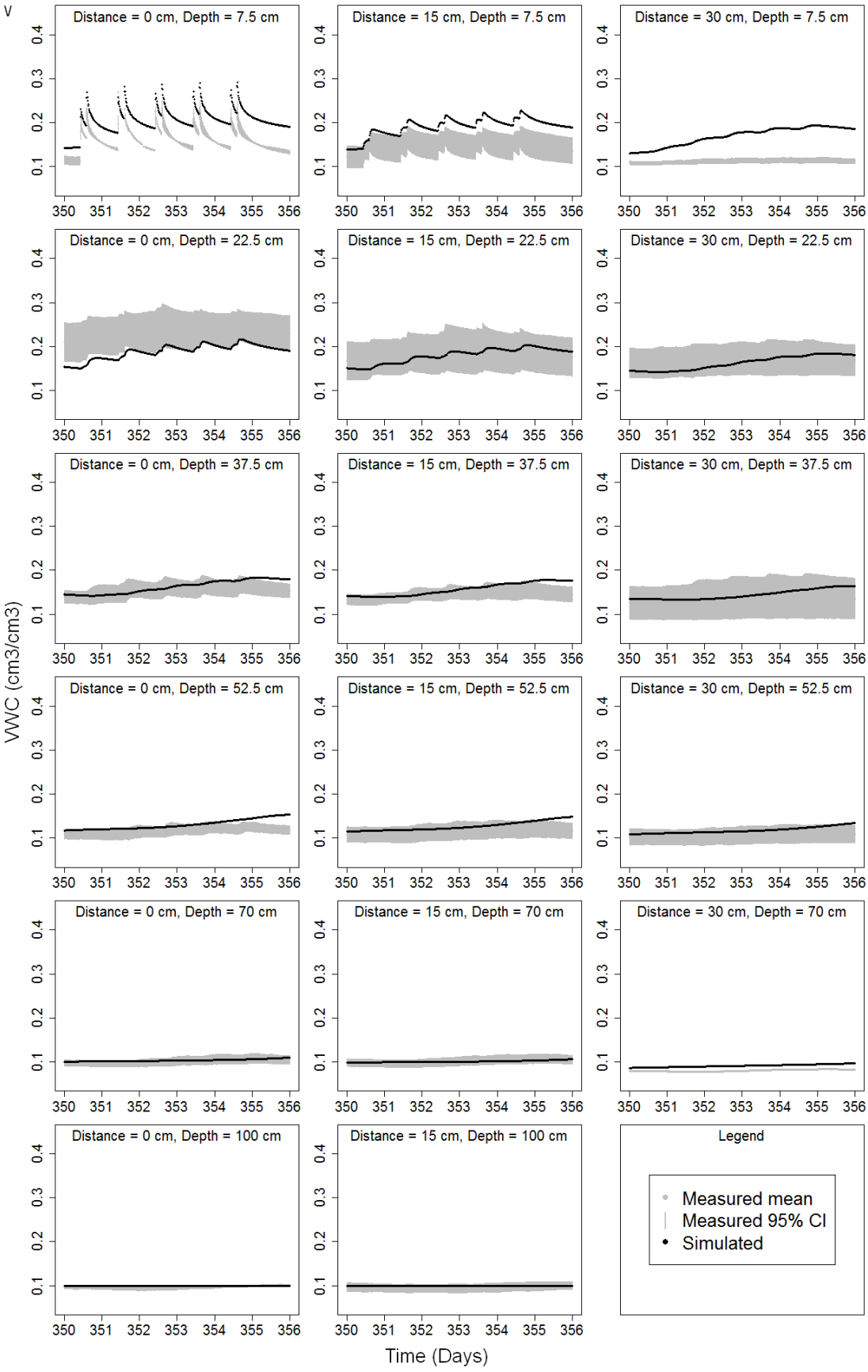
V
Distance = 0 cm, Depth = 7.5 cm
Distance = 15 cm, Depth = 7.5 cm
Distance = 30 cm, Depth = 7.5 cm
Distance = 0 cm, Depth = 22.5 cm
Distance = 15 cm, Depth = 22.5 cm
Distance = 30 cm, Depth = 22.5 cm
Distance = 0 cm, Depth = 37.5 cm
Distance = 15 cm, Depth = 37.5 cm
Distance = 30 cm, Depth = 37.5 cm
Distance = 0 cm, Depth = 52.5 cm
Distance = 15 cm, Depth = 52.5 cm
Distance = 30 cm, Depth = 52.5 cm
Distance = 0 cm, Depth = 70 cm
Distance = 15 cm, Depth = 70 cm
Distance = 30 cm, Depth = 70 cm
Distance = 0 cm, Depth = 100 cm
Distance = 15 cm, Depth = 100 cm
Legend
Measured mean
Measured 95% CI
Simulated
VWC (cm3/cm3)
Time (Days)
0.1
0.2
0.3
0.4
350
351
352
353
354
355
356

Figure C-2. Time evolution at each probe location of the measured and simulated VWCs using DSSAT-2D with the RETC estimated soil parameters. Plots for each probe location include the predicted VWCs, average probe measured VWCs, and 95% probe measured VWC confidence intervals vs. time for treatments A) 30-H-1 rep 1, B) 30-H-2 rep 1, C) 30-L-1 rep 1, D) 30-L-2 rep 1, E) 20-H-1 rep 1, F) 20-H-2 rep 1, G) 10-H-2 rep 1, H)10-H-1 rep 1, I) 20-L-1 rep 1, J) 20-L-2 rep 1, K) 10-L-2 rep 1, L) 10-L-1 rep 1, M) 10-H-2 rep 2, N) 10-H-2 rep 3, O) 10-H-1 rep 2, P) 10-H-2 rep 3, Q) 30-L-1 rep 2, R) 30-L-1 rep 3, S) 30-L-2 rep 2, T) 30-L-2 rep 3, U) 20-H-1 rep 2, V) 20-H-2 rep 2.

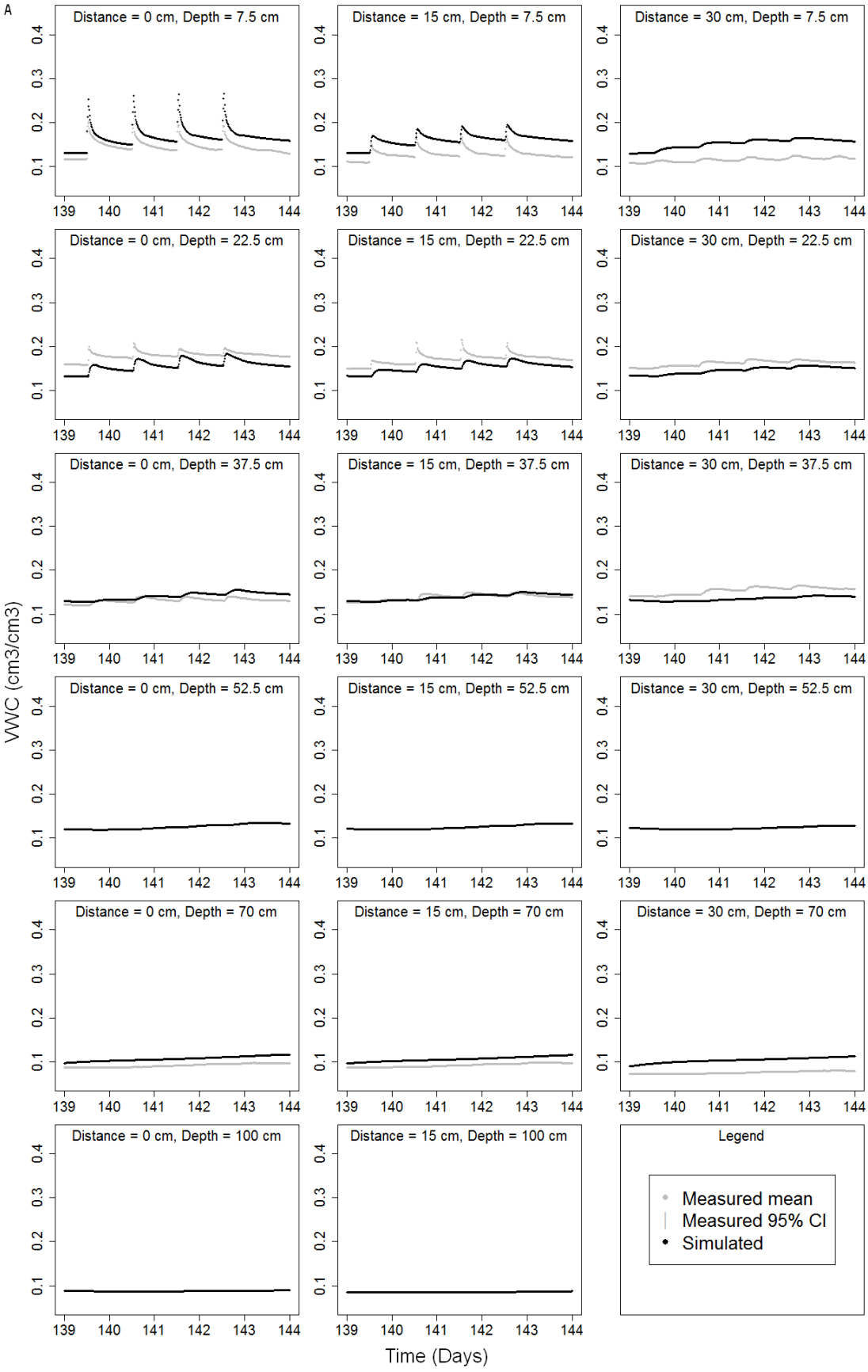
A
Distance = 0 cm, Depth = 7.5 cm
Distance = 15 cm, Depth = 7.5 cm
Distance = 30 cm, Depth = 7.5 cm
Distance = 0 cm, Depth = 22.5 cm
Distance = 15 cm, Depth = 22.5 cm
Distance = 30 cm, Depth = 22.5 cm
Distance = 0 cm, Depth = 37.5 cm
Distance = 15 cm, Depth = 37.5 cm
Distance = 30 cm, Depth = 37.5 cm
Distance = 0 cm, Depth = 52.5 cm
Distance = 15 cm, Depth = 52.5 cm
Distance = 30 cm, Depth = 52.5 cm
Distance = 0 cm, Depth = 70 cm
Distance = 15 cm, Depth = 70 cm
Distance = 30 cm, Depth = 70 cm
Distance = 0 cm, Depth = 100 cm
Distance = 15 cm, Depth = 100 cm
Legend
Measured mean
Measured 95% CI
Simulated
VWC (cm3/cm3)
Time (Days)
0.1
0.2
0.3
0.4
139
140
141
142
143
144

B

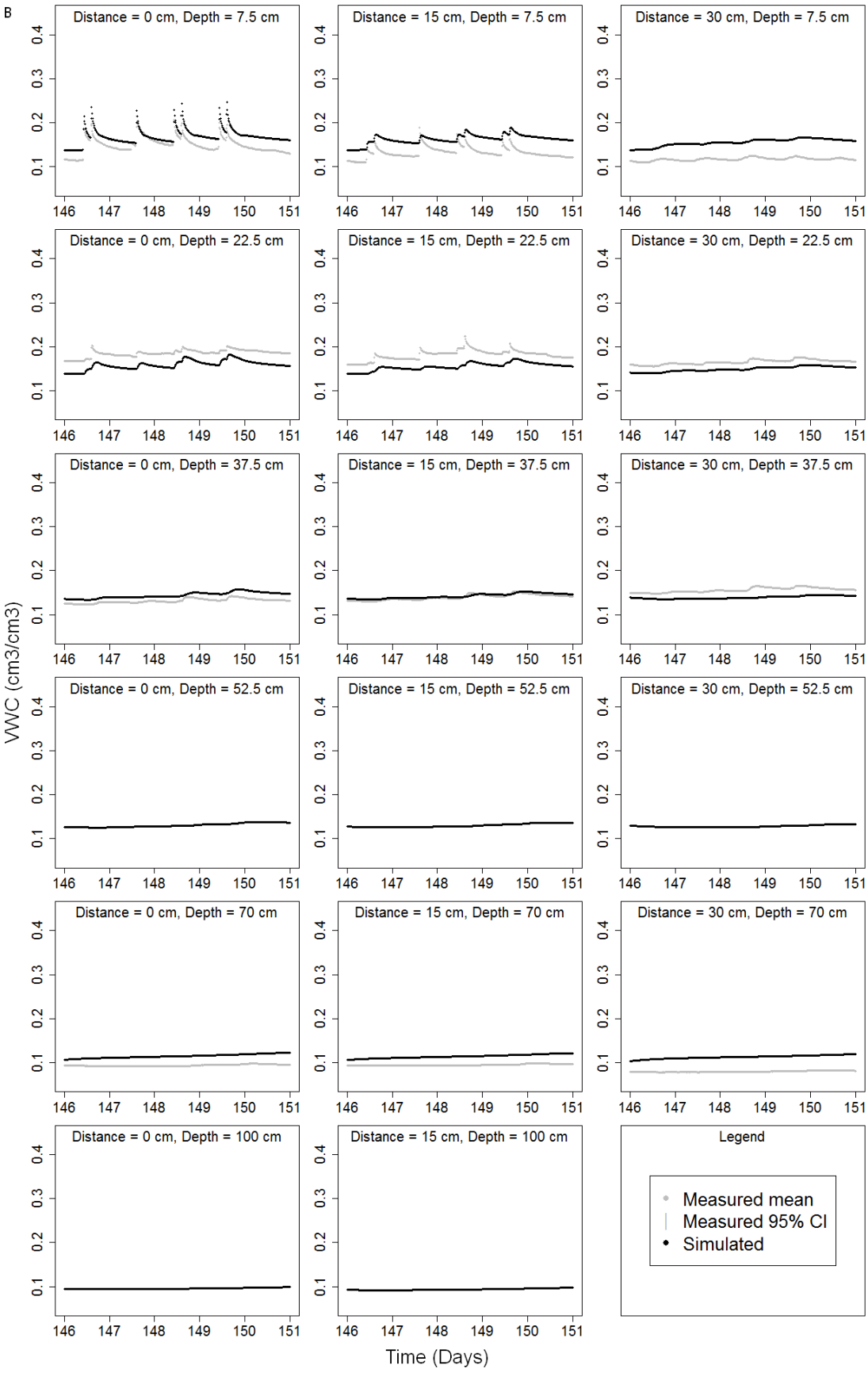
Distance = 0 cm, Depth = 7.5 cm
Distance = 15 cm, Depth = 7.5 cm
Distance = 30 cm, Depth = 7.5 cm
Distance = 0 cm, Depth = 22.5 cm
Distance = 15 cm, Depth = 22.5 cm
Distance = 30 cm, Depth = 22.5 cm
Distance = 0 cm, Depth = 37.5 cm
Distance = 15 cm, Depth = 37.5 cm
Distance = 30 cm, Depth = 37.5 cm
Distance = 0 cm, Depth = 52.5 cm
Distance = 15 cm, Depth = 52.5 cm
Distance = 30 cm, Depth = 52.5 cm
Distance = 0 cm, Depth = 70 cm
Distance = 15 cm, Depth = 70 cm
Distance = 30 cm, Depth = 70 cm
Distance = 0 cm, Depth = 100 cm
Distance = 15 cm, Depth = 100 cm
Legend
Measured mean
Measured 95% CI
Simulated
VWC (cm3/cm3)
Time (Days)
0.1
0.2
0.3
0.4
146
147
148
149
150
151

c

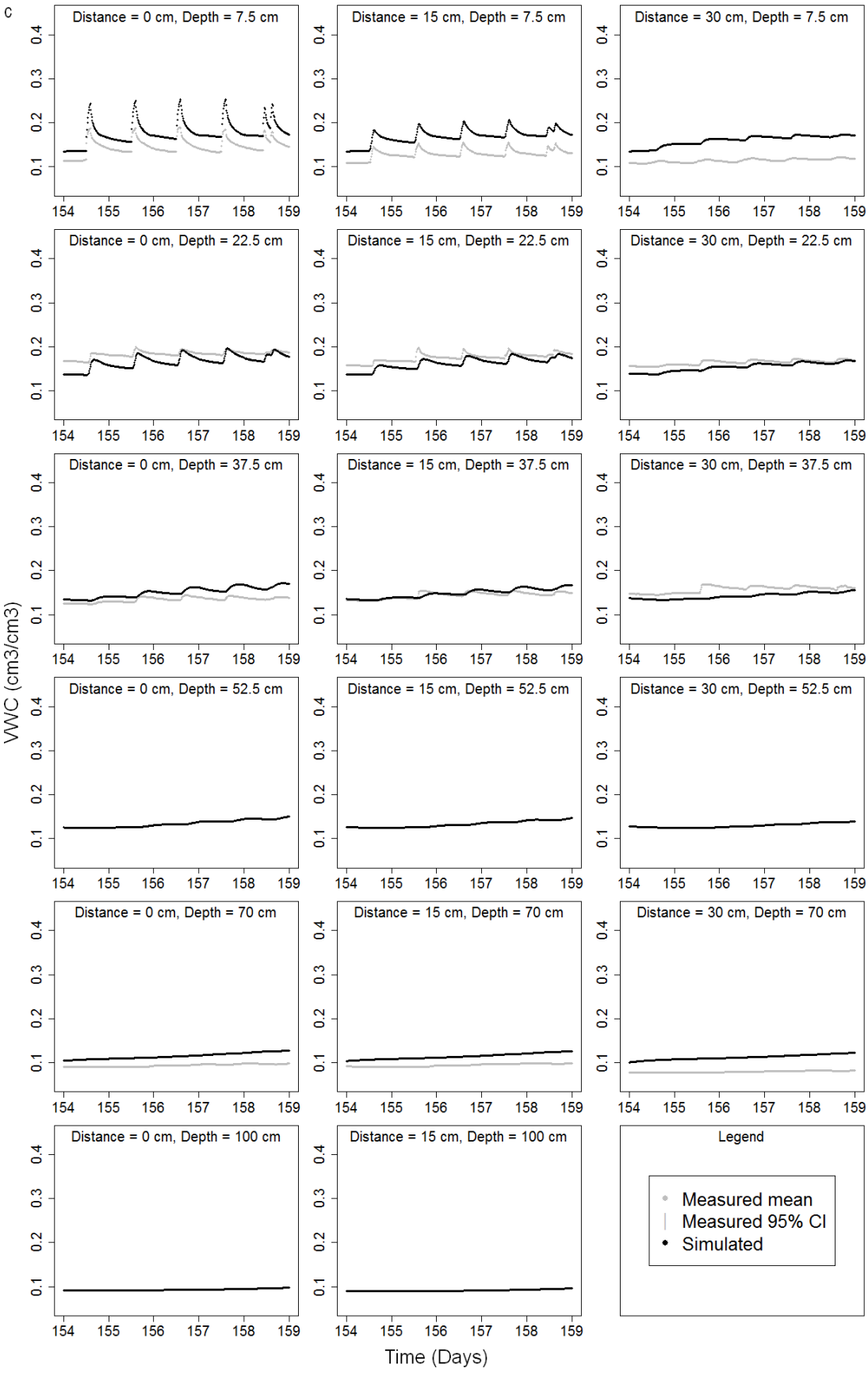
Distance = 0 cm, Depth = 7.5 cm
Distance = 15 cm, Depth = 7.5 cm
Distance = 30 cm, Depth = 7.5 cm
Distance = 0 cm, Depth = 22.5 cm
Distance = 15 cm, Depth = 22.5 cm
Distance = 30 cm, Depth = 22.5 cm
Distance = 0 cm, Depth = 37.5 cm
Distance = 15 cm, Depth = 37.5 cm
Distance = 30 cm, Depth = 37.5 cm
Distance = 0 cm, Depth = 52.5 cm
Distance = 15 cm, Depth = 52.5 cm
Distance = 30 cm, Depth = 52.5 cm
Distance = 0 cm, Depth = 70 cm
Distance = 15 cm, Depth = 70 cm
Distance = 30 cm, Depth = 70 cm
Distance = 0 cm, Depth = 100 cm
Distance = 15 cm, Depth = 100 cm
Legend
Measured mean
Measured 95% CI
Simulated
VWC (cm3/cm3)
Time (Days)
0.1
0.2
0.3
0.4
154
155
156
157
158
159

D

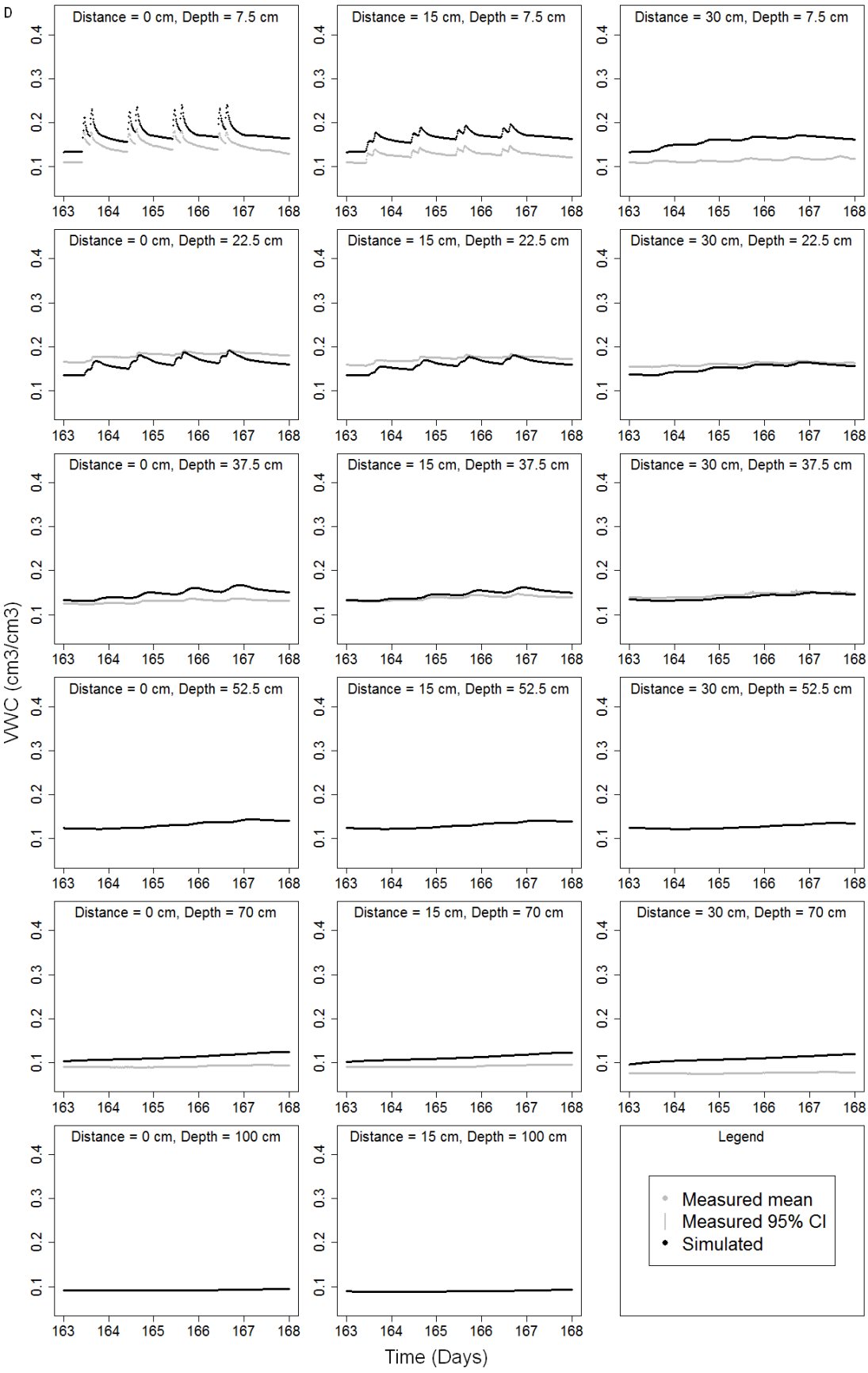
Distance = 0 cm, Depth = 7.5 cm
Distance = 15 cm, Depth = 7.5 cm
Distance = 30 cm, Depth = 7.5 cm
Distance = 0 cm, Depth = 22.5 cm
Distance = 15 cm, Depth = 22.5 cm
Distance = 30 cm, Depth = 22.5 cm
Distance = 0 cm, Depth = 37.5 cm
Distance = 15 cm, Depth = 37.5 cm
Distance = 30 cm, Depth = 37.5 cm
Distance = 0 cm, Depth = 52.5 cm
Distance = 15 cm, Depth = 52.5 cm
Distance = 30 cm, Depth = 52.5 cm
Distance = 0 cm, Depth = 70 cm
Distance = 15 cm, Depth = 70 cm
Distance = 30 cm, Depth = 70 cm
Distance = 0 cm, Depth = 100 cm
Distance = 15 cm, Depth = 100 cm
Legend
Measured mean
Measured 95% CI
Simulated
VWC (cm3/cm3)
Time (Days)

E

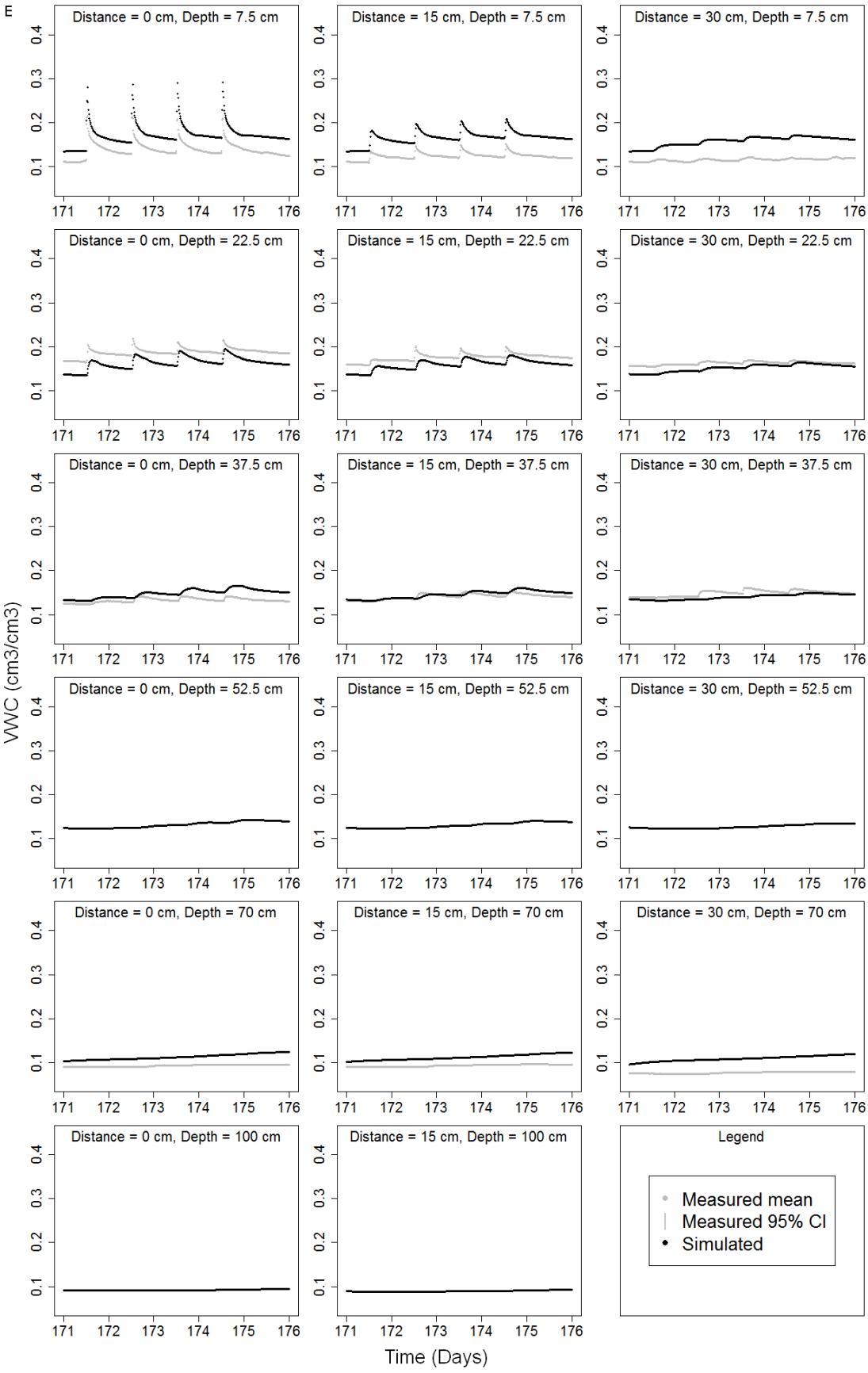
Distance = 0 cm, Depth = 7.5 cm
Distance = 15 cm, Depth = 7.5 cm
Distance = 30 cm, Depth = 7.5 cm
Distance = 0 cm, Depth = 22.5 cm
Distance = 15 cm, Depth = 22.5 cm
Distance = 30 cm, Depth = 22.5 cm
Distance = 0 cm, Depth = 37.5 cm
Distance = 15 cm, Depth = 37.5 cm
Distance = 30 cm, Depth = 37.5 cm
Distance = 0 cm, Depth = 52.5 cm
Distance = 15 cm, Depth = 52.5 cm
Distance = 30 cm, Depth = 52.5 cm
Distance = 0 cm, Depth = 70 cm
Distance = 15 cm, Depth = 70 cm
Distance = 30 cm, Depth = 70 cm
Distance = 0 cm, Depth = 100 cm
Distance = 15 cm, Depth = 100 cm
Legend
Measured mean
Measured 95% CI
Simulated
VWC (cm3/cm3)
Time (Days)
0.1
0.2
0.3
0.4
171
172
173
174
175
176

F

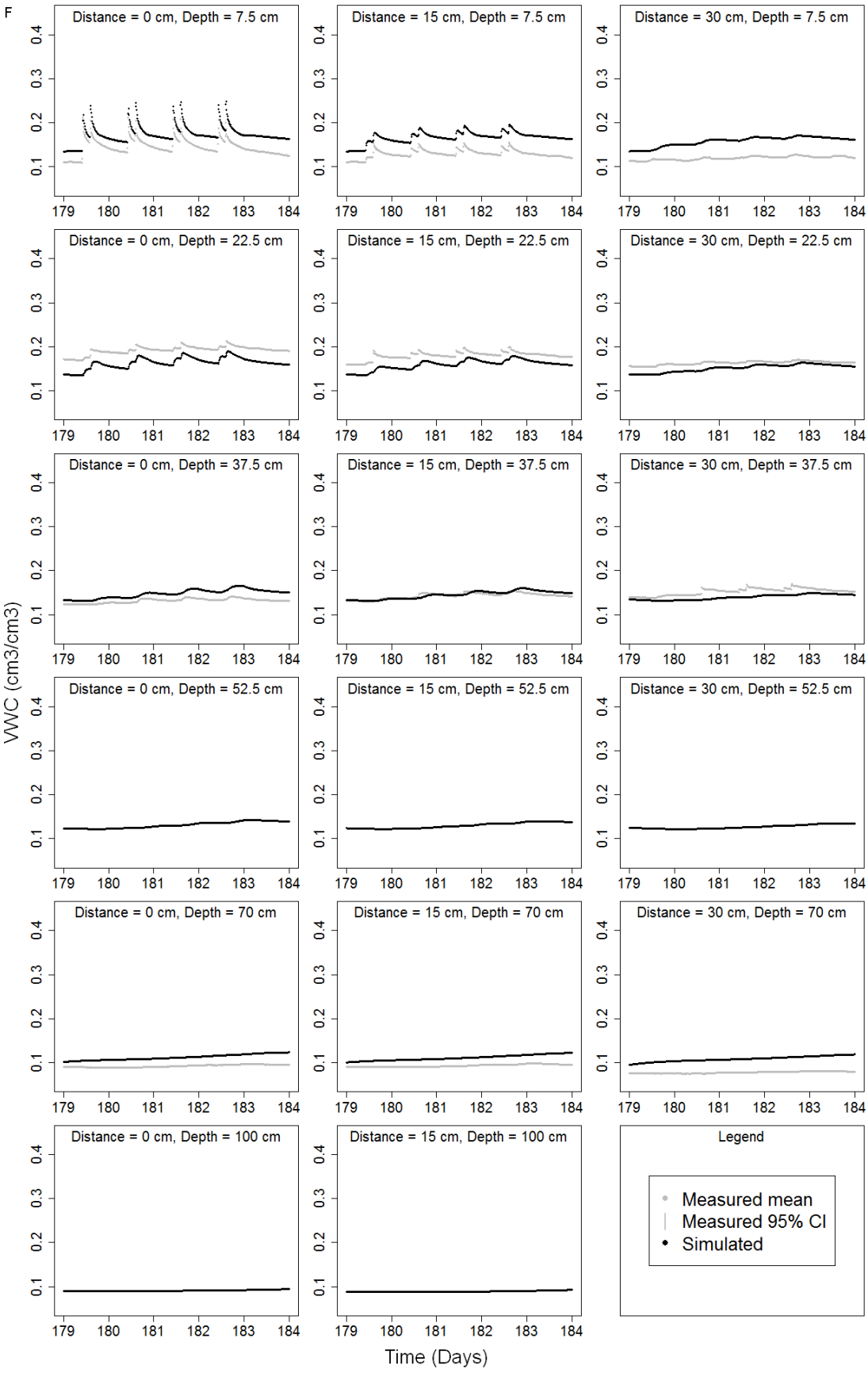
Distance = 0 cm, Depth = 7.5 cm
Distance = 15 cm, Depth = 7.5 cm
Distance = 30 cm, Depth = 7.5 cm
Distance = 0 cm, Depth = 22.5 cm
Distance = 15 cm, Depth = 22.5 cm
Distance = 30 cm, Depth = 22.5 cm
Distance = 0 cm, Depth = 37.5 cm
Distance = 15 cm, Depth = 37.5 cm
Distance = 30 cm, Depth = 37.5 cm
Distance = 0 cm, Depth = 52.5 cm
Distance = 15 cm, Depth = 52.5 cm
Distance = 30 cm, Depth = 52.5 cm
Distance = 0 cm, Depth = 70 cm
Distance = 15 cm, Depth = 70 cm
Distance = 30 cm, Depth = 70 cm
Distance = 0 cm, Depth = 100 cm
Distance = 15 cm, Depth = 100 cm
Legend
Measured mean
Measured 95% CI
Simulated
VWC (cm3/cm3)
Time (Days)
0.1
0.2
0.3
0.4
179
180
181
182
183
184

G

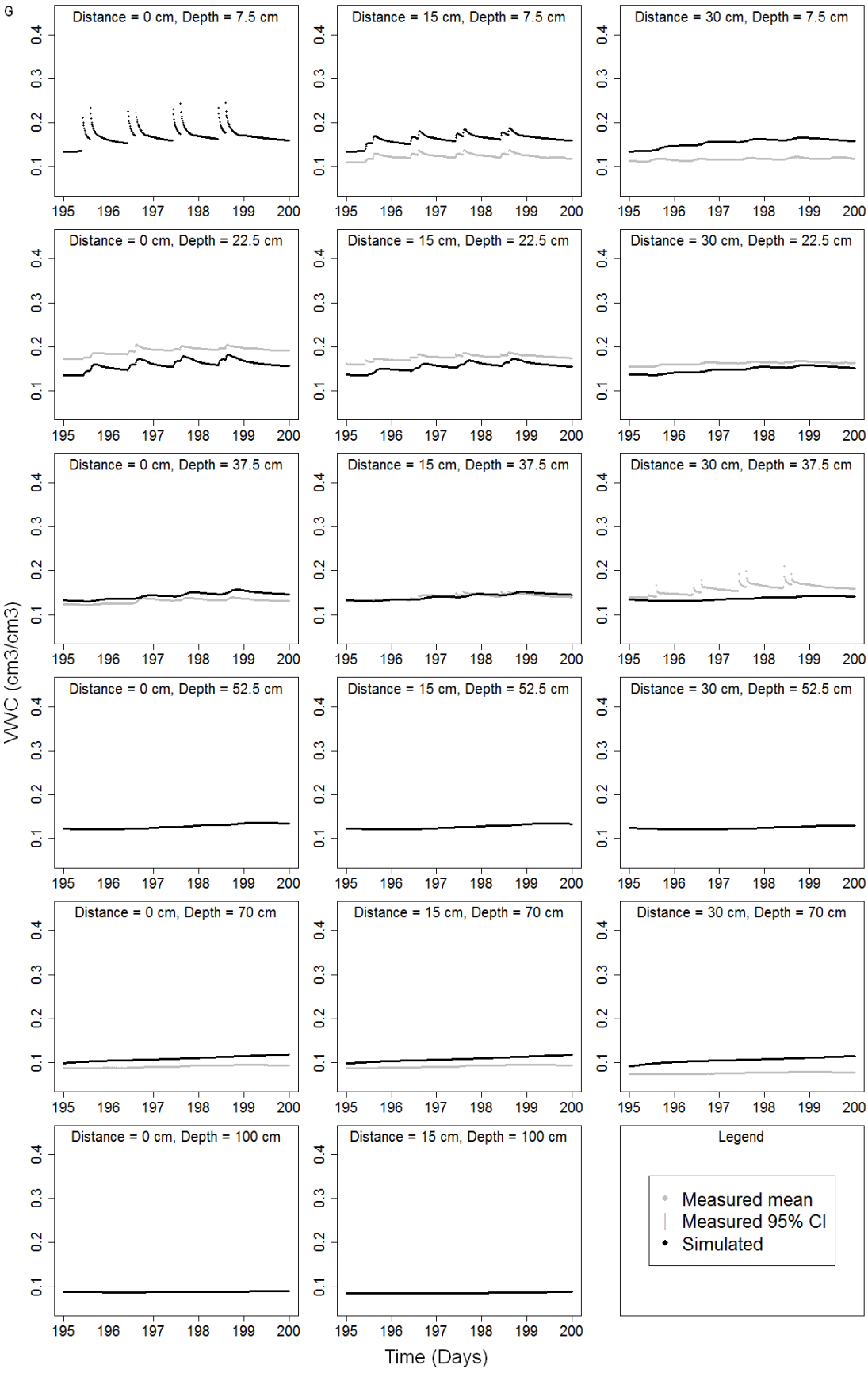
Distance = 0 cm, Depth = 7.5 cm
Distance = 15 cm, Depth = 7.5 cm
Distance = 30 cm, Depth = 7.5 cm
Distance = 0 cm, Depth = 22.5 cm
Distance = 15 cm, Depth = 22.5 cm
Distance = 30 cm, Depth = 22.5 cm
Distance = 0 cm, Depth = 37.5 cm
Distance = 15 cm, Depth = 37.5 cm
Distance = 30 cm, Depth = 37.5 cm
Distance = 0 cm, Depth = 52.5 cm
Distance = 15 cm, Depth = 52.5 cm
Distance = 30 cm, Depth = 52.5 cm
Distance = 0 cm, Depth = 70 cm
Distance = 15 cm, Depth = 70 cm
Distance = 30 cm, Depth = 70 cm
Distance = 0 cm, Depth = 100 cm
Distance = 15 cm, Depth = 100 cm
Legend
Measured mean
Measured 95% CI
Simulated
VWC (cm3/cm3)
Time (Days)
0.1
0.2
0.3
0.4
195
196
197
198
199
200

H

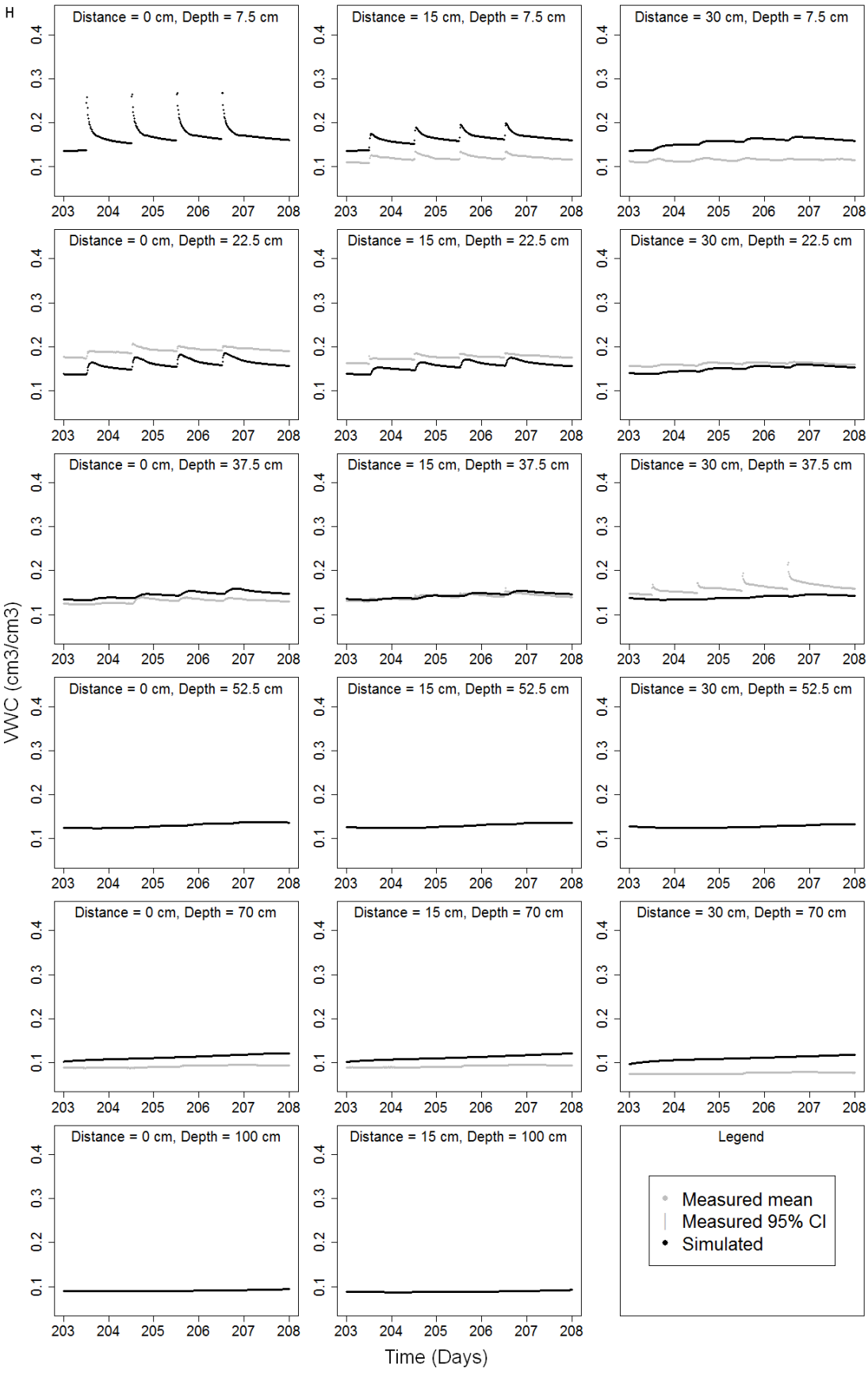
Distance = 0 cm, Depth = 7.5 cm
Distance = 15 cm, Depth = 7.5 cm
Distance = 30 cm, Depth = 7.5 cm
Distance = 0 cm, Depth = 22.5 cm
Distance = 15 cm, Depth = 22.5 cm
Distance = 30 cm, Depth = 22.5 cm
Distance = 0 cm, Depth = 37.5 cm
Distance = 15 cm, Depth = 37.5 cm
Distance = 30 cm, Depth = 37.5 cm
Distance = 0 cm, Depth = 52.5 cm
Distance = 15 cm, Depth = 52.5 cm
Distance = 30 cm, Depth = 52.5 cm
Distance = 0 cm, Depth = 70 cm
Distance = 15 cm, Depth = 70 cm
Distance = 30 cm, Depth = 70 cm
Distance = 0 cm, Depth = 100 cm
Distance = 15 cm, Depth = 100 cm
Legend
Measured mean
Measured 95% CI
Simulated
VWC (cm3/cm3)
Time (Days)

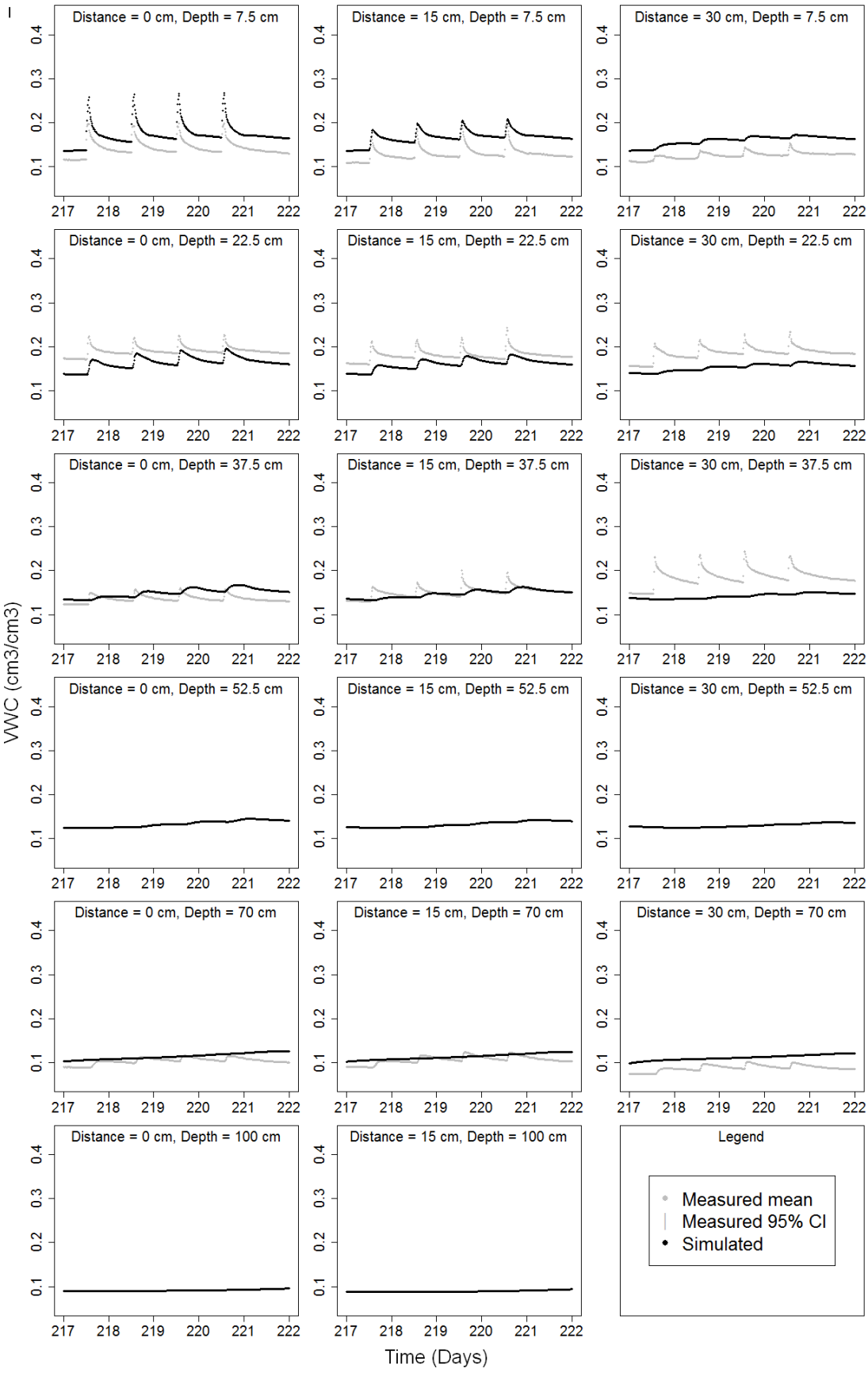
Distance = 0 cm, Depth = 7.5 cm
Distance = 15 cm, Depth = 7.5 cm
Distance = 30 cm, Depth = 7.5 cm
Distance = 0 cm, Depth = 22.5 cm
Distance = 15 cm, Depth = 22.5 cm
Distance = 30 cm, Depth = 22.5 cm
Distance = 0 cm, Depth = 37.5 cm
Distance = 15 cm, Depth = 37.5 cm
Distance = 30 cm, Depth = 37.5 cm
Distance = 0 cm, Depth = 52.5 cm
Distance = 15 cm, Depth = 52.5 cm
Distance = 30 cm, Depth = 52.5 cm
Distance = 0 cm, Depth = 70 cm
Distance = 15 cm, Depth = 70 cm
Distance = 30 cm, Depth = 70 cm
Distance = 0 cm, Depth = 100 cm
Distance = 15 cm, Depth = 100 cm
Legend
Measured mean
Measured 95% CI
Simulated
VWC (cm3/cm3)
Time (Days)
0.1
0.2
0.3
0.4
217
218
219
220
221
222

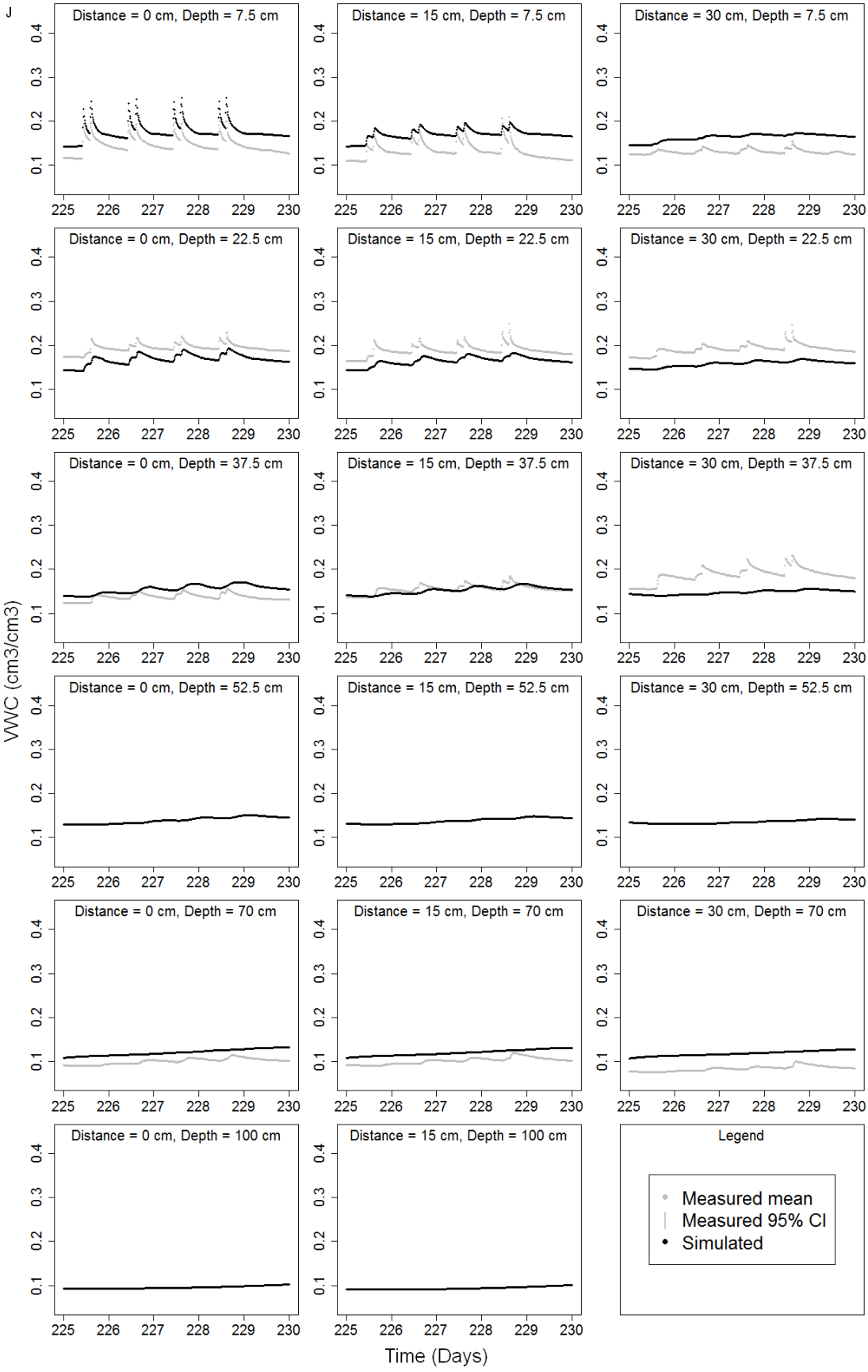
Distance = 0 cm, Depth = 7.5 cm
Distance = 15 cm, Depth = 7.5 cm
Distance = 30 cm, Depth = 7.5 cm
Distance = 0 cm, Depth = 22.5 cm
Distance = 15 cm, Depth = 22.5 cm
Distance = 30 cm, Depth = 22.5 cm
Distance = 0 cm, Depth = 37.5 cm
Distance = 15 cm, Depth = 37.5 cm
Distance = 30 cm, Depth = 37.5 cm
Distance = 0 cm, Depth = 52.5 cm
Distance = 15 cm, Depth = 52.5 cm
Distance = 30 cm, Depth = 52.5 cm
Distance = 0 cm, Depth = 70 cm
Distance = 15 cm, Depth = 70 cm
Distance = 30 cm, Depth = 70 cm
Distance = 0 cm, Depth = 100 cm
Distance = 15 cm, Depth = 100 cm
Legend
Measured mean
Measured 95% CI
Simulated
VWC (cm3/cm3)
Time (Days)
0.1
0.2
0.3
0.4
225
226
227
228
229
230

K

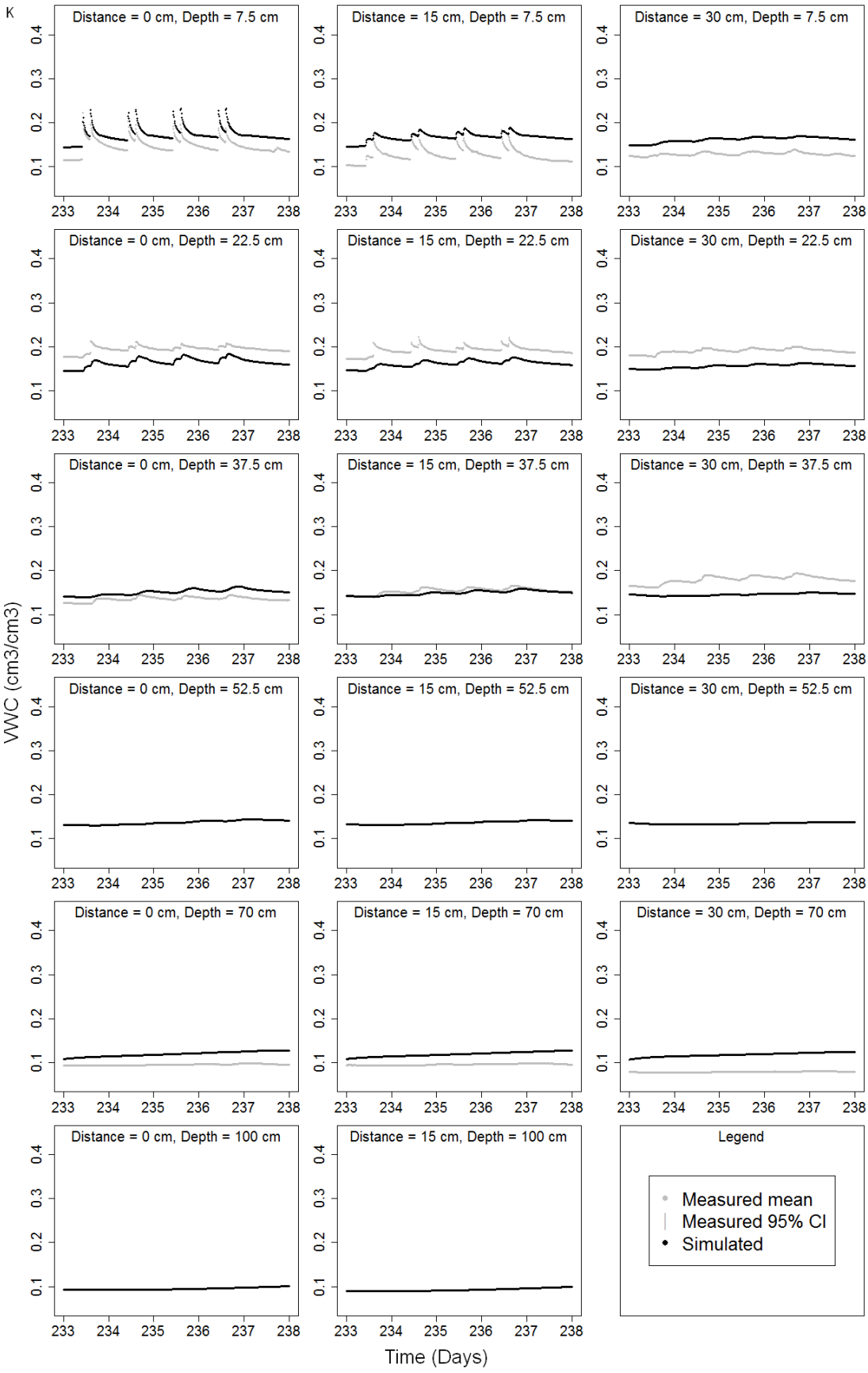
Distance = 0 cm, Depth = 7.5 cm
Distance = 15 cm, Depth = 7.5 cm
Distance = 30 cm, Depth = 7.5 cm
Distance = 0 cm, Depth = 22.5 cm
Distance = 15 cm, Depth = 22.5 cm
Distance = 30 cm, Depth = 22.5 cm
Distance = 0 cm, Depth = 37.5 cm
Distance = 15 cm, Depth = 37.5 cm
Distance = 30 cm, Depth = 37.5 cm
Distance = 0 cm, Depth = 52.5 cm
Distance = 15 cm, Depth = 52.5 cm
Distance = 30 cm, Depth = 52.5 cm
Distance = 0 cm, Depth = 70 cm
Distance = 15 cm, Depth = 70 cm
Distance = 30 cm, Depth = 70 cm
Distance = 0 cm, Depth = 100 cm
Distance = 15 cm, Depth = 100 cm
Legend
Measured mean
Measured 95% CI
Simulated
VWC (cm3/cm3)
Time (Days)
0.1
0.2
0.3
0.4
233
234
235
236
237
238

L

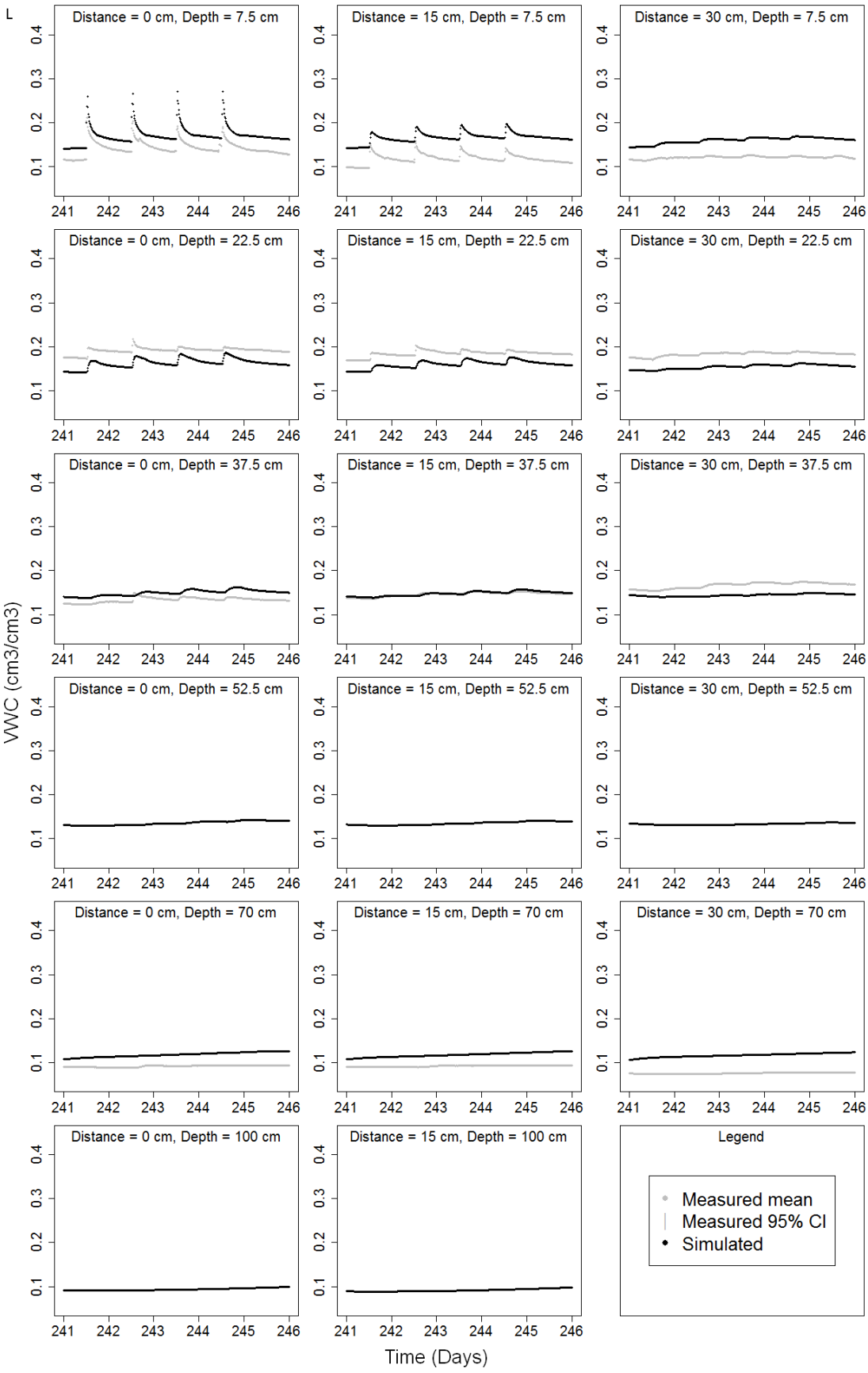
Distance = 0 cm, Depth = 7.5 cm
Distance = 15 cm, Depth = 7.5 cm
Distance = 30 cm, Depth = 7.5 cm
Distance = 0 cm, Depth = 22.5 cm
Distance = 15 cm, Depth = 22.5 cm
Distance = 30 cm, Depth = 22.5 cm
Distance = 0 cm, Depth = 37.5 cm
Distance = 15 cm, Depth = 37.5 cm
Distance = 30 cm, Depth = 37.5 cm
Distance = 0 cm, Depth = 52.5 cm
Distance = 15 cm, Depth = 52.5 cm
Distance = 30 cm, Depth = 52.5 cm
Distance = 0 cm, Depth = 70 cm
Distance = 15 cm, Depth = 70 cm
Distance = 30 cm, Depth = 70 cm
Distance = 0 cm, Depth = 100 cm
Distance = 15 cm, Depth = 100 cm
Legend
Measured mean
Measured 95% CI
Simulated
VWC (cm3/cm3)
Time (Days)
0.1
0.2
0.3
0.4
241
242
243
244
245
246

M

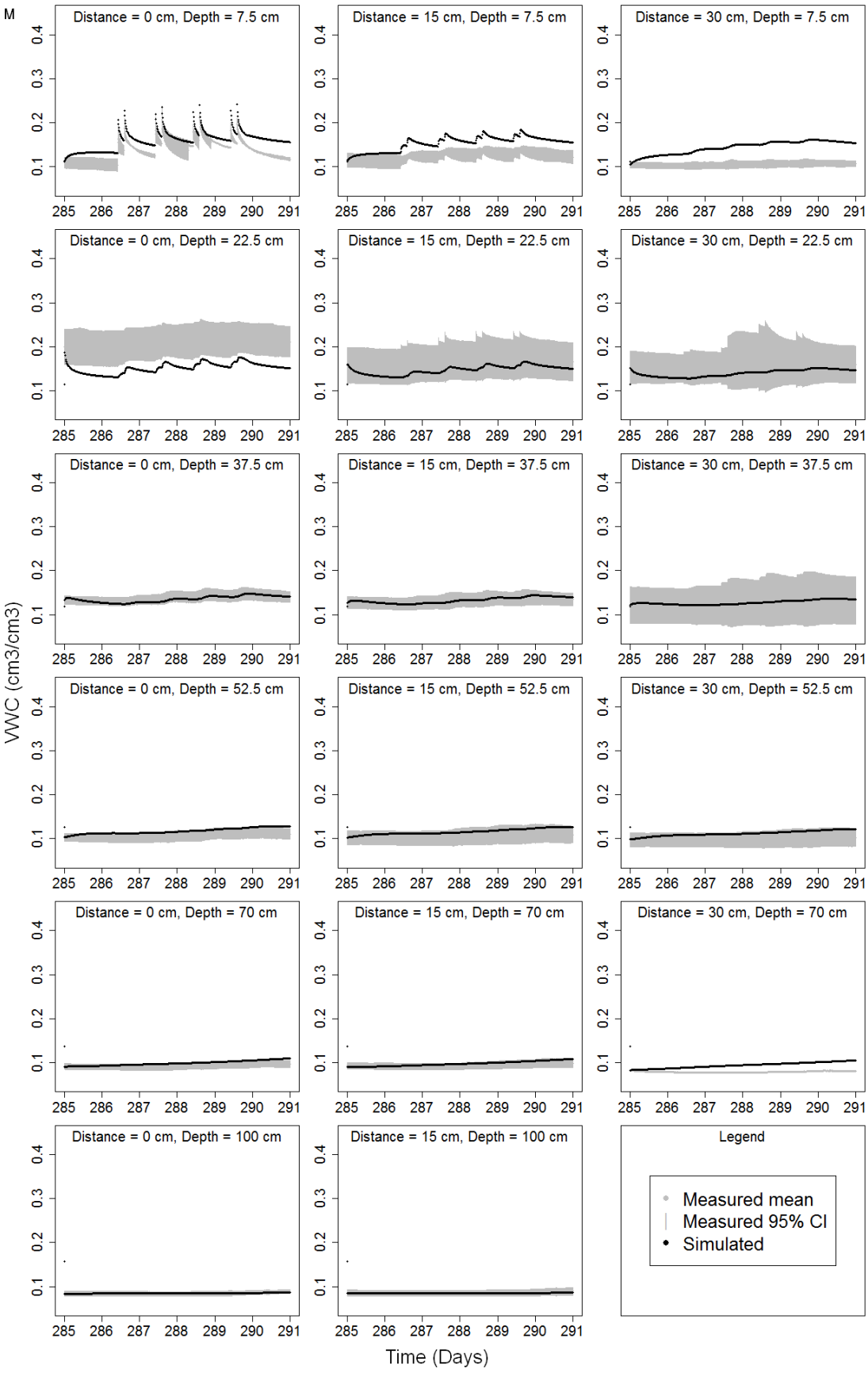
Distance = 0 cm, Depth = 7.5 cm
Distance = 15 cm, Depth = 7.5 cm
Distance = 30 cm, Depth = 7.5 cm
Distance = 0 cm, Depth = 22.5 cm
Distance = 15 cm, Depth = 22.5 cm
Distance = 30 cm, Depth = 22.5 cm
Distance = 0 cm, Depth = 37.5 cm
Distance = 15 cm, Depth = 37.5 cm
Distance = 30 cm, Depth = 37.5 cm
Distance = 0 cm, Depth = 52.5 cm
Distance = 15 cm, Depth = 52.5 cm
Distance = 30 cm, Depth = 52.5 cm
Distance = 0 cm, Depth = 70 cm
Distance = 15 cm, Depth = 70 cm
Distance = 30 cm, Depth = 70 cm
Distance = 0 cm, Depth = 100 cm
Distance = 15 cm, Depth = 100 cm
Legend
Measured mean
Measured 95% CI
Simulated
VWC (cm3/cm3)
Time (Days)
0.1
0.2
0.3
0.4
285
286
287
288
289
290
291

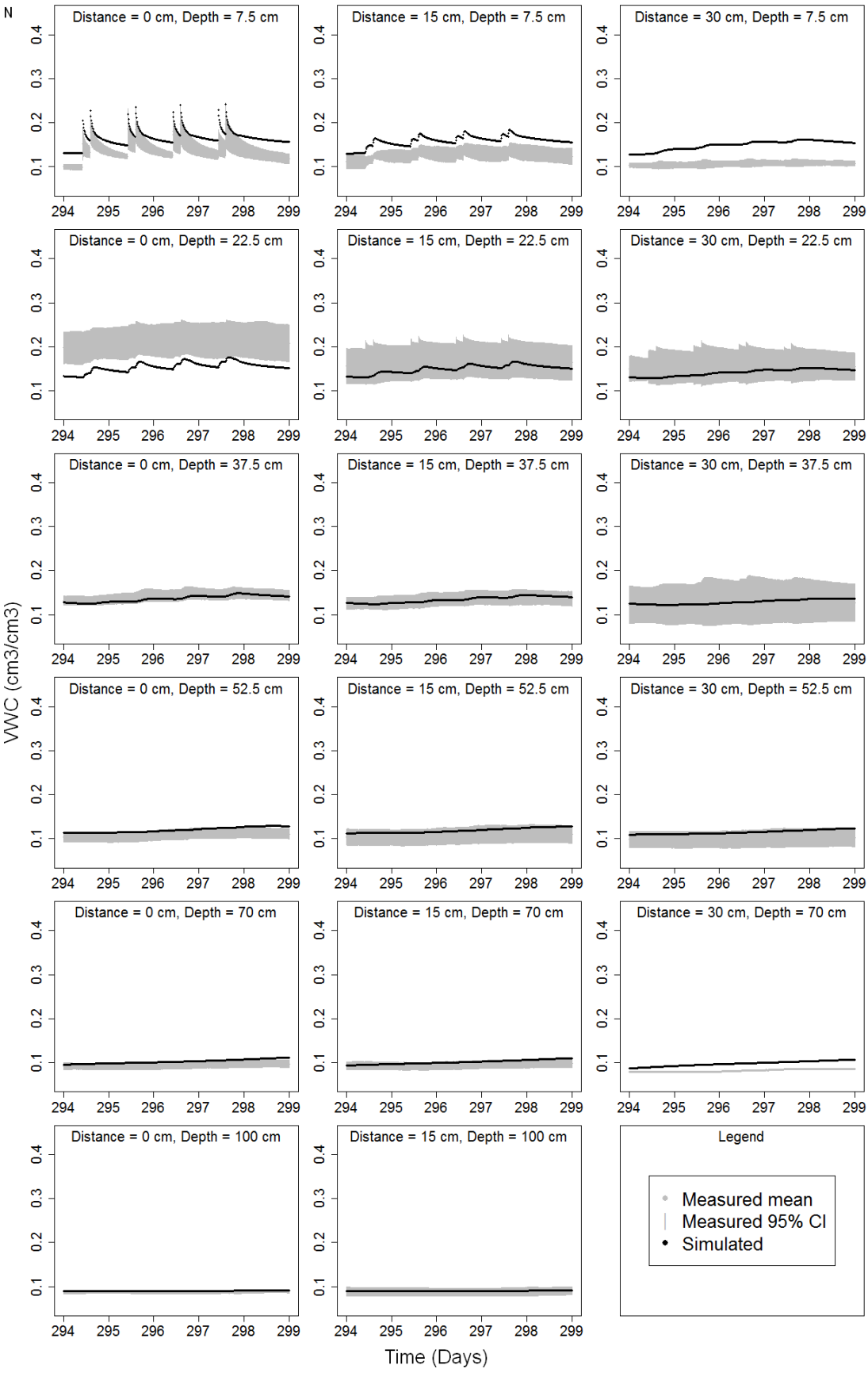
Distance = 0 cm, Depth = 7.5 cm
Distance = 15 cm, Depth = 7.5 cm
Distance = 30 cm, Depth = 7.5 cm
Distance = 0 cm, Depth = 22.5 cm
Distance = 15 cm, Depth = 22.5 cm
Distance = 30 cm, Depth = 22.5 cm
Distance = 0 cm, Depth = 37.5 cm
Distance = 15 cm, Depth = 37.5 cm
Distance = 30 cm, Depth = 37.5 cm
Distance = 0 cm, Depth = 52.5 cm
Distance = 15 cm, Depth = 52.5 cm
Distance = 30 cm, Depth = 52.5 cm
Distance = 0 cm, Depth = 70 cm
Distance = 15 cm, Depth = 70 cm
Distance = 30 cm, Depth = 70 cm
Distance = 0 cm, Depth = 100 cm
Distance = 15 cm, Depth = 100 cm
Legend
Measured mean
Measured 95% CI
Simulated
VWC (cm3/cm3)
Time (Days)
0.1
0.2
0.3
0.4
294
295
296
297
298
299

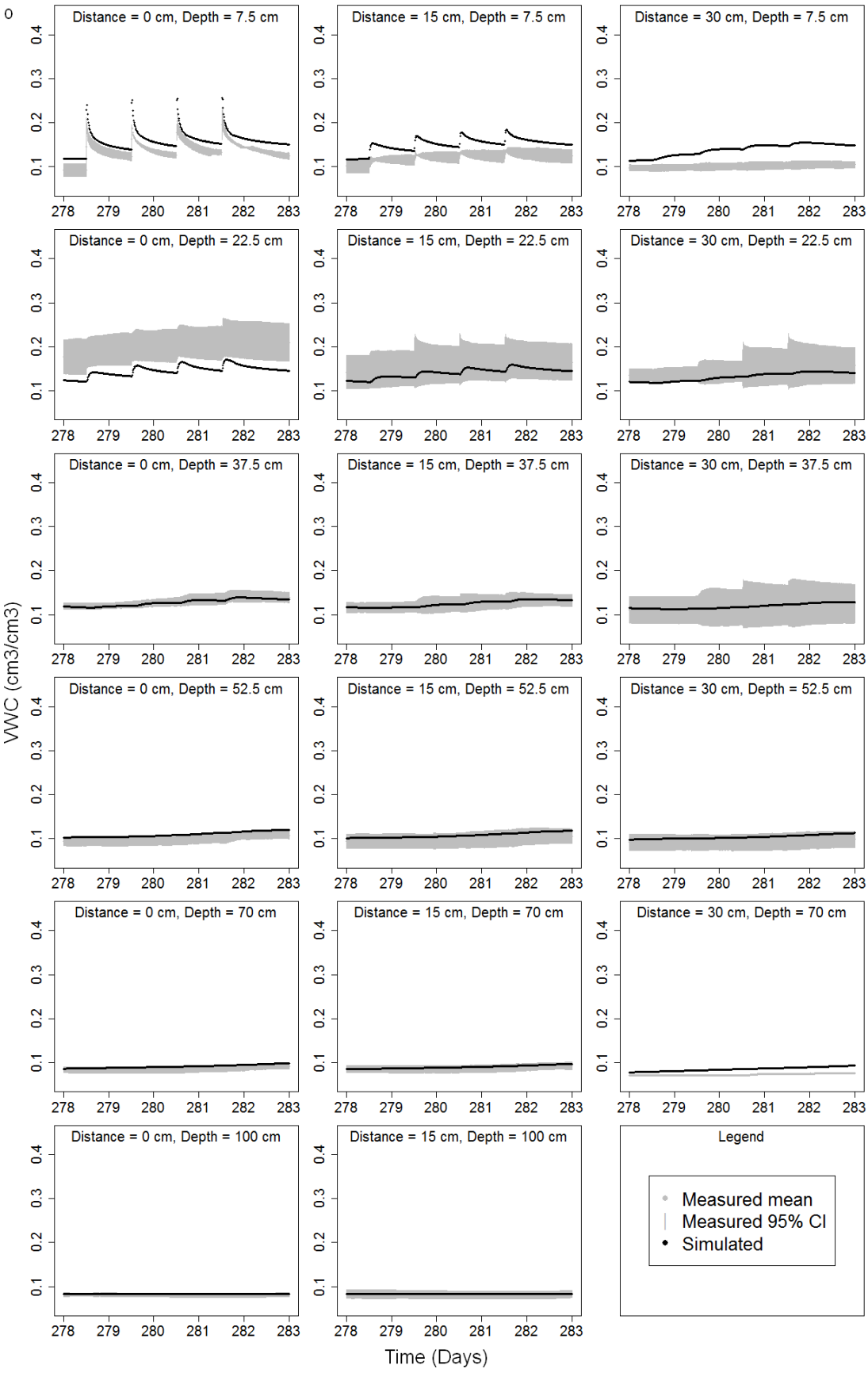
Distance = 0 cm, Depth = 7.5 cm
Distance = 15 cm, Depth = 7.5 cm
Distance = 30 cm, Depth = 7.5 cm
Distance = 0 cm, Depth = 22.5 cm
Distance = 15 cm, Depth = 22.5 cm
Distance = 30 cm, Depth = 22.5 cm
Distance = 0 cm, Depth = 37.5 cm
Distance = 15 cm, Depth = 37.5 cm
Distance = 30 cm, Depth = 37.5 cm
Distance = 0 cm, Depth = 52.5 cm
Distance = 15 cm, Depth = 52.5 cm
Distance = 30 cm, Depth = 52.5 cm
Distance = 0 cm, Depth = 70 cm
Distance = 15 cm, Depth = 70 cm
Distance = 30 cm, Depth = 70 cm
Distance = 0 cm, Depth = 100 cm
Distance = 15 cm, Depth = 100 cm
Legend
Measured mean
Measured 95% CI
Simulated
VWC (cm3/cm3)
Time (Days)
0.1
0.2
0.3
0.4
278
279
280
281
282
283

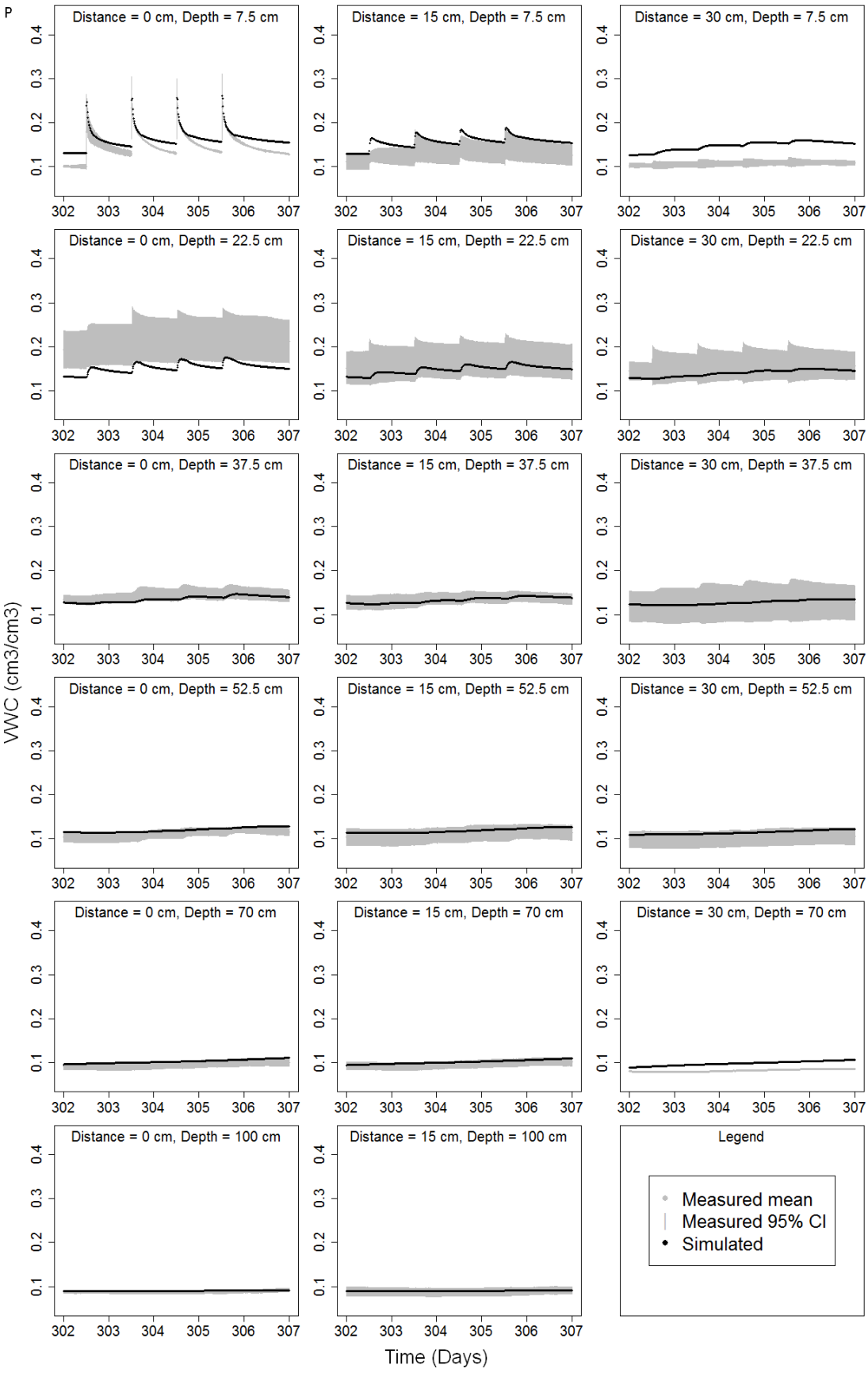
P
Distance = 0 cm, Depth = 7.5 cm
Distance = 15 cm, Depth = 7.5 cm
Distance = 30 cm, Depth = 7.5 cm
Distance = 0 cm, Depth = 22.5 cm
Distance = 15 cm, Depth = 22.5 cm
Distance = 30 cm, Depth = 22.5 cm
Distance = 0 cm, Depth = 37.5 cm
Distance = 15 cm, Depth = 37.5 cm
Distance = 30 cm, Depth = 37.5 cm
Distance = 0 cm, Depth = 52.5 cm
Distance = 15 cm, Depth = 52.5 cm
Distance = 30 cm, Depth = 52.5 cm
Distance = 0 cm, Depth = 70 cm
Distance = 15 cm, Depth = 70 cm
Distance = 30 cm, Depth = 70 cm
Distance = 0 cm, Depth = 100 cm
Distance = 15 cm, Depth = 100 cm
Legend
Measured mean
Measured 95% CI
Simulated
VWC (cm3/cm3)
Time (Days)
0.1
0.2
0.3
0.4
302
303
304
305
306
307

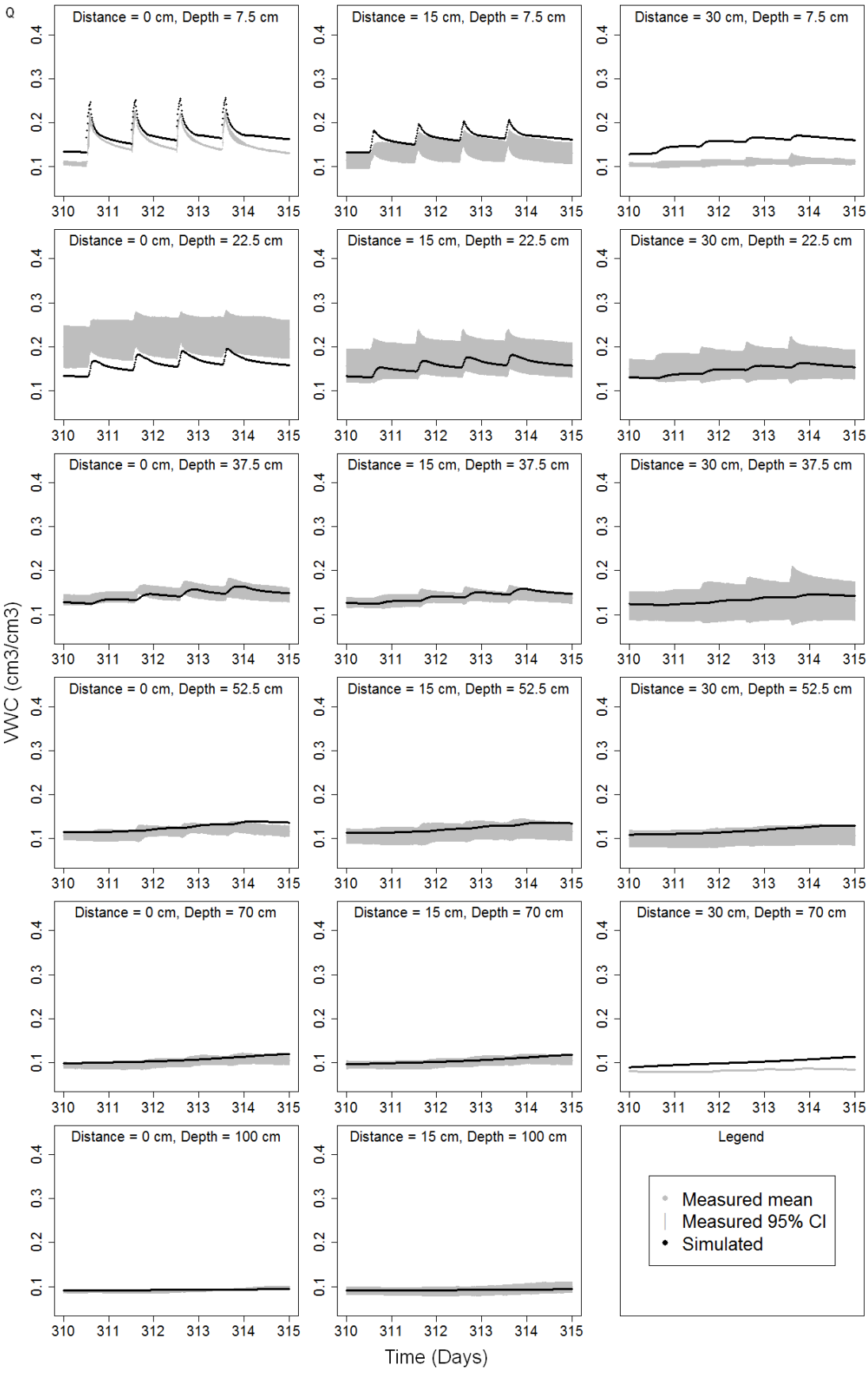
Q
Distance = 0 cm, Depth = 7.5 cm
Distance = 15 cm, Depth = 7.5 cm
Distance = 30 cm, Depth = 7.5 cm
Distance = 0 cm, Depth = 22.5 cm
Distance = 15 cm, Depth = 22.5 cm
Distance = 30 cm, Depth = 22.5 cm
Distance = 0 cm, Depth = 37.5 cm
Distance = 15 cm, Depth = 37.5 cm
Distance = 30 cm, Depth = 37.5 cm
Distance = 0 cm, Depth = 52.5 cm
Distance = 15 cm, Depth = 52.5 cm
Distance = 30 cm, Depth = 52.5 cm
Distance = 0 cm, Depth = 70 cm
Distance = 15 cm, Depth = 70 cm
Distance = 30 cm, Depth = 70 cm
Distance = 0 cm, Depth = 100 cm
Distance = 15 cm, Depth = 100 cm
Legend
Measured mean
Measured 95% CI
Simulated
VWC (cm3/cm3)
Time (Days)
0.1
0.2
0.3
0.4
310
311
312
313
314
315

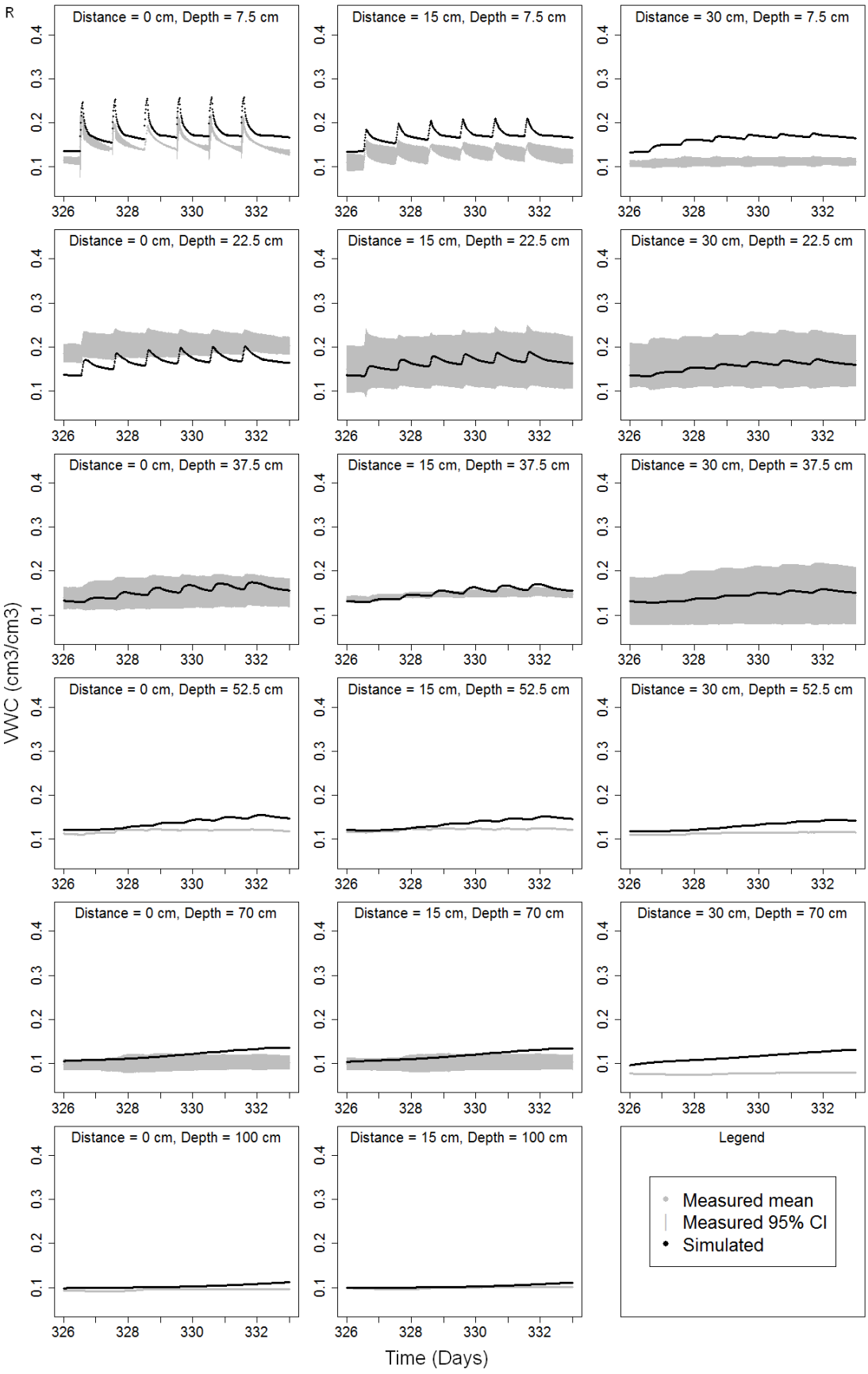
R
Distance = 0 cm, Depth = 7.5 cm
Distance = 15 cm, Depth = 7.5 cm
Distance = 30 cm, Depth = 7.5 cm
Distance = 0 cm, Depth = 22.5 cm
Distance = 15 cm, Depth = 22.5 cm
Distance = 30 cm, Depth = 22.5 cm
Distance = 0 cm, Depth = 37.5 cm
Distance = 15 cm, Depth = 37.5 cm
Distance = 30 cm, Depth = 37.5 cm
Distance = 0 cm, Depth = 52.5 cm
Distance = 15 cm, Depth = 52.5 cm
Distance = 30 cm, Depth = 52.5 cm
Distance = 0 cm, Depth = 70 cm
Distance = 15 cm, Depth = 70 cm
Distance = 30 cm, Depth = 70 cm
Distance = 0 cm, Depth = 100 cm
Distance = 15 cm, Depth = 100 cm
Legend
Measured mean
Measured 95% CI
Simulated
VWC (cm3/cm3)
Time (Days)
0.1
0.2
0.3
0.4
326
328
330
332

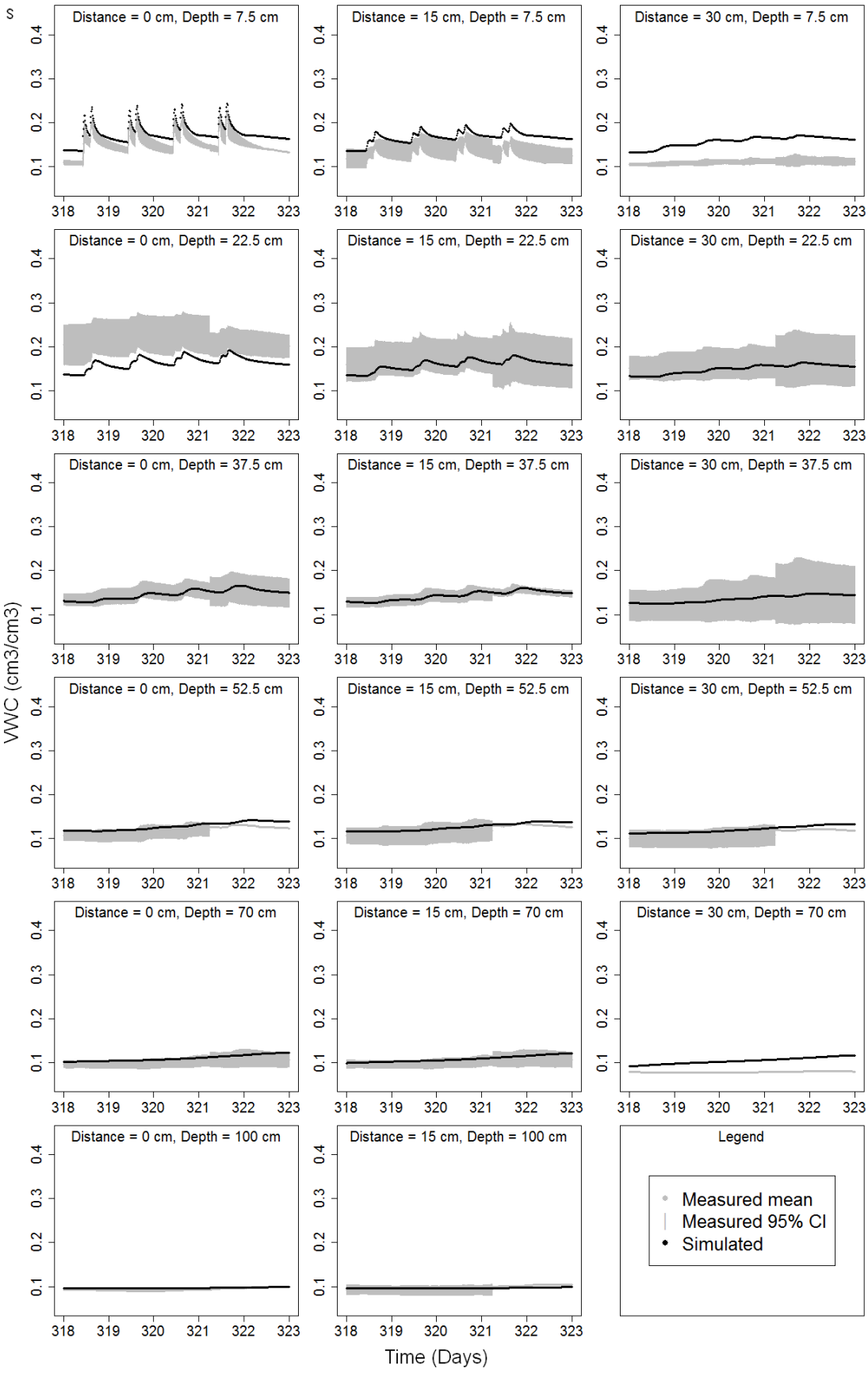
S
Distance = 0 cm, Depth = 7.5 cm
Distance = 15 cm, Depth = 7.5 cm
Distance = 30 cm, Depth = 7.5 cm
Distance = 0 cm, Depth = 22.5 cm
Distance = 15 cm, Depth = 22.5 cm
Distance = 30 cm, Depth = 22.5 cm
Distance = 0 cm, Depth = 37.5 cm
Distance = 15 cm, Depth = 37.5 cm
Distance = 30 cm, Depth = 37.5 cm
Distance = 0 cm, Depth = 52.5 cm
Distance = 15 cm, Depth = 52.5 cm
Distance = 30 cm, Depth = 52.5 cm
Distance = 0 cm, Depth = 70 cm
Distance = 15 cm, Depth = 70 cm
Distance = 30 cm, Depth = 70 cm
Distance = 0 cm, Depth = 100 cm
Distance = 15 cm, Depth = 100 cm
Legend
Measured mean
Measured 95% CI
Simulated
VWC (cm3/cm3)
Time (Days)
0.1
0.2
0.3
0.4
318
319
320
321
322
323

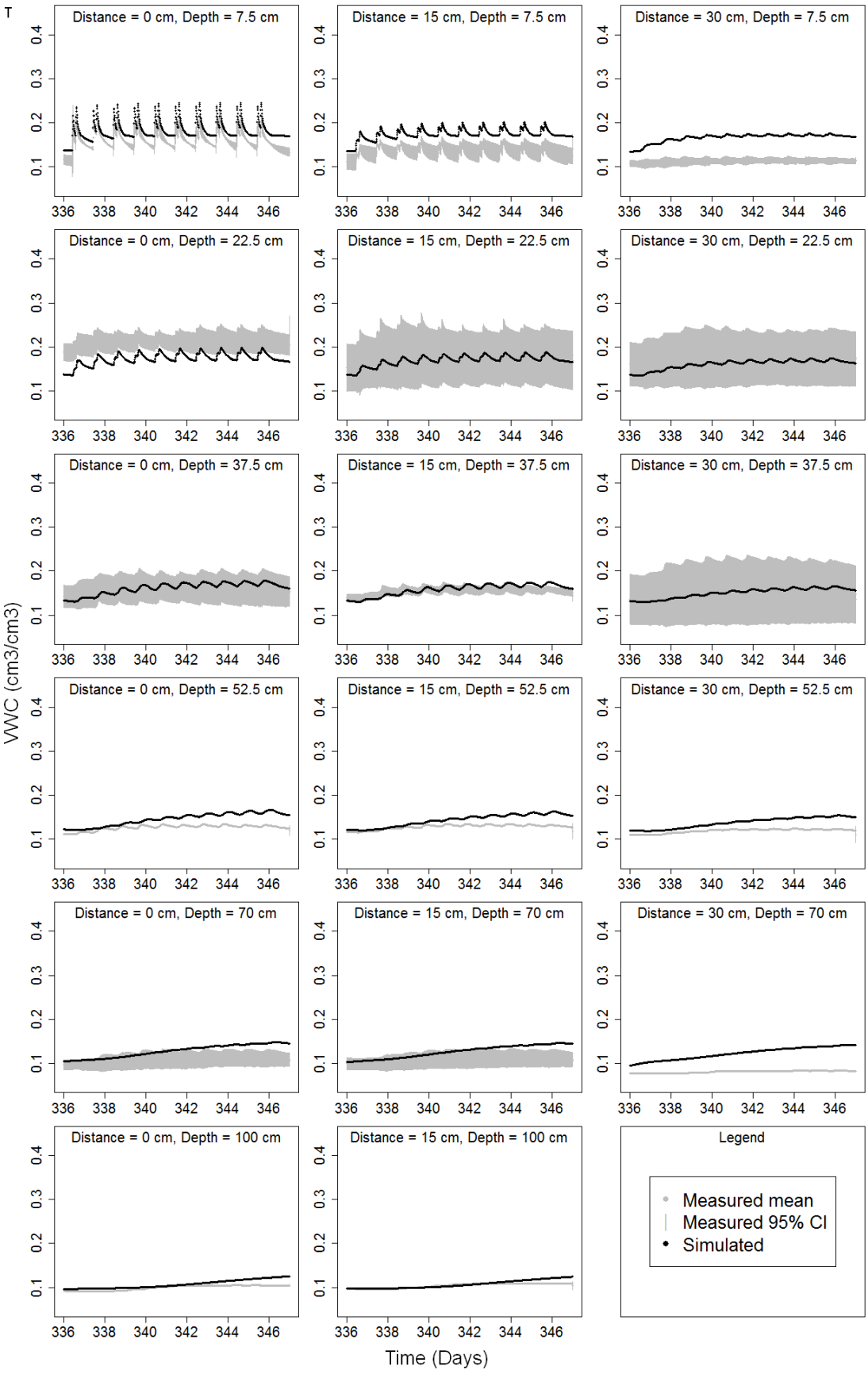
T
Distance = 0 cm, Depth = 7.5 cm
Distance = 15 cm, Depth = 7.5 cm
Distance = 30 cm, Depth = 7.5 cm
Distance = 0 cm, Depth = 22.5 cm
Distance = 15 cm, Depth = 22.5 cm
Distance = 30 cm, Depth = 22.5 cm
Distance = 0 cm, Depth = 37.5 cm
Distance = 15 cm, Depth = 37.5 cm
Distance = 30 cm, Depth = 37.5 cm
Distance = 0 cm, Depth = 52.5 cm
Distance = 15 cm, Depth = 52.5 cm
Distance = 30 cm, Depth = 52.5 cm
Distance = 0 cm, Depth = 70 cm
Distance = 15 cm, Depth = 70 cm
Distance = 30 cm, Depth = 70 cm
Distance = 0 cm, Depth = 100 cm
Distance = 15 cm, Depth = 100 cm
Legend
Measured mean
Measured 95% CI
Simulated
VWC (cm3/cm3)
Time (Days)
0.1
0.2
0.3
0.4
336
338
340
342
344
346

u

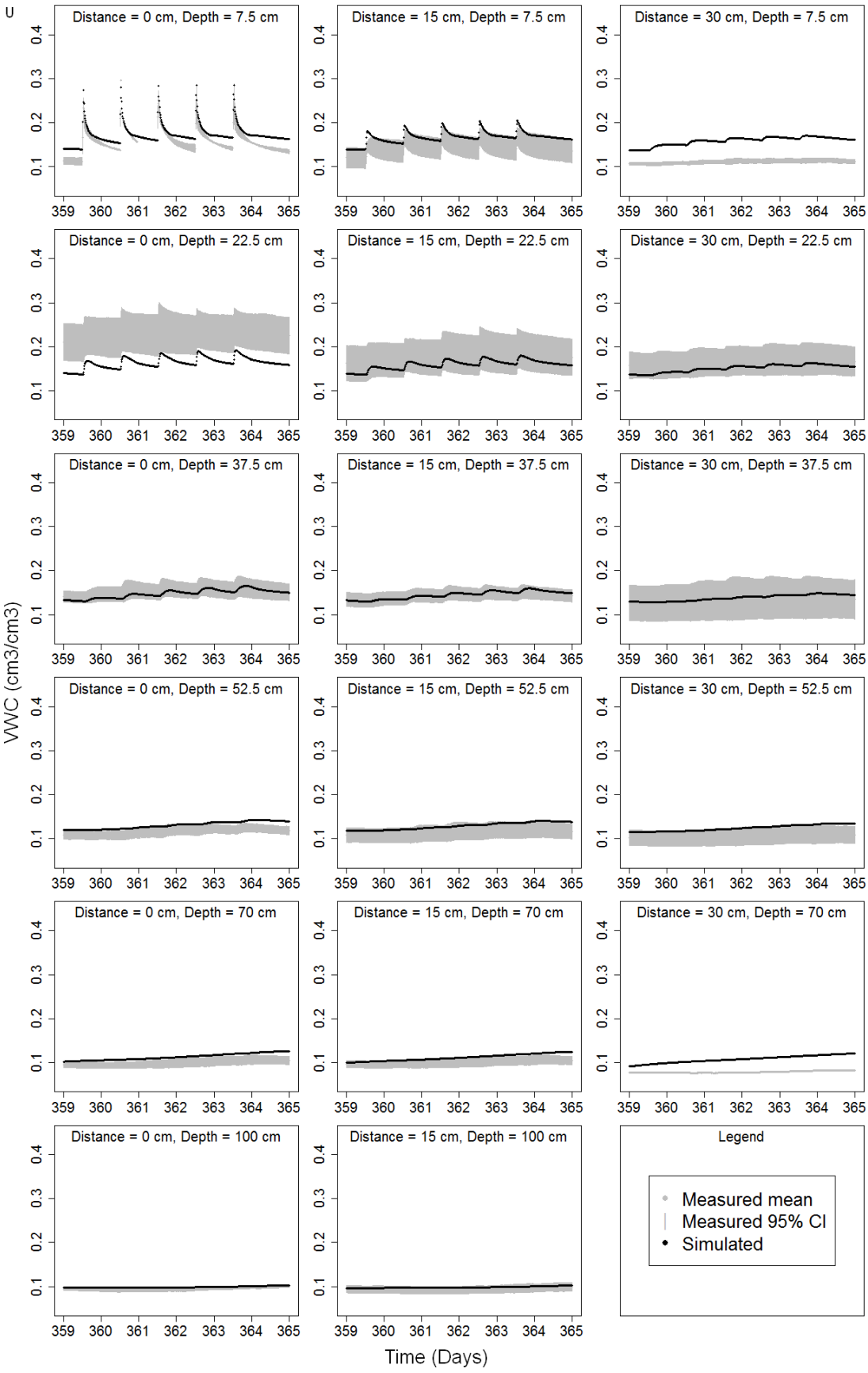
Distance = 0 cm, Depth = 7.5 cm
Distance = 15 cm, Depth = 7.5 cm
Distance = 30 cm, Depth = 7.5 cm
Distance = 0 cm, Depth = 22.5 cm
Distance = 15 cm, Depth = 22.5 cm
Distance = 30 cm, Depth = 22.5 cm
Distance = 0 cm, Depth = 37.5 cm
Distance = 15 cm, Depth = 37.5 cm
Distance = 30 cm, Depth = 37.5 cm
Distance = 0 cm, Depth = 52.5 cm
Distance = 15 cm, Depth = 52.5 cm
Distance = 30 cm, Depth = 52.5 cm
Distance = 0 cm, Depth = 70 cm
Distance = 15 cm, Depth = 70 cm
Distance = 30 cm, Depth = 70 cm
Distance = 0 cm, Depth = 100 cm
Distance = 15 cm, Depth = 100 cm
Legend
Measured mean
Measured 95% CI
Simulated
VWC (cm3/cm3)
Time (Days)

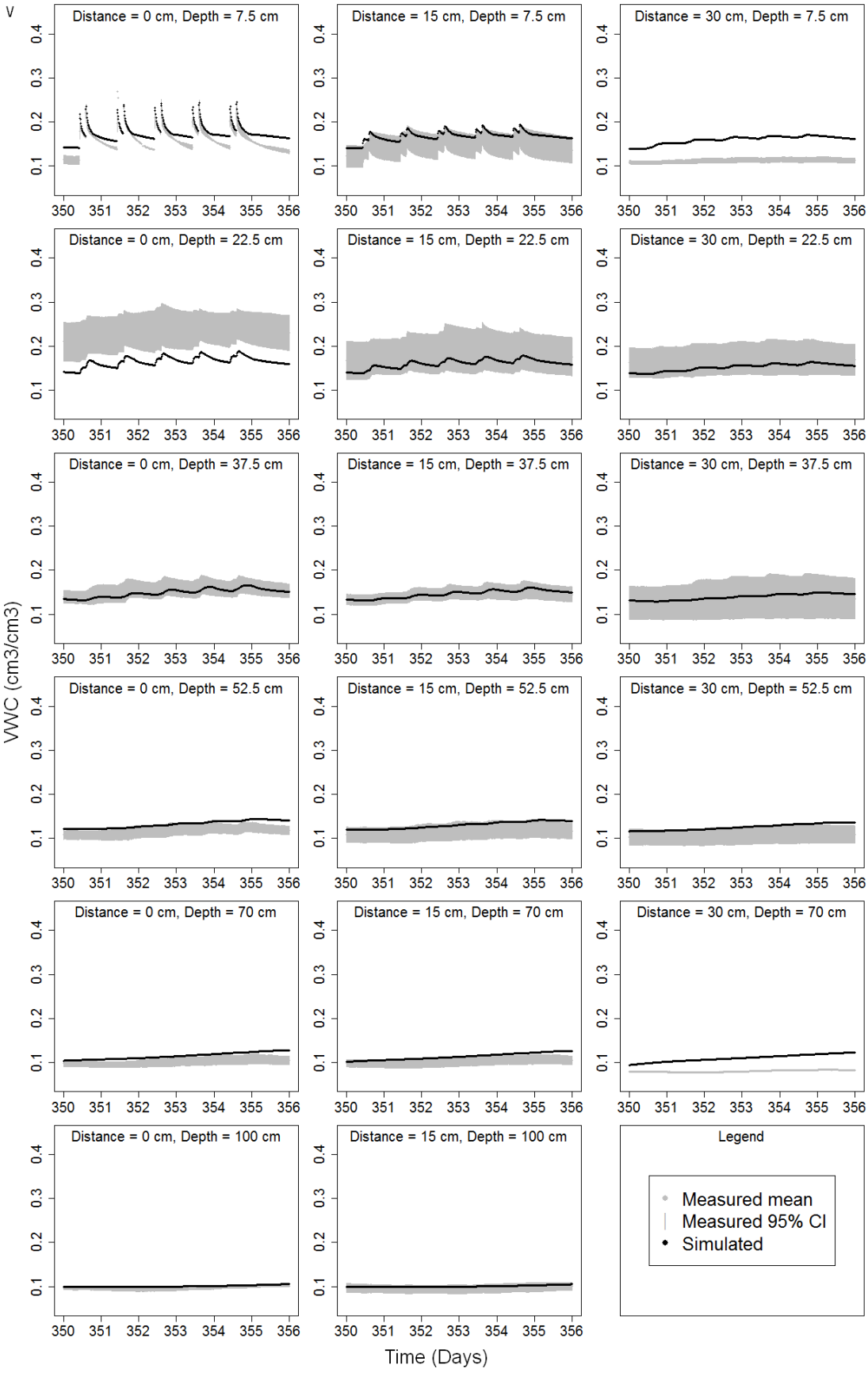
V
Distance = 0 cm, Depth = 7.5 cm
Distance = 15 cm, Depth = 7.5 cm
Distance = 30 cm, Depth = 7.5 cm
Distance = 0 cm, Depth = 22.5 cm
Distance = 15 cm, Depth = 22.5 cm
Distance = 30 cm, Depth = 22.5 cm
Distance = 0 cm, Depth = 37.5 cm
Distance = 15 cm, Depth = 37.5 cm
Distance = 30 cm, Depth = 37.5 cm
Distance = 0 cm, Depth = 52.5 cm
Distance = 15 cm, Depth = 52.5 cm
Distance = 30 cm, Depth = 52.5 cm
Distance = 0 cm, Depth = 70 cm
Distance = 15 cm, Depth = 70 cm
Distance = 30 cm, Depth = 70 cm
Distance = 0 cm, Depth = 100 cm
Distance = 15 cm, Depth = 100 cm
Legend
Measured mean
Measured 95% CI
Simulated
VWC (cm3/cm3)
Time (Days)
0.1
0.2
0.3
0.4
350
351
352
353
354
355
356

LIST OF REFERENCES

Andersson, K., Ohlsson, T., Olsson, P., 1998. Screening life cycle assessment (LCA) of tomato ketchup: a case study. Journal of Cleaner Production 6, 277-288.

Antón, A., Montero, J.I., Muñoz, P., Castells, F., 2005. LCA and tomato production in Mediterranean greenhouses. International Journal of Agricultural Resources Governance and Ecology 4, 102-112.

Asano, T., Burton, F.L., Leverenz, H.L., Tsuchihashi, R., Tchobanoglous, G., 2007. Water Reuse: issues, Technologies and Applications. Metcalf and Eddy, Inc.

Baroni, G., Facchi, A., Gandolfi, C., Ortuani, B., Horeschi, D., Van Dam, J.C., 2009. Uncertainty in the determination of soil hydraulic parameters and its influence on the performance of two hydrological models of different complexity. Hydrology and Earth System Sciences Discussions 6, 4065-4105.

Barretto de Figueiredo, E., Panosso, A.R., Romao, R., La Scala Jr, N., 2010. Greenhouse gas emission associated with sugar production in southern Brazil. Carbon Balance Management 5, 1-7.

Beauchemin, K.A., Janzen, H.H., Little, S.M., McAllister, T.A., McGinn, S.M., 2010. Life cycle assessment of greenhouse emissions from beef production in western Canada: a case study. Agricultural Systems 103, 371-379.

Bedard-Haughn, A., Matson, A.L., Pennock, D.J., 2006. Land use effects on gross nitrogen mineralization, nitrification, and N_2O emissions in ephemeral wetlands. Soil Biology and Biochemistry 38, 3398-3406.

Bengston, T. O., 1987. The hydrologic effects from intense ground-water pumpage in east-central Hillsborough County, Florida. In: Karst hydrogeology: engineering and environmental applications. Beck, B.F., Wilson, W.L. (editors), Proceedings of the Second Multidisciplinary Conference on Sinkholes and the Environmental Impacts of Karst. A. A. Balkema Publishers, Rotterdam, Netherlands.

Berndt, M.P., Hatzell, H.H., Crandall, C.A., Turtora, M., Pittman, J.R., Oaksford, E.T., 1998. Water quality in the Georgia-Florida coastal plain, Georgia and Florida, 1992-96. United States Geological Survey Circular 1151. United States Geological Survey, Reston, VA, USA.

Bernstein, L., Bosch, P., Canziani, O., Chen, Z., Christ, R., Davidson, O., Hare, W., Huq, S., Karoly, D., Kundzewicz, Z., Liu, J., Lohmann, U., Manning, M., Matsuno, T., Menne, B., Metz, B., Mirza, M., Nicholls, N., Nurse, L., Pachauri, R., Palutikof, J., Parry, M., Qin, D., Ravindranath, N., Reisinger, A., Ren, J., Riahi, K., Rosenzweig, C., Rusticucci, M., Schneider, S., Sokona, Y., Solomon, S., Stott, P., Stouffer, R., Sugiyama, T., Swart, R., Tirpak, D., Vogel, C., Yohe, G., 2007. Climate change 2007 - synthesis report. An assessment of the Intergovernmental Panel on Climate Change, Cambridge University Press, Cambridge, UK.

Brandt, A., Bresler, E., Diner, N., Ben-Asher, I., Heller, J., Goldberg, D., 1971. Infiltration from a trickle source: I. Mathematical models. Soil Science Society of America Journal 35, 675-682.

Brentrup, F., Küsters, J., Kuhlmann, H., Lammel, J., 2004. Environmental impact assessment of agricultural production systems using the life cycle assessment methodology: I. Theoretical concept of a LCA method tailored to crop production. European Journal of Agronomy 20, 247-264.

Bresler, E., 1977. Trickle-drip irrigation: principles and application to management. Advances in Agronomy 29, 343-393.

Bresler, E., 1977. Trickle-drip irrigation: Principles and application to management. Advances in Agronomy 29, 343-393.

Bresler, E., Heller, J., Diner, N., Ben-Asher, I., Brandt, A., Goldberg, D., 1971. Infiltration from a trickle source: II. Experimental data and theoretical predictions. Soil Science Society of America Journal 35, 683-689.

Breve, M.A., Skaggs, R.W., Parsons, J.E., Gilliam, J.W., 1997. DRAINMOD-N: A Nitrogen Model for Artificially Drained Lands. Transactions of the American Society of Agricultural Engineers 40, 1067-1075.

Brooks, R.H., Corey, A.T., 1966. Properties of porous media affecting fluid flow. Proceedings of the American Society of Civil Engineering, Journal of Irrigation Drainage Division IR2, 61-68.

Bruinsma, J. (editor), 2003. World agriculture: towards 2015/2030: an FAO perspective. Earthscan, London, UK.

Burkhart, M. R., James, D. E., 1999. Agricultural-nitrogen contributions to hypoxia in the Gulf of Mexico. Journal of Environmental Quality 28, 850-859.

Burney, J.A., Davis, S.J., Lobell, D.B., 2010. Greenhouse gas mitigation by agricultural intensification. Proceedings of the National Academy of Sciences of the United States of America 107, 12052-12057.

Campbell Scientific, 2011. CS616 and CS625 water content reflectometers instruction manual. Campbell Scientific, Logan, UT, USA.

Cantliffe, D., Gilreath, P., Haman, D., Hutchinson, C., Li, Y., McAvoy, G., Migliaccio, K., Olczyk, T., Olson, S., Parmenter, D., Santos, B., Shukla, S., Simonne, E., Stanley, C., Whidden, A., 2009. Review of nutrient management systems for Florida vegetable producers: a white paper from the UF/IFAS vegetable fertilizer task force. Florida Cooperative Extension Service Document HS1156, University of Florida, Gainesville, FL, USA.

Carlsson, A., 1997. Greenhouse gas emissions in the life-cycle of carrots and tomatoes. IMES/EESS Report No. 24, Lund University, Lund, Sweden.

Caruso, G., Rapoport, H.F., Gucci, R., 2013. Long-term evaluation of yield components of young olive trees during the onset of fruit production under different irrigation regimes. Irrigation Science 31, 37-47.

Casey, J.W., Holden, N.M., 2003. A systematic description and analysis of GHG emissions resulting from Ireland's milk production using LCA methodology. In: Proceedings of the Fourth International Conference on Life Cycle Assessment in the Agri-Food Sector, Bygholm, Denmark.

Cassel, D.K., Nielsen, D.R., 1986. Field capacity and available water capacity. In: Agronomy 9-1. Methods of Soil Analysis, 2nd ed. Klute, A., Dinauer, R.C. (editors), American Society of Agronomy, Madison, WI, USA, pp. 493-544.

Ceschia, E., Beziat, P., Dejoux, J.F., Aubinet, M., Bernhofer, Ch., Bodson, B., Buchmann, N., Carrar, A., Cellier, P., Di Tommasi, P., Elbers, J.A., Eugster, W., Grunwald, T., Jacobs, C.M.J., Jans, W.W.O., Jones, M., Kutsch, W., Lanigan, G., Magliulo, E., Marloie, O., Moors, E.J., Moureaux, C., Olioso, A., Osborne, B., Sanz, M.J., Saunders, M., Smith, P., Soegaard, H., Wattenbach, M., 2010. Management effects on net ecosystem carbon and GHG budgets at European crop sites. Agriculture, Ecosystems, and Environment 139, 363-383.

Coelho, E.F., Or, D. ,1996. Flow and uptake patterns affecting soil water sensor placement for drip irrigation management. Transactions of the American Society of Agricultural Engineers 39, 2007-2016.

Copenhagen Accord, 2009. Decision 2/CP.15. United Nations Climate Change Conference 2009, Copenhagen, Denmark.

Cote, C.M., Bristow, K.L., Philip, C.B., Freeman, J.C., Thorburn, J., 2003. Analysis of soil wetting and solute transport in subsurface trickle irrigation. Irrigation Science 22, 143-156.

Davies, J.N., Hobson, G.E., 1981. The constituents of tomato fruits the influence of the environment, nutrition and genotype. CRC Critical Reviews in Food Science and Nutrition 15, 205-280.

Del Grosso, S.J., Ogle, S., Wirth, J., Skiles, S., 2008. U.S. Agriculture and Forestry Greenhouse Gas Inventory: 1990-2005. United States Department of Agriculture Technical Bulletin 1921, United States Department of Agriculture, Washington, DC, USA.

Del Grosso, S.J., Parton, W.J., Mosier, A.R., Walsh, M.K., Ojima, D.S., Thornton, P.E., 2006. DAYCENT National-scale simulations of nitrous oxide emissions from cropped soils in the United States. Journal of Environmental Quality 35, 1451-1460.

Di, H. J., Cameron, K.C., 2002. Nitrate leaching in temperate agroecosystems: sources, factors and mitigating strategies. Nutrient Cycling in Agroecosystems 46, 237-256.

Dukes, M.D., Simonne, E.H., Davis, W.E., Studstil, D.W., Hochmuth, R., 2003. Effect of sensor-based high frequency irrigation on bell pepper yield and water use. In: Proceeding of 2nd International Conference of Irrigation and Drainage, Phoenix, AZ, USA, pp. 665-674.

Dukes, M.D., Zotarelli, L., Morgan, K.T., 2010. Use of irrigation technologies for vegetable crops in Florida. HortTechnology 20, 133-142.

Dukes, M.D., Zotarelli, L., Scholberg, J.M., Munoz-Carpena, R., 2006. Irrigation and nitrogen best management practices under drip irrigated vegetable production. In: Proceedings of the World Environmental & Water Resources Congress. Omaha, NE, USA, May 21-25, 2006.

Dutton, R., Jiao, J., Tsujita, M.J., Grodzinsk, B., 1988. Whole plant CO_2 exchange measurements for nondestructive estimation of growth. Plant Physiology 86, 355-358.

Eggleston, H.S., Buendia L., Miwa K., Ngara T., Tanabe K., 2006. 2006 IPCC guidelines for national greenhouse gas inventories. Institute for Global Environmental Strategies, Hayama, Japan.

Elmaloglou, S.T., Malamos, N., 2003. A method to estimate soil-water movement under a trickle surface line source, with water extraction by roots. Irrigation and Drainage 52, 273-284.

Fischlin, A., Midgeley, G., 2007. Ecosystems, their properties, goods and services. In: Climate change 2007: impacts, adaptation and vulnerability. Contribution of working group II to the fourth assessment report of the intergovernmental panel on climate change. Parry, M.L., Canziani, O.F., Palutikof, J.P., Hanson, C.E., van der Linden, P.J. (editors), Cambridge University Press, Cambridge, U.K.

Fisher, P.D., 1995. An alternative plastic mulching system for improved water management in dryland maize production. Agricultural Water Management 27, 155-166.

Florida Department of Agriculture and Consumer Services, 2010. Florida agriculture statistical directory 2010. Florida Department of Agricultural and Consumer Services, Division of Marketing and Development, Tallahassee, FL, USA.

Fraisse, C.W., Hu, Z., Simonne, E.H., 2010. Effect of El Niño-Southern Oscillation on the number of leaching rain events in Florida and implications on nutrient management for tomato. HortTechnology 20, 120-132.

Gan, Y., Liang, C., Huang, G., Malhi, S.S., Brandt, S.A., Katepa-Mupondwa, F., 2012. Carbon footprint of canola and mustard is a function of the rate of N fertilizer. International Journal of Life Cycle Assessment 17, 58-68.

Gardner, W.R., Mayhugh, M.S., 1958. Solutions and tests of the diffusion equation for the movement of water in soil. Soil Science Society of America Proceedings 22, 197-201.

Gijsman, A.J., Jagtap, S.S., Jones, J.W., 2002. Wading through a swamp of complete confusion: how to choose a method for estimating soil water retention parameters for crop models. European Journal of Agronomy 18, 75-105.

Glades Crop Care, Inc., 1999. Crop profile for south Florida tomatoes. Glades Crop Care, Inc., Jupiter, Florida, USA.

Golden Software, Inc., 2011. Surfer Version 10.1. Golden Software, Inc., Golden, CO, USA.

Gowdish, L., Muñoz-Carpena, R., 2009. An improved Green-Ampt infiltration and redistribution method for uneven multistorm series. Vadose Zone Journal 8, 470-479.

Gowdish, L.C., 2007. An improved Green-Ampt soil infiltration and redistribution method and its application to 1-dimensional and quasi 3-dimensional (point source) flow domains. Doctoral dissertation, University of Florida, Gainesville, FL, USA.

Graboski, M., 2002. Fossil energy use in the manufacture of corn ethanol. National Corn Growers Association, Chesterfield, MO, USA.

Guo, L.B., Gifford, R.M., 2002. Soil carbon stocks and land use change: a meta analysis. Global Change Biology 4, 345-360.

Gupta, S.C., Farrell, D.A., Larson, W.,E., 1974. Determining effective soil water diffusivities from one-step outflow experiments. Soil Science Society of America Journal 38, 710-716.

Hansen, J., Sato, M., Ruedy, R., Lo, K., Lea, D.W., Medina-Elizade, M., 2006. Global temperature change. Proceedings of the National Academy of Sciences of the United States of America 103, 14288-14293.

Hillel D., 1998. Environmental Soil Physics. San Diego, CA: Academic.

Hillier, J., Hawes, C., Squire, G., Hilton, A., Wale, S., Smith, P., 2009. The carbon footprints of food crop production. International Journal of Agricultural Sustainability 7, 107-118.

Hillier, J., Walter, C., Malin, D., Garcia-Suarez, T, Mila-i-Canals, L., Smith, P., 2011. A farm-focused calculator for emissions from crop and livestock production. Environmental Modeling and Software 26, 1070-1078.

Hochmuth, G. C., Hochmuth, R. C., Olson, S. M., 2008. Polyethylene Mulching for Early Vegetable Production in North Florida.Florida Cooperative Extension Service Circular 805, University of Florida, Gainesville, FL, USA.

Hoogenboom, G., Jones, J.W., Wilkens, P.W., Porter, C.H., Hunt, L.A., Boote, K.J., Singh, U., Uryasev, O., Lizaso, J.I., Gijsman, A.J., White, J.W., Batchelor, W.D., Tsuji, G.Y., 2009. Decision Support System for Agrotechnology Transfer Version 4.5 [CD-ROM]. University of Hawaii, Honolulu, HI, USA.

Hoogenboom, G., Jones,J. W., Porter, C. H., Wilkens, P. W., Boote, K. J., Batchelor, W. D., Hunt, L. A., Tsuji, G. Y. (editors), 2003. Decision Support System for Agrotechnology Transfer Version 4.0. University of Hawaii, Honolulu, HI.

Ibarra, L., Flores, J., Diaz-Perez, J.C., 2001. Growth and yield of muskmelon in response to plastic mulch and row covers. Scientia Horticulturae 87, 139-145.

Ingwersen, W.W., 2012. Life cycle assessment of fresh pineapple from Costa Rica. Journal of Cleaner Production 35, 1-12.

Intergovernmental Panel on Climate Change, 2006. 2006 IPCC Guidelines for National Greenhouse Gas Inventories, Prepared by the National Greenhouse Gas Inventories Programme, Eggleston, H.S., Buendia, L., Miwa, K., Ngara, T., and Tanabe, K. (editors),IGES, Japan.

International Fertilizer Industry Association and the Food and Agriculture Organization of the United Nations, 2001. Global estimates of gaseous emissions of NH_3, NO, and N_2O from agricultural land. International Fertilizer Industry Association and the Food and Agriculture Organization of the United Nations, Rome, Italy.

Ippisch, O., Vogel, H.J., Bastian, P., 2006. Validity limits for the Van Genuchten-Mualem model and implications for parameter estimation and numerical simulation. Advances in Water Resources 29, 1780-1789.

Jansson, S. L., Persson, J., 1982. Mineralization and immobilization of soil nitrogen. In: Nitrogen in Agricultural Soils. Stevenson, F. J. (editor), Agronomy Monograph 22. American Society of Agronomy, Madison, WI.pp. 229-248.

Jones, C.D., Fraisse, C.W., Ozores-Hampton, M., 2012. Quantification of greenhouse gas emissions from open field-grown Florida tomato production. Agricultural Systems 113, 64-72.

Jones, J. W., Hoogenboom, G., Porter, C. H., Boote, K. J., Batchelor, W. D., Hunt, L. A., Wilkens, P. W., Singh, U., Gijsman, A. J., Ritchie, J. T., 2003. The DSSAT cropping system model. European Journal of Agronomy 18, 235-265.

Jones, J.W., Hoogenboom, G., Porter, C.H., Boote, K.J., Batchelor, W.D., Hunt, L.A., Wilkens, P.W., Singh, U., Gijsman, A.J., Ritchie, J.T., 2003. The DSSAT cropping system model. European Journal of Agronomy 18, 235-265.

Kasperbauer, M.J., Hunt, P.G., 1989. Mulch surface color affects yield of fresh-market tomatoes. Jounral of the American Society of Horitcultural Science 114, 216-219.

Kendall, A., Chang, B., 2009. Estimating life cycle greenhouse gas emissions from corn-ethanol: a critical review of current U.S. practices. Journal of Cleaner Production 17, 1175-1182.

Kenny, J. F., Barber, N. L., Hutson, S. S., Linsey, K. S., Lovelace, J. K., Maupin, M. A., 2009. Estimated use of water in the United States in 2005.US Geological Survey Circular 1344. Reston, VA: US Geological Survey.

Kim, S., Dale, B.E., Jenkins, R., 2009. Life cycle assessment of corn grain and corn stover in the United States. The International Journal of Life Cycle Assessment 14, 160-174.

Klute, A., 1986. Methods of soil analysis, part 1. Physical and Mineralogical Methods, 2nd ed. American Society of Agronomy, Soil Science Society of America, Inc., Madison, WI, USA.

Kosugi, K., Hopmans, J.W., Dane, J.H., 2002. Parametric models. In: Methods of Soil Analysis, part 4, Physical Methods. Dane, J.H., Topp, G.C. (editors). Soil Science Society of America, Madison, WI, USA, pp. 739-755.

Lal, R., 2004.Carbon emission from farm operations. Environment International 30, 981-990.

Li, F., Guo, A., Wei, H., 1999. Effects of clear plastic film mulch on yield of spring wheat. Field Crops Research 63, 79-86.

Li, J. S., Zhang, J. J., Ren, L., 2003. Water and nitrogen distribution as affected by fertigation of ammonium nitrate from a point source. Irrigation Science 22, 19-30.

Locascio, S. J., 2005. Management of irrigation for vegetables: past, present, and future. HortTechnology 15, 482-485.

Looper, J.P., Baxter, E.V., 2011. An assessment of distributed flash flood forecasting accuracy using radar and rain gauge input for a physics-based distributed hydrologic model. Journal of Hydrology 412-413, 114-132.

Mace, A., Rudolph, D.L., Kachanoski, R.G., 1998. Suitability of parametric models to describe the hydraulic properties of an unsaturated coarse sand and gravel. Ground Water 36, 465-475.

Machado, R.M.A., do Rosario, M., Oliveira, G., Portas, C.A.M., 2003. Tomato root distribution, yield and fruit quality under subsurface drip irrigation. Plant and Soil 255, 333-341.

Marquardt, D.W., 1963. An algorithm for least-squares estimation of nonlinear parameters. Journal of the Society for Industrial and Applied Mathematics 11, 431-441.

McSwiney, C.P., Robertson, G.P., 2005. Nonlinear response of N_2O flux to incremental fertilizer addition in a continuous maize (*Zea mays* L.) cropping system. Global Change Biology 11, 1712-1719.

Meehl, G.A., Stocker, T.F., Collins, W.D., Friedlingstein, P., Gaye, A.T., Gregory, J.M., Kitoh, A., Knutti, R., Murphy, J.M., Noda, A., Raper, S.C.B., Watterson, I.G., Weaver, A.J., Zhao, Z.C., 2007. Global climate projections. In: Climate change 2007: the physical science basis. Contribution of Working Group I to the Fourth Assessment Report of the Intergovernmental Panel on Climate Change. Solomon, S., Qin, D., Manning, M., Chen, Z., Marquis, M., Averyt, K.B., Tignor, M., Miller, H.L. (editors), Cambridge University Press, Cambridge, UK.

Meinshausen, M., Meinshausen, N., Hare, W., Raper, S. C. B., Frieler, K., Knutti, R., Frame, D. J., Allen, M. R., 2009. Greenhouse-gas emission targets for limiting global warming to 2 °C. Nature 458, 1158-1162.

Molle, F., Berkoff, J., 2009. Cities vs. agriculture: a review of intersectoral water re-allocation. Natural Resources Forum 33, 6-18.

Mordini, M., Nemecek, T., Gaillard, G., 2009. Carbon & water footprint of orange and strawberries. Federal Department of Economic Affairs, Zurich, Switzerland.

Mualem, Y., 1976. A new model predicting the hydraulic conductivity of unsaturated porous media. Water Resources Research 12, 513-522.

Mueller, D.K., Helsel, D.R., 1996. Nutrients in the nation's waters: Too much of a good thing? United States Geological Survey Circular 1136. United States Geological Survey, Reston, VA, USA.

Muñoz, P., Antón, A., Montero, J.I., Castells, F., 2004. Using LCA for the improvement of waste management in greenhouse tomato production. In: Proceedings of the Fourth International Conference on Life Cycle Assessment in the Agri-Food Sector, Bygholm, Denmark.

Nagy, R.C., Lockaby, B.G., Helms, B., Kalin, L., Stoeckel, D., 2010. Water resources and land use and cover in a humid region: the Southeastern United States. Journal of Environmental Quality 40, 867-878.

O'Connor, G.A., Elliott, H.A., Bastian, R.K., 2008. Degraded water reuse: an overview. Journal of Environmental Quality 37, S-157-S-168.

Olson, S.M., 2011. Mulching. In: Vegetable production handbook for Florida 2010-2011. Olson, S.M., Santos, B. (editors). University of Florida, Gainesville, FL, USA.

Olson, S.M., Santos, B., 2011. Vegetable production handbook for Florida, 2010-2011. University of Florida Institute of Food and Agricultural Sciences, Gainesville, FL, USA.

Olson, S.M., Stall, W.M., Vallad, G.E., Webb, S.E., Smith, S.A., Simonne, E.H., McAvoy, E.J., Santos, B.M., 2010. Tomato production in Florida. In: Vegetable production handbook for Florida 2010-2011. Olson, S.M., Santos, B. (editors), University of Florida, Gainesville, FL, USA.

Pachepsky, Y., Timlin, D., Rawls, W., 2003. Generalized Richard's equation to simulate water transport in unsaturated soils. Journal of Hydrology 272, 3-13.

Pitts, D.J., Clark, G.A., Alvarez, J., Everett, P.H., Grimm, J.M., 1988. A comparison of micro to subsurface irrigation of tomatoes. Proceedings of the Florida State Horticultural Society 101, 393-397.

Provenzano, G., 2007. Using HYDRUS-2D simulation model to evaluate wetted soil volume in subsurface drip irrigation systems. Journal of Irrigation and Drainage Engineering 133, 342-349.

R Development Core Team, 2011. R: A language and environment for statistical computing. R Foundation for Statistical Computing, Vienna, Austria.

Rawls, W.J., Ahuja, L.R., Brakensiek, D.L., 1992. Estimating soil hydraulic properties from soils data. In: Indirect Methods for Estimating the Hydraulic Properties of Unsaturated Soils. Van Genuchten, M.Th., Leij, F.J., Lund, L.J. (editors). University of California, Riverside, CA, USA, pp. 329-340.

Reichardt, K., Nielsen, D.R., Biggar, J.W., 1972. Scaling of horizontal infiltration into homogenous soils. Soil Science Society of America Proceedings 36, 241-245.

Richards, L.A. 1931. Capillary conduction of liquids in porous mediums. Physics 1, 318-333.

Ritchie, J.T., 1985. An user-orientated model of the soil water balance in wheat. In: Wheat Growth and Modeling. Day, W., Atkin, R.K., (editors). Plenum Press, New York, NY, USA, pp. 293-305.

Ritchie, J.T., 1985. An user-orientated model of the soil water balance in wheat. In: Wheat Growth and Modeling. Day, W., Atkin, R.K. (editors). Plenum Press, New York, NY, USA, pp. 293-305.

Ritchie, J.T., 1998. Soil water balance and water stress. In: Understanding Options for Agricultural Production. Tsuji, G.Y., Hoogenboom, G., Thornton, P. K. (editors). Kluwer Academic Publishers, Dordrecht, Netherlands, pp. 99-128.

Ritchie, J.T., 1998. Soil water balance and water stress. In: Understanding Options for Agricultural Production. Tsuji, G.Y., Hoogenboom, G., Thornton, P.K. (editors). Kluwer Academic Publishers, Dordrecht, Netherlands, pp. 99-128.

Roberts, R., Lazarovitch, N., Warrick, A.W., Thompson, T.L., 2009. Modeling salt accumulation with subsurface drip irrigation using HYDRUS-2D. Soil Science Society of America Journal 73, 233-240.

Robertson, G.P., Paul, E.A., Harwood, R.R., 2000. Greenhouse gases in intensive agriculture: contributions of individual gases to the radiative forcing of the atmosphere. Science 289, 1922-1925.

Rogelj, J., Nabel, J., Chen, C., Hare, W., Markmann, K., Meinshausen, M., Schaeffer, M., Macey, K., Höhne, N., 2010. Copenhagen Accord pledges are paltry. Nature 464, 1126-1128.

Rogner, H.-H., Zhou, D., Bradley, R., Crabbé, P., Edenhofer, O., Hare, B., Kuijpers, L., Yamaguchi, M., 2007. Introduction. In: Climate change 2007: mitigation. Contribution of Working Group III to the Fourth Assessment Report of the Intergovernmental Panel on Climate Change. Metz, B., Davidson, O.R., Bosch, P.R., Dave, R., Meyer, L.A. (editors), Cambridge University Press, Cambridge, UK.

Romero, C.C., Dukes, M.D., Baigorria, G.A., Cohen, R.C., 2008. Comparing theoretical irrigation requirement and actual irrigation for citrus in Florida. Agricultural Water Management 96, 473-483.

Roos, E., Sundberg, C., Hansson, P., 2010. Uncertainties in the carbon footprint of food products: a case study on table potatoes. The International Journal of Life Cycle Assessment 15, 478-488.

Rosenzweig, C., Strzepek, K.M., Major, D.C., Iglesias, A., Yates, D.N., McCluskey, A., Hillel, D., 2004. Water resources for agriculture in a changing climate: international case studies. Global Environment Change Part A 14, 345-360.

Rubin, J., 1968. Theoretical analysis of two-dimensional, transient flow of water in unsaturated and partly unsaturated soils. Soil Science Society of America Proceedings 32, 607-615.

Sato, S., Morgan, K.T., Ozores-Hampton, M., Mahmoud, K., Simonne, E.H., 2010. Nutrient balance and use efficiency in sandy soils cropped with tomato under seepage irrigation. Soil Science Society of America Journal 76, 1867-1876.

Saxton, K.E., Rawls, W.J., 2006. Soil water characteristics estimates by texture and organic matter for hydrologic solutions. Soil Science Society of America Journal 70, 1569-1578.

Schaap, M.G., Leij, F.J., 2000. Improved prediction of unsaturated hydraulic conductivity with the Mualem-Van Genuchten Model. Soil Science Society of America Journal 64, 843-851.

Scholberg, J.M.S., 1996. Adaptive use of crop growth models to simulate the growth of field-grown tomato. Doctoral dissertation, University of Florida, Gainesville, FL, USA.

Schroder, J. H., 2006. Soil moisture-based drip irrigation for efficient use of water and nutrients and sustainability of vegetables cropped on coarse soils. Masters thesis, University of Florida, Gainesville, FL, USA.

Schwartzman, M., Zur, B., 1986. Emitter spacing and geometry of wetted soil volume. Journal of Irrigation and Drainage Engineering 112, 242-253.

Shrestha, N., Geerts, S., Raes, D., Horemans, S., Soentjens, S., Maupas, F., Clouet, P., 2010. Yield response of sugar beets to water stress under Western European conditions. Agricultural Water Management 97, 346-350.

Shukla, S., Jaber, F.H., 2005. Groundwater recharge in shallow water table conditions. Paper No. 05-2088, presented at the 2005 ASAE Annual International Meeting, Tampa, FL, USA, July 17-20, 2005. The American Society of Agricultural Engineers, St. Joseph, MI, USA.

Simonne, E., Studstill, D., Hochmuth, R., Olczyk, T., Dukes, M., Munoz-Carpena, R., Li, Y., 2003. Drip Irrigation: The BMP Era - An Integrated Approach to Water and Fertilizer Management for Vegetables Grown with Plasticulture. Florida Cooperative Extension Service, IFAS, University of Florida HS917, Gainesville, FL, USA.

Simonne, E.H., Dukes, M.D., Haman, D.Z., 2004. Principles and practices of irrigation management for vegetables. In: Vegetable production guide for Florida. Olsen, S. M., Simonne, E. H. (editors). University of Florida, Gainesville, FL, USA, p. 33-39.

Simonne, E.H., Dukes, M.D., Zotarelli, L., 2010. Principles and practices of irrigation management for vegetables. In: Vegetable production handbook for Florida 2010-2011. Olson, S.M., Santos, B. (editors), University of Florida, Gainesville, FL, USA.

Simonne, E.H., Ozores-Hampton, M., 2006. Challenges and opportunities for extension research educators involved in best management practices. HortTechnology 16, 403-407.

Simmone, E., Hutchinson, C., DeValerio, J., Hochmuth, R., Treadwell, D., Wright, A., Sants, B., Whidden, A., McAvoy, G., Zhao, X., Olczyk, T., Gazula, A., Ozores-Hampton, M., 2010. Current knowledge, gaps, and future needs for keeping water and nutrients in the root zone of vegetables grown in Florida. HortTechnology 20, 143-152.

Simunek, J., Van Genuchten, M.Th., Sejna, M., 2006. The HYDRUS software package for simulating the two- and three-dimensional movement of water, heat, and multiple solutes in variably-saturated media, Version 1.0. PC Progress, Prague, Czech Republic.

Skaggs, T.H., Trout, T.J., Rothfuss, Y., 2010. Drip irrigation water distribution patterns: Effects of emitter rate, pulsing, and antecedent water. Soil Science Society of America Journal 74, 1886-1896.

Skaggs, T.H., Trout, T.J., Simunek, J., Shouse, P.J., 2004. Comparison of HYDRUS-2D simulations of drip irrigation with experimental observations. Journal of Irrigation and Drainage Engineering 130, 304-310.

Smajstrla, A.G., Locascio, S.J., 1996. Tensiometer-controlled, drip-irrigation scheduling of tomato. Applied Engineering in Agriculture 12, 315-319.

Smith, P., Martino, D., Cai, Z., Gwary, D., Janzen, H., Kumar, P., McCarl, B., Ogle, S., O'Mara, F., Rice, C. Scholes, B., Sirotenko, O., 2007. Agriculture. In: Climate Change 2007: Mitigation. Contribution of Working Group III to the Fourth Assessment Report of the Intergovernmental Panel on Climate Change. Metz, B., Davidson, O.R., Bosch, P.R., Dave, R., Meyer, L.A. (editors). Cambridge University Press, New York, NY, USA.

Snyder, C.S., Bruulsema, T.W., Jensen, T.L., Fixen, P.E., 2009. Review of greenhouse gas emissions from crop production systems and fertilizer management effects. Agriculture, Ecosystems and Environment 133, 247-266.

Soil Survey Staff, 2004. Particle size analysis method 3A1a1. In: Soil survey laboratory methods manual. Burt, R. (editor). Soil survey investigations report no. 42, version 4. Natural Resources Conservation Service, United States Department of Agriculture, National Soil Survey Center, Lincoln, NE, USA.

Soil Survey Staff, 2011. Web soil survey. Natural Resources Conservation Service, United States Department of Agriculture. Retrieved 06.01.2011 from http://websoilsurvey.nrcs.usda.gov/.

Southwest Florida Water Management District, 2006. Southern water use caution area recovery strategy. Retrieved 05.01.2011 from http://www.swfwmd.state.fl.us/documents/plans/swuca_recovery_strategy.pdf

Spreen, T., Dwivedi, P., Goodrich-Schneider, R., 2010. Estimating the carbon footprint of Florida orange juice. Proceedings in Food System Dynamics, 95-101.

Tak, H.I., Bakhtiyar, Y., Ahmad, F., Inam, A., 2012. Effluent quality parameters for safe use in agriculture. In: Water quality, soil and managing irrigation of crops. Lee, T.S. (editor), InTech, Rijeka, Croatia.

Talbot, C.A., Ogden, F.L., Or, D., 2004. Comment of “Layer averaged Richards’ equation with lateral flow” by Kumar, P. Advances in Water Resources 27, 1041-1042.

Tiemeyer, B., Kahle, P., Lennartz, B., 2010. Designing monitoring programs for artificially drained catchments. Vadose Zone Journal 9, 14-24.

Topp, G.C., 1980. Electromagnetic determination of soil water content measurements in coaxial transmission lines. Water Resources Research 16, 574-582.

Tsuji, G.Y., Uehara, G., Balas, S., (editors), 1994. DSSAT Version 3. University of Hawaii, Honolulu, HI, USA.

Tuller, M., Or, D., 2001. Hydraulic conductivity of variably saturated porous media: film and corner flow in angular pore space. Water Resources Research 37, 1257-1276.

United Nations Framework Convention on Climate Change, 2009. Decision 2/CP.15 Copenhagen Accord, pp. 4-10.

United States Department of Agriculture, Soil Conservation Service, 1972. National Engineering Handbook, Hydrology, Section 4. Washington, DC, USA.

United States Environmental Protection Agency, 2005. Emission facts: average carbon dioxide emissions resulting from gasoline and diesel fuel. U.S. EPA # 420-F-05-001, Environmental Protection Agency, Washington, DC, USA.

United States Environmental Protection Agency, 2010. 2010 US Greenhouse Gas Inventory Report: Inventory of U.S. Greenhouse Gas Emissions and Sinks, 1990-2008. U.S. EPA # 430-R-10-006, Environmental Protection Agency, Washington, DC, USA.

University of Florida Department of Soil and Water Science, 2012. Florida Soil Characterization Database. Retrieved 09.01.2012 from The Florida Soil Characterization Retrieval System http://soils.ifas.ufl.edu/flsoils/.

Van Genuchten, M.Th., 1980. A closed-form equation for predicting the hydraulic conductivity of unsaturated soils. Soil Science Society of America Journal 44, 892-898.

Van Genuchten, M.Th., Leij, F., Yates, S., 1991. The RETC code for quantifying the hydraulic functions of unsaturated soils.Technical Report EPA/600/2-91/065, US Environmental Protection Agency.

Van Genuchten, M.Th., Nielsen, D.R., 1985. On describing and predicting the hydraulic properties of unsaturated soils. Annales Geophysicae 3, 615-628.

Vazquez, N., Pardo, A., Suso, M.L., Quemada, M., 2005. A methodology for measuring drainage and nitrate leaching in unevenly irrigated vegetable crops. Plant and Soil 269, 297-308.

Vorosmarty, C. J., Green P., Salisbury J., Lammers, R.B., 2000. Global water resources: vulnerability from climate change and population growth. Science 289, 284-288.

Wan, Y., El-Swaify, S.A., 1999. Runoff and soil erosion as affected by plastic mulch in a Hawaiian pineapple field. Soil and Tillage Research 52, 29-35.

Wang, D., Shannon, M.C., Grieve, C.M., Yates, S.R., 2000. Soil water and temperature regimes in drip and sprinkler irrigation, and implications to soybean emergence. Agricultural Water Management 43, 15-28.

Warrick, A.W., 1985. Point and line infiltration - calculation of the wetted soil surface. Soil Science Society of America Journal 49, 1581-1583.

Weinheimer, J., Rajan, N., Johnson, P., Maas, S., 2010. Carbon footprint: a new farm management consideration in the Southern High Plains. Selected paper prepared for presentation at the Agricultural and Applied Economics Association‘s 2010 AAEA, CAES and WAEA Joint Annual Meeting, July 25-27, 2010, Denver, Colorado, USA.

Williams, A.G., Audsley, E., Sandars, D.L. 2006. Energy and environmental burdens of organic and non-organic agriculture and horticulture. Aspects of Applied Biology 79, 19-23.

Williams, J.R., Jones, C.A., Dyke, P.T., 1984. A modeling approach to determining the relationships between erosion and soil productivity. Transactions of American Society of Agricultural Engineers 27, 129-144.

World Meteorological Organization, 2006. Greenhouse gas bulletin: the state of greenhouse gases in the atmosphere using global observations up to December 2004. World Meteorological Organization, Geneva, Switzerland.

Zotarelli, L., Dukes, M.D., Scholberg, J.M., Hanselman, T., Le Femminella, K., Munoz-Carpena, R., 2008. Nitrogen and water use efficiency of zucchini squash for a plastic mulch bed system on a sandy soil. Scientia Horticulurae 116, 8-16.

Zotarelli, L., Dukes, M.D., Scholberg, J.M.S., Munoz-Carpena, R., Icerman, J., 2009. Tomato nitrogen accumulation and fertilizer use efficiency on a sandy soil, as affected by nitrogen rate and irrigation scheduling. Agricultural Water Management 96, 1247-1258.

Zotarelli, L., M.D. Dukes, Morgan, K.T., 2010.Interpretation of Soil Moisture Content to Determine Soil Field Capacity and Avoid Over-Irrigating Sandy Soils Using Soil Moisture Sensors. Florida Cooperative Extension Service AE 460.

Zotarelli, L., Scholberg, J.M., Dukes, M.D., Munoz-Carpena, R., 2007. Monitoring of nitrate leaching in sandy soils: comparison of three methods. Journal of Environmental Quality 36, 953-962.

Zotarelli, L., Scholberg, J.M., Dukes, M.D., Munoz-Carpena, R., Icerman, J., 2009. Tomato yield, biomass accumulation, root distribution and irrigation water use efficiency on a sandy soil, as affected by nitrogen rate and irrigation scheduling. Agricultural Water Management 96, 23-34.

BIOGRAPHICAL SKETCH

Curtis Jones graduated *magna cum laude* with a Bachelor of Science degree in agricultural and biological engineering from the University of Florida in 2006. During this time he was introduced to crop modeling and worked on projects related to irrigation management and climate impacts on agricultural risk. After graduating, he worked for Water & Air Research Inc., an environmental consulting firm, focusing on water quality monitoring projects. In 2008 he began graduate school at the University of Florida, where he was awarded an Alumni Fellowship by the Department of Agricultural and Biological Engineering to pursue a Doctoral degree.